

# Control of monomer sequence distribution : strategic approaches based on novel insights in atom transfer radical copolymerisation

**Citation for published version (APA):**

Chambard, G. (2000). *Control of monomer sequence distribution : strategic approaches based on novel insights in atom transfer radical copolymerisation*. [Phd Thesis 1 (Research TU/e / Graduation TU/e), Chemical Engineering and Chemistry]. Technische Universiteit Eindhoven. <https://doi.org/10.6100/IR539072>

**DOI:**

[10.6100/IR539072](https://doi.org/10.6100/IR539072)

**Document status and date:**

Published: 01/01/2000

**Document Version:**

Publisher's PDF, also known as Version of Record (includes final page, issue and volume numbers)

**Please check the document version of this publication:**

- A submitted manuscript is the version of the article upon submission and before peer-review. There can be important differences between the submitted version and the official published version of record. People interested in the research are advised to contact the author for the final version of the publication, or visit the DOI to the publisher's website.
- The final author version and the galley proof are versions of the publication after peer review.
- The final published version features the final layout of the paper including the volume, issue and page numbers.

[Link to publication](#)

**General rights**

Copyright and moral rights for the publications made accessible in the public portal are retained by the authors and/or other copyright owners and it is a condition of accessing publications that users recognise and abide by the legal requirements associated with these rights.

- Users may download and print one copy of any publication from the public portal for the purpose of private study or research.
- You may not further distribute the material or use it for any profit-making activity or commercial gain
- You may freely distribute the URL identifying the publication in the public portal.

If the publication is distributed under the terms of Article 25fa of the Dutch Copyright Act, indicated by the "Taverne" license above, please follow below link for the End User Agreement:

[www.tue.nl/taverne](http://www.tue.nl/taverne)

**Take down policy**

If you believe that this document breaches copyright please contact us at:

[openaccess@tue.nl](mailto:openaccess@tue.nl)

providing details and we will investigate your claim.

# Control of Monomer Sequence Distribution

Strategic Approaches based on Novel Insights in  
Atom Transfer Radical Copolymerisation

Grégory Chambard

CIP-DATA LIBRARY TECHNISCHE UNIVERSITEIT EINDHOVEN

Chambard, Grégory

Control of monomer sequence distribution: strategic approaches based on novel insights in atom transfer radical copolymerisation / by Gregory Chambard.

Eindhoven: Technische Universiteit Eindhoven, 2000.

Proefschrift.

ISBN 90-386-2622-3

NUGI 813

Trefwoorden: polymerisatie; radicaalreacties / reactiekinetiek / copolymeren; chemische samenstelling / styreen / butylacrylaat

Subject headings: polymerization; radical reactions / reaction kinetics / copolymers; chemical composition / styrene / butyl acrylate

© 2000, Grégory Chambard

Druk: Universiteitsdrukkerij Technische Universiteit Eindhoven

Omslag: Karin Verheijen

# Control of Monomer Sequence Distribution

Strategic Approaches based on Novel Insights in  
Atom Transfer Radical Copolymerisation

PROEFSCHRIFT

ter verkrijging van de graad van doctor aan de  
Technische Universiteit Eindhoven, op gezag van de  
Rector Magnificus, prof. dr. M. Rem, voor een  
commissie aangewezen door het College voor  
Promoties in het openbaar te verdedigen  
op dinsdag 19 december 2000 om 16.00 uur

door

Grégory Chambard

geboren te Prinsenbeek

Dit proefschrift is goedgekeurd door de promotoren:

prof. dr. ir. A.L. German

en

prof. dr. T. Fukuda

Copromotor:

dr. ir. B. Klumperman

*‘Ο χρησιμὸν εἶδως, οὐχ ὁ πολλὸν εἶδως, σοφός*

*Niet hij is wijs, die veel weet, maar hij, die nuttige dingen weet*

Aischylos



# Table of Contents

<b>TABLE OF CONTENTS</b>	7
<b>CHAPTER 1 INTRODUCTION</b>	11
1.1 History	12
1.2 Free-Radical Polymerisation	12
1.3 Chemical Composition Distribution: Intramolecular Composition Drift	13
1.4 Objective of This Thesis	15
1.5 Outline of This Thesis	16
References	17
<b>CHAPTER 2 FREE-RADICAL COPOLYMERISATION OF STYRENE AND BUTYL ACRYLATE</b>	19
2.1 Introduction	20
2.2 Copolymerisation	21
2.3 Anomalies in Copolymerisation	24
2.3.1 Bootstrap model	24
2.3.2 Preferential absorption model	27
2.3.3 Summary	30
2.4 Experimental	31
2.5 Results and Discussion	32
2.6 Conclusions	36
References	36
<b>CHAPTER 3 ATOM TRANSFER RADICAL POLYMERISATION</b>	39
3.1 Introduction	40
3.2 Living Radical Polymerisation	40
3.3 Atom Transfer Radical Polymerisation (ATRP)	43
3.3.1 Mechanism of ATRP	43
3.3.2 Kinetic description of ATRP in constant density reactors	46
3.3.3 Different components in ATRP	49
3.3.3.1 Transition metal complex	49
3.3.3.2 Monomer	54
3.3.3.3 Solvent	55
3.3.3.4 Initiator	55



3.3.4	<i>Peculiarities</i>	56
3.3.5	<i>Possibilities and limitations</i>	57
3.4	<b>Future Prospects</b>	59
	<b>References</b>	59

## CHAPTER 4 *ATOM TRANSFER RADICAL HOMOPOLYMERISATIONS OF STYRENE AND BUTYL ACRYLATE* 63

4.1	<b>Introduction</b>	64
4.2	<b>Rate Coefficients for Propagation and Termination</b>	64
4.3	<b>Determination of <math>k_{act}</math></b>	68
4.3.1	<i>Background</i>	68
4.3.2	<i>Nitroxide exchange experiments</i>	69
4.3.3	<i>Experimental</i>	71
4.3.4	<i>Results and discussion</i>	73
4.4	<b>Determination of <math>k_{deact}</math></b>	78
4.4.1	<i>Sensitivity test</i>	78
4.4.1.1	<i>Influence of alkyl halide initiator activation process</i>	81
4.4.1.2	<i>Influence of <math>k_t^0</math></i>	83
4.4.2	<i>Experimental</i>	85
4.4.3	<i>Results and discussion</i>	87
4.4.3.1	<i>Homopolymerisations of S and BA</i>	87
4.4.3.2	<i>Kinetic experiments</i>	89
4.5	<b>Conclusions</b>	91
	<b>References</b>	92

## CHAPTER 5 *ATOM TRANSFER RADICAL COPOLYMERISATIONS OF STYRENE AND BUTYL ACRYLATE* 95

5.1	<b>Copolymerisation Models</b>	96
5.2	<b>Reactivity Ratios in the S/BA Copolymerisation</b>	99
5.2.1	<i>General</i>	99
5.2.2	<i>Determination of reactivity ratios in ATRP</i>	99
5.2.3	<i>Effect of the ATRP equilibria on the observed reactivity ratios</i>	102
5.2.4	<i>Summary</i>	106
5.2.5	<i>Experimental</i>	107
5.2.6	<i>Results and discussion</i>	108
5.2.6.1	<i>Low-conversion free-radical copolymerisations</i>	108
5.2.6.2	<i>Reactivity ratios in ATRP</i>	110

<b>5.3</b>	<b>Modelling of the ATRP Copolymerisations of S and BA</b>	112
5.3.1	<i>Evolution of <math>-\ln(1-\xi)</math></i>	112
5.3.2	<i>Experimental</i>	114
5.3.3	<i>Results and discussion</i>	115
5.3.3.1	<i>Assessment of living character</i>	115
5.3.3.2	<i>Evolution of <math>-\ln(1-\xi)</math> as a function of <math>f_S^0</math></i>	117
5.3.3.3	<i>Modelling of the ATRP copolymerisations of S and BA</i>	119
5.3.3.4	<i>Influence of reactivity ratios, <math>k_{act}</math> and <math>k_{deact}</math></i>	122
<b>5.4</b>	<b>Conclusions</b>	125
	<b>References</b>	125

## **CHAPTER 6    *SYNTHESIS AND CHARACTERISATION OF INTRAMOLECULARLY HETEROGENEOUS COPOLYMERS*** 127

<b>6.1</b>	<b>Introduction</b>	128
<b>6.2</b>	<b>Block Copolymerisation</b>	128
6.2.1	<i>Definition and application</i>	128
6.2.2	<i>Phase separation</i>	129
6.2.3	<i>Synthesis</i>	131
6.2.4	<i>Experimental</i>	132
6.2.5	<i>Results and discussion</i>	135
6.2.5.1	<i>Indications of block existence</i>	135
6.2.5.2	<i>Problems</i>	138
6.2.5.3	<i>Phase separation</i>	143
6.2.6	<i>Concluding remarks</i>	145
<b>6.3</b>	<b>Gradient Copolymerisation</b>	146
6.3.1	<i>Synthesis</i>	146
6.3.2	<i>Experimental</i>	149
6.3.3	<i>Results and discussion</i>	150
6.3.4	<i>Concluding remarks</i>	154
<b>6.4</b>	<b>Conclusions</b>	155
	<b>References</b>	155

<b>EPILOGUE</b>	157
<b>APPENDIX: SIMULATION PROGRAMS</b>	159
<b>GLOSSARY</b>	165
<b>SUMMARY</b>	171
<b>RÉSUMÉ</b>	175
<b>SAMENVATTING</b>	179
<b>DANKWOORD</b>	183
<b>CURRICULUM VITAE</b>	185

# *1*

## *Introduction*

**Synopsis:** A general introduction is presented to the reader. The concept of intramolecular composition drift is discussed and the investigated lines of research are validated. Hereafter, the outline of the thesis is given in detail.

## 1.1 HISTORY

Since the beginning of times, man has had a profound interest in his environment and has tried to manipulate it to control the course of events and herewith his own destiny. He has always investigated nature, attempted to understand it and, in dribs and drabs, he has contrived new tools to do so. He started investigating systematically the complex world surrounding him, hereby essentially marking the beginning of science. The Egyptians and Greek bestowed mankind with algebra and provided the knowledge to create majestic edifices of their civilization. Astronomy afforded the knowledge to sail the oceans of the world, while physics allowed man to construct machines that took over heavy tasks.

The definition of the elements by Lavoisier in 1789 opened the door to a completely new category of science: chemistry. It enabled one to understand how matter is built up of building blocks, and why materials behave as they do. Furthermore, fundamental knowledge provided the tool to actually produce new materials that could substitute traditional materials, such as wood, stone and iron. The invention of Bakelite marked the beginning of a new class in chemistry, called polymer chemistry. Although polymers had been synthesised and used in the 19<sup>th</sup> century as well, Bakelite was the first truly synthetic thermoset. However, it was not until the 1920s that a fundamental basis was provided to explain the extraordinary properties of polymers. Staudinger<sup>1</sup> proposed that polymeric materials consist of long-chain molecules that, in turn, are built up of low-molecular-weight building blocks called monomers.

Polymer chemistry has evolved very rapidly since then, and fundamental knowledge has ensured that it is no longer mainly empirical.

## 1.2 FREE-RADICAL POLYMERISATION

One of the most convenient ways to produce polymeric material on an industrial scale is through free-radical polymerisation<sup>2</sup>. It allows the synthesis of a wide gamut of homopolymers, while at the same time virtually any combination of monomers can be employed to produce copolymers. Moreover, the technique is relatively insensitive towards all kinds of impurities, notably water, and only requires the absence of oxygen. Today, the majority of all polymeric materials is produced using free-radical polymerisation techniques. Unfortunately, however, control of the incorporation of the monomer species into the polymeric chain is not possible in free-radical

polymerisation. A growing radical in a polymerisation reaction usually exists and grows only for 0.1-1 seconds before it undergoes bimolecular termination reactions. Control of molecular weight is only limitedly achievable with the variation of initiator concentration or with the use of transfer agents, while in general molecular-weight distributions are broad. Furthermore, in copolymerisation the growing radical adds monomer in a random way, governed by its relative reactivities towards both monomers. This lack of control confines the versatility of the free-radical process, because the microscopic polymer properties, such as chemical composition distribution, molecular-weight distribution and tacticity, are key parameters that determine the macroscopic behaviour of the polymer. The absence of control of the incorporation of monomer into the polymeric chain implies that many macroscopic properties cannot be influenced to a large extent.

Today, the 'simple' homo- and copolymers that are prepared using free-radical polymerisation no longer suffice in specific applications. The requirements that have to be met are simply too severe and create a demand for more advanced (co)polymers. Block copolymers with amphiphilic properties, star-shaped and hyperbranched polymers have become more and more important in recent years. To comply with these ever growing demands, polymer chemistry has resorted to the application of living polymerisation techniques, such as anionic polymerisation<sup>3</sup>, group-transfer polymerisation<sup>4</sup>, and several others. In these polymerisation methods, the polymeric chain grows during the whole reaction time, which enables one to produce copolymers with a special chemical composition distribution simply by adjusting the reaction conditions. In addition stereoregular control of the incorporation of the monomer unit in some cases is possible. Nevertheless, all these polymerisation techniques have major drawbacks. For instance, they require ultra-pure reagents and, more important, not all monomers available can be polymerised. This renders living polymerisation techniques less interesting from a commercial point of view.

### **1.3 CHEMICAL COMPOSITION DISTRIBUTION: INTRAMOLECULAR COMPOSITION DRIFT**

As mentioned before, the way both monomers are distributed in a copolymer determines in great part its physical properties. Two copolymers can have the same *overall* chemical composition, but totally different chemical composition *distributions*. The properties of these copolymers will also differ to a large extent.

Three examples of copolymers with the same overall chemical composition, but with different chemical composition distributions are schematically depicted in Figure 1.1.

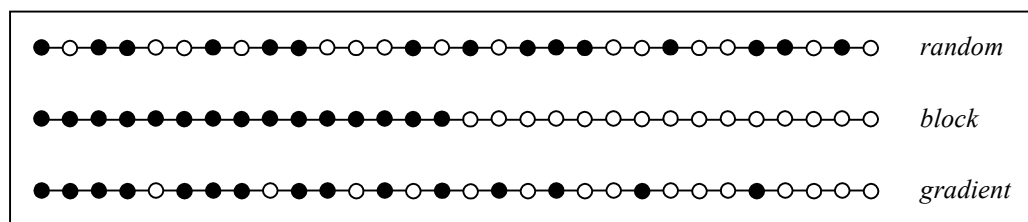


**Figure 1.1** Three different chemical composition distributions of copolymers with the same overall chemical composition.

In a random copolymer, both monomers are distributed randomly along the polymeric chain. During chain growth, the two monomers are incorporated according to their reactivities. The properties of the copolymer are very often an average of the properties of the homopolymers. The glass transition temperature, for instance, will be in between those of the homopolymers, the exact temperature being dependent on the overall chemical composition of the copolymer.

In a block copolymer, the monomer species are not distributed homogeneously, but they are present in separate blocks. In a diblock copolymer, for instance, the two monomers have been built into the polymeric chain consecutively during the growth of the chain. These block copolymers can exhibit amphiphilic properties, *i.e.* the characteristics of the corresponding homopolymers are retained in each block. Due to incompatibility, these block copolymers can exhibit micro-phase separation.

A copolymer that can be regarded as an intermediate form also exists, in which the chemical composition gradually changes along the polymeric chain, *i.e.* a gradient copolymer. During chain growth, the ratio of monomers incorporated changes. This phenomenon is called intramolecular composition drift, *i.e.* the process in which a shift occurs in the build-in ratio of the two monomers during the time of growth of the copolymer, leading to the formation of chemically heterogeneous polymeric chains. The macroscopic properties of gradient copolymers have not been investigated thoroughly. Although gradient copolymers will definitely possess characteristics different from random copolymers, it is plausible that they show somewhat less pronounced amphiphilic properties.

It is clear that in order to tune the chemical composition distribution, it is necessary to understand and control the process of intramolecular composition drift. When this is achieved, the knowledge may be used to produce copolymers with pre-defined intramolecular sequence distributions.

## 1.4 OBJECTIVE OF THIS THESIS

This thesis aims at investigating the possibility to synthesise copolymers with an intramolecularly heterogeneous chemical composition distribution using convenient polymerisation techniques. The radical copolymerisation of styrene and butyl acrylate has been chosen as a model system, since their homopolymers show markedly different chemical and physical properties. This, obviously, is of great importance when investigating the effect of chemical composition distribution on the final macroscopic properties of the copolymer.

Two lines of research have been investigated: *first*, free-radical copolymerisation systems that, according to literature might show a molecular-weight dependence of their chemical composition. In these systems, the polymeric chain is generally formed in less than one second, and it is believed that during this time interval the polymeric coil changes its direct environment by preferential absorption of one of the two monomer species. The preferential absorption enhances the incorporation of this monomer, which leads to a change in chemical composition along the polymer chain. This results in a snowball effect, since the effect of preferential sorption by the polymeric coil will become even more pronounced. The feasibility of utilising this spontaneously occurring intramolecular composition drift will be investigated.

A *second* line of interest concerns the application of living radical polymerisation (LRP) techniques as a tool to control the incorporation of monomer into the growing polymeric chain. In LRP irreversible chain-stopping events are minimised relative to propagation by a reversible activation/deactivation process. The radicals are reversibly transformed into dormant species and, consequently, the polymeric chains grow during the whole reaction time. Additionally, they are allowed to add only one or a few monomer units per activation/deactivation cycle. These characteristics should in principle permit the control of the chemical composition distribution, since when knowledge on the reaction kinetics is available, the monomer composition can be altered at each moment during the polymerisation to control the incorporation of monomer species. Unfortunately, until now the stereoregular incorporation of monomer units into the polymeric chain has not been possible. However, since termination reactions are relatively less important and only few monomer units are built into the polymeric chain per activation step, control of molecular-weight and chemical composition distribution is possible.

This second line of research should lead to improved understanding of living radical polymerisation. On the basis of this better basic insight it will then be attempted to synthesise copolymers with well-defined intramolecular composition distributions.



## 1.5 OUTLINE OF THIS THESIS

In chapter 2, the first line of research will be discussed. After a short introduction on copolymerisation kinetics, two theories explaining anomalous behaviour in free-radical copolymerisation will be presented to the reader. The feasibility of using these models to describe and control the process of intramolecular composition drift will be tested. Thereto, the molecular-weight dependence of copolymer composition is investigated by assessing reactivity ratios of styrene/butyl acrylate copolymerisations with and without the use of a chain-transfer agent.

In chapter 3, a general overview on living radical polymerisation techniques is presented to the reader. The basic concepts of Atom Transfer Radical Polymerisation (ATRP), as well as its kinetics are discussed. The differences and similarities between classical free-radical polymerisation and ATRP are highlighted. Hereafter, the role of various compounds in ATRP is described.

Since the mechanisms that govern ATRP are currently still a matter of discussion, the homopolymerisations of styrene and butyl acrylate are dealt with first in chapter 4. This chapter should therefore be considered as a springboard towards the copolymerisation of styrene and butyl acrylate. The attention is focused on the determination of activation and deactivation rate coefficients. A novel method involving exchange reactions with subsequent analysis by high-performance liquid chromatography to determine the activation rate coefficients is provided. Evaluation of the results of kinetic experiments to obtain the deactivation rate coefficients then conclude chapter 4.

Chapter 5 will then turn towards the copolymerisation of styrene and butyl acrylate by ATRP. The reactivity ratios for this system will be evaluated and compared with the reactivity ratios obtained for the corresponding free-radical copolymerisation to investigate the impact of the ATRP equilibria on the kinetic behaviour of the system. It is attempted to harmonise the rate of polymerisation with the kinetic insights in the homopolymerisations and to explain and model any possible discrepancies.

In Chapter 6, the reactivity ratios, together with the kinetic information on the rate of polymerisation are exploited to produce copolymers of styrene and butyl acrylate with pre-defined chemical composition distributions. Block copolymers are synthesised and problems occurring during the synthesis are discussed. A three-step strategy for the synthesis of gradient copolymers is proposed, using the kinetic parameters obtained in chapter 4 and 5. The block and gradient copolymers are subjected to fundamental chemical analyses by size exclusion chromatography and nuclear magnetic resonance spectroscopy. A possible relation between the chemical

composition distribution and the macroscopic behaviour of the copolymer is investigated by means of differential scanning calorimetry.

Finally, the results presented throughout the thesis are brought into perspective in the epilogue. Beside the goals that have been achieved, expected future developments are discussed in this chapter as well.

## REFERENCES

- <sup>1</sup> Staudinger, H., *Chem. Ber.* (1920), 53, 1073
- <sup>2</sup> Moad, G.; Solomon, D.H. In *The Chemistry of Free Radical Polymerization*, 1<sup>st</sup> ed.; Elsevier Science Ltd.: Oxford, 1995
- <sup>3</sup> Iván, B.; Kennedy, J.P. *Macromolecules* 1990, 23, 2880
- <sup>4</sup> Webster, O.W.; Hertler, W.R.; Sogah, D.Y.; Farnham, W.B.; Rajanbabu, T.V. *J. Am. Chem. Soc.* 1983, 105, 5706



# 2

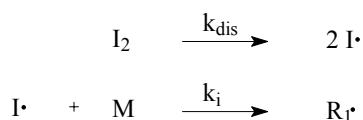
## *Free-Radical Copolymerisation of Styrene and Butyl Acrylate*

**Synopsis:** In this chapter, the feasibility of introducing intramolecular composition drift via conventional free-radical copolymerisation is investigated. Two theoretical models to describe this compositional heterogeneity are discussed, the first involving preferential absorption of one of the two monomers by the polymeric coil and the second considering composition-dependent partitioning. The system styrene/butyl acrylate is chosen, since it is previously claimed that the chemical composition of the corresponding copolymers is dependent on molecular weight. Free-radical copolymerisation of styrene and butyl acrylate is performed to test the chain-length dependence of the chemical composition of the copolymers. Thereto, reactivity ratios using copolymers with different chain lengths are assessed. At 90°C, no molecular-weight dependence of the reactivity ratios is observed, while the dependence at 50°C is insignificant and can probably be ascribed to inaccuracies in the integration process of the butyl acrylate region in the <sup>1</sup>H NMR spectra. On the basis of these findings, it is judged that conventional free-radical copolymerisation cannot be used to create pre-desired compositional heterogeneity in the polymeric chain.

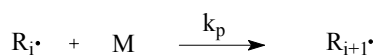
## 2.1 INTRODUCTION

Free-radical polymerisation comprises essentially three distinguishable features, *viz.* initiation, propagation and termination<sup>1,2</sup>. The general scheme for free-radical homopolymerisation is depicted in scheme 2.1.

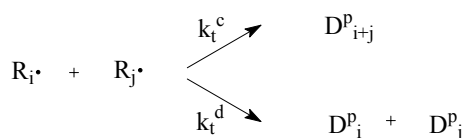
*Initiation:*



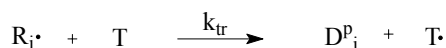
*Propagation:*



*Bimolecular termination:*



*Transfer:*



**Scheme 2.1 Free-radical homopolymerisation scheme.**

Generally, in the initiation step a primary radical ( $I\cdot$ ) is formed by dissociation of an initiator ( $I_2$ ), usually a peroxide or an azo-compound. This primary radical can react with monomer ( $M$ ) to yield a carbon-centred radical ( $R_1\cdot$ ). The carbon-centred radical can now add monomer until it undergoes bimolecular termination, which can occur either by combination or by disproportionation. It should be noted that growing polymeric radicals can also be terminated by transfer reactions with a transfer agent, solvent or even a polymeric chain ( $T$ ). In this case, the radical will be transferred from the growing polymeric radical to the transfer agent, which, in turn, can re-initiate polymerisation.

Two features characterise the conventional free-radical polymerisation system. First, chains grow very fast and the average lifetime of the growing radical chains is in the order of only a second or even less. Second, the addition of monomer to the polymeric radical most often occurs without any selectivity, *i.e.* stereoregular incorporation of

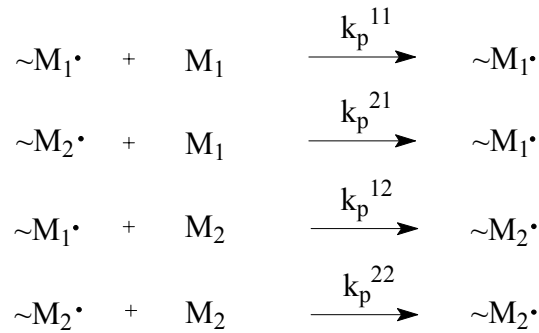
monomer is only claimed in special cases<sup>3</sup>. These characteristics impede control of molecular-weight distribution, tacticity and, in the case of copolymers, intramolecular chemical composition distribution.

It is evident that the characteristics of the polymeric chain are determined by all fundamental reaction steps in the polymerisation process, see Scheme 2.1. However, since initiation, transfer and termination events only account for a very small part of the polymeric chain, the kinetic behaviour of a free-radical polymerisation system can be described by considering the propagation steps only. After all, the propagation steps occur much more frequently and therefore the growth of a polymeric chain is mainly consisted of propagation. For this reason, the kinetics of free-radical polymerisation will be focused on the propagation steps in the following discussion.

## 2.2 COPOLYMERISATION

The situation becomes slightly more complicated when two different monomers are copolymerised. In this case, two monomers participate in the propagation steps and, as a result, polymeric radicals with different chain ends exist. In general, these radicals will not exhibit the same affinities towards both monomer species. In addition, interactions between monomer and solvent, monomer and copolymer, monomer and growing polymeric radicals and even between both monomers may exist. These interactions affect the intrinsic reactivities of the radicals and, therefore, have a strong influence on the composition of the resulting copolymer and its macroscopic properties.

In order to describe the copolymerisation and to explain copolymer compositions, sequence distributions and average propagation rate coefficients, several models have been proposed. One should bear in mind that these models are mere approximations of the complex process of copolymerisation. The simplest one is the terminal unit model<sup>4,5</sup> that disregards any of the physical interactions stated above and, beside the two monomer species, only takes into account two growing radicals with different monomer units at their chain ends. The terminal unit model (TUM) thus considers the following four propagation reactions:



**Scheme 2.2 Propagation reactions in a copolymerisation according to the terminal model.**

The superscripts in the propagation rate coefficients in Scheme 2.2 denote the terminal, *i.e.* radical bearing, unit in the growing polymeric radical and the monomer unit to be added, respectively. As can be seen in Scheme 2.2, two homopropagation and two crosspropagation reactions exist. The ratio of the instantaneously incorporated monomers can be expressed as the ratio of the appropriate differential equations following from mass balances of both monomers in a constant density batch reactor:

$$\frac{d[M_1]}{d[M_2]} = \frac{k_p^{11}[\sim M_1\cdot][M_1] + k_p^{21}[\sim M_2\cdot][M_1]}{k_p^{12}[\sim M_1\cdot][M_2] + k_p^{22}[\sim M_2\cdot][M_2]} \quad (2.1)$$

In Eq. (2.1) the concentrations of both radicals are unknown and cannot be determined experimentally. Fortunately, this equation can be simplified by assuming a steady state in the radical concentrations, *i.e.* the concentrations of both  $\sim M_1\cdot$  and  $\sim M_2\cdot$  are supposed to be constant during the growth of a polymeric chain. Note that this does not necessarily imply that the radical concentrations may not change during the reaction. A mass balance for  $\sim M_1\cdot$  or  $\sim M_2\cdot$  then results in:

$$k_p^{12}[\sim M_1\cdot][M_2] = k_p^{21}[\sim M_2\cdot][M_1] \quad (2.2)$$

The cross propagation rate coefficients in Eq. (2.1),  $k_p^{ij}$ , can be expressed in terms of reactivity ratios:

$$r_1 = \frac{k_p^{11}}{k_p^{12}} \quad \text{and} \quad r_2 = \frac{k_p^{22}}{k_p^{21}}$$

These reactivity ratios are defined as the ratio of the homopropagation and crosspropagation rate coefficients and denote the relative tendency of a radical to homopropagate. When the steady-state assumption and the reactivity ratios are used to eliminate the radical concentrations and the crosspropagation rate coefficients, the differential copolymer composition equation, or Mayo-Lewis equation can be derived<sup>4,5</sup>:

$$F_1 = \frac{r_1 f_1^2 + f_1(1-f_1)}{r_1 f_1^2 + 2f_1(1-f_1) + r_2(1-f_1)^2} \quad (2.3)$$

Eq. (2.3) reflects the relation between the instantaneous mole fraction of monomer 1 in the monomer mixture at the locus of polymerisation ( $f_1$ ) and the mole fraction of monomer 1 in the instantaneously formed copolymer ( $F_1$ ). The reactivity ratios can be determined with this relation by performing copolymerisations and subsequently analysing the copolymer composition. Evidently, the monomer conversion,  $\xi$ , has to be kept low in these cases, since the monomer composition should not change. By fitting the  $F_1$  vs.  $f_1$  data to Eq. (2.3), a set of reactivity ratios is obtained. Once the reactivity ratios for a specific copolymerisation system are known, the resulting instantaneous copolymer composition can be calculated at any given monomer composition at the locus of polymerisation. Reactivity ratios have been determined for a number of systems<sup>6</sup> and generally the relationship between copolymer composition and monomer composition is well described.

In a similar way, expressions can be derived for the average propagation rate coefficient and for the sequence distributions vs. monomer composition at the locus of polymerisation. In general however, these expressions derived from the terminal model give only a qualitative description and do not quantitatively describe the experimentally observed data very well. In these cases more complicated models, such as the penultimate unit model<sup>7,8</sup> or monomer complex participation model<sup>9</sup> should be considered to derive the corresponding expressions. Obviously, a better description of the system is gained, but additional parameters need to be introduced. The penultimate unit model takes into account influences of the penultimate unit in the polymeric radical on its reactivity. As a consequence, eight different propagation steps are now involved in the copolymerisation instead of only four. In the



penultimate unit model, therefore, six reactivity ratios are introduced. The four monomer reactivity ratios are classical and two radical reactivity ratios were introduced by Fukuda *et al.*<sup>10</sup>. The complex participation model assumes complex formation between the two monomer species. The radicals exhibit a different reactivity towards this complex species compared to the free monomer and, as a consequence, this complex behaves like a third species that can add to the polymeric radical.

Copolymerisation models have been extensively discussed in many literature reviews<sup>11,12,13</sup>. In this chapter reactivity ratios will be investigated by assessing copolymer composition data and for this purpose the terminal model suffices.

## 2.3 ANOMALIES IN COPOLYMERISATION

All copolymerisation models mentioned before are based on intrinsic reactivities of the species involved. Any discrepancy between experimental data and the TUM is explained by oversimplification in the TUM regarding the intrinsic reactivities of the reacting species involved. In some cases, the reactivity of the growing polymeric radical is refined, *e.g.* in the penultimate unit model, while in other cases the reactivity of the monomer species is believed to change due to the formation of complexed species, *e.g.* the complex participation model.

Copolymer composition, sequence distributions and propagation rate coefficients, however, are not only dependent on the reactivities of the participating reacting species, but also on their relative concentrations at the locus of polymerisation. After all, in the mathematical expressions for these parameters the monomer composition at the locus of polymerisation is important. When the intrinsic reactivities of the radicals towards the monomer species are correct, but for some reason the monomer composition at the locus of polymerisation differs from the bulk composition, this will have an effect on the experimentally observed reactivity ratios. In the following sections, two models that explain changes in observed reactivity ratios by considering the monomer composition at the locus of polymerisation will be presented.

### 2.3.1 Bootstrap model

For a number of systems, a solvent dependence of the reactivity ratios is reported<sup>14,15</sup>. The free-radical copolymerisations involving  $\alpha$ -unsaturated acids and amides show that the reactivity ratios for these monomers are higher in non-polar solvents compared to those in polar solvents. Harwood *et al.*<sup>14</sup> suggested that these variations

are caused by reaction mixture heterogeneity rather than by a change in intrinsic reactivities of growing radicals. Depending on the way in which the growing polymeric radical is solvated, the monomer composition in its vicinity may differ substantially from the overall one. This difference leads to copolymers having different chemical composition and, according to Eq. (2.1), different reactivity ratios are found. This is very clearly illustrated by the copolymerisation of styrene (S) and methacrylic acid (MAA) in 1,4-dioxane and in tetrachloromethane ( $\text{CCl}_4$ )<sup>14</sup>, see Figure 2.1. When performing low-conversion copolymerisations to determine reactivity ratios, Harwood *et al.* found  $r_S=0.59$  and  $r_{MAA}=0.66$  for the copolymerisations in 1,4-dioxane and  $r_S=0.08$  and  $r_{MAA}=0.75$  for the copolymerisations in  $\text{CCl}_4$ . This is

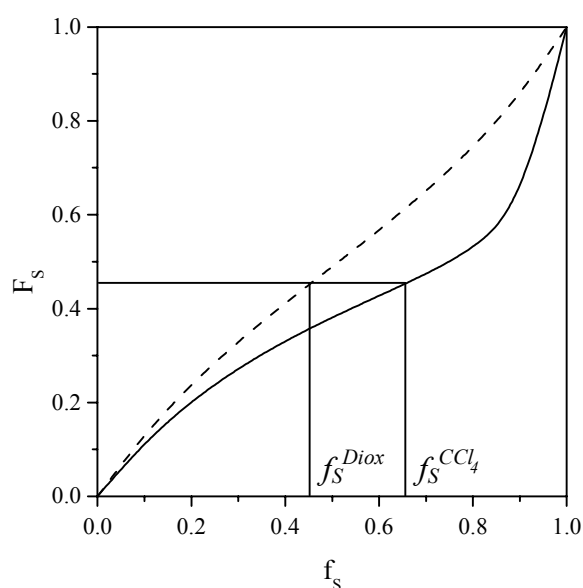


**Figure 2.1** Instantaneous copolymer composition as a function of overall monomer composition for S/MAA copolymerisations in  $\text{CCl}_4$  (—) and dioxane (---).

reflected in Figure 2.1, where the difference in  $F_S$  vs.  $f_S$  between both solvents is evident. However, Harwood and co-workers stated that this discrepancy does not find its origin in a difference in intrinsic reactivities of the propagating radicals. The evidence for the fact that this discrepancy is not due to differences in intrinsic reactivities of growing radicals is found in the analysis of the microstructures, *i.e.* sequence distributions, of two copolymers with the same overall chemical composition ( $F_S \approx 0.46$ ), but that were prepared in 1,4-dioxane and  $\text{CCl}_4$ . It should be emphasised that these copolymers

were prepared at different initial monomer compositions, *viz.*  $f_S^{Diox}$  and  $f_S^{CCl_4}$ . The microstructures of the two copolymers proved to be identical, hereby demonstrating that the intrinsic reactivities of the growing polymeric radicals towards the monomer species are identical in both solvents. The monomer compositions at the locus of polymerisation must have been identical for the copolymers prepared in 1,4-dioxane and  $\text{CCl}_4$ , respectively. On the grounds of these findings, Harwood and co-workers suggested that the monomer composition in the vicinity of the polymeric radical is dependent on the structure of the radical itself. This idea seems to be somewhat surprising, but is actually quite plausible, given the fact that time constants for

polymerisation are much smaller than time constants for diffusion of monomer. This phenomenon has been denominated as the ‘bootstrap effect’<sup>15</sup>.

In an attempt to quantify this bootstrap effect and relate it to experimentally obtained reactivity ratios, a distribution coefficient,  $K^A$ , can be defined as follows<sup>16</sup>:

$$K^A = \frac{[M_1^A]/[M_2^A]}{[M_1^0]/[M_2^0]} \quad (2.4)$$

In Eq. (2.4),  $[M_1^A]/[M_2^A]$  denotes the ratio of both monomer concentrations at the locus of polymerisation in solvent A, while  $[M_1^0]/[M_2^0]$  represents the overall ratio in this solvent. The apparent reactivity ratios for the terminal model can now be expressed in terms of this distribution coefficient:

$$\begin{aligned} r_1^A &= r_1^0 \cdot K^A \\ r_2^A &= r_2^0 / K^A \end{aligned} \quad (2.5)$$

Eqs. (2.5) express the apparent reactivity ratios in solvent A as a function of reference reactivity ratios and the distribution coefficient in solvent A. In order to quantify the partition coefficient, the reactivity ratios obtained from bulk copolymerisations are taken as reference values. Note that in bulk copolymerisations the monomer composition at the locus of polymerisation can differ as well from the overall monomer composition.

The bootstrap model seems to be applicable to a number of copolymerisation systems, among which styrene/maleic anhydride<sup>16,17</sup> and styrene/acrylonitrile<sup>18</sup>. Since it is based on the idea that the growing polymeric coil is in equilibrium with its environment it is therefore logical that the distribution coefficient,  $K^A$ , is dependent on the composition of the polymeric radical, as was also proposed in the initial paper<sup>15</sup>. This has also been recognised by Klumperman and Kraeger<sup>18</sup>, who suggested a linear dependence of  $K$  on copolymer composition:

$$K^A = \alpha \cdot F_1 + \beta \quad (2.6)$$

Should the distribution coefficient be dependent on the composition of the growing radical, and  $K^A > 1$  (this is a matter of definition) and  $dK^A/dF_1 > 0$  then this would lead to a compositional heterogeneity within a single chain. This can be seen as follows.

When  $K^A > 1$ , the monomer ratio in the vicinity of the growing radical will be richer in  $M_1$  compared to the overall ratio. Since  $K^A$  increases with an increasing amount of  $M_1$  in the copolymer, see Eq. (2.6), the monomer ratio in the copolymer coil will even further increase. As the polymer grows, it becomes richer and richer in  $M_1$  and a compositional gradient along the copolymer chain will be the result. On the other hand, when  $K^A > 1$  and  $dK^A/dF_1 < 0$ , the snowball effect does not take place. The presence of  $M_1$  in the copolymer ensures a lower distribution coefficient, which results in a lower fraction of  $M_1$  in the monomer composition in the direct vicinity of the growing radical. The fraction of  $M_1$  in the copolymer will decrease resulting in an increase in  $K^A$ . In this case, the dependence of the distribution coefficient on copolymer composition does not lead to chemically heterogeneous copolymers. Clearly, when  $K^A$  is not dependent of copolymer composition, intramolecular composition drift will not occur either.

### 2.3.2 Preferential absorption model

Related to the bootstrap effect seems to be the dependence of copolymer composition on molecular weight for copolymerisation systems like styrene/methacrylic acid (S/MAA) and styrene/acrylamide (S/AAM)<sup>19,20</sup>, but also for systems containing comonomer pairs with less pronounced functionalities such as styrene/butyl acrylate (S/BA)<sup>21</sup>. For the system S/MAA, for instance, Semchikov *et al.*<sup>22</sup> investigated the molecular-weight dependence by performing copolymerisations using different initiators and chain-transfer agents. Semchikov and co-workers performed low-conversion copolymerisation using various concentrations of 2,2-azobis(isobutyronitrile) (AIBN), or benzoyl peroxide (BP) or tetrabromomethane (CBr<sub>4</sub>) to obtain copolymers with varying molecular weights. These authors compared the composition of these copolymers with those of fractionated copolymers of S and MAA. These copolymers had been prepared under the same conditions, but at low initiator concentration and without the use of a chain-transfer agent. The copolymers of S and MAA were precipitated from a 1% acetone-methanol solution by a mixture of diethyl ether and petroleum ether. Semchikov *et al.*<sup>22</sup> reported a marked dependence of the copolymer composition of S/MAA copolymers on the initiator and chain-transfer agent concentration. When the copolymer composition was plotted versus chain length, a similar behaviour was observed for all copolymers, see Figure 2.2.

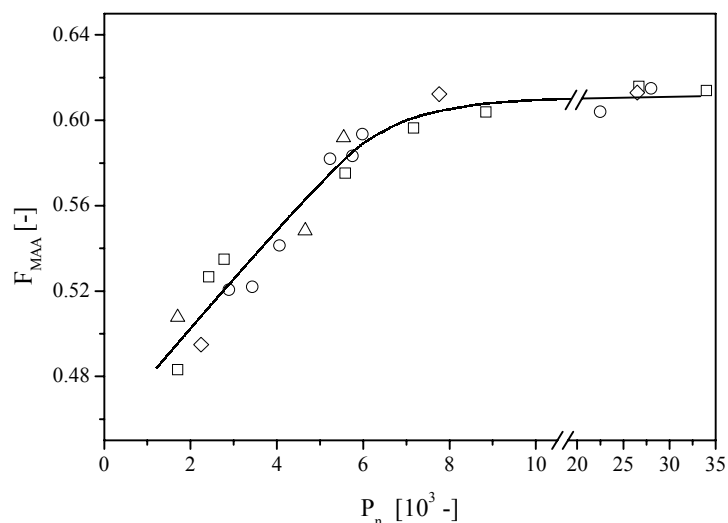


**Figure 2.2** Copolymer composition as a function of chain length for S/MAA copolymers prepared with different initiators (○: AIBN; ◇: BP) or chain-transfer agent (△: CBr<sub>4</sub>) compared to fractionated copolymers (□).

From Figure 2.2, one can see that regardless of the initiator or chain-transfer agent employed, copolymers with the same chain length have the same overall chemical composition. Moreover, the fractionated copolymers show identical behaviour. The dependence of copolymer composition on molecular weight as depicted in Figure 2.2 suggests one single explanation. The underlying reason for this behaviour should be found in the copolymer itself, since all copolymers show the same dependence. Bearing in mind the bootstrap effect, the results displayed in Figure 2.2 can be fully explained by the fact that a growing polymeric radical is able to control its own environment, thus creating a different local monomer composition within the polymeric coil compared to the overall monomer composition. Semchikov *et al.* explained this molecular-weight dependence by preferential absorption of one of the two monomers by the polymeric coil<sup>21,22</sup>. To describe this favoured absorption, Semchikov introduced a so-called preferential absorption coefficient ( $\lambda$ ), which expresses to what extent the polymeric coil absorbs the monomer<sup>23</sup>. This preferential absorption coefficient is related to the refractive index increment and can experimentally be obtained using light-scattering techniques. Semchikov and co-workers investigated the chain-length dependence of this preferential absorption coefficient and found that for some systems it increases with increasing chain length. For copolymers prepared via bulk copolymerisation of S/MAA, the results are collected in Figure 2.3.

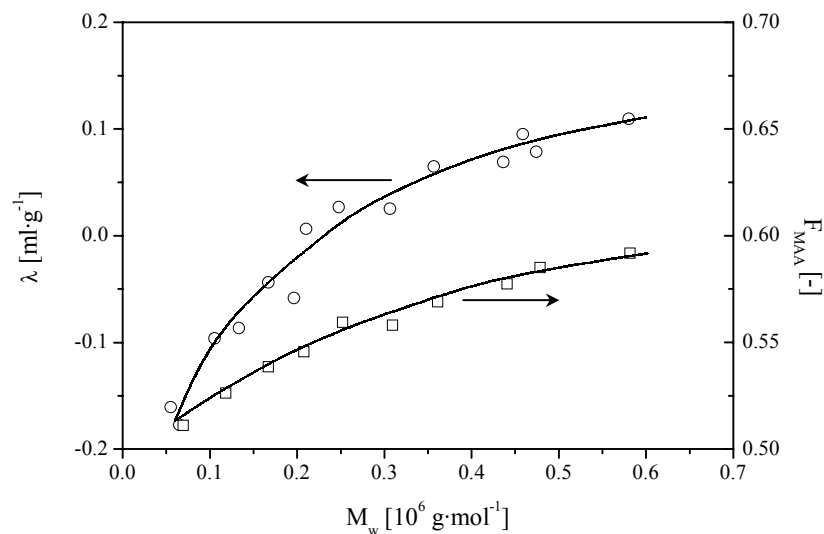


**Figure 2.3** Preferential absorption coefficient,  $\lambda$  ( $\circ$ ), and fraction of methacrylic acid in the copolymer,  $F_{MAA}$  ( $\square$ ), as a function of molecular weight ( $M_w$ ) in a bulk copolymerisation of styrene and methacrylic acid.

As can be seen from Figure 2.3, the preferential absorption coefficient increases with increasing chain length. The monomer mixture in the vicinity of the polymeric radical, therefore, becomes richer in methacrylic acid during growth. Intramolecular composition drift occurs and the composition gradually changes towards MAA rich. Although the evidence is seemingly very convincing, several critical notes should be made concerning the experimental procedures that Semchikov *et al.* used in their investigations. An important point concerns the fractionation procedure. Copolymers of S and MAA, for instance, were precipitated from a 1% acetone-methanol solution by a mixture of diethyl ether and petroleum ether to separate the copolymers according to chemical composition. Two major problems arise when a fractionation procedure is used. In the first place, it is well possible that during the fractionation process, separation not only occurs on the basis of chemical composition, but also on molecular weight. In the subsequent analysis, therefore, it is unclear whether these fractions are narrow as far as molecular weight is concerned. Second, the probability that fractions with a certain chemical composition are lost, simply because they do not precipitate, is considerable. The conclusions that are drawn from the copolymer composition data as a function of molecular weight therefore have to be taken with care.

Three different cases for  $\lambda$  may exist in copolymerisations:

1. *no preferential absorption occurs ( $\lambda = 0$ ).*
2. *preferential absorption occurs, but  $\lambda$  does not depend on molecular weight ( $\lambda = C$ ).*
3. *preferential absorption occurs and  $\lambda$  is dependent on molecular weight ( $\lambda = f(MW)$ ).*

In case 1, it is obvious that undisturbed copolymerisation takes place and that the intramolecular copolymer composition distribution is homogeneous in all chains. The monomer composition in the vicinity of the growing polymeric radical is the same as the overall monomer composition. This case can be related to the bootstrap model where the distribution coefficient equals 1. Case 2 is in complete analogy with the bootstrap model where  $K^A \neq 1$ . In this case the chemical composition distribution is homogeneous, but the measured reactivity ratios are actually apparent reactivity ratios. Analogous to the bootstrap model, the preferential absorption coefficient in this case is constant and not dependent on molecular weight. Case 3 is quite a complex one; according to the preferential absorption theory, the preferential absorption coefficient,  $\lambda$ , is dependent on the molecular weight of the growing polymeric radical.

### 2.3.3 Summary

The fundamental difference between the bootstrap theory and the preferential absorption theory lies in the different dependences of their essential parameters ( $K^A$  on copolymer composition and  $\lambda$  on molecular weight, respectively). It is clear that in order to exploit this spontaneously occurring intramolecular composition drift, a thorough understanding of these parameters is of paramount importance. In this chapter, the copolymerisation of styrene (S) and butyl acrylate (BA) will be investigated. According to Semchikov *et al.*<sup>21</sup> this system, although the monomers do not possess any pronounced polar characteristics, exhibits preferential absorption. Since their report lacks any details, the dependence of copolymer composition on molecular weight will be checked by performing low-conversion copolymerisations with and without the use of a chain-transfer agent. Since we want to exploit any unusual free-radical copolymerisation kinetics to produce chemically heterogeneous copolymers, the reactivity ratios will be assessed to investigate whether this approach is viable for the system S/BA.

## 2.4 EXPERIMENTAL

### *Materials:*

Styrene (>99% stabilised by 4-*tert*-butylcatechol, Merck) and butyl acrylate (>99% stabilised by monomethyl ether hydroquinone, Aldrich) were distilled under reduced pressure and stored at -18°C. Prior to use, the monomers were subsequently passed through a column to remove residual inhibitor. An appropriate inhibitor remover (Aldrich) was used for each monomer. 2,2'-Azobis(isobutyronitrile) (AIBN, Fluka) was recrystallised once from methanol. 2-Mercapto ethanol (>99%, Merck) was used as chain-transfer agent and was used as received. All other chemicals were not purified prior to use.

### *Copolymerisations:*

Styrene/butyl acrylate copolymers were prepared at 50°C and 90°C in bulk. Optimal monomer compositions in the recipe were calculated applying the Tidwell-Mortimer criterion<sup>24</sup> and using literature values of the reactivity ratios<sup>25</sup>:  $r_S=0.95$  and  $r_B=0.18$ . Appropriate amounts of styrene and butyl acrylate, together with AIBN ( $5 \cdot 10^{-3}$  M) were mixed in a 100 mL round-bottom flask equipped with a magnetic stirrer and reflux condenser. The reaction mixture was then subdued to three freeze-pump-thaw cycles to remove residual oxygen. At both optimal monomer compositions, five copolymerisations were carried out. Conversion was determined gravimetrically and was kept below 1% in most cases. Hereafter, the reaction mixtures were freeze-dried and subsequently dried in a vacuum oven at room temperature for 1 day.

### *Analysis:*

Copolymer composition was determined by <sup>1</sup>H NMR on a 400 MHz Bruker at 50°C in CDCl<sub>3</sub>. Peak areas of the proton resonances at  $\delta=7$  ppm (phenyl) and  $\delta=3.8$  ppm (methoxyl) were taken to calculate copolymer composition. Copolymer composition versus monomer composition data were fitted to Eq. (2.2) using non-linear least squares fitting which yields the most accurate values of both reactivity ratios<sup>26,27</sup>. No alternative method was tested. For size exclusion chromatography (SEC), the copolymers were dissolved in stabilised tetrahydrofuran at 1 mg·mL<sup>-1</sup> and filtrated using 0.2  $\mu$ m filters. Molecular weights were determined by SEC with a Waters Model 510 pump and Waters 712 WISP using 4 PL-gel mix C columns (300mm×7.5mm, Polymer Laboratories) at 40°C with tetrahydrofuran as eluent at a flow rate of 1 mL·min<sup>-1</sup>. A Waters 410 differential refractive index detector was used. Data acquisition was performed with Millennium-32 3.05 software. Polystyrene



standards with narrow molecular-weight distributions (Polymer Laboratories) were used for calibration. The molecular weights of the copolymers were calculated relative to polystyrene.

## 2.5 RESULTS AND DISCUSSION

Copolymerisations of S and BA were carried out at 50°C and 90°C in the presence and absence of chain-transfer agent (CTA). The Tidwell-Mortimer criterion<sup>24</sup> was used to obtain the best estimates for the reactivity ratios and five experiments were performed at each monomer composition. The ‘average’ experimental conditions, *i.e.* experimental conditions for the sets of five experiments, together with the average molecular weights and chemical compositions for the sets of five copolymerisations at each initial monomer composition are given in Table 2.1. For the copolymerisations at 50°C in the presence of chain-transfer agent, *i.e.* A1802 1-5 and A1902 1-5, the conversion was kept low as well, but was not determined accurately. It is possible, however, that conversion in these two cases is somewhat higher compared to the other experiments. The polymerisation reactions were quenched as soon as polymer was visually detected by precipitation in methanol. At lower molecular weights, therefore, it is likely that precipitation only occurs at higher conversion, since solubility increases with decreasing molecular weight.

**Table 2.1 Average experimental conditions for the copolymerisations of S and BA.**

<i>Experiment</i>	<i>T</i> [°C]	[CTA] [mol·L <sup>-1</sup> ]	<i>f<sub>S</sub></i> [-]	<i>F<sub>S</sub></i> [-]	<i>M<sub>n</sub></i> [g·mol <sup>-1</sup> ]	$\xi$ [-]
A2101 1-5	50	0	0.676	0.72	~10 <sup>6</sup>	< 0.01
A2401 1-6	50	0	0.085	0.28	~10 <sup>6</sup>	< 0.01
A1802 1-5	50	0.02	0.677	0.69	~7·10 <sup>3</sup>	n.d.
A1902 1-5	50	0.02	0.084	0.27	~2·10 <sup>4</sup>	n.d.
A0807 1-5	90	0	0.676	0.73	~5·10 <sup>5</sup>	< 0.01
A1607 1-5	90	0	0.084	0.26	~5·10 <sup>5</sup>	< 0.04
A2107 1-5	90	0.02	0.676	0.72	~5·10 <sup>4</sup>	< 0.01
A2207 1-5	90	0.02	0.083	0.25	~1·10 <sup>5</sup>	< 0.01

Since the chemical composition of S/BA copolymers can be described by the terminal unit model<sup>25,28</sup>, it is possible to determine the reactivity ratios using the monomer composition and the resulting copolymer composition. The values of  $F_S$  as a function of  $f_S$  are therefore fitted to Eq. (2.2) using non-linear least squares statistics.

The resulting reactivity ratios with their 95% joint-confidence intervals for the copolymerisations of S and BA at 50°C and 90°C are depicted in Figures 2.4a and b, respectively.

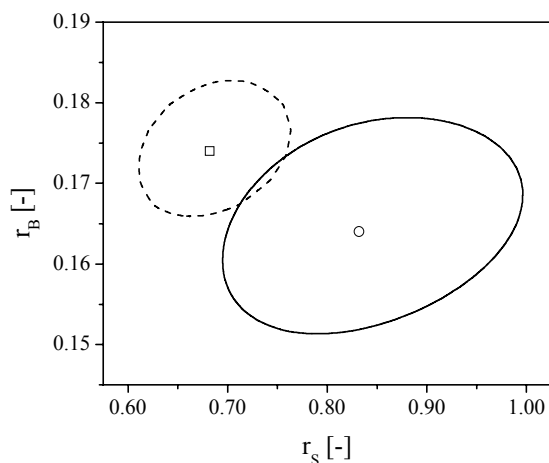


**Figure 2.4a** 95% joint confidence intervals for S/BA copolymerisations at 50°C. No CTA added (—); [CTA]=0.02 mol·L<sup>-1</sup> (---).

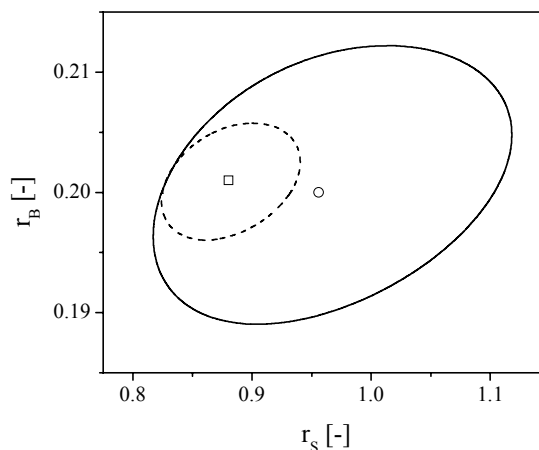


**Figure 2.4b** 95% joint confidence intervals for S/BA copolymerisations at 90°C. No CTA added (—); [CTA]=0.02 mol·L<sup>-1</sup> (---).

The sets of reactivity ratios for the copolymerisations of S and BA at 50°C and 90°C in the absence and presence of chain-transfer agent are collected in Table 2.2.

**Table 2.2** Reactivity ratios for copolymerisations of S and BA at 50°C and 90°C in the presence and absence of chain-transfer agent.

[CTA] [mol·L <sup>-1</sup> ]	T [°C]	r <sub>S</sub> [-]	r <sub>B</sub> [-]
0	50	0.83	0.16
0.02	50	0.69	0.17
0	90	0.96	0.20
0.02	90	0.88	0.20

When looking at Figures 2.4a and b, it is clear that the reactivity ratios are in very good agreement with literature values<sup>28</sup>, *i.e.*  $r_S=0.95$  and  $r_B=0.18$ . A second point that immediately catches the eye is the difference in size of the joint-confidence intervals of the reactivity ratios for the copolymerisations with and without chain-transfer agent. The 95% joint-confidence intervals for the copolymerisations with chain-transfer agent are both smaller than the ones for the copolymerisations that were conducted in the absence of chain-transfer agent. The origin of this seems to lie in the

amount of scatter on the  $F_S$  vs.  $f_S$  data in the high  $F_S$  regions. This scatter is more pronounced in the copolymerisations without chain-transfer agent. The reason for this can be found in the integration of the  $^1\text{H}$  NMR spectra for these copolymerisations at high  $F_S$ , see Figure 2.5.

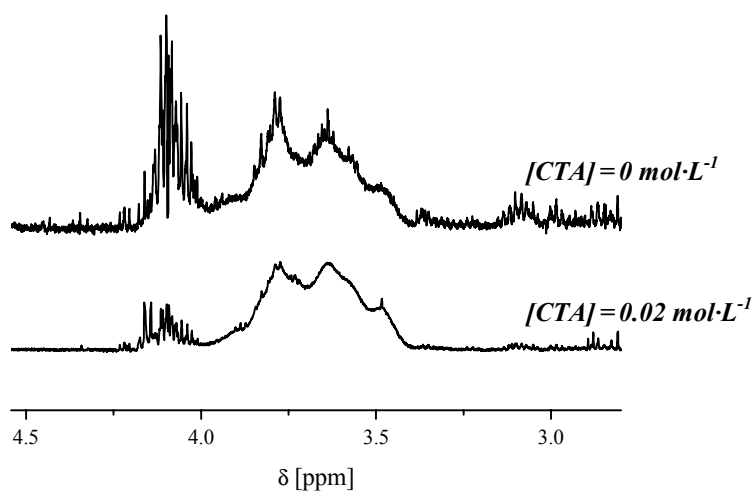


*Figure 2.5 BA region in the  $^1\text{H}$  NMR spectra of copolymers prepared in the absence and in the presence of chain-transfer agent.*

It seems that an interfering peak ( $\delta=4.1\text{-}4.2$ ) next to the BA peak ( $\delta=3.4\text{-}4.0$ ) in the  $^1\text{H}$  NMR spectrum of the copolymers prepared in the absence of chain-transfer agent complicates the integration of the BA peak. It is unclear what species is responsible for the peak in the  $^1\text{H}$  NMR spectrum. This interfering peak is always present, but at high molecular weights it partially overlaps with the BA peak. In the integration of the BA region the interfering peak has not been taken into account. As a result, the integral values for the BA copolymerisations without chain-transfer agent contain a considerable error, leading to a larger 95% joint-confidence interval.

A third interesting point concerns the differences in the positions of the 95% joint-confidence intervals of copolymerisations in the presence and the absence of chain-transfer agent. When they are compared, no significant effect of molecular weight is visible. This is very clear at  $90^\circ\text{C}$ , where the 95% joint-confidence intervals for both copolymerisations completely coincide. It has to be noted that molecular weights of the copolymers prepared with and without chain-transfer agent at  $90^\circ\text{C}$  do not differ to the same extent as the copolymers prepared at  $50^\circ\text{C}$ . Nevertheless, according to Figures 2.2 and 2.3 an order of magnitude difference in molecular weight should be enough to indicate the slightest molecular-weight dependence of copolymer composition, especially in the observed region of molecular weights.

Even though Figure 2.4a suggests a molecular-weight dependence, since the two 95% joint confidence intervals are not overlapping, it is very hard to believe that these minor differences are caused by differences in local monomer concentrations. It should be stressed that molecular weights of the copolymers prepared in the presence of chain-transfer agent are roughly 2-3 orders of magnitude lower than those of the copolymers prepared in the absence of chain-transfer agent. The insignificance of the difference in reactivity ratios becomes clear when the copolymer composition is plotted against molecular weight, see Figure 2.6:

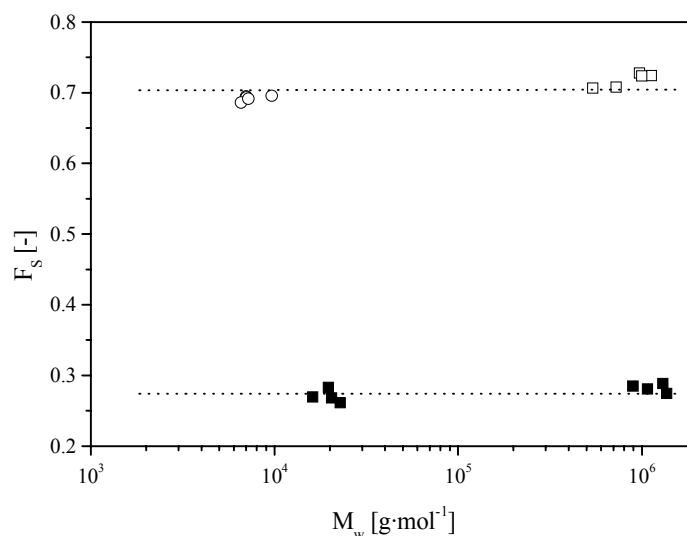


**Figure 2.6 vs. Copolymer composition vs. molecular weight for S/BA copolymerisations at 50°C in bulk with  $f_s^0=0.085$  and  $f_s^0=0.676$  in the presence of CTA (● and ○, respectively) and in the absence of CTA (■ and □, respectively).**

As can be seen from Figure 2.6, no significant difference in chemical composition between high and low-molecular-weight material is observed. One could argue that the chemical compositions for the low-molecular-weight copolymers are somewhat lower than for copolymers with high molecular weights. In an attempt to explain these minor differences in copolymer composition it might be wise to look at possible initiator effects on the copolymer composition at small chain lengths. It is known that propagation rate coefficients are chain-length dependent<sup>29</sup>, especially at low chain lengths, *i.e.* less than 10 monomer units. It is plausible that the propagation rate coefficients of S and BA radicals are affected by the chain length in a different way, causing a different instantaneous composition at low molecular weights. However, the copolymers prepared in the presence of chain-transfer agent have molecular weights of at least  $7 \cdot 10^3$  g·mol<sup>-1</sup>, *i.e.* 60 to 70 monomer units. Small changes in the chemical composition at short chain lengths can therefore not be completely responsible for the difference in observed reactivity ratios.

A more plausible explanation for the shift of the 95% joint-confidence intervals can be found once again in the complications that we have come across during the integration of the BA region in the  $^1\text{H}$  NMR spectra. In the integration of this region, the interfering peak has never been taken into account. When this peak is overlapping with the BA peak, which is the case for the high-molecular-weight polymers in particular, the amount of BA in the copolymer is systematically underestimated. This leads to a higher  $F_S$  at high  $f_S$  for copolymers prepared in the absence of chain-transfer agent. When the data are now fitted with Eq. (2.3),  $r_S$  is affected most and a higher  $r_B$  will fit the data best. Apparently, the effect of the interfering peak is more noticeable in the copolymerisations at 50°C.

In summary, the effect of molecular weight on copolymer composition for the conventional free-radical copolymerisation of S and BA is not observed in our experimental work, which is in contrast to the report of Semchikov *et al.*<sup>21</sup>.

## 2.6 CONCLUSIONS

The conventional copolymerisation of S and BA has been investigated to assess the feasibility of synthesising copolymers bearing an intramolecular compositional gradient. Reactivity ratios have thereto been studied in copolymerisations of S and BA in the presence and in the absence of chain-transfer agent. Neither at 50°C nor at 90°C a significant molecular-weight dependence could be detected. It can therefore be stated that neither the preferential absorption nor the bootstrap effect do not significantly occur in the bulk free-radical copolymerisation of S and BA. As a consequence, intramolecular composition drift will not occur and the application of living radical polymerisation techniques seems to be necessary to produce intramolecularly heterogeneous copolymers.

## REFERENCES

- <sup>1</sup> Flory, P.J., *Principles of Polymer Chemistry*, Cornell University Press, Ithaca: New York, 1953
- <sup>2</sup> Walling, C., *Free Radicals in Solution*, Wiley: New York, 1957
- <sup>3</sup> Nakano, T.; Okamoto, Y. In *Controlled Radical Polymerization*; Matyjaszewski, K., Ed.; ACS Symposium Series No. 685; American Chemical Society: Washington DC, 1997; p 451
- <sup>4</sup> Mayo, F.R.; Lewis, F.M. *J. Am. Chem. Soc.* **1944**, *66*, 1594
- <sup>5</sup> Alfrey Jr., T.; Goldfinger, G. *J. Chem. Phys.* **1944**, *12*, 205
- <sup>6</sup> Greenley, R.Z. *J. Macromol. Sci., Chem.* **1980**, *A14*, 445

- 7 Merz, E.; Alfrey Jr., T.; Goldfinger, G. *J. Polym. Sci.* **1946**, *1*, 75
- 8 Ham, G.E. *J. Polym. Sci.* **1954**, *14*, 87
- 9 Cais, R.E.; Farmer, R.G.; Hill, D.J.T.; O'Donnell, J.H. *Macromolecules* **1979**, *12*, 835
- 10 Fukuda, T.; Ma, Y.D.; Inagaki, H. *Macromolecules* **1985**, *18*, 17
- 11 Tirrell, D.A. In *Encyclopedia of Polymer Science and Technology*, vol. 4, Wiley: New York, 1986; p. 192
- 12 Fukuda, T.; Kubo, K.; Ma, Y.D. *Prog Polym. Sci.* **1992**, *17*, 875
- 13 Coote, M.L.; Davis, T.P. *Prog. Polym. Sci.* **1999**, *24*, 1217
- 14 Plochocka, K.; Harwood, H.J. *Am. Chem. Soc., Div., Polym. Chem., Polym. Prepr.* **1978**, *19*, 240
- 15 Harwood, H.J. *Makromol. Chem., Macromol. Symp.* **1987**, *10/11*, 331
- 16 Klumperman, B.; O'Driscoll, K.F. *Polymer* **1993**, *34* (6), 1032
- 17 Klumperman, B.; Brown, P.G. *Macromolecules* **1994**, *27*, 6100
- 18 Klumperman, B.; Kreager, I.R. *Macromolecules* **1994**, *27*, 1529
- 19 Semchikov, Yu.D.; Smirnova, L.A.; Knyazeva, T.Ye.; Bulgakova, S.A.; Voskoboinik, G.A.; Sherstyanykh, V.I. *Polym. Sci. U.S.S.R.* **1984**, *26* (4), 780
- 20 Semchikov, Yu.D.; Izvolenskii, V.V.; Smirnova, L.A.; Kopylova, N.A.; Sveshnikova, T.G. *Polym. Sci. Series A* **1993**, *35* (5), 594
- 21 Semchikov, Yu.D.; Smirnova, L.A.; Knyazeva, T.Ye.; Bulgakova, S.A.; Sherstyanykh, V.I. *Eur. Polym. J.* **1990**, *26* (8), 883
- 22 Semchikov, Yu.D.; Smirnova, L.A.; Kopylova, N.A.; Izvolenskii, V.V. *Eur. Polym. J.* **1996**, *32* (10), 1213
- 23 Zivny, A.; Pouchly, J.; Solc, K. *Coll. Czech Chem. Comm.* **1967**, *130*, 41
- 24 Tidwell, P.W.; Mortimer, G.A. *J. Polym. Sci., Part A* **1963**, *3*, 369
- 25 Dubé, M.A.; Penlidis, A.; O'Driscoll, K.F. *Can. J. Chem. Eng.* **1990**, *68*, 974
- 26 Van Herk, A.M. *J. Chem. Ed.* **1995**, *72*, 138
- 27 Van Herk, A.M.; Dröge, T. *Macromol. Theory Simul.* **1997**, *6*, 1263
- 28 Dubé, M.A.; Penlidis, A.; O'Driscoll, K.F. *Can. J. Chem. Eng.* **1990**, *68*, 974
- 29 Moad, G.; Solomon, D.H., *The Chemistry of Free Radical Polymerization*, 1<sup>st</sup> ed., Elsevier Science Ltd.: Oxford, 1995



# 3

## *Atom Transfer Radical Polymerisation*

**Synopsis:** In chapter 2 it has been shown that in conventional free-radical polymerisation control of copolymer structure is not possible. Therefore, a start is made with the application of living radical polymerisation techniques. Since these living radical techniques are different from conventional free-radical polymerisation, it seems recommendable to introduce the reader to the existing living radical polymerisation techniques with a general overview. Hereafter, the attention is focused on one particular case: atom transfer radical polymerisation. The kinetics, as well as the general role of the most important components involved, are discussed.



## 3.1 INTRODUCTION

Conventional free-radical polymerisation is a widely used technique to produce polymeric material on an industrial scale<sup>1</sup>. It is applicable to a wide gamut of monomers, while at the same time it is inert towards water and many common impurities. Nevertheless, full control of polymer microstructure, *e.g.* molecular-weight distribution and, in the case of copolymers, intramolecular chemical composition distribution, is generally not possible and can only be achieved with living polymerisation techniques such as anionic polymerisation<sup>2</sup>, group transfer polymerisation<sup>3,4</sup> or metallocene catalysed polymerisation<sup>5</sup>.

In the last few decades, however, so-called living radical polymerisation techniques<sup>6</sup> have been developed that combine the facility of free-radical polymerisation with the advantages of the above-mentioned living polymerisation techniques. In other words, a wide variety of polymers now in principle can be produced via free-radical polymerisation techniques, while an increased control of the incorporation of monomer units into the polymeric chain is gained.

This chapter gives an overview of living radical polymerisation techniques available nowadays and focuses on atom transfer radical polymerisation.

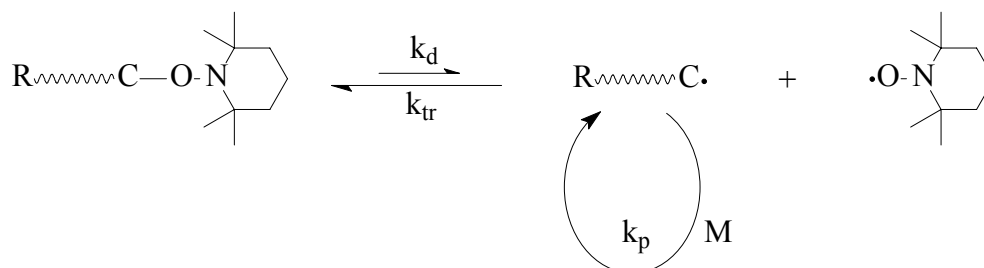
## 3.2 LIVING RADICAL POLYMERISATION

The development of living radical polymerisation was inspired by the work of Otsu *et al.*<sup>7</sup> on the use of disulfides to polymerise styrene and methyl methacrylate. The disulfides photochemically dissociate resulting in the formation of S-centred radicals that can not only polymerise but also reversibly terminate growing radicals. Additionally, these radicals can also participate in transfer processes. Application of these so-called iniferters (*initiator*, *transfer* agent and *terminating* agent) allows the synthesis of block copolymers<sup>8</sup>. A drawback of the iniferter system is that it is subject to side-reactions, which lead to a loss of chain-end functionality<sup>9</sup>.

Druliner and co-workers<sup>10</sup> developed a system where long-living oxygen-centred radicals, formed by reaction with electron acceptors, enable acrylate block copolymer synthesis. Arvanitopoulos *et al.*<sup>11</sup> used cobaloximes in living radical polymerisation under photochemical conditions. To polymerise acrylates, the procedure reported by Arvanitopoulos was modified by Wayland *et al.*<sup>12</sup>.

One of the more promising and thoroughly studied living radical polymerisation techniques seems to be nitroxide-mediated polymerisation, which was first discovered

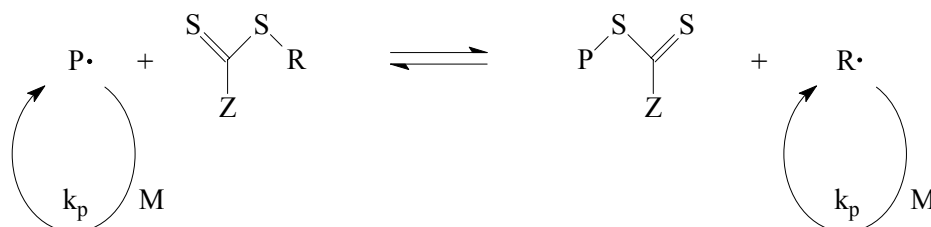
by Solomon and Rizzardo<sup>13,14</sup> in 1985, and experienced a revival with the work of Georges *et al.*<sup>15,16</sup>. The basis of nitroxide-mediated polymerisation lies in the reversible trapping of the growing polymeric radicals by a stable free nitroxide radical, *e.g.* 2,2,6,6-tetramethylpiperide-*N*-oxyl (TEMPO), see Scheme 3.1.



**Scheme 3.1** Schematic representation of nitroxide-mediated living radical polymerisation.

The C-O bond of the alkoxyamine is thermally labile and will be homolytically cleaved at elevated temperatures, yielding a free nitroxide and a reactive radical that is capable to restart propagation until recombination with the nitroxide takes place. This reversible trapping/dissociation ensures a sufficiently low stationary radical concentration, since  $k_d \ll k_{tr}$  and in this way it competes with termination reactions. Usually, nitroxide-mediated living radical polymerisation is conducted at high temperatures ( $> 110^\circ\text{C}$ ), although recent literature reports the polymerisation at low temperatures<sup>17,18</sup>. A major disadvantage of nitroxide-mediated living radical polymerisation remains the limited number of monomers, more notably styrene and its derivatives, to which it can be applied.

A system that emerged in 1998 and that is certainly worth mentioning is reversible addition-fragmentation chain transfer (RAFT) polymerisation<sup>19,20</sup>. RAFT uses dithioesters to ensure fast interchange of growing radicals and dormant species, see Scheme 3.2. An activating group (Z) ensures efficient addition and fragmentation of the RAFT group.



**Scheme 3.2** Schematic representation of reversible addition-fragmentation chain transfer polymerisation.

If the exchange reaction is fast in comparison with propagation, the radical is interchanged over all chains during the polymerisation. It is this characteristic feature that yields narrow molecular-weight distributions and enables the production of well-defined polymers with the RAFT polymerisation technique. An additional radical flux is necessary in RAFT to initiate polymerisation and compensate for the loss of functional chains due to bimolecular termination. A strategically important aspect of the RAFT process is that it can be applied to virtually any monomer, regardless of the functional groups present.

Atom transfer radical polymerisation (ATRP) is another sprig of the family of living radical polymerisation techniques, and was reported by Sawamoto *et al.*<sup>21</sup> and Matyjaszewski *et al.*<sup>22</sup>. It encompasses the use of a transition metal complex to reversibly deactivate growing polymeric radicals by transforming them into dormant species. In the following sections the attention is focused on ATRP.

In living polymerisation systems the number-average molecular weight,  $M_n$ , increases linearly with fractional conversion ( $\xi$ ). The molecular weight at the end of the reaction is determined by the ratio of the initial concentrations of monomer ( $[M]_0$ ) and initiator ( $[I]_0$ ):

$$M_n = \frac{[M]_0}{[I]_0} \xi \quad (3.1)$$

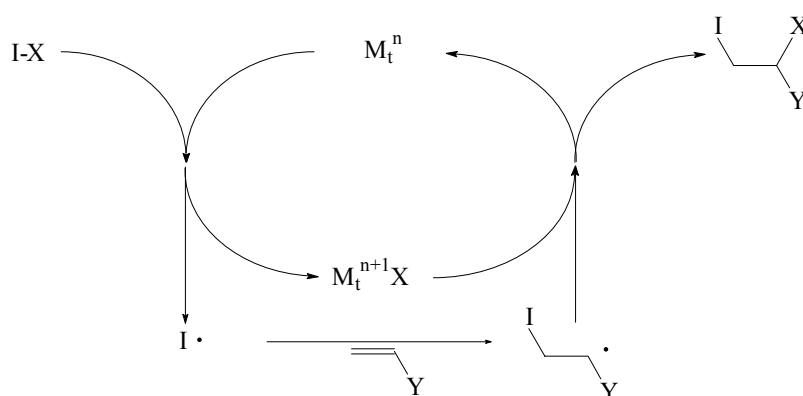
It should be stressed that bimolecular termination reactions cannot be prevented in living radical polymerisations. As a consequence, bimolecular termination reactions take place. When the stationary radical concentrations in living radical polymerisation and conventional free-radical polymerisation are equal, the same number of terminated chains will be generated. However, since in living radical polymerisations much more chains are initiated, the relative amount of terminated chains is less.

Generally, in living radical polymerisation the amount of terminated chains should not exceed 5% relative to the total number of chains present in the system<sup>23</sup>, although it should be noted that this is rather an arbitrary rule.

## 3.3 ATOM TRANSFER RADICAL POLYMERISATION (ATRP)

### 3.3.1 Mechanism of ATRP

Atom transfer radical polymerisation is essentially based on a well-known organic reaction that is called atom transfer radical addition (ATRA)<sup>24</sup>. ATRA is based on the halogen exchange from an alkyl halide to a transition-metal complex. This process generates a radical, which is able to add an alkene to form a transient product radical to which the halide atom is transferred back, see Scheme 3.3. Copper<sup>25</sup> and other transition metals with a  $d^n$  electronic structure such as nickel<sup>26,27</sup>, palladium<sup>28</sup>, ruthenium<sup>29</sup> and iron<sup>30</sup> have been used in ATRA.

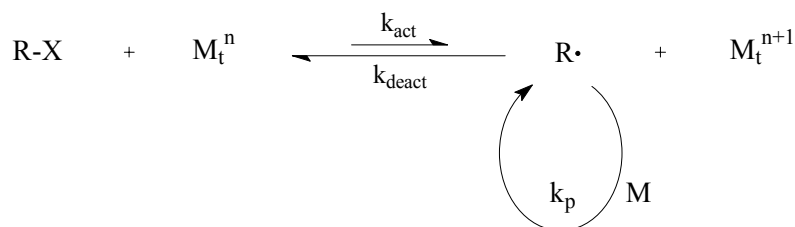


*Scheme 3.3 General mechanism of atom transfer radical addition (ATRA).*

The mechanism is believed to proceed via an inner-sphere electron transfer<sup>31</sup>, which reversibly generates the radical ( $I\cdot$ ) and the oxidised metal complex ( $M_t^{n+1}X$ ). The radical that is formed after the addition of the alkene is generally much less stabilised than the radical that existed before. The subsequent reaction of the newly formed radical with  $M_t^{n+1}X$  is therefore irreversible and explains why only one alkene addition can take place in ATRA. It is assumed that the intermediate species are free radicals and that neither solvent-cage effects, nor coordination with the metal centre occurs.

ATRA can be extended to ATRP when the radical that is formed after addition of the unsaturated substrate is sufficiently stabilised. In that case, the reaction of this radical with  $M_t^{n+1}X$  will no longer be irreversible and, as a consequence, the addition of many alkene units is possible. This process will continue until all of the substrate has been consumed. ATRP therefore relies on the equilibrium between halide-end-capped species (or dormant species) and propagating radicals, see Scheme 3.4. The halide

atom (X) is transferred from the dormant species (R-X) to the transition-metal complex and a radical ( $\text{R}\cdot$ ) is formed that is able to add monomer (M). For reasons of simplicity, the deactivating species is denoted as  $\text{M}_t^{n+1}$  instead of  $\text{M}_t^{n+1}\text{X}$ .



**Scheme 3.4** Equilibrium between dormant and radical species in atom transfer radical polymerisation (ATRP).

In this equilibrium,  $k_{act}$  and  $k_{deact}$  stand for the activation and deactivation rate parameters, respectively. Note that the initiation step in ATRP involves a halide species (I-X) and is completely analogous to the equilibrium as depicted in Scheme 3.4. As in ATRA, it is believed that free radicals are involved in ATRP. The equilibrium can be considered as an additional element in the conventional free-radical polymerisation scheme. There are strong indications that this concept is a true representation of the actual mechanism, among which are the following:

- copolymer microstructures are similar to those of copolymers prepared by free-radical polymerisation, which suggests a mechanism involving free radicals.
- reactivity ratios obtained in ATRP copolymerisation are similar to those obtained in conventional free-radical copolymerisation<sup>32</sup>.
- performing ATRP using  $\text{M}_t^{n+1}$  and a conventional free-radical initiator as point of departure results in a controlled polymerisation system<sup>33,34</sup>. The alkyl halide and  $\text{M}_t^{n+1}$  are formed *in situ* by the halide transfer from the  $\text{M}_t^{n+1}$  to the carbon-centred radical.
- oxygen inhibits the polymerisation reaction<sup>35</sup>.

It should be noted, however, that these indications are far from conclusive, since there are no indications that contradict a concerted halide abstraction/monomer insertion mechanism. For the sake of clarity and simplicity, in the remainder of this thesis it will be assumed that ATRP obeys conventional free-radical kinetics on the understanding that the equilibrium between dormant species and growing radicals plays a crucial role.

In order for ATRP to produce well-defined polymers, the equilibrium has to meet several requirements<sup>36,37,38</sup>:

1. *Initiation must be fast in comparison with propagation.*
2. *The equilibrium constant, i.e.  $k_{act}/k_{deact}$ , must be in a proper range in order to maintain a proper stationary concentration of radicals.*
3. *The time constant of deactivation must be low as compared to the time constant of propagation.*

The first condition is to ensure that all chains will grow during the whole reaction time. The second requirement should be obeyed, because it is necessary to keep the stationary radical concentration low in order to minimise bimolecular termination reactions relative to propagation reactions. If the equilibrium constant would be too high, the stationary concentration of radicals would be too high. Since termination is proportional to  $[R\cdot]^2$  and propagation to  $[R\cdot]$ , this would lead to an increase in termination relative to propagation. In other words, the equilibrium as defined in Scheme 3.4 should be almost completely on the dormant species side. If this is the case, termination is minimised and end-group functionality is largely retained throughout polymerisation. Obviously, decrease in termination can only be obtained at the expense of the rate of polymerisation. The radical concentration should therefore not be too low, in order to maintain a reasonable rate of polymerisation. In general, a radical concentration of  $10^{-7}$  or  $10^{-8}$  is a reasonable compromise<sup>36</sup>.

The third condition determines the number of propagation steps per activation/deactivation cycle. In order to have control of the molecular-weight distribution, the number of activation/deactivation cycles during the whole polymerisation time should be large enough<sup>39,40</sup>. If the third requirement is met, polymers with narrow molecular-weight distributions are obtained.

A simple calculation demonstrates the importance of the equilibrium. The probability of a radical to be still living after  $i$  propagation steps is expressed by Eq. (3.2).

$$p^{i \text{ living}} = \left( \frac{R_p}{R_p + R_t} \right)^i = \left( \frac{k_p[M]}{k_p[M] + 2k_t[R\cdot]} \right)^i \quad (3.2)$$

When polymerising styrene in bulk at 110°C up to a chain length of 100 and only 5% of the total chains may be involved in termination reactions,  $R_p \approx 2000 \cdot R_t$ . When using  $k_p = 1600 \text{ L}\cdot\text{mol}^{-1}\cdot\text{s}^{-1}$ <sup>41</sup>,  $k_t \sim 10^8 \text{ L}\cdot\text{mol}^{-1}\cdot\text{s}^{-1}$  and  $[M] \sim 10 \text{ mol}\cdot\text{L}^{-1}$ , it is clear that the

radical concentration should not exceed  $4 \cdot 10^{-8} \text{ mol} \cdot \text{L}^{-1}$ . The ratio of  $k_{act}$  and  $k_{deact}$  should therefore be sufficiently low.

### 3.3.2 Kinetic description of ATRP in constant density reactors

In order to describe the kinetics of ATRP, it is necessary to consider the reactions in Scheme 2.1 and taking into account the ATRP equilibrium as well. The rate of reaction is a key factor in the description of polymerisation kinetics, and can be expressed as the rate of consumption of monomer:

$$-\frac{d[M]}{dt} = k_p [R \cdot] [M] \quad (3.3)$$

The radical concentration in equation (3.3) originates from dormant species according to the ATRP equilibrium depicted in Scheme 3.4. After the equilibrium has set in, the radical concentration can be expressed by:

$$[R \cdot] = \frac{k_{act} [M_t^n] [R-X]}{k_{deact} [M_t^{n+1}]} \quad (3.4)$$

In order to describe the rate of polymerisation, it is necessary to find analytical expressions for  $[R \cdot]$ ,  $[M_t^{n+1}]$ ,  $[R-X]$  and  $[M_t^n]$ . Since  $[R \cdot]$  and  $[M_t^{n+1}]$  change relatively considerable more during the reaction than the concentrations of dormant species and  $M_t^n$ , a closer look has to be cast on the time derivatives of  $[R \cdot]$  and  $[M_t^{n+1}]$ , see Eqs. (3.5) and (3.6)<sup>39</sup>.

$$\frac{d[R \cdot]}{dt} = k_{act} [R-X] [M_t^n] - k_{deact} [R \cdot] [M_t^{n+1}] - 2\bar{k}_t [R \cdot]^2 \quad (3.5)$$

$$\frac{d[M_t^{n+1}]}{dt} = k_{act} [R-X] [M_t^n] - k_{deact} [R \cdot] [M_t^{n+1}] \quad (3.6)$$

Note that thermal initiation has been neglected in these equations. The evolution of  $[R \cdot]$  and  $[M_t^{n+1}]$  in time is not straightforward, since the radicals are subject to bimolecular termination (with an average termination rate constant,  $\bar{k}_t$ ), while  $M_t^{n+1}$

can be regarded as a persistent radical. Considering the fact that  $[M_t^{n+1}] = 0$  and  $[R\cdot] = 0$  at the beginning of the reaction,  $[M_t^{n+1}]$  and  $[R\cdot]$  initially increase linearly with time:

$$\frac{d[R\cdot]}{dt} = \frac{d[M_t^{n+1}]}{dt} = k_{act}[I-X]_0[M_t^n]_0 \quad (3.7)$$

At this stage, bimolecular termination of the radicals is competing with reversible deactivation due to the low  $M_t^{n+1}$  concentration. When  $k_t \sim 10^8 \text{ L}\cdot\text{mol}^{-1}\cdot\text{s}^{-1}$  and  $k_{deact} \sim 10^7 \text{ L}\cdot\text{mol}^{-1}\cdot\text{s}^{-1}$ <sup>42</sup>, termination dominates at the beginning of the reaction:

$$R_t = 2k_t[R\cdot]^2 > R_{deact} = k_{deact}[R\cdot][M_t^{n+1}] \quad (3.8)$$

After all, in the beginning  $[R\cdot] = [M_t^{n+1}]$  and when  $k_{deact}$  is an order of magnitude smaller than  $k_t$ , bimolecular termination will prevail. However, as time elapses, the transient radicals,  $R\cdot$ , undergo bimolecular termination, which, as a consequence, induces an excess of the  $M_t^{n+1}$  species. The reversible deactivation reaction therefore becomes more dominant and  $[R\cdot]$  will eventually go through a maximum, after which it monotonously decreases. The  $M_t^{n+1}$  species, on the other hand, does not undergo any kind of termination and increases in concentration throughout the reaction. In general, the concentrations of growing radicals, dormant species,  $M_t^n$  and  $M_t^{n+1}$  never reach steady state values. This phenomenon is well-known as the persistent radical effect<sup>43,44</sup> and occurs whenever there are transient radicals ( $R\cdot$ ) and persistent radicals ( $M_t^{n+1}$ ) present.

Subtracting (3.6) from (3.5) and integration of the resulting expression with respect to  $t$  leads to:

$$[R\cdot] - [M_t^{n+1}] = \int_0^t -2k_t[R\cdot]^2 dt \quad (3.9)$$

Looking at Eq. (3.9) it can be expected that for larger values of  $t$ ,  $[R\cdot]$  is much smaller than  $[M_t^{n+1}]$ . For a common ATRP system involving CuBr to polymerise styrene,  $[R\cdot]$  can be estimated relative to  $[M_t^{n+1}]$ . After all, since the relative number of inactive chains at the end of the reaction is limited to 5%, *i.e.*  $[R-X] \approx [I-X]_0$  and  $[M_t^n] \approx [M_t^n]_0$ , the system is governed by a quasi-equilibrium:



$$K = \frac{k_{act}}{k_{deact}} = \frac{[M_t^{n+1}][R\cdot]}{[M_t^n]_0[I-X]_0} \quad (3.10)$$

When using  $k_{act}=0.45 \text{ L}\cdot\text{mol}^{-1}\cdot\text{s}^{-1}$ <sup>45</sup>,  $k_{deact}=1.1\cdot 10^7 \text{ L}\cdot\text{mol}^{-1}\cdot\text{s}^{-1}$ <sup>42,45</sup>,  $[\text{Cu}^+]_0=5\cdot 10^{-2} \text{ mol}\cdot\text{L}^{-1}$  and  $[\text{PS-Br}]_0=5\cdot 10^{-2} \text{ mol}\cdot\text{L}^{-1}$ , together with a reasonable value for  $[R\cdot]$  ( $10^{-7} \text{ mol}\cdot\text{L}^{-1}$ ), a deactivator concentration of  $1\cdot 10^{-3} \text{ mol}\cdot\text{L}^{-1}$  is reached. It is clear that  $[R\cdot]\ll[M_t^{n+1}]$  and therefore it is allowed to neglect the  $[R\cdot]$  term in the left-hand side of Eq. (3.9).

Using the quasi-equilibrium, the  $[M_t^{n+1}]$  term in (3.9) can be substituted yielding:

$$K[M_t^n]_0[I-X]_0 = 2k_t[R\cdot]\int_0^t [R\cdot]^2 dt \quad (3.11)$$

Eq. (3.11) can easily be integrated yielding analytical expressions for  $[R\cdot]$  and  $[M_t^{n+1}]$ <sup>39,44</sup>.

$$[R\cdot] = \left( \frac{k_{act}[I-X]_0[M_t^n]_0}{6k_{deact}k_t} \right)^{1/3} t^{-1/3} \quad (3.12)$$

$$[M_t^{n+1}] = \left( \frac{k_{act}6k_t[I-X]_0^2[M_t^n]_0^2}{k_{deact}} \right)^{1/3} t^{1/3} \quad (3.13)$$

Eq. (3.12) can now be substituted into (3.3) and subsequent integration leads to:

$$-\ln(1-\xi) = \ln\left(\frac{[M]_0}{[M]}\right) = \frac{3}{2}k_p \left( \frac{k_{act}[I-X]_0[M_t^n]_0}{6k_{deact}k_t} \right)^{1/3} t^{2/3} \quad (3.14)$$

Eq. (3.14) can be used to monitor the monomer consumption as a function of time. It has to be noted that it only holds at longer times, *i.e.* a few milliseconds after the start of the reaction when  $[R\cdot]\ll[M_t^{n+1}]$ . Furthermore, the derivation assumes that no deactivating species is present at the beginning of the reaction; that the cumulative number of terminated chains is negligible (<5%) and that thermal initiation is absent.

In many cases, however, a deactivating species is added at the beginning of the reaction. When  $[M_t^{n+1}]_0 \gg 0$ ,  $[M_t^{n+1}] \approx [M_t^{n+1}]_0$  and Eq. (3.15) is obtained directly from Eqs. (3.3) and (3.4):

$$\ln\left(\frac{[M]_0}{[M]}\right) = k_p \frac{k_{act}}{k_{deact}} \frac{[I-X]_0 [M_t^n]_0}{[M_t^{n+1}]_0} t \quad (3.15)$$

### 3.3.3 Different components in ATRP

As already mentioned in section 3.3.1, many different species are involved in the ATRP process. All these components have their specific roles in the mechanism and their behaviour is in many cases very complex. In the following sections, the most important components will be discussed in some detail.

#### 3.3.3.1 Transition metal complex

The transition metal complex serves as catalyst in ATRP. Upon complex formation, the properties are determined by the interactions between transition metal ion and ligands. To perform a successful ATRP reaction, the complex should have a suitable equilibrium position between the oxidized and reduced state, determined by its redox potential. Furthermore, appropriate exchange dynamics should be created between the dormant and active species. These dynamics are responsible for the deactivation process of the radical that needs to be fast to secure control of the polymerisation reaction.

##### *Transition metal.*

The properties of the complex are for the greater part determined by the selection of the transition metal. The category of  $d^n$  transition metals is most suitable for application in catalysis for organic synthesis. The first requirement for the transition metal ion is the ability to participate in an inner sphere one-electron transfer cycle to promote atom transfer and to accommodate the transferred halide atom from the dormant species, R-X, in the inner coordination sphere. Furthermore, to prevent side-reactions the metal should have a high selectivity for halide transfer and consequently a low affinity for alkyl radicals and hydrogen atoms on alkyl groups. In addition, the metal should not be a strong Lewis acid that could ionise certain end-groups to carbocations.

At present,  $Ni^{46,47}$ ,  $Fe^{48}$ ,  $Ru^{21}$ , and  $Cu^{22}$  have been successfully applied in ATRP polymerisations. The latter, however, besides the fact that it has been studied most

extensively, has proven to be the most widely applicable transition metal in ATRP. In the remainder of this chapter, therefore,  $\text{Cu}^+$  and  $\text{Cu}^{2+}$  is used synonymously with  $\text{M}_t^n$  and  $\text{M}_t^{n+1}$ , respectively.

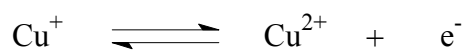
#### *Ligand.*

The ligand in ATRP is vital and serves several purposes. First, the ligand should affect the redox potential of the transition metal ion in such a way that the equilibrium between dormant species and propagating radicals is shifted towards the dormant species. For instance, electron-withdrawing substituents stabilise  $\text{M}_t^n$ , while electron-donating substituents favour  $\text{M}_t^{n+1}$  stabilisation. Steric effects, in addition, also affect the redox potential. When substituents on the ligand hamper the accommodation of the transferred halide atom, the resulting transition metal complex will be less active in ATRP.

Second, it should solubilise the transition metal ion in order to maintain proper control of the polymerisation reaction. A decreased solubility of the transition metal complex might imply a lower concentration of deactivating species, *i.e.*  $\text{M}_t^{n+1}$ , which ultimately results in broadening of molecular-weight distributions and an increase in the contribution of termination events to the polymerisation process. For the  $\text{Cu}/(2\text{-pyridine carbaldehyde } 3,3\text{-diphenyl propyl imine})_2$  complex, it is known that the oxidised state is much less soluble in organic solvents than the complex in its reduced state<sup>49</sup>. A decrease in deactivator concentration would lead to inefficient deactivation, resulting in broadening of the molecular-weight distribution. Matyjaszewski *et al.*<sup>42</sup> successfully applied modified bipyridines such as 4,4'-di-(*t*-butyl)-bipyridine, 4,4'-di-(*n*-heptyl)-bipyridine and 4,4'-di-(nonyl)-bipyridine. The alkyl groups reduce polarity, thereby increasing the complex solubility compared to complexes with unsubstituted bipyridine, leading to a homogeneous reaction mixture.

#### *Electronic interplay between transition metal and ligand.*

In aqueous solution the redox potential for the oxidation reaction of cuprous ions, as shown in Scheme 3.5, is  $-153 \text{ mV}^{50}$ .



**Scheme 3.5** Oxidation/reduction of a cuprous ion.

The same oxidation reaction for the  $\text{Cu}/(\text{bipyridine})_2$  complex in aqueous solution results in a redox potential of  $120 \text{ mV}^{51}$ , which shows the stabilising effect of  $\text{Cu}^+$  by

the ligand. When ligands raise this redox potential even more, this could lead to cationic polymerisation, which is the case for the  $\text{Cu}(\text{MeCN})_4$  complex<sup>52</sup>. So, it is clear that the transition metal complexes should have redox potentials that lie in a certain window, in order to be suitable for ATRP. The ligand should sufficiently stabilise  $\text{Cu}^+$  in order to keep  $[\text{R}\cdot]$  low enough to minimise termination relative to propagation. At the same time, it should not raise the redox potential in such a way that no halogen atom can be abstracted from the alkyl halide species. In general, ligands that are good  $\sigma$ -donors and  $\pi$ -acceptors lower the electron density on the copper centre and therefore preferentially stabilise the lower oxidation state.

The geometry of the copper complex influences its electronic and steric characteristics to a large extent. In general, a  $\text{Cu}^+$  complex has a tetrahedral geometry.  $\text{Cu}^{2+}$  complexes are generally believed to be square planar, see Figure 3.1.

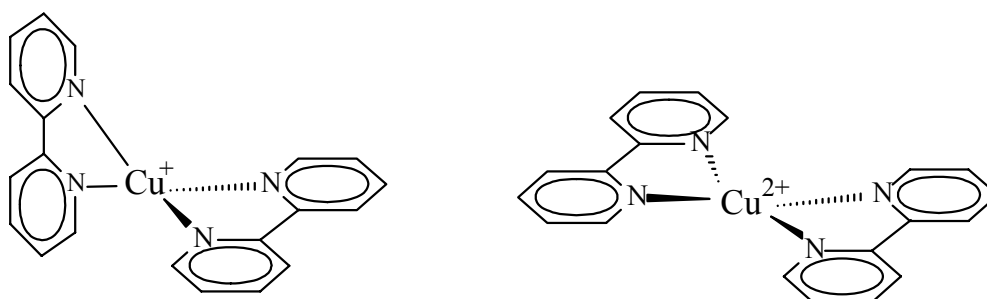


**Figure 3.1** Tetrahedral geometry of  $\text{Cu}^+/(bpy)_2$  complex and square planar geometry of  $\text{Cu}^{2+}/(bpy)_2$  complex.

The  $\text{Cu}^+$  complex should be able to accommodate for a counter ion belonging to the copper salt, e.g. a  $\text{Br}^-$  when  $\text{CuBr}$  is used. This probably occurs in the outer coordination sphere, which implies that the counter ion is not directly bonded to the copper centre. Upon oxidation of the copper complex by  $\text{R-X}$  into  $\text{X}^-$  and  $\text{Cu}^{2+}$ , it has to host a halide atom from the dormant species. Most straightforward would be that both the halide and the counter ion are present around the square planar structure in the outer coordination sphere of the complex. Secondly, both ions could be coordinated to form an octahedral-like structure with the halide and the counter ion weakly bonded in the inner sphere along the Z-axis of the complex, at some distance from the copper centre, see Figure 3.2. A third possibility is a penta-coordinated  $\text{Cu}^{2+}$  complex, as proposed by both Haddleton<sup>53</sup> and Matyjaszewski<sup>54</sup>, with the transferred halide in the inner coordination sphere, forming a trigonal bipyramidal structure as shown in Figure 3.2. The counter anion will again be present in the outer coordination sphere.

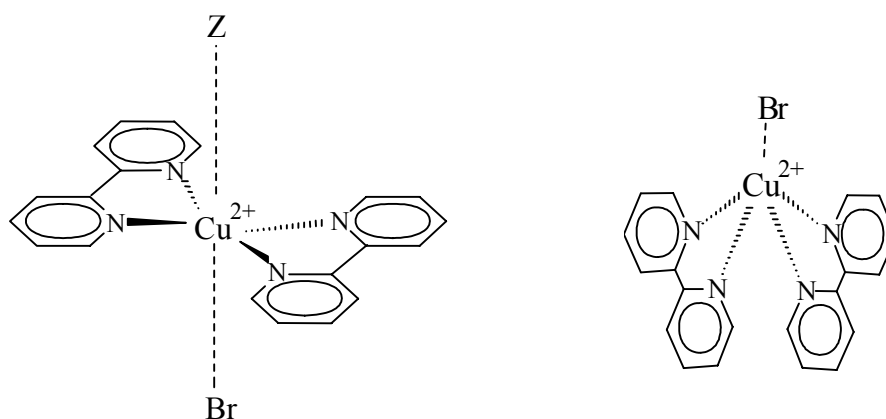
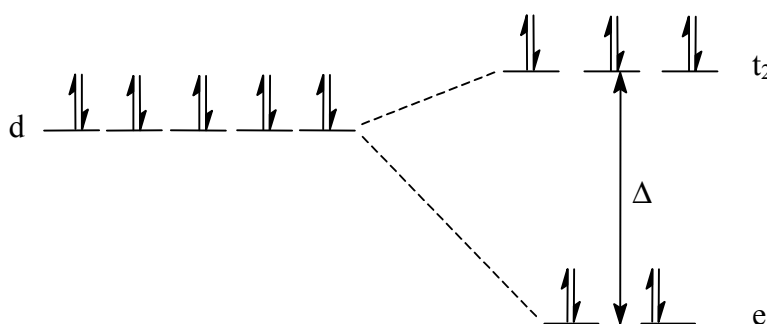


**Figure 3.2** Possible geometries of the  $\text{Cu}^{2+}$  complex after halide transfer. Left: an octahedral geometry; right: a trigonal bipyramidal geometry.

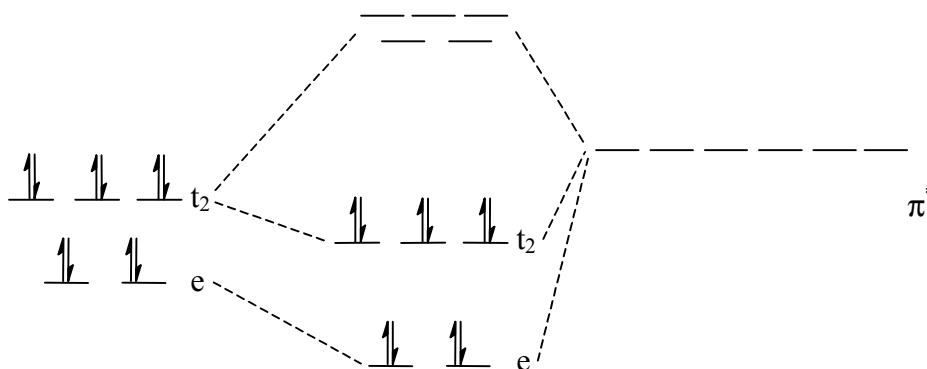
It is clear that when going from  $\text{Cu}^+$  to  $\text{Cu}^{2+}$ , substituents on the ligands may cause steric hindrance. Especially ligands with bulky substituents situated on the ortho-positions are unfavourable for the formation of  $\text{Cu}^{2+}$  and will consequently be suitable for ATRP.

Upon formation of a  $\text{Cu}^+$  complex with tetrahedral symmetry, the 3d orbitals will split up into two energy levels, see Scheme 3.6.



**Scheme 3.6** Schematic representation of the splitting of the d-orbitals of the copper centre with a tetrahedral configuration upon complexation with a ligand.

The tetrahedral field splitting,  $\Delta$ , is dependent on the interaction between the ligand and the Cu centre and increases with increasing interaction. The resulting  $t_2$  and e energy levels of the metal centre can be lowered when the ligand involved is a so-called  $\pi$ -acceptor. This is the case when the energy level of the lowest unoccupied molecular orbital (LUMO) of the ligand, the  $\pi^*$ -orbital, is comparable to the original d-orbitals of the copper centre. When this is the case, back donation from the electron density on the metal centre takes place (Scheme 3.7).



**Scheme 3.7**  $\pi$ -back donation occurring when the energy level of the  $\pi^*$ -orbital is close to the d-orbitals of the metal centre.

Copper complexes with ligands that are good  $\pi$ -acceptors are known to be able to give charge-transfer transitions in the UV/Vis-spectrum by excitation of electrons in complex-orbitals coming from the d-orbitals of the metal. This transition is called

metal to ligand charge transfer or MLCT. The lower the  $\pi^*$ -orbital, the more back donation occurs, the larger the energy barrier for MLCT and the lower the wavelength at which the MLCT band is visible in the UV/Vis spectrum.

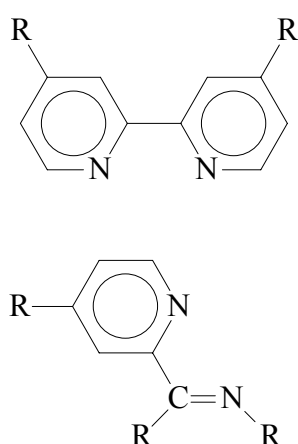


**Figure 3.3** General structures of bipyridine (upper case) and Schiff's base (lower case) ligands.

Good  $\sigma$ -donors and  $\pi$ -acceptors like bipyridines and Schiff's bases of pyridine-carboxaldehyde are able to act as suitable ligands for  $\text{Cu}^+$ . Although they both have comparable  $\sigma$ -bonding, the latter has a lower lying LUMO<sup>55</sup> and is therefore superior in stabilising  $\text{Cu}^+$  as compared to bipyridines. As mentioned earlier, the substituents on the para-positions in the bipyridine ligand, as well as those in the Schiff's base ligand, may alter the electronic

structure of the ligand as well. For instance, electron withdrawing groups, such as  $-\text{CN}$ , decrease the energy of the vacant  $\pi^*$  significantly, hereby favouring stabilisation of  $\text{Cu}^+$ . This electronic effect is additional to possible steric effects of the substituents on the redox potential. It should be noted, however, that the steric effects of substituents on the ortho-positions are much more pronounced than when they are located on the para-position.

Not only bipyridines and Schiff's bases are suitable ligands with favourable electronic characteristics. Boutevin *et al.*<sup>56</sup> reported ATRP reactions of styrene catalyzed by

CuCl with the commercially available ligands phenanthroline and 4,7-diphenyl-phenanthroline. Using phenanthroline ligands leads to a successful ATRP in solution polymerisation with 1,2-dimethoxybenzene as solvent. Bulk polymerisations with the same ligand resulted in poor control of molecular weight due to the low solubility of the copper complex in non-polar environments. Using 4,7-diphenyl-phenanthroline, on the other hand, leads to good control of molecular weight up to 50% conversion, despite the fact that the system is still not completely homogeneous.

A completely different class of ligands comprise the multi-dentate amine ligands. Xia *et al.*<sup>57</sup> used simple linear amines such as tetramethylethylenediamine (TMEDA), *N,N,N',N''*-pentamethyldiethylenetriamine (PMDETA) and *N,N,N',N'',N''',N''''*-hexamethyltriethylenetetramine (HMTETA) to polymerise styrene, methyl acrylate and methyl methacrylate.

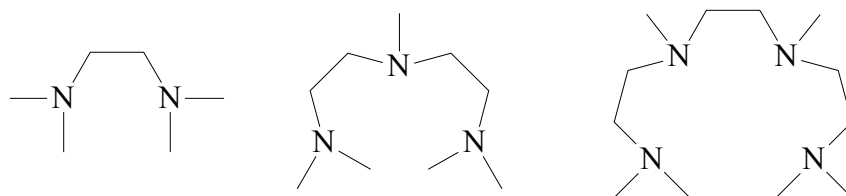


Figure 3.4 Structures of TMEDA (left), PMDETA (middle) and HMTETA (right).

Despite the fact that these ligands do not possess  $\pi$ -electrons and give rise to heterogeneous reaction mixtures, they are still able to stabilise  $\text{Cu}^+$  sufficiently to ensure control of polymerisation. They even have some advantages over the bipyridine and Schiff's base ligands, since they are cheaper, easier to modify, give almost colourless reaction mixtures and, due to the heterogeneity of the reaction mixture, enable facile removal of the catalyst after the reaction has been completed. However, given the fact that they give rise to very high polymerisation rates combined with the reaction mixture's heterogeneity, they are not suitable for kinetic investigations and modelling of the polymerisation reaction.

### 3.3.3.2 Monomer

As opposed to ionic living polymerisation, a wide variety of monomers has been found to polymerise successfully by ATRP. It includes monomers that are applied in conventional free-radical polymerisation, like styrenes<sup>42,58</sup>, (meth)acrylates<sup>53,59,60</sup>, as well as monomers with more pronounced functional groups such as acrylonitrile<sup>61</sup> and 2-hydroxyethyl acrylate<sup>62</sup>. Armes *et al.* recently reported the direct atom transfer radical polymerisation of salts of acidic monomers<sup>63,64</sup>. The effect of monomer

structure has been studied by Qiu *et al.* with a series of substituted styrenes<sup>58</sup>. Monomers having electron-withdrawing substituents polymerise faster and give better control of molecular-weight distribution than monomers with electron-donating substituents. The authors explain the differences by stating that electron-withdrawing substituents increase the propagation rate constant as well as the equilibrium constant. These substituents therefore increase monomer reactivity (higher  $k_p$ ) and lower the stability of the dormant species (higher  $K$ ).

Until now, however, ATRP is limited to stabilised vinyl monomers, which implies that  $\alpha$ -olefins and vinyl esters cannot be polymerised with ATRP.

### 3.3.3.3 Solvent

ATRP is very often performed in solution. This has the advantage that heat transfer is rather easy to control and that viscosity can be kept low, in comparison with bulk polymerisation. Dilution has a significant effect on the reaction rate, which becomes clear when we look at Eq. (3.14), where  $\ln([M]_0/[M])$  vs. time is dependent on both  $[I-X]_0$  and  $[M]_i^n$ . A lower viscosity can only be obtained at the expense of a lowered reaction rate, and a balance between reaction rate and viscosity has to be found.

Most ATRP reactions are carried out in non-polar solvents, such as xylene<sup>65</sup> and diphenylether<sup>42</sup>, although more polar solvents have been applied as well<sup>42,61</sup>.

A prerequisite of the solvent is that it must not have any interactions with the catalyst. It has been reported that ATRP reactions in dimethylformamide were less successful<sup>66</sup> yielding polymers with relatively high polydispersities. Similarly, the addition of 5% pyridine to the reaction mixture<sup>42</sup> caused the reaction rate to drop dramatically.

Another important aspect of the solvents is their ability to participate in side-reactions. For instance, when polymerising styrene in polar solvents at higher temperatures, HBr elimination occurs<sup>67</sup>. This leads to a loss of functionality during the polymerisation and should therefore be avoided in ATRP. Likewise, solvents that will participate in radical transfer processes should not be used when the production of high-molecular-weight material is aimed at. Due to the longer reaction time needed to produce high-molecular-weight material, the amount of dead polymeric chains as a result of chain-transfer processes is much more significant. However, when low molecular weights are the objective, the application of solvents such as toluene and xylene is permitted.

### 3.3.3.4 Initiator

The main role of the initiator (I-X) is to generate chains at the start of the reaction that will be able to add monomer during polymerisation. Usually, alkyl halides are used as initiators in ATRP.



For successful control of molecular weight and molecular-weight distribution, the initiator needs to fulfil two important requirements. First, the initiator should quantitatively generate chains, *i.e.* upon dissociation all radicals should lead to the formation of a dormant species. Recombination of initiator-derived radicals would lead to higher molecular weight than was targeted for and is therefore unfavourable. Second, the dissociation of the alkyl halide should be fast in comparison with propagation. If this is not the case, this leads to broadening of the molecular-weight distribution. The dissociation energy of the carbon-halide bond of the initiator should therefore be sufficiently low to facilitate a rapid transfer of the halide radical from the alkyl halide to the transition metal species. Since the carbon-fluoride bond is too strong, alkyl fluoride cannot be used. Iodine would be a good leaving group, but unfortunately it participates in side-reactions when polymerising styrene<sup>68</sup>. Alkyl bromides and chlorides are most successful in ATRP.

The structure of the alkyl part is also of importance. Usually, a structure resembling the monomer involved in polymerisation is used to ensure fast initiation of polymerisation by the initiator radical, although this is not a law of the Medes and Persians. For polymerisations of styrene 1-phenyl ethylbromide can be used, while for the polymerisation of methyl methacrylate ethyl 2-bromoisobutyrate is suitable. Another class of very efficient and universally applicable initiators was reported by Percec *et al.*<sup>69,70</sup> and are called the arenosulfonyl chlorides, see Figure 3.5. These arenosulfonyl chlorides homolytically dissociate between the sulphur and the chlorine atom and yield highly reactive sulfonyl radicals. This leads to much faster initiation than in the case when *e.g.* ethyl 2-bromoisobutyrate is used. On the other hand, when using arenosulfonyl chlorides, more bimolecular termination takes place in the beginning of the reaction due to the high radical flux, although it must be noted that primary radicals derived from arenosulfonyl chlorides can only recombine after addition of at least one monomer unit.

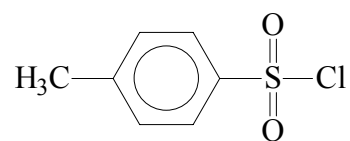
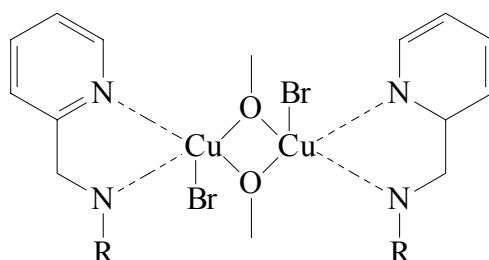


**Figure 3.5** Arenosulfonylchloride initiator.

### 3.3.4 Peculiarities

The mechanism of the ATRP system still is an obscure and not completely understood issue. Whether or not it follows the classical radical polymerisation scheme is still a matter of debate. Observations that seem to contradict the current point of view, among other things, concern the effect of phenols in ATRP reactions<sup>71,72</sup> reported by Haddleton *et al.* Phenol, as well as a range of substituted phenols, which normally act

as free-radical inhibitors<sup>73</sup> in ATRP appear to accelerate the polymerisation. The authors acknowledge the fact that these compounds usually perform better as inhibitor when oxygen is present. In view of the absence of an induction period, which is normally always observed when polymerising methyl methacrylate with copper/Schiff's base ligands, Haddleton *et al.* conclude that phenols definitely have an effect on the reaction mechanism. In fact, they suggested the formation of a bridged copper complex as depicted in Scheme 3.8.



**Scheme 3.8** Proposed structure of bridged copper species upon addition of phenol.

At the beginning of polymerisation, phenol rapidly forms the bridged copper species, which then could abstract a halogen atom from the dormant species. The existence of these dinuclear copper species, albeit in the solid state, has been demonstrated by single crystal X-ray diffraction. A parallel can be drawn with the accelerating effect of water on the polymerisation of methyl methacrylate<sup>74</sup>. In this case, it has been speculated that dinuclear species are formed as well. These dinuclear species could be responsible for the accelerating effect.

This kind of behaviour clearly shows that the origin of the active species in ATRP, as well as the mechanism, is still not clarified.

### 3.3.5 Possibilities and limitations

Up to the present moment, numerous publications have reported the successful application of ATRP to produce well-defined polymers.

Concerning homopolymerisations, styrene and methyl methacrylate are the most intensively studied monomers<sup>36</sup>. Styrene can be polymerised up to molecular weights of  $90000 \text{ g}\cdot\text{mol}^{-1}$ , although it should be noted that good control ( $\text{PDI} < 1.1$ ) is only obtained when molecular weights remain below  $30000 \text{ g}\cdot\text{mol}^{-1}$ . A temperature of  $110^\circ\text{C}$  is typically applied<sup>42</sup>. Methyl methacrylate can be polymerised up to much higher molecular weights ( $180000 \text{ g}\cdot\text{mol}^{-1}$ ), without significant loss of control of the molecular-weight distribution<sup>75</sup>.

Furthermore, as already mentioned earlier in section 3.3.3.2, also substituted styrenes, (meth)acrylates, acrylonitrile and even some acids can be polymerised. Since ATRP is relatively tolerant towards functional groups, the preparation of polymers bearing functional groups is possible. So far, current ATRP systems are not able to polymerise monomers that yield less stabilised radicals such as  $\alpha$ -olefins, vinyl acetate and vinyl chloride.

A very important possibility of ATRP is the relatively easy preparation of block copolymers, and almost any combination of blocks has been reported in literature<sup>76,77</sup>. The reports on the ATRP equivalent of statistical copolymerisations, however, are not abundant. Only copolymerisation of methyl methacrylate/butyl methacrylate<sup>32</sup>, styrene/methyl methacrylate<sup>78</sup>, methyl methacrylate/methyl acrylate<sup>79</sup>, methyl methacrylate/butyl acrylate<sup>79,59,80</sup> and styrene/butyl acrylate<sup>81</sup> have been reported up to now. The most sought-after question in these investigations is whether the reactivity ratios of the monomers are equal to those observed in free-radical polymerisation, since this could give a clue about the radical nature of the ATRP process. Since in controlled polymerisation techniques all chains grow during the whole reaction time, it is necessary to investigate polymerisations up to higher conversions. Haddleton *et al.*<sup>32</sup> were the first to compare reactivity ratios of the copolymerisation of methyl acrylate and methyl methacrylate in free-radical polymerisation and in ATRP. Although they did not investigate the system up to high conversions, they concluded that reactivity ratios were similar for both polymerisation techniques. Roos and Müller<sup>80</sup> investigated the copolymerisation of butyl acrylate and butyl methacrylate, but also did not investigate the system up to higher conversion. Arehart *et al.*<sup>81</sup> looked into the copolymerisation of styrene and butyl acrylate and analysed the comonomer ratio in the residual monomer mixture as a function of conversion. Arehart and co-workers found a decreasing rate of polymerisation in time and ascribed this effect to the occurrence of side-reactions, which cause an increased amount of termination. These side-reactions, as they speculate, are due to a change in monomer feed composition that shifts towards butyl acrylate rich as a result of composition drift. This change of environment has an enhancing effect on the activation of styrene dormant species. This enhanced activation causes an increase in the radical concentration, which ultimately results in more bimolecular termination.

Not only in homogeneous systems ATRP has been successfully applied. There are a few reports on the emulsion polymerisations of various monomers<sup>74,82</sup>. Notwithstanding the fact that latex stability and control of molecular weight are difficult to achieve, the prospects of applying ATRP to heterogeneous systems seem very bright.

### 3.4 FUTURE PROSPECTS

It seems that enough qualitative knowledge on ATRP is available to produce ‘simple’ well-defined polymers. Molecular weight and molecular-weight distribution have been proven to be easily controllable, and the synthesis of block copolymers, given the fact that it only concerns two consecutive homopolymerisations, has been mastered fairly smoothly.

However, at present thorough quantitative knowledge on ATRP, which is absolutely necessary when the production of more sophisticated polymers is desired, is still lacking. The synthesis of copolymers with a compositional gradient along the chain, for instance, is still a difficult task and requires detailed kinetic knowledge on the ATRP system. So far, little quantitative data is available on the activation and deactivation of dormant species and growing radicals, respectively. Reactivity ratios in ATRP copolymerisation have been given attention rarely.

Fundamental knowledge on the parameters that govern ATRP, such as the activation and deactivation rate parameters, as well as accurate and reliable reactivity ratios, therefore is of utmost importance. When this vital information becomes available, not only copolymers with well-defined molecular weights can be produced, but also with truly well-defined intramolecular chemical composition distributions.

The strategy of the following chapters is therefore chosen to be logical and simple. The copolymerisation system styrene/butyl acrylate has been chosen as a model system. In the first step, the fundamental kinetic parameters that govern the ATRP of styrene and butyl acrylate will be investigated. General guidelines to obtain information on the activation and deactivation rate coefficients will be provided. Hereafter, the coefficients will be used to assess their applicability in the ATRP copolymerisation of styrene and butyl acrylate. In the third and last step, the kinetic knowledge will be used to synthesise copolymers of styrene and butyl acrylate with pre-defined intramolecular composition distribution.

### REFERENCES

- <sup>1</sup> Moad, G., Solomon, D.H., *The Chemistry of Free Radical Polymerization*, 1<sup>st</sup> ed., Elsevier Science Ltd.: Oxford, 1995
- <sup>2</sup> Iván, B.; Kennedy, J.P. *Macromolecules* **1990**, *23*, 2880
- <sup>3</sup> Webster, O.W.; Hertler, W.R.; Sogah, D.Y.; Farnham, W.B.; Rajanbabu, T.V. *J. Am. Chem. Soc.* **1983**, *105*, 5706
- <sup>4</sup> Webster, O.W. *Makromol. Chem., Macromol. Symp.* **1990**, *33*, 133

- 5 Kaminsky, W.; Miri, M.; Sinn, H.; Woldt R. *Makromol. Chem., Rapid Commun.* **1983**, *4*, 417
- 6 Darling, T.R.; Davis, T.P.; Fryd, M.; Gridnev, A.A.; Haddleton, D.M.; Ittel, S.D.; Matheson Jr.,  
R.R.; Moad, G.; Rizzardo, E. *J. Polym. Sci.: Part A: Polym. Chem.* **2000**, *38*, 1708
- 7 Otsu, T.; Yoshida, M. *Makromol. Chem., Rapid Commun.* **1982**, *3*, 127
- 8 Nair, C.P.R.; Chaumont, P.; Clouet, G. *J. Macromol. Sci., Chem.* **1990**, *A27*, 791
- 9 Turner, S.R.; Blevins, R.W. *Macromolecules* **1990**, *23*, 1856
- 10 Druliner, J.D.; *Macromolecules* **1991**, *24*, 6079
- 11 Arvanitopoulos, L.D.; Greuel M.P.; Harwood, H.J. *Polym. Prepr.* **1994**, *35*, 549
- 12 Wayland, B.B.; Poszmik, G.; Mukerjee, S.L. *J. Am. Chem. Soc.* **1994**, *116*, 7943
- 13 Solomon, D.H.; Rizzardo, E.; Cacioli, P. *European Patent Application* **1985**, 135 280 A2
- 14 Rizzardo, E. *Chem. Aust.* **1987**, *54*, 32
- 15 Georges, M.K.; Veregin, R.P.N.; Kazmaier, P.M.; Hamer, G.K. *Macromolecules* **1993**, *26*, 2987
- 16 Georges, M.K.; Veregin, R.P.N.; Kazmaier, P.M.; Hamer, G.K. *Macromolecules* **1993**, *26*, 5316
- 17 Grimaldi, S.; Finet, J.-P.; Zeghdaoui, A.; Tordo, P.; Benoit, D.; Gnanou, Y.; Fontanille, M.; Nicol,  
P.; Pierson, J.-F. *Polym. Prepr.* **1997**, *38* (1), 651
- 18 Benoit, D.; Grimaldi, S.; Finet, J.-P.; Tordo, P.; Fontanille, M.; Gnanou, Y. *Polym. Prepr.* **1997**,  
*38* (1), 729
- 19 Le, T.; Moad, G.; Rizzardo, E.; Thang, S.H. PCT Int. Appl. WO 9801478 A1 980115 (1998)
- 20 Chiefari, J.; Chong, Y.K.; Ercole, F.; Krstina, J.; Jeffery, J.; Le, T.P.T.; Mayadunne, R.T.A.; Meijs,  
G.F.; Moad, C.L.; Moad, G.; Thand, S.H. *Macromolecules* **1998**, *31*, 5559
- 21 Kato, M.; Kamigaito, M.; Sawamoto, M.; Higashimura, T. *Macromolecules* **1995**, *28*, 1721
- 22 Wang, J.S.; Matyjaszewski, K. *Macromolecules* **1995**, *28*, 7901
- 23 Greszta, D.; Mandare, D.; Matyjaszewski, M. *Macromolecules* **1994**, *27*, 638
- 24 Kharash, M.S.; Jensen, E.U.; Urry, W.H. *Science* **1945**, *102*, 128
- 25 Bellus, D. *Pure Appl. Chem.* **1985**, *57*, 1827
- 26 Lee, G.M.; Weinreb, S.M. *J. Org. Chem.* **1990**, *55*, 1281
- 27 Grove, D.M.; van Koten, G.; Verschuuren, A.H.M. *J. Mol. Catal.* **1988**, *45*, 169
- 28 Tsuji, J.; Sato, K.; Nagashima, H. *Chem. Lett.* **1981**, 1169
- 29 Kamigata, N.; Sawada, H.; Kobayashi, M. *Tetrahedron Lett.* **1979**, 159
- 30 Asscher, M.; Vofsi, D. *J. Chem. Soc.* **1963**, *1963*, 1887
- 31 Miessler, G.L.; Tarr, D.A., *Inorganic Chemistry*; Prentice Hall: Englewood Cliffs, 1991
- 32 Haddleton, D.M.; Crossman, M.C.; Hunt, K.H.; Topping, C.; Waterson, C.; Suddaby, K.G.  
*Macromolecules* **1997**, *30*, 3992
- 33 Wang, J.S.; Matyjaszewski, K. *Macromolecules* **1995**, *28*, 7572
- 34 Moineau, G.; Dubois, Ph.; Jérôme, R.; Senninger, T.; Teyssié, Ph. *Macromolecules* **1998**, *31*, 545
- 35 Matyjaszewski, K.; Coca, S.; Gaynor, S.G.; Wei, M.; Woodworth, B.E. *Macromolecules* **1998**, *31*,  
5967
- 36 Matyjaszewski, K., *Controlled Radical Polymerization*; ACS Symposium Series No. 685;  
American Chemical Society: Washington DC, 1997
- 37 Matyjaszewski, K. *Chem. Eur. J.* **1999**, *5* (11), 3095
- 38 Matyjaszewski, K. *J. Macromol. Sci. – Pure Appl. Chem.* **1997**, *A34*(10), 1785
- 39 Fukuda, T.; Goto, A.; Ohno, K. *Macromol. Rapid Commun.* **2000**, *21*, 151
- 40 Goto, A.; Fukuda, T. *Macromolecules* **1997**, *30*, 4272

- 41 Buback, M. Gilbert, R.G.; Hutchinson, R.A.; Klumperman, B.; Kuchta, F.-D.; Manders, B.G.; O'Driscoll, K.F.; Russell, G.T.; Schweer, J. *Macromol. Chem. Phys.* **1995**, *196*, 3267
- 42 Matyjaszewski, K.; Patten, T.E.; Xia, J. *J. Am. Chem. Soc.* **1997**, *119*, 674
- 43 Fischer, H. *J. Am. Chem. Soc.* **1986**, *108*, 3925
- 44 Fischer, H. *Macromolecules* **1997**, *30*, 5666
- 45 Ohno, K.; Goto, A.; Fukuda, T.; Xia, J.; Matyjaszewski, K. *Macromolecules* **1998**, *31*, 2699
- 46 Granel, C.; Teyssié, Ph.; DuBois, Ph.; Jérôme, R. *Macromolecules* **1996**, *29*, 8576
- 47 Uegaki, H.; Kotani, Y.; Kamigaito, M.; Sawamoto, M. *Macromolecules* **1997**, *30*, 2249
- 48 Ando, T.; Kamigaito M.; Sawamoto, M. *Macromolecules* **1997**, *30*, 4507
- 49 De Man, P.A.P. *Graduation Thesis*; Technische Universiteit Eindhoven: Eindhoven, 1998
- 50 Latimer, W.M., *The Oxidation States of the Elements and Their Potentials in Aqueous Solution*, 2<sup>nd</sup> ed., Prentice Hall: New York, 1952
- 51 James, B.R.; Williams, R.J.P. *J. Chem. Soc.* **1961**, 2007
- 52 Haddleton, D.M.; Shooter, A.J.; Hannon, M.J.; Barker, J.A. *Polym. Prepr.* **1997**, *38(1)*, 679
- 53 Haddleton, D.M.; Jasieczek, C.B.; Hannon, M.J.; Shooter, A.J. *Macromolecules* **1997**, *30*, 2190
- 54 Matyjaszewski, K. *Curr. Opin. So. St. Mat. Sci.* **1996**, *1*, 769
- 55 Reinhold, J.; Benedix, R.; Birner, P.; Hennig, H. *Inorg. Chim. Acta* **1979**, *33*, 209
- 56 Destarac, M.; Bessière, J.-M.; Boutevin, B. *Macromol. Rapid Commun.* **1997**, *18*, 967
- 57 Xia, J.; Matyjaszewski, K. *Macromolecules* **1997**, *30*, 7697
- 58 Qiu, J.; Matyjaszewski, K. *Macromolecules* **1997**, *30*, 5643
- 59 Moineau, G.; Minet, M.; Dubois, Ph.; Teyssié, Ph.; Senninger, T.; Jérôme, R. *Macromolecules* **1999**, *32*, 27
- 60 Xia, J.; Gaynor, S.G.; Matyjaszewski, K. *Macromolecules* **1998**, *31*, 5958
- 61 Jo, S.M.; Paik, H.-J.; Matyjaszewski, K. *Polym. Prepr.* **1997**, *38(1)*, 697
- 62 Coca, S.; Jasieczek, C.B.; Beers, K.L.; Matyjaszewski, K. *J. Polym. Sci. Polym. Chem. Ed.* **1998**, *36*, 1417
- 63 Ashford, E.J.; Naldi, V.; O'Dell, R.; Billingham, N.C.; Armes, S.P. *Chem. Commun.* **1999**, 1285
- 64 Wang, X.-S.; Jackson, R.A.; Armes, S.P. *Macromolecules* **2000**, *33*, 255
- 65 Haddleton, D.M.; Crossman, M.C.; Dana, B.H.; Duncalf, D.J.; Heming, A.M.; Kukulj, D.; Shooter, A.J. *Macromolecules* **1999**, *32*, 2110
- 66 Pascual, S.; Coutin, B.; Tardi, M.; Polton, A.; Vairon, J.-P. *Macromolecules* **1999**, *32*, 1432
- 67 Wei, M.; Matyjaszewski, K.; Patten, T.E. *Polym. Prepr.* **1997**, *38(1)*, 683
- 68 Davis, K.; O'Malley, J.; Paik, H.-J.; Matyjaszewski, K. *Polym. Prepr.* **1997**, *38(1)*, 687
- 69 Percec, V.; Barboiu, B. *Macromolecules* **1995**, *28*, 7970
- 70 Percec, V.; Barboiu, B.; Neumann, A.; Ronda, J.C.; Zhao, M. *Macromolecules* **1996**, *29*, 3665
- 71 Haddleton, D.M.; Shooter, A.J. *Polym. Prepr.* **1997**, *38(1)*, 738
- 72 Haddleton, D.M.; Shooter, A.J.; Heming, A.M.; Crossman, M.C.; Duncalf, D.J.; Morsley, S.R. In *Controlled Radical Polymerization*; Matyjaszewski, K., Ed.; ACS Symposium Series No. 685; American Chemical Society: Washington DC, 1997; p 284
- 73 Moad, G., Solomon, D.H., *The Chemistry of Free Radical Polymerization*, 1<sup>st</sup> ed., Elsevier Science Ltd.: Oxford, 1995, 260
- 74 Chambard, G; de Man, P.A.P.; Klumperman, B. *Macromol. Symp.* **2000**, *150*, 45
- 75 Grimaud, T.; Matyjaszewski, K. *Macromolecules* **1997**, *30*, 2216
- 76 Shipp, D.A.; Wang, J.-L.; Matyjaszewski, K. *Macromolecules* **1998**, *31*, 8005

- <sup>77</sup> Cassebras, M.; Pascual, S.; Polton, A.; Tardi, M.; Vairon, J.-P. *Macromol. Rapid Commun.* **1999**, *20*, 261
- <sup>78</sup> Kotani, Y.; Kamigaito, M.; Sawamoto, M. *Macromolecules* **1998**, *31*, 5582
- <sup>79</sup> Uegaki, H.; Kotani, Y.; Kamigaito, M.; Sawamoto, M. *Macromolecules* **1998**, *31*, 6756
- <sup>80</sup> Roos, S.G.; Müller, A.H.E.; Matyjaszewski, K. *Macromolecules* **1999**, *32*, 8331
- <sup>81</sup> Arehart, S.V.; Matyjaszewski, K. *Macromolecules* **1999**, *32*, 2221
- <sup>82</sup> Gaynor, S.G.; Qiu, J.; Matyjaszewski, K. *Macromolecules* **1999**, *31*, 5951

# 4

## *ATRP Homopolymerisations of Styrene and Butyl Acrylate*

**Synopsis:** Prior to the description of the ATRP copolymerisation of styrene and butyl acrylate, the homopolymerisations are dealt with. The goal of this chapter is twofold. First, kinetic data on the important parameters that govern the ATRP homopolymerisations of styrene and butyl acrylate are necessary to describe the ATRP copolymerisation and, therefore, need to be obtained. Second, performing the homopolymerisations of styrene and butyl acrylate enables one to familiarise with the ATRP system and to master experimental difficulties, thereby optimising the polymerisation procedure.

Since quantitative data on the kinetics of ATRP is scarce in current literature, this chapter will mainly focus on the determination of fundamental parameters in ATRP, more notably the activation and deactivation rate coefficients for polystyrene and poly(butyl acrylate) dormant species and growing radical, respectively. The implication of these parameters on the rate of polymerisation is evaluated thoroughly.



## 4.1 INTRODUCTION

When aiming at the control of the copolymerisation reaction of styrene (S) and butyl acrylate (BA), a certain number of parameters that determine the course of the homopolymerisation reactions have to be identified and evaluated. For this purpose, it is wise to take a look at Eq. (3.14) from the previous chapter again.

$$-\ln(1-\xi) = \ln\left(\frac{[M]_0}{[M]}\right) = \frac{3}{2}k_p \left(\frac{k_{act}[I-X]_0[M_t^n]_0}{6k_{deact}k_t}\right)^{1/3} t^{2/3} \quad (3.14)$$

It should be kept in mind that several assumptions have been made to derive Eq. (3.14), as is also stated in chapter 3. If thermal initiation, for instance, plays a significant role in the ATRP of S and BA, the kinetics of the homopolymerisations do not obey Eq. (3.14). In that case, the thermal initiation should be quantified and taken into account.

It is clear from Eq. (3.14), that in principle four rate parameters play a role in the kinetics of the homopolymerisation. The initial concentrations of catalyst,  $[M_t^n]_0$ , and initiator,  $[I-X]_0$ , can be varied independently. The propagation rate constant,  $k_p$ , the termination rate constant,  $k_t$ , and the activation and deactivation rate coefficients,  $k_{act}$  and  $k_{deact}$ , respectively, are the parameters that are inherent to the system itself. The ATRP system, therefore, is determined only by these four rate parameters and in order to describe the homopolymerisations of S and BA, it is necessary to quantify these parameters.

## 4.2 RATE COEFFICIENTS FOR PROPAGATION AND TERMINATION

The first parameter,  $k_p$ , can easily be implemented in the kinetic analyses, since it is well known for a number of monomers, including S and BA, over a large range of temperatures. The most accurate and reliable propagation rate constants have been determined using pulsed-laser polymerisation<sup>1</sup> and subsequent analysis by size exclusion chromatography (SEC). However, one should always keep in mind that the values of these propagation rate constants have been measured for conventional free-radical polymerisation. As already pointed out in chapter 3, the exact mechanism of ATRP is still unclear and there could well be a possibility that it does not follow conventional free-radical-polymerisation schemes. Nevertheless, considering the

strong indications in favour of a free-radical mechanism, it seems justifiable to assume that the propagation rate constants in ATRP equal to those for free-radical polymerisation. We therefore use the following Arrhenius equations for the propagation rate constants for S<sup>2</sup> and BA<sup>3</sup>.

$$k_p^S = 10^{7.63} e^{-\frac{32.5 \cdot 10^3}{R \cdot T}} \quad (4.1)$$

$$k_p^{BA} = 10^{7.28} e^{-\frac{17.5 \cdot 10^3}{R \cdot T}} \quad (4.2)$$

In these expressions,  $R$  is the gas constant (8.314 J·mol<sup>-1</sup>·K<sup>-1</sup>) and  $T$  is the temperature in Kelvin. At 110°C, the propagation rate constant for S equals 1.58·10<sup>3</sup> L·mol<sup>-1</sup>·s<sup>-1</sup> and for BA 7.84·10<sup>4</sup> L·mol<sup>-1</sup>·s<sup>-1</sup>.

For the bimolecular termination rate coefficients,  $k_t$ , we also can use the existing knowledge on free-radical termination. Bimolecular termination is known to be diffusion-controlled and depends on the diffusion coefficient of the radicals in the reaction medium. A common way to express the termination rate constant in terms of diffusion coefficients is via the so-called Smoluchovski equation<sup>4,5</sup>, Eq. (4.3).

$$k_t^{i,j} = 2\pi\sigma p(D_i + D_j)N_A \quad (4.3)$$

In this equation,  $\sigma$  is the capture radius of the termination reaction,  $p$  is the so-called spin multiplicity factor,  $D_i$  is the diffusion coefficient of a polymeric radical with chain length  $i$  and  $N_A$  is Avogadro's number.

In classical free-radical polymerisation, small radicals are generated during the whole reaction and bimolecular termination therefore predominantly occurs by short-short or short-long termination. As the average chain length hardly changes during the polymerisation reaction, the average termination rate coefficient only depends on the viscosity of the medium, *i.e.* on the weight fraction of polymer in the system. In ATRP, however, as in other living radical polymerisations such as nitroxide-mediated living radical polymerisation, generation of small radicals only occurs in the beginning of the reaction. Chains grow during the complete reaction time and it is therefore necessary to account for the chain-length dependence of the average termination rate coefficient in addition to the weight fraction of polymer.

There are numerous theoretical models reported in literature that describe the chain length dependence of termination rate coefficients. In view of the Smoluchovski

equation stated above, it seems logical to look at the chain-length-dependent diffusion coefficient,  $D_i$ . For methyl methacrylate and butyl methacrylate, the chain-length-dependent diffusion coefficient can empirically be described by Eq. (4.4)<sup>6</sup>.

$$D_i = D_0 i^{-(0.664+2.02w_p)} \quad (4.4)$$

The diffusion coefficient in Eq. (4.4),  $D_i$ , is not only a function of chain length,  $i$ , but also of the viscosity of the reaction mixture, reflected by the weight fraction of polymer,  $w_p$ .  $D_0$  is the diffusion coefficient of the monomer species. This empirical equation has been determined for both butyl methacrylate and methyl methacrylate oligomers in both butyl methacrylate and methyl methacrylate matrices at concentration above  $c^*$ , *i.e.* the concentration at which chain overlap commences. Surprisingly -and fortunately- it also seems to describe data on styrene oligomers in a matrix of polystyrene<sup>7</sup>.

When Eq. (4.4) is substituted into the Smoluchowski equation, an expression for the chain-length-dependent termination rate coefficient,  $k_t^{i,j}$ , is obtained:

$$k_t^{i,j} = 2\pi\sigma p(D_0 i^{-(0.664+2.02w_p)} + D_0 j^{-(0.664+2.02w_p)})N_A \quad (4.5)$$

Fortunately, expression (4.5) can be simplified for an ATRP system. A characteristic feature of ATRP should be that the initiator is consumed at the beginning of the reaction and that, consequently, all chains start growing at the same time. Strictly speaking, this situation is never attained, but low polydispersities strongly indicate that the initiation time is much shorter than the total duration of the polymerisation. It is therefore justified to assume that all chains grow during approximately the whole reaction time. This has two important implications. First, at any moment in time, all chains have approximately the same chain length and, as a consequence, only bimolecular termination involving two polymeric radicals of the same chain length occurs. The chain-length-dependent termination rate coefficient can therefore be simplified and written as follows:

$$k_t^{i,i} = k_t^0 i^{-(0.664+2.02w_p)} \quad (4.6)$$

In Eq. (4.6)  $k_t^0$  is the termination rate coefficient for a polymer with chain length 1. Second, given the fact that all chains start at approximately the same moment, it is possible to relate the chain length,  $i$ , to the overall conversion. The chain length and the weight fraction of polymer are related to the fractional conversion,  $\xi$ , as follows, see Eqs. (4.7) and (4.8), respectively.

$$i = 1 + \frac{[M]_0}{[I-X]_0} \xi \quad (4.7)$$

$$w_p = w_{M,0} \xi \quad (4.8)$$

The monomer weight fraction at the start of the reaction is denoted as  $w_{M,0}$ . The chain-length dependent termination rate coefficient can be expressed as function of conversion by substituting Eqs. (4.7) and (4.8) into (4.6) yielding Eq. (4.9).

$$k_t^\xi = k_t^0 \left( 1 + \frac{[M]_0}{[I-X]_0} \xi \right)^{-(0.664+2.02 \cdot w_{M,0} \cdot \xi)} \quad (4.9)$$

The termination rate coefficient is monotonously decreasing upon increasing conversion. For a polymerisation reaction with  $[M]_0 = 100 \cdot [I-X]_0$  and  $k_t^0 = 1 \cdot 10^8 \text{ L} \cdot \text{mol}^{-1} \cdot \text{s}^{-1}$ , the value of  $k_t^\xi$  is plotted in Figure 4.1.

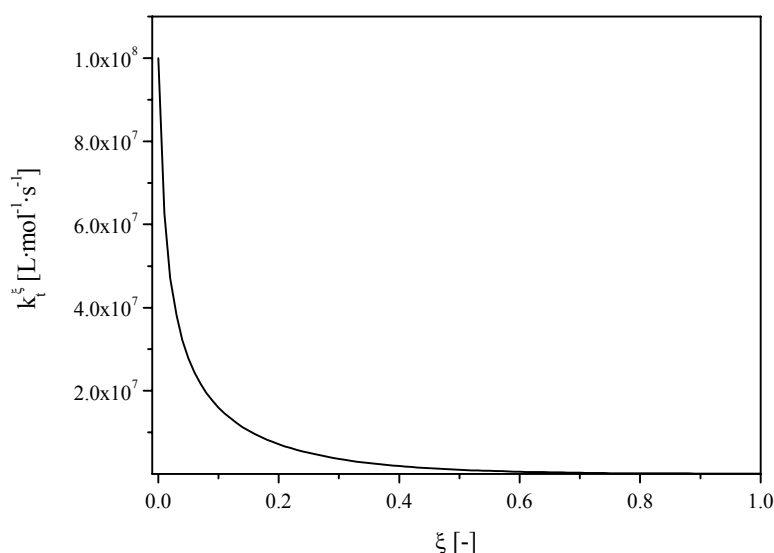


*Figure 4.1 Evolution of  $k_t^\xi$  as a function of fractional conversion for a polymerisation reaction with  $[M]_0 = 100 \cdot [I-X]_0$  and  $k_t^0 = 1 \cdot 10^8 \text{ L} \cdot \text{mol}^{-1} \cdot \text{s}^{-1}$ .*

The expression for the conversion-dependent termination rate coefficient will thus be used in Eq. (3.11) to describe ATRP homopolymerisations. As a consequence, the evolution of  $\ln([M]_0/[M])$  vs. time does no longer show a  $2/3$  order dependence, but becomes much more complex.

## 4.3 DETERMINATION OF $k_{ACT}$

### 4.3.1 Background

Fukuda *et al.*<sup>8</sup> introduced a simple method to experimentally determine the activation rate coefficient using size exclusion chromatography (SEC). In their method, the macroinitiator is added together with monomer, the transition metal complex (the authors used a  $Cu^+/(2,2'$ -di-(4-nonyl)-4,4'-bipyridine)<sub>2</sub> complex) and a conventional free-radical initiator such as *tert*-butyl hydroperoxide. According to Fukuda *et al.* the technique is based on decreasing the rate of deactivation by the reaction of the radicals originating from the conventional free-radical initiator with the  $Cu^{2+}$  species. The lifetime of the radicals originating from the macroinitiator will therefore increase and more monomer units are added before deactivation takes place. The decrease of the macroinitiator concentration then obeys pseudo-first order kinetics and this can then be monitored by SEC according to:

$$\ln\left(\frac{S_0}{S_t}\right) = k_{act}[Cu^+]_0 \cdot t \quad (4.10)$$

In this relation  $S_0$  and  $S_t$  are the normalised areas of the macroinitiator peaks in SEC at the beginning of the reaction and at time  $t$ . In order to get good resolution in SEC the amount of conventional free-radical initiator must be fine-tuned, which is a difficult and often impractical task. If the concentration of radicals derived from the conventional free-radical initiator is too low, the concentration of  $Cu^{2+}$  species is too high. The radicals originating from the macroinitiator will then only add a few monomer units before being deactivated again. The difference in molecular weights between the resulting product and the original macroinitiator will be too low to get good resolution in SEC. On the other hand, when the concentration of the initiator-derived radicals is too high, the radicals coming from the macroinitiator would bimolecularly terminate prematurely. In this case as well, resolution in SEC is too poor to extract quantitative data from these experiments. Furthermore, with this

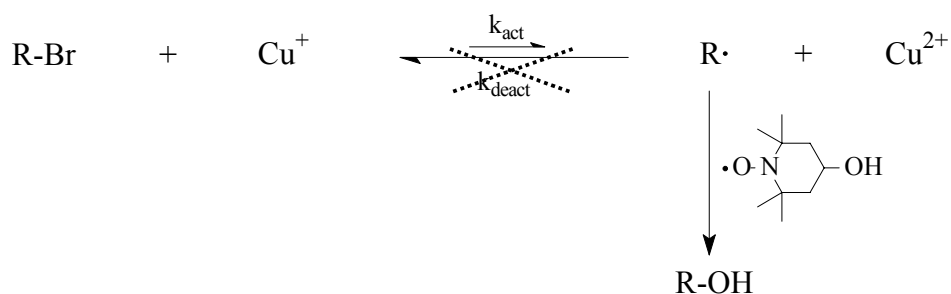
method  $k_{act}$  can only be determined in the presence of a monomer, preferably a monomer with a high propagation rate constant, in order to ensure good peak separation in SEC. Very recently, Fukuda *et al.* reported a second method to determine activation rate coefficients<sup>9</sup>. The method is based on a similar principle, *i.e.* the impediment of reversible deactivation, and also in this case pseudo-first order kinetics are obtained. Only, in this method they use a stable free radical (2,2,6,6-tetramethylpiperidine-*N*-oxyl or TEMPO) to trap the radical originating from the macroinitiator. The decrease in concentration of the macroinitiator can be monitored by means of <sup>1</sup>H NMR.

### 4.3.2 Nitroxide exchange reactions

The method that is used in this section to determine the activation rate coefficients of polystyrene (PS) and poly(butyl acrylate) (PBA) dormant species utilises exchange reactions that are also the basis for determining the dissociation rate constants of alkoxyamines<sup>10</sup>.

As already mentioned, the activation rate coefficient of the macroinitiator,  $k_{act}$ , can be determined when the deactivation of the radical that is formed after halogen abstraction is minimized. This can be assured by trapping the radical immediately and irreversibly by another species. A very effective way to trap the radicals is by using stable free radicals, in particular nitroxides. These nitroxides are known to react with carbon-centred radicals at almost diffusion-controlled rates<sup>11</sup>.

We consider a system comprising solvent, transition metal complex, *e.g.* Cu/(4,4'-*n*-heptyl-2,2'-bipyridine)<sub>2</sub>, macroinitiator (R-Br) and a hydroxy-functional stable free nitroxide (4-hydroxy-2,2,6,6-tetramethylpiperidine-*N*-oxyl, hydroxy-TEMPO). Upon heating, the halide atom will be transferred from the macroinitiator to the copper complex. The radicals formed are then irreversibly trapped by the stable nitroxide radical to yield a hydroxy-functional species, R-OH (Scheme 4.1). Note that the deactivating species is denoted as Cu<sup>2+</sup>.



*Scheme 4.1 Exchange reactions with hydroxy-TEMPO.*

In order to obtain an irreversible second-order reaction, the only fate of the radicals originating from the macroinitiator must be to be trapped by hydroxy-TEMPO. Transformation back to the dormant species should be prevented, which can be achieved by using an excess of hydroxy-TEMPO. When neglecting transfer reactions, the probability of R· being trapped by hydroxy-TEMPO,  $p_{tr}$ , obeys equation (4.11). Note that hydroxy-TEMPO is abbreviated with T.

$$p_{tr} = \frac{k_{tr} \cdot [T]}{k_{tr} \cdot [T] + k_{deact} \cdot [Cu^{2+}] + k_t \cdot [R\cdot]} \quad (4.11)$$

When using  $[T]=0.1 \text{ mol}\cdot\text{L}^{-1}$ , together with appropriate values for the trapping rate constant ( $k_{tr} \approx 10^8 \text{ L}\cdot\text{mol}^{-1}\cdot\text{s}^{-1}$  <sup>11</sup>), the termination rate constant ( $k_t \approx 10^8 \text{ L}\cdot\text{mol}^{-1}\cdot\text{s}^{-1}$  <sup>12</sup>), the deactivation rate coefficient ( $k_{deact} \approx 10^7 \text{ L}\cdot\text{mol}^{-1}\cdot\text{s}^{-1}$  <sup>8</sup>), the radical concentration ( $[R\cdot] \approx 5 \cdot 10^{-3} \text{ mol}\cdot\text{L}^{-1}$ ) and deactivator concentration ( $[Cu^{2+}] \approx 5 \cdot 10^{-3} \text{ mol}\cdot\text{L}^{-1}$ ), this probability nearly equals 1 and all radicals are clearly trapped by the nitroxide.

For an irreversible second-order reaction, as depicted in Scheme 4.1, in a constant density batch process, the following differential equation holds:

$$-\frac{d[R - Br]}{dt} = k_{act} [R - Br][Cu^+] \quad (4.12)$$

When we take into account that the  $[Cu^+]$  decreases as well in the exchange reactions, the general solution for Eq. (4.12) is:

$$\ln\left(\frac{[R - Br]_0}{[R - Br]_t}\right) + \ln\left(\frac{[Cu^+]_0 - [R - Br]_0 + [R - Br]_t}{[Cu^+]_0}\right) = ([Cu^+]_0 - [R - Br]_0)k_{act} \cdot t \quad (4.13)$$

Experimentally, the macroinitiator can be separated from the hydroxy-functional product by quantitative HPLC. Therefore, the decrease in concentration of dormant species can be monitored as a function of time. When the left-hand side of Eq. (4.13) is plotted vs. time, a linear relationship is obtained whose slope corresponds to  $([Cu^+]_0 - [R - Br]_0) \cdot k_{act}$ .

The method is actually similar to the one that Fukuda *et al.* proposed<sup>9</sup>, but the analysis in our investigation rests on the application of high performance liquid chromatography (HPLC) in combination with evaporative light scattering detection.

### 4.3.3 Experimental

#### *Materials:*

The ligand, 4,4'-di-*n*-heptyl-2,2'-bipyridine (dHbpy), was synthesised according to a literature procedure<sup>13</sup>. Styrene (S, Aldrich, 99%) and butyl acrylate (BA, Aldrich, 99+%) were distilled and stored over molecular sieves. *p*-Xylene (Aldrich, 99+% HPLC grade) and dry *N,N*-dimethylformamide (DMF, Biosolve, 99.8%) were stored over molecular sieves and used without further purification. Butyl acetate (BuAc, Merck, 99+%), 1,4-dioxane (Biosolve, 99.8%) and 1-butanol (Aldrich, 99.8% HPLC grade) were used as received. CuBr (Aldrich, 98%), ethyl 2-bromoisobutyrate (Aldrich, 98%) and hydroxy-TEMPO (Aldrich) were used without further purification.

#### *Macroinitiator synthesis:*

Polystyrene (PS-Br) and poly(butyl acrylate) (PBA-Br) macroinitiators were synthesised using ATRP. *p*-Xylene (10.0 g), monomer (10.0 g of S or 12.3 g of BA, 0.0960 mol), ethyl 2-bromoisobutyrate (0.624 g,  $3.20 \cdot 10^{-3}$  mol) and dHbpy (0.549 g,  $1.56 \cdot 10^{-3}$  mol) were mixed in a 100 mL round-bottom flask. The mixture was then purged with argon for 30 min, after which CuBr (0.112 g,  $7.81 \cdot 10^{-4}$  mol) was added. The reaction mixture was homogenized and purged with argon for another 30 min, after which the reaction mixture was heated to 110 °C. After elapse of a certain period of time, the reaction mixture was quenched and passed over a column with aluminumoxide (activated, neutral, Brockman I, STD grade approx. 150 mesh, 58Å, Aldrich) to remove the copper catalyst using stabilized tetrahydrofuran (AR, Biosolve) as eluent. After subsequent drying, the dry polymers were dissolved in stabilised tetrahydrofuran at 1 mg·mL<sup>-1</sup> and filtrated using 0.2 µm filters. The molecular weights were determined by size exclusion chromatography (SEC) with a Waters Model 510 pump and Waters 712 WISP using 4 PL-gel mix C columns (300mm×7.5mm, Polymer Laboratories) at 40°C and tetrahydrofuran as the eluent. The eluent flow rate was 1.0 mL·min<sup>-1</sup>. Calibration was performed with polystyrene standards with narrow molecular-weight distributions (Polymer Laboratories). They were 1600 g·mol<sup>-1</sup> for PS-Br ( $M_w/M_n=1.08$ ) and 2300 g·mol<sup>-1</sup> for PBA-Br ( $M_w/M_n=1.16$ ). The BA polymers were not corrected with Mark-Houwink



parameters from literature<sup>14</sup>, since molecular weights were too small for the parameters to be applicable.

#### *Exchange reactions:*

Exchange reactions were carried out in *p*-xylene, 1,4-dioxane, butyl acetate, 1-butanol and DMF. A typical procedure for an exchange reaction with PS-Br in *p*-xylene is as follows. *p*-Xylene (10 mL), hydroxy-TEMPO (0.172 g,  $1.00 \cdot 10^{-3}$  mol), dHbpy (0.141 g,  $4.01 \cdot 10^{-4}$  mol) and PS-Br (0.0792 g,  $5.00 \cdot 10^{-5}$  mol) were mixed in a 100 mL round-bottom flask. Note that a 20-fold excess of hydroxy-TEMPO relative to PS-Br has been used. The mixture was then degassed by purging with argon for at least 30 minutes, after which CuBr (0.0287 g,  $2.00 \cdot 10^{-4}$  mol) was added. The reaction mixture was homogenized and purged with argon for another 15 minutes. After this time period, the reaction mixture was immersed in an oil bath at 110°C. The time to heat the reaction mixtures to the desired temperature was calculated to be less than 1 min. To monitor the reaction, after regular time intervals 0.5 mL samples were taken through a septum and immediately quenched.

#### *HPLC measurements:*

Prior to analysis, the samples from the exchange experiments were passed through a column of activated alumina, after which they were subjected to drying. The samples were then dissolved in CH<sub>2</sub>Cl<sub>2</sub> (Aldrich, HPLC grade) and analyzed by HPLC using an Alliance Waters 2690 Separation Module and a Jordi Gel DVB polyamine column (250mm×4.6mm, Alltech) at 40 °C. The gradient program changed from 100% heptane to 100% CH<sub>2</sub>Cl<sub>2</sub> in 15 min, then to 80/20 CH<sub>2</sub>Cl<sub>2</sub>/THF in 25 min. After 5 min, the eluent was changed to 100% CH<sub>2</sub>Cl<sub>2</sub> in 5 min, after which the gradient was changed to 100% heptane in 5 min. Detection was carried out using a multi-wavelength and multi-angle PL-EMD 960 evaporative light scattering detector (ELSD) (Polymer Laboratories). Data acquisition was done using Millennium-32 3.05 software.

#### *Data analysis:*

When using the ELSD detector to analyse the samples from the exchange reactions, two fundamental problems arise. First, the detector response signal,  $R_{ELSD}$ , is not the same for the macroinitiator (R-Br in Scheme 4.1) and for the trapped species (R-OH in Scheme 4.1). Second, the detector response signal is not simply linearly dependent on concentration, [C], but is scaled with a power law<sup>15</sup>:

$$R_{ELSD} = \alpha[C]^\beta \quad (4.14)$$

These problems can be solved by calibrating the ELSD detector for all compounds that are important in Eq. (4.13). The hydroxy-functional species, however, were not available as pure compounds and, therefore, direct calibration for these compounds was not possible. Fortunately, the total concentration of polymeric species is constant in each experiment. This mass balance holds when R· is exclusively trapped by the nitroxide and transformed into R-OH, while termination is negligible. Using Eq. (4.11) with the appropriate parameters and concentrations, it is clear that termination plays a minor role and that the mass balance holds.

Calibration curves for the ELSD response signal as a function of concentration of macroinitiator (R-Br) were obtained by determining the peak areas of samples with known concentrations and injection volumes. To be able to construct the calibration curves for PS-OH and PBA-OH, exchange reactions for both PS-Br and PBA-Br were carried out and samples were taken at timed intervals. The samples were carefully weighed, so as to exactly know the total amount of polymeric species, *i.e.* R-Br + R-OH. Subsequently, the concentration of R-Br was calculated using the experimentally obtained calibration curve. Then, the concentration of the trapped species (R-OH) was calculated with the mass balance and a calibration curve for R-OH was constructed.

For the exchange reactions in general, the data were analysed by first correcting the ELSD chromatograms with the calibration curves for the non-linear concentration dependence. Then, using the mass balance, the corrected chromatograms were normalized on the total peak area. The relative peak area of the R-Br species was then calculated and used in (4.13).

#### 4.3.4 Results and discussion

An example of a series of HPLC chromatograms for an exchange reaction in *p*-xylene using PS-Br is shown in Figure 4.2. It has to be stressed that direct calibration of the hydroxy-functional species is not possible, since model compounds were not available.

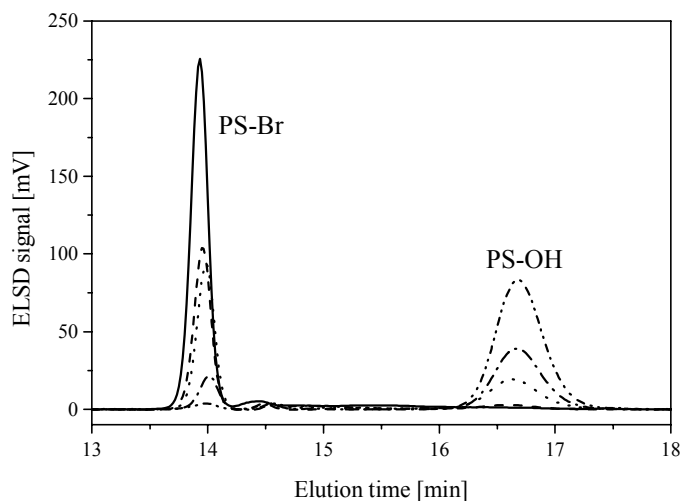


**Figure 4.2** HPLC chromatograms for an exchange reaction with PS-Br in p-xylene at 110 °C at  $t=0$  s (—),  $t=60$  s (---),  $t=180$  s (···),  $t=300$  s (-·-·) and  $t=600$  s (- - -).

The peak at an elution time of 14 minutes corresponds to the macroinitiator species, PS-Br, and it is clear that this peak is decreasing in time. The hydroxy-functional species, PS-OH, should elute at longer time, due to polar interactions with the amino-functional column. The peak at 16.6 minutes increase in time and can therefore be assigned to the hydroxy-functional species, PS-OH.

The calibration curves for the detector response signal as a function of concentration for PS-Br and PS-OH as well as PBA-Br and PBA-OH are depicted in Figures 4.3a and 4.3b, respectively. The calibration curves for PS-Br and PBA-Br measured with calibration samples of known concentrations are very well described by a power law, *i.e.* Eq. (4.14), as are the calibration curves for PS-OH and PBA-OH.

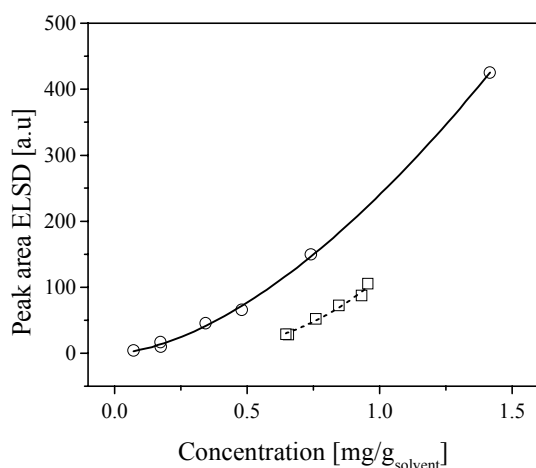


**Figure 4.3a** Calibration curves for ELSD quantification in HPLC analyses: PS-Br dormant species (—○—) and PS-OH trapped species (- - □ - -).

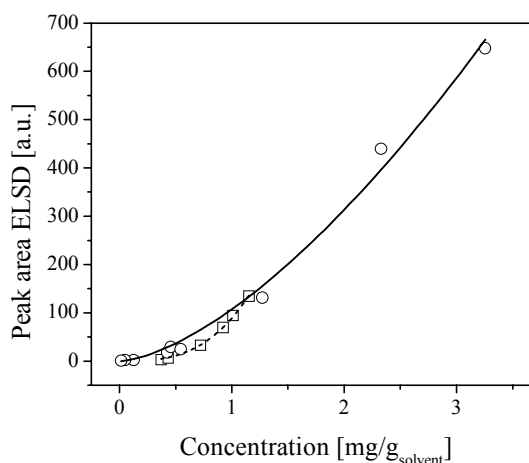


**Figure 4.3b** Calibration curves for ELSD quantification in HPLC analyses: PBA-Br dormant species (—○—) and PBA-OH trapped species (- - □ - -).

It has to be noted, however, that for the macroinitiators the fitted power laws behave according to theory<sup>15</sup>, while the ones for the hydroxy-functional species, although they are fitted nicely, have very high values for the exponent,  $\beta$ , in the power law. According to theory, this exponent should be between 1.5 and 1.7, which is the case for both macroinitiators (1.64 for PS-Br and 1.55 for PBA-Br). For PS-OH and PBA-OH these values are as high as 3.14 and 2.98, respectively. It is suspected that in the filtration step, where the copper catalyst is removed from the reaction mixture, not 100% of the polymeric species is retrieved. When this happens, the mass balance based calculation does not hold anymore and a wrong [R-OH] is calculated. This could lead to deviations in the power law that is obtained after fitting. However, in the filtration step, hydroxy-TEMPO is not retained by the filter material and it is therefore likely that the trapped polymeric species (R-OH) is not retained either. It has been assessed that at least 90% of all polymeric material is recovered after filtration. These deviations do not have a significant influence on the power laws as depicted in Figures 4.3. The origin of the high exponent values still is unknown. In our calculations, we did not take into account any possible loss of material during the filtration step. The calibration curves in Figures 4.3 have been used in the quantification of the exchange reactions.

In Figures 4.4a and 4.4b, the second-order reaction plots, see Eq. (4.13), are displayed for exchange reactions in *p*-xylene using PS macroinitiator and PBA macroinitiator, respectively. For reasons of clarity, the left-hand side of Eq. (4.13) is abbreviated with  $\ln(A) + \ln(B)$ .

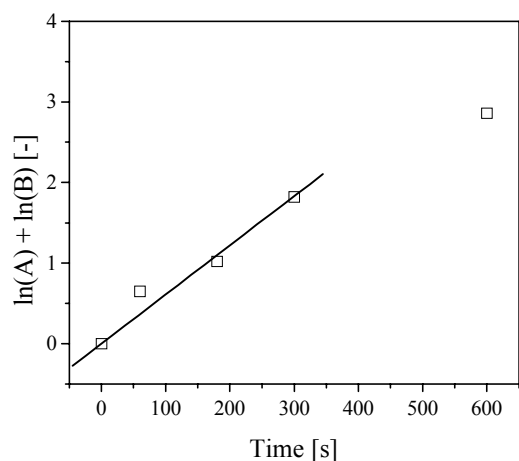


*Figure 4.4a Second-order reaction plots of an exchange reaction of PS-Br in *p*-xylene at 110 °C.*

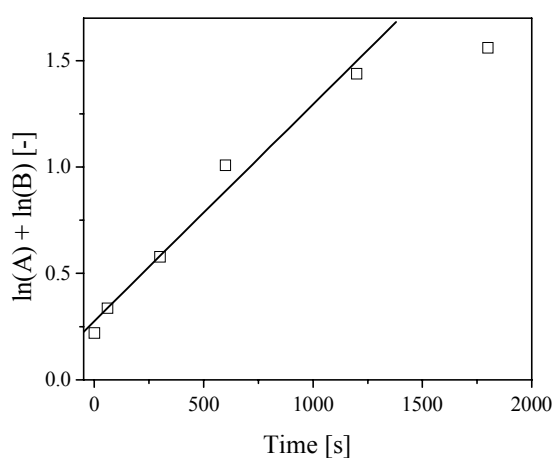


*Figure 4.4b Second-order reaction plots of an exchange reaction of PBA-Br in *p*-xylene at 110 °C.*

From fitting the data in Figures 4.4 to Eq. (4.13), the activation rate coefficients for PS and PBA dormant species can be calculated from the slopes. Note that the linear fit

in Figure 4.4b does not pass through the origin due to the fact that at  $t=0$  a small part of the macroinitiator had already dissociated and reacted with the hydroxy-TEMPO. This, however, does not affect the kinetics and the values of the activation rate coefficients. The resulting activation rate coefficients are  $0.43 \text{ L}\cdot\text{mol}^{-1}\cdot\text{s}^{-1}$  for PS-Br and  $0.075 \text{ L}\cdot\text{mol}^{-1}\cdot\text{s}^{-1}$  for PBA-Br in *p*-xylene at  $110 \text{ }^\circ\text{C}$ . The value for the activation rate coefficient for PS-Br,  $k_{act}^S$ , is in very good agreement with data reported by Fukuda *et al.*<sup>8</sup>, who found a value of  $0.45 \text{ L}\cdot\text{mol}^{-1}\cdot\text{s}^{-1}$  in styrene at  $110^\circ\text{C}$ . The value for the activation rate coefficient for PBA-Br,  $k_{act}^B$ , is almost a factor 6 lower than  $k_{act}^S$ . This is probably due to the lower stability of the PBA radical compared to the PS radical with its stabilising phenyl group.

It is of great importance that when extracting data from the second-order plots, one should always look closely at the HPLC chromatograms to evaluate the accuracy of the data. This is especially important when almost all macroinitiator has depleted and the R-Br peak is very small compared to the R-OH peak. The initial presence of dead material in the macroinitiator is then relatively more important. This is reflected in Figures 4.4, where the data points at large reaction times do not obey Eq. (4.13).

Since in copolymerisations of S and BA composition drift occurs, the polarity of the reaction mixture changes during polymerisation. It is therefore interesting to investigate the activation rate coefficients in solvents of varying polarity. Butyl acetate (BuAc) has been chosen as solvent, because its structure resembles the monomer BA. In addition to butyl acetate, the exchange reactions were also performed in 1,4-dioxane, 1-butanol and *N,N*-dimethylformamide (DMF) according to the same procedure. The results of these experiments are summarised in Table 4.1.

**Table 4.1** Activation rate coefficients,  $k_{act}$ , measured in solvents of varying polarity.

solvent	dielectric constant at $110 \text{ }^\circ\text{C}$ <sup>16</sup>	$k_{act} \text{ (L}\cdot\text{mol}^{-1}\cdot\text{s}^{-1}\text{)}$	
		PS-Br	PBA-Br
<i>p</i> -xylene	2.14	0.43	0.075
1,4-dioxane	2.06	0.17	0.033
BuAc	4.04	0.27	0.086
1-butanol	8.88	0.48	4.3
DMF	27.3	0.26	0.088

The data in Table 4.1 clearly demonstrate a marked effect of the solvent on the activation process of PS and PBA dormant species. In the following discussion, we have tried to ascribe the effect of solvent to particular characteristics, hereby taking the reactions in *p*-xylene as reference. Three categories have been defined: solvent

polarity, reflected in the dielectric constant  $\epsilon$ , coordinating ability and finally hydrogen bonding ability.

1,4-Dioxane seems to impede dissociation of both dormant species, although it has a dielectric constant similar to that of *p*-xylene. The decrease in activation rate coefficients may be due to interactions between 1,4-dioxane and the copper complex, since ethers may act as ligands<sup>13</sup>. Coordinating solvents may saturate the coordination sphere of the copper complex temporarily and so decrease the rate coefficient.

The influence of butyl acetate on the activation rate coefficients of PS-Br and PBA-Br is not consistent, and does not support Matyjaszewski's<sup>17</sup> hypothesis that activation of the PS macroinitiator is enhanced in more polar media. On the contrary, the activation of a PS macroinitiator is hampered in butyl acetate, resulting in lower  $k_{act}^S$ . The increase in  $k_{act}^B$  is very small and can be explained by stabilization of the radical by butyl acetate. The radical is more easily formed, which increases  $k_{act}^B$ .

When the effect of solvent polarity is further investigated, it is interesting to look at the activation rate coefficient data for 1-butanol. 1-Butanol has a very high dielectric constant,  $\epsilon=8.88$  at 110°C, and it is therefore expected that the activation rate coefficient of PS dormant species will be dramatically decreased, while that of PBA dormant species will increase. However, when considering the data in Table 4.1 we see that the activation rate coefficient for PBA macroinitiator drastically increases from 0.075 L·mol<sup>-1</sup>·s<sup>-1</sup> in *p*-xylene to 4.3 L·mol<sup>-1</sup>·s<sup>-1</sup> in 1-butanol. Although this is consistent with increasing  $k_{act}^B$  with increasing solvent polarity, the effect is peculiarly pronounced. This could be related to the presence of the hydroxyl group, which could enhance activation of dormant species. Similarly, Haddleton *et al.*<sup>18</sup> found that the addition of phenols to an ATRP reaction of methyl methacrylate enhanced the reaction rate. Furthermore, the addition of water also has a rate enhancing effect on the polymerisation of methyl methacrylate<sup>19</sup>. It is rather peculiar in this respect that the hydroxyl group of the hydroxy-TEMPO does not affect the activation rate coefficient of PS-Br in *p*-xylene compared to literature values<sup>8</sup>, although it is present in a relatively high concentration in the exchange reactions.

The overall effect of 1-butanol on the activation rate coefficient of PS dormant species,  $k_{act}^S$ , is limited, since the negative effect of polarity is, presumably, compensated by the enhancing effect of the presence of the hydroxy group.

DMF combines a high polarity with the ability to act as ligand in the copper complex, which should decrease  $k_{act}^S$ . This is indeed the case, although the effect is not as pronounced as we might expect. For  $k_{act}^B$ , polar solvents clearly enhance activation, although the ability to act as a ligand suppresses the activation. The value of 0.088 L·mol<sup>-1</sup>·s<sup>-1</sup> suggests that solvent polarity dominates.

In all data analyses, the presence of any dead material in the macroinitiators has been neglected. Although this may not be correct, the HPLC peak for the dormant species, R-Br, almost completely disappears at the end of the reaction, see Figures 4.2, which indicates that the amount of inactive chains in the macroinitiator is negligible, *viz.* <2%. This small amount of inactive dormant species is not likely to interfere with the quantitative analyses of the activation rate coefficients.

The effect of solvent polarity, coordinating ability and the presence of a hydroxy group is qualitatively summarised in Table 4.2.

**Table 4.2 Effects of solvent polarity, coordinating ability and presence of hydroxy groups on activation rate coefficients.**

<i>Solvent</i>	<i>PS-Br</i>	<i>PBA-Br</i>
Polarity	-	+
Coordinating ability	-	-
Hydroxy group	+	+

## 4.4 DETERMINATION OF $k_{\text{DEACT}}$

### 4.4.1 Sensitivity test

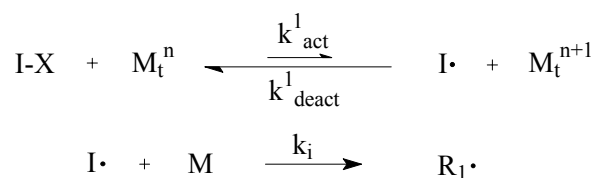
Since the activation rate coefficients for PS and PBA dormant species are known, it is possible to obtain the deactivation rate coefficients by performing so-called kinetic experiments. These kinetic experiments encompass homopolymerisations of S and BA while monitoring the rate of polymerisation. In principle, these data can be used in Eq. (3.14) together with accurate values for  $k_p$  and  $k_t^\xi$ .

Using this approach, several problems arise. First, the termination rate constant is not well known because of three reasons. The expression for the conversion-dependent termination rate constant, Eq. (4.9), in principle holds for methyl and butyl methacrylate oligomers in methyl and butyl methacrylate matrices. The present investigation deals with PS and PBA in a *p*-xylene solution. Furthermore, at elevated temperatures, *e.g.* at 110°C, these termination rate constants have not been determined. For S and BA, a typical polymerisation temperature of 110°C is applied. Finally, in the derivation of Eq. (4.9) it has been assumed that the concentration of polymer exceeds  $c^*$ , *i.e.* the concentration at which chains start overlapping. Since in ATRP all chains start growing at the beginning of the reaction, it takes a while to reach the value of  $c^*$ .

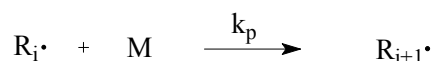
Another problem arises on recognising that Eq. (3.11) does not take into account the initiation process, *i.e.* the activation and deactivation of the alkyl halide initiator. In general, one expects different activation and deactivation rate coefficients of the alkyl halide initiator compared to those of the PS and PBA dormant species.

In view of these complications, it seems obvious to study the effect of the initiation process on the course of the polymerisation, as well as the effect of changes in the termination rate constant. We therefore assume a model system, in which only initiation, propagation and termination reactions occur, as well as activation of dormant species and deactivation of polymeric radicals, see Scheme 4.2. Transfer reactions, as well as thermal initiation are not taken into account. This model can be assessed *ab initio* with the aid of computer simulations by simultaneously solving the differential equations (4.15) as derived from Scheme 4.2, varying the different parameters independently.

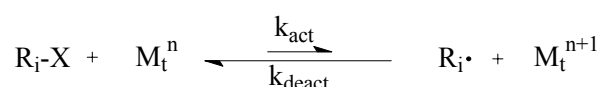
*Initiation:*



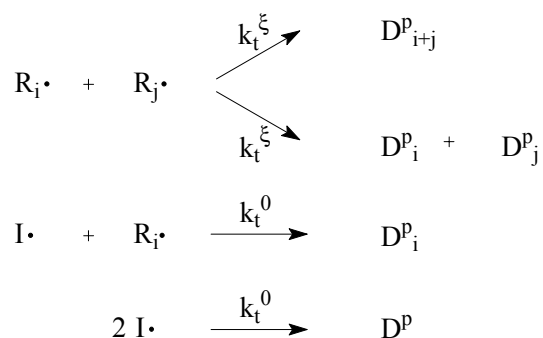
*Propagation:*



*ATRP equilibrium:*



*Bimolecular termination:*



**Scheme 4.2 Fundamental reaction steps in an ATRP system used for simulations.**



It should be stressed that transfer reactions and thermal initiation have been neglected, and for bimolecular termination by combination and disproportionation both rate coefficients are assumed to be equal. For this termination rate constant, Eq. (4.9) will be used, despite the drawbacks mentioned earlier. The termination events involving initiator-derived radicals,  $I\cdot$ , are assumed to be governed by  $k_t^0$ , *i.e.* the termination rate coefficient for small species. As far as the initiation process is concerned, it is known from literature that the initiation step can be up to 10 times faster than propagation<sup>20</sup>. However, in the simulations the initiation step is assumed to be equally fast as the subsequent propagation steps, *i.e.*  $k_i = k_p$ . Additionally, the propagation rate coefficient is assumed to be independent of the chain length of the growing radical. The mass balances for  $[I-X]$ ,  $[I\cdot]$ ,  $[R\cdot]$ ,  $[R-X]$ ,  $[M]$ ,  $[M_t^n]$  and  $[M_t^{n+1}]$  for an ATRP system in a constant density batch process as depicted in Scheme 4.2 are the following:

$$\frac{d[I-X]}{dt} = -k_{act}^1 [I-X][M_t^n] + k_{deact}^1 [I\cdot][M_t^{n+1}] \quad (4.15a)$$

$$\frac{d[I\cdot]}{dt} = k_{act}^1 [I-X][M_t^n] - k_{deact}^1 [I\cdot][M_t^{n+1}] - 2k_t^0 [I\cdot]^2 - 2k_t^0 [I\cdot][R\cdot] - k_i [I\cdot][M] \quad (4.15b)$$

$$\frac{d[R\cdot]}{dt} = k_{act} [R-X][M_t^n] - k_{deact} [R\cdot][M_t^{n+1}] + k_i [I\cdot][M] - 2k_t^0 [I\cdot][R\cdot] - 2k_t^\xi [R\cdot]^2 \quad (4.15c)$$

$$\frac{d[R-X]}{dt} = -k_{act} [R-X][M_t^n] + k_{deact} [R\cdot][M_t^{n+1}] \quad (4.15d)$$

$$\frac{d[M]}{dt} = -k_p [R\cdot][M] - k_i [I\cdot][M] \quad (4.15e)$$

$$\frac{d[M_t^n]}{dt} = -k_{act}^1 [I-X][M_t^n] + k_{deact}^1 [I\cdot][M_t^{n+1}] - k_{act} [R-X][M_t^n] + k_{deact} [R\cdot][M_t^{n+1}] \quad (4.15f)$$

$$\frac{d[M_t^{n+1}]}{dt} = k_{act}^1 [I-X][M_t^n] - k_{deact}^1 [I\cdot][M_t^{n+1}] + k_{act} [R-X][M_t^n] - k_{deact} [R\cdot][M_t^{n+1}] \quad (4.15g)$$

The computer simulations are carried out with Mathematica 4.0 software, see the appendix.

#### 4.4.1.1 Influence of alkyl halide initiator activation process

The initial concentrations of all compounds involved, as well as the values for the parameters described in section 4.2 are collected in Table 4.3. Common values for the initial concentrations and  $k_t^0$  have been chosen, and literature data on the activation and deactivation rate coefficients for respectively R-X and R· were taken. The values of  $k_{act}^1$  and  $k_{deact}^1$  were varied in the simulations.

**Table 4.3 Initial concentrations and parameters used in the simulation of the ATRP system as depicted in Scheme 4.2**

Parameter / Concentration	Value
$[I-X]_0$	$5 \cdot 10^{-2} \text{ mol} \cdot \text{L}^{-1}$
$[M_t^n]_0$	$5 \cdot 10^{-2} \text{ mol} \cdot \text{L}^{-1}$
$[M]_0$	$4.2 \text{ mol} \cdot \text{L}^{-1}$
$k_{act}$	$0.45 \text{ L} \cdot \text{mol}^{-1} \cdot \text{s}^{-1} \text{ }^8$
$k_{deact}$	$1.1 \cdot 10^7 \text{ L} \cdot \text{mol}^{-1} \cdot \text{s}^{-1} \text{ }^{8,13}$
$k_p$	$1572 \text{ L} \cdot \text{mol}^{-1} \cdot \text{s}^{-1} \text{ }^2$
$k_t^0$	$1 \cdot 10^8 \text{ L} \cdot \text{mol}^{-1} \cdot \text{s}^{-1} \text{ }^{12}$

Figures 4.5 show how the evolution of  $-\ln(1-\xi)$  with time is affected by the initiation process. The data from Table 4.3 were used, together with various values for the activation and deactivation rate coefficients of the initiator,  $k_{act}^1$  and  $k_{deact}^1$ , respectively.

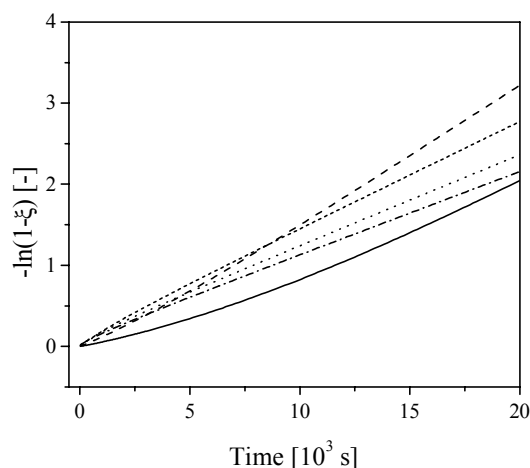


**Figure 4.5a Evolution of  $-\ln(1-\xi)$  in time for different values of  $k_{act}^1$ :  $k_{deact}^1 = 1.1 \cdot 10^7 \text{ L} \cdot \text{mol}^{-1} \cdot \text{s}^{-1}$ ,  $k_{act}^1 = 0.001 \text{ L} \cdot \text{mol}^{-1} \cdot \text{s}^{-1}$  (—),  $0.01 \text{ L} \cdot \text{mol}^{-1} \cdot \text{s}^{-1}$  (---),  $0.1 \text{ L} \cdot \text{mol}^{-1} \cdot \text{s}^{-1}$  (-.-),  $0.45 \text{ L} \cdot \text{mol}^{-1} \cdot \text{s}^{-1}$  (···) and  $1 \text{ L} \cdot \text{mol}^{-1} \cdot \text{s}^{-1}$  (—·—). Other parameters see Table 4.3.**

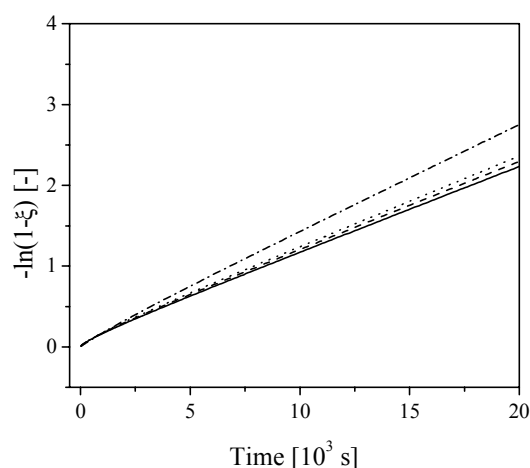


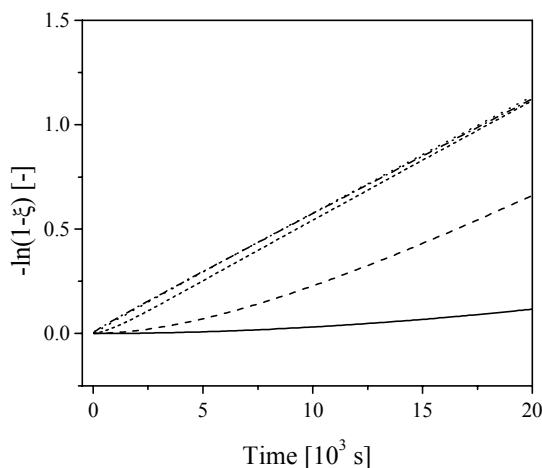
**Figure 4.5b Evolution of  $-\ln(1-\xi)$  in time for different values of  $k_{deact}^1$ :  $k_{act}^1 = 0.45 \text{ L} \cdot \text{mol}^{-1} \cdot \text{s}^{-1}$ ,  $k_{deact}^1 = 1.1 \cdot 10^6 \text{ L} \cdot \text{mol}^{-1} \cdot \text{s}^{-1}$  (—),  $5 \cdot 10^6 \text{ L} \cdot \text{mol}^{-1} \cdot \text{s}^{-1}$  (---),  $1.1 \cdot 10^7 \text{ L} \cdot \text{mol}^{-1} \cdot \text{s}^{-1}$  (-.-) and  $1 \cdot 10^8 \text{ L} \cdot \text{mol}^{-1} \cdot \text{s}^{-1}$  (···). Other parameters see Table 4.3.**

Figures 4.5 demonstrate that the reversible initiation step has a significant influence on the rate of polymerisation. The differences as displayed in Figures 4.5 can be fully explained by the concentration of dormant species in the ATRP system.

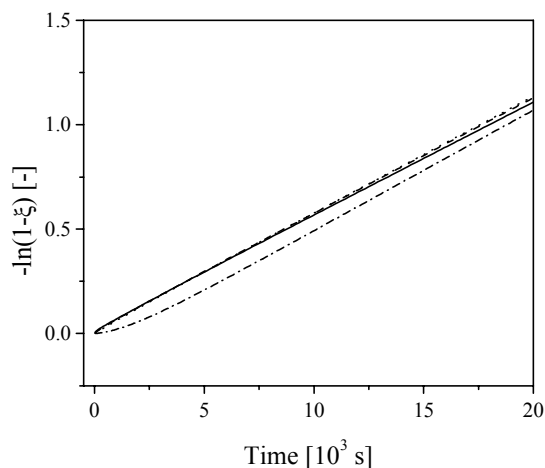
Figure 4.5a shows that upon increasing  $k^I_{act}$  from  $10^{-3}$  to  $10^{-2}$  L·mol<sup>-1</sup>·s<sup>-1</sup>, the rate of polymerisation increases. This is fairly logical, since it takes less time to transform the initiator species into active radicals, which can be transformed into dormant species after addition of monomer and subsequent deactivation. A too high  $k^I_{act}$ , however, causes a relatively high radical concentration at the very beginning of the reaction, which is reflected in an initially high reaction rate. Nevertheless, the system is paying its price, since the high initial radical concentration results in an enhanced contribution of bimolecular termination relative to reversible deactivation. As a consequence, the concentration of dormant species is lowered and the reaction rate is lower.

Figure 4.5b shows a somewhat peculiar behaviour of the ATRP system. Upon increasing  $k^I_{deact}$  the reaction rate also increases. Yet, this behaviour can also be clarified when looking at the total number of active chains present in the system. When  $k^I_{deact}$  decreases, the transformation back to the alkyl halide is too slow and the initial radical concentration again increases dramatically. This high radical concentration is responsible for the increased contribution of bimolecular termination in comparison with reversible deactivation. Consequently, the eventual concentration of dormant species will be lower.

The pessimistic conclusion that could be drawn from the observations displayed in Figures 4.5 is that if we want to be able to describe the kinetics of ATRP homopolymerisation, very accurate knowledge on the initiation step is indispensable. There is, however, a way to render the ATRP system less sensitive towards changes in the initiation process. After all, bimolecular termination can be minimised by the addition of Cu<sup>2+</sup> species. In this way, a relatively high initial radical concentration would not immediately result in loss of active chains, since the deactivation by reaction with a Cu<sup>2+</sup> species is competing with bimolecular termination. In the simulations, 5% of Cu<sup>2+</sup> species relative to Cu<sup>+</sup>, *i.e.*  $[M_t^{n+1}]_0 = 2.5 \cdot 10^{-3}$  mol·L<sup>-1</sup>, has been added. The results are plotted in Figures 4.6.



**Figure 4.6a** Evolution of  $-\ln(1-\xi)$  in time for different values of  $k^I_{act}$ ;  $k^I_{deact}=1.1\cdot 10^7 \text{ L}\cdot\text{mol}^{-1}\cdot\text{s}^{-1}$  and  $[\text{Cu}^{2+}]_0=2.5\cdot 10^{-3} \text{ mol}\cdot\text{L}^{-1}$ ;  $k^I_{act}=0.001 \text{ L}\cdot\text{mol}^{-1}\cdot\text{s}^{-1}$  (—),  $0.01 \text{ L}\cdot\text{mol}^{-1}\cdot\text{s}^{-1}$  (---),  $0.1 \text{ L}\cdot\text{mol}^{-1}\cdot\text{s}^{-1}$  (-·-·)  $0.45 \text{ L}\cdot\text{mol}^{-1}\cdot\text{s}^{-1}$  (···) and  $1 \text{ L}\cdot\text{mol}^{-1}\cdot\text{s}^{-1}$  (-·-·). Other parameters see Table 4.3.



**Figure 4.6b** Evolution of  $-\ln(1-\xi)$  in time for different values of  $k^I_{deact}$ ;  $k^I_{act}=0.45 \text{ L}\cdot\text{mol}^{-1}\cdot\text{s}^{-1}$  and  $[\text{Cu}^{2+}]_0=2.5\cdot 10^{-3} \text{ mol}\cdot\text{L}^{-1}$ ;  $k^I_{deact}=1.1\cdot 10^6 \text{ L}\cdot\text{mol}^{-1}\cdot\text{s}^{-1}$  (—),  $1.1\cdot 10^7 \text{ L}\cdot\text{mol}^{-1}\cdot\text{s}^{-1}$  (···),  $1.1\cdot 10^8 \text{ L}\cdot\text{mol}^{-1}\cdot\text{s}^{-1}$  (-·-·) and  $1\cdot 10^9 \text{ L}\cdot\text{mol}^{-1}\cdot\text{s}^{-1}$  (-·-·). Other parameters see Table 4.3.

As can be seen in Figure 4.6a, the effect of the activation of the alkyl halide initiator has been drastically diminished. There still is some kind of threshold for approximately  $0.1 \text{ L}\cdot\text{mol}^{-1}\cdot\text{s}^{-1}$ , above which  $k^I_{act}$  should be in order to minimise the effect on the course of polymerisation. This threshold value is very low and it is expected that in real ATRP systems  $k^I_{act}$  is much higher. For 1-phenyl ethylbromide, for instance, the  $k^I_{act}$  has been determined and equals  $0.45 \text{ L}\cdot\text{mol}^{-1}\cdot\text{s}^{-1}$ <sup>9</sup>, which implies that in this case no influence of the initiation of the alkyl halide initiator on the rate of polymerisation is expected.

The same holds for  $k^I_{deact}$ , since from Figure 4.6b we can see that when this deactivation rate coefficient is high enough, the rate of polymerisation is not affected. For ATRP homopolymerisations of S in diphenyl ether, this deactivation rate coefficient is calculated from rate data in combination with information on the activation rate coefficient and was found to be  $1.1\cdot 10^7 \text{ L}\cdot\text{mol}^{-1}\cdot\text{s}^{-1}$ <sup>8,13</sup>.

These simulations show that the influence of the initiation step on the course of polymerisation can be minimised by addition of  $\text{Cu}^{2+}$ .

#### 4.4.1.2 Influence of $k_t^0$

Another parameter that might have an influence on the rate of polymerisation is the chain-length-dependent termination rate coefficient,  $k_t^\xi$ . To get insight into the sensitivity towards this parameter, simulations have been carried out with different values of  $k_t^0$  and using the same concentrations and parameters as listed in Table 4.3,

together with  $k_{act}^I=0.45 \text{ L}\cdot\text{mol}^{-1}\cdot\text{s}^{-1}$  and  $k_{deact}^I=1.1\cdot 10^7 \text{ L}\cdot\text{mol}^{-1}\cdot\text{s}^{-1}$ . The results of these simulations are depicted in Figure 4.7.

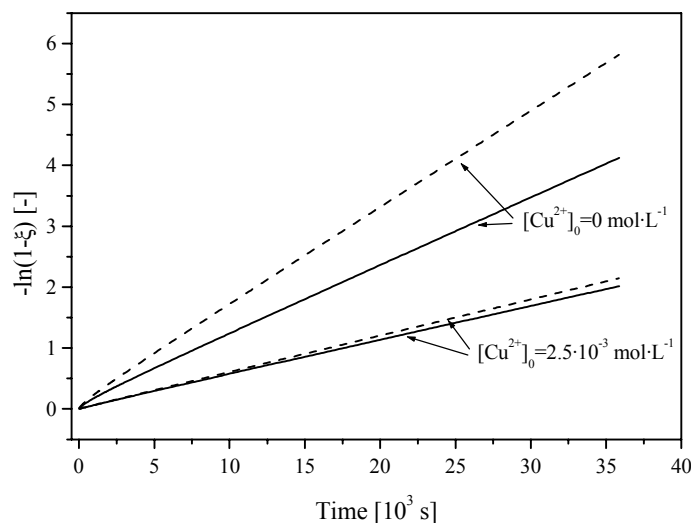


**Figure 4.7** Evolution of  $-\ln(1-\xi)$  in time as a function of  $k_t^0$  in the absence of  $\text{Cu}^{2+}$  and with  $[\text{Cu}^{2+}]_0=2.5\cdot 10^{-3} \text{ mol}\cdot\text{L}^{-1}$ ;  $k_t^0=1\cdot 10^8 \text{ L}\cdot\text{mol}^{-1}\cdot\text{s}^{-1}$  (—),  $k_t^0=5\cdot 10^7 \text{ L}\cdot\text{mol}^{-1}\cdot\text{s}^{-1}$  (---).

As was the case with the initiation process, the polymerisation rate is much less affected by changes in  $k_t^0$  when a small amount of deactivating species is present. The presence of  $\text{Cu}^{2+}$  species at the start of the reaction allows reversible deactivation to compete with bimolecular termination from the outset. The system does not have to build up the concentration of the persistent radical.

The simulations demonstrate the usefulness of the addition of a small amount of  $\text{Cu}^{2+}$ . The course of the ATRP reaction is much less affected by the initiation process and uncertainties in the chain-length-dependent termination rate coefficient when a small amount of  $\text{Cu}^{2+}$  is added, typically 5 mol% on total Cu basis. However, this implies that Eq. (3.14) no longer applies and that Eq. (3.15) has to be used to assess the evolution of  $-\ln(1-\xi)$  with time<sup>21</sup>:

$$-\ln(1-\xi) = \ln\left(\frac{[M]_0}{[M]}\right) = k_p \frac{k_{act}}{k_{deact}} \frac{[R-X]_0 [M_t^n]_0}{[M_t^{n+1}]_0} t \quad (3.15)$$

When  $\ln([M]_0/[M])$  or  $-\ln(1-\xi)$  is plotted vs. time, the ratio of  $k_{act}$  and  $k_{deact}$  can be determined on using the initial concentrations of alkyl halide initiator,  $\text{Cu}^+$  and  $\text{Cu}^{2+}$ .

If  $k_{act}$  is accurately known, the explicit values of the deactivation rate coefficient can be calculated.

In the following sections, ATRP homopolymerisations of S and BA will be studied. In order to obtain reliable quantitative information on the deactivation rate coefficients, a small amount of initial  $Cu^{2+}$  will be applied. However, in order to get acquainted with the ATRP system and to optimise the reaction conditions in such a way that the results are reproducible, homopolymerisations of S and BA in the absence of an initial amount of  $Cu^{2+}$  will be carried out. Furthermore, these homopolymerisations allow us to test whether our ATRP system resulted in good control of the polymerisations of S and BA.

#### 4.4.2 Experimental

##### *Materials:*

The copper ligand, 4,4'-di-*n*-heptyl-2,2'-bipyridine (dHbpy), was synthesised according to a literature procedure<sup>13</sup>. Styrene (S, Aldrich, 99%) and butyl acrylate (BA, Aldrich, 99+%) were distilled and stored over molecular sieves. *p*-Xylene (Aldrich, 99+% HPLC grade) was stored over molecular sieves and used without further purification. Ethyl 2-bromoisobutyrate (Aldrich, 98%) was used as received, as well as  $CuBr_2$  (Aldrich, 99%).  $CuBr$  (Aldrich, 99,999%) was used as received, stored in a glove box under a nitrogen atmosphere and used in the 'kinetic experiments'.  $CuBr$  (Aldrich, 98%) was also used as received and used for the homopolymerisations.

##### *Procedure for homopolymerisations without $Cu^{2+}$ :*

A typical homopolymerisation of S is conducted in the following way. In a 100 mL three-necked round-bottom flask equipped with a magnetic stirrer, *p*-xylene (5.00 g) was mixed with S (5.00 g, 0.0480 mol), dHbpy (0.338 g,  $9.60 \cdot 10^{-4}$  mol) and ethyl 2-bromoisobutyrate (0.0940 g,  $4.82 \cdot 10^{-4}$  mol). While stirring, the reaction mixture was degassed by purging with dry argon for at least 45 minutes. Hereafter,  $CuBr$  (0.0689 g,  $4.80 \cdot 10^{-4}$  mol) was added and the reaction mixture was homogenised and purged with dry argon for another 15 minutes. After this, the reaction mixture was placed in a thermostatically controlled oil bath at 110°C. Samples from the reaction mixture were withdrawn through a septum with a syringe and cooled down immediately. Monomer conversion was determined by gas chromatography using a HP 5890 gas chromatograph equipped with an AT Wax column (Alltech, length 30 m, film thickness 1.0  $\mu$ m) and an auto sampler. The remainder of the samples was used for molecular weight analysis. For this purpose, the samples were passed through a column with aluminumoxide (activated, neutral, Brockman I, STD grade approx. 150

mesh, 58Å, Aldrich) to remove the copper catalyst using stabilized tetrahydrofuran (AR, Biosolve) as eluent. After subsequent drying, the dry polymers were dissolved in stabilised tetrahydrofuran at 1 mg·mL<sup>-1</sup> and filtrated using 0.2 µm filters. The molecular weights were determined by size exclusion chromatography (SEC) with a Waters Model 510 pump and Waters 712 WISP using 4 PL-gel mix C columns (300mm×7.5mm, Polymer Laboratories) at 40°C and tetrahydrofuran as the eluent. The eluent flow rate was 1.0 mL·min<sup>-1</sup>. Calibration was performed with polystyrene standards with narrow molecular-weight distributions (Polymer Laboratories). The BA polymers were not corrected with Mark-Houwink parameters from literature<sup>14</sup>, since molecular weights were too small for the parameters to be applicable. A Waters 410 differential refractometer was used for detection. Data acquisition was done with Millennium-32 3.05 software.

*Procedure for 'kinetic experiments' to determine  $k_{deact}$ :*

The experimental procedure for the homopolymerisations of S and BA is similar to those described in the previous paragraph. However, in order to rule out the effects of the initiation process and uncertainties in the chain-length-dependent termination rate coefficient on the course of the reaction, 5% of CuBr<sub>2</sub> based on the total amount of copper was added. A typical kinetic experiment with S was performed using the following procedure. In a 100 mL three-necked round-bottom flask, *p*-xylene (5.00 g) was mixed with S (5.00 g, 0.0480 mol), dHbpy (0.338 g, 9.60·10<sup>-4</sup> mol), CuBr<sub>2</sub> (5.40·10<sup>-3</sup> g, 2.42·10<sup>-5</sup> mol) and ethyl 2-bromoisobutyrate (0.0940 g, 4.82·10<sup>-4</sup> mol). While stirring, the reaction mixture was degassed by purging with dry argon for at least 45 minutes. Hereafter, CuBr (0.0654 g, 4.56·10<sup>-4</sup> mol) was added and the reaction mixture was homogenised and purged with dry argon for another 15 minutes. After this, the reaction mixture was placed in an oil bath at 110°C. Samples from the reaction mixture were withdrawn with a syringe through a septum and cooled down immediately. Monomer conversion was determined by gas chromatography using a HP 5890 gas chromatograph equipped with an AT Wax column (Alltech, length 30 m, film thickness 1.0 µm) and an auto sampler.

### 4.4.3 Results and discussion

#### 4.4.3.1 Homopolymerisations of S and BA

In Figure 4.8, the  $-\ln(1-\xi)$  vs. time plots of homopolymerisations of S and BA are displayed.

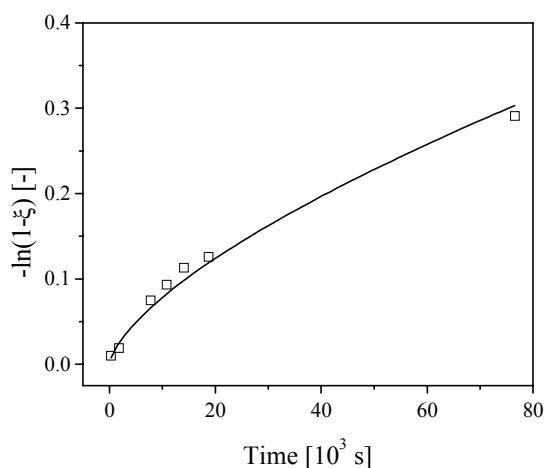


*Figure 4.8a Evolution of  $-\ln(1-\xi)$  in time for a homopolymerisation of S in p-xylene at 110°C.*

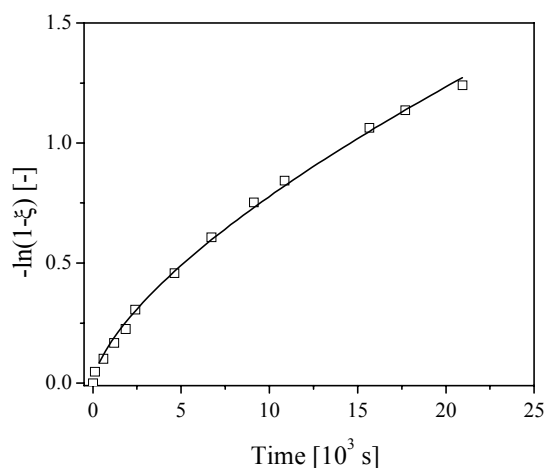


*Figure 4.8b Evolution of  $-\ln(1-\xi)$  in time for a homopolymerisation of BA in p-xylene at 110°C.*

Since no  $\text{CuBr}_2$  was added, the experimental data in Figures 4.8 have been fitted to Eq. (3.14) and as can be seen, the data are well described. This is, however, somewhat unexpected if we recognise that in reality  $k_t$  is conversion-dependent, but is considered constant in this evaluation. Furthermore, the ATRP system that we used for these homopolymerisations made use of (only) 98% pure  $\text{CuBr}$ , and therefore 2% of  $\text{Cu}^{2+}$  species was present from the very start of the reaction. Looking at Figures 4.6 and 4.7, it is expected that the evolution of  $-\ln(1-\xi)$  in time should not show such a decrease in slope when  $\text{CuBr}_2$  is present.

If we consider all variables and parameters that can be responsible for the decreasing slope in the evolution of  $-\ln(1-\xi)$  with time, the following possible explanations can be postulated. First, the propagation rate constant is decreasing during polymerisation. This is merely a hypothetical explanation, since there is no evidence for this reported for free-radical polymerisation. Even if ATRP would not obey a conventional free-radical mechanism, a decrease of  $k_p$  with conversion would not be expected to occur. Second, the concentration of dormant species is decreasing during polymerisation. If this were the case, we would expect this to happen at the start of the reaction in particular, since at that moment the radical concentration has its maximum value. In this small period of time, bimolecular termination causes a decrease in the



concentration of the dormant species. This allows the deactivator concentration to build up according to the persistent radical effect. After this period, bimolecular termination takes place only moderately and the concentration of dormant species will not decrease much anymore. Furthermore, the 2% of  $\text{Cu}^{2+}$  species should ensure fast deactivation immediately after the start of the polymerisation. A decrease in dormant species concentration, therefore, is no plausible reason for a decreasing reaction rate. A third possibility could be a decrease of  $[\text{Cu}^+]$ . This could be due to bimolecular termination of the radicals, or by the presence of traces of oxygen in the reaction mixture. As we discussed earlier, bimolecular termination should play only a minor role after the persistent radical concentration has been built up and can therefore not be held responsible for the effects observed. On the other hand, oxygen might well be introduced into the reaction mixture when samples are taken through the septum. The oxygen then could react either with polymeric radicals or with  $\text{Cu}^+$ . Assuming comparable reactivities towards  $\text{R}\cdot$  and  $\text{Cu}^+$  with the latter being present in much larger concentrations ( $[\text{Cu}^+]:[\text{R}\cdot] \sim 10^{-3} \text{ mol}\cdot\text{L}^{-1}:10^{-7} \text{ mol}\cdot\text{L}^{-1}$ ), the oxygen is more likely to oxidise the  $\text{Cu}^+$ .

In the light of this explanation, it is interesting to take a look at Figure 4.9, where two polymerisations of BA are displayed. These homopolymerisations have been conducted at almost identical conditions, *i.e.* the initial concentrations of alkyl halide and catalyst were almost the same. However, in one experiment the polymerisation rate drops dramatically from the fifth data point on. It is suspected, although no hard proof is present, that when taking this sample for the fifth data point, a small amount of oxygen was introduced via the syringe, causing  $[\text{Cu}^+]$  to decrease.

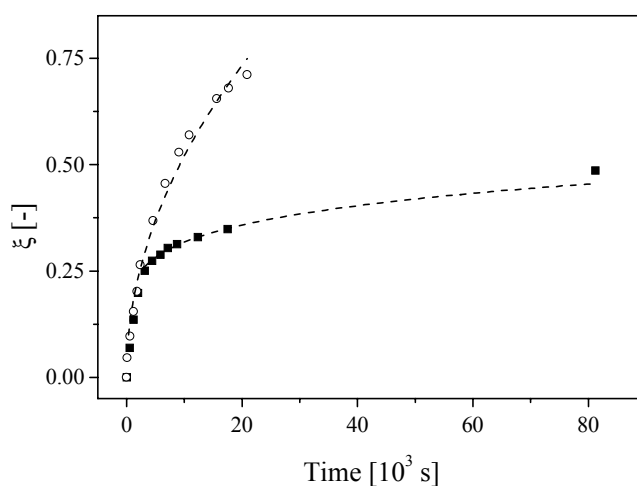


**Figure 4.9** Conversion-time histories for two polymerisations of BA in *p*-xylene. ■: Presumably with oxygen introduced during the reaction ( $[\text{BA}] = 3.78 \text{ mol}\cdot\text{L}^{-1}$ ,  $[\text{Cu}^+] = 0.0187 \text{ mol}\cdot\text{L}^{-1}$ ,  $[\text{I-Br}] = 0.0186 \text{ mol}\cdot\text{L}^{-1}$ ); ○: without oxygen ( $[\text{BA}] = 3.78 \text{ mol}\cdot\text{L}^{-1}$ ,  $[\text{Cu}^+] = 0.0168 \text{ mol}\cdot\text{L}^{-1}$ ,  $[\text{I-Br}] = 0.0222 \text{ mol}\cdot\text{L}^{-1}$ ) at  $110^\circ\text{C}$ .

It can clearly be seen that in the beginning both reactions proceed at the same rate and that suddenly the rate drops dramatically. This makes it plausible that even a minor amount of oxygen in the system will hamper any kinetic investigation on ATRP polymerisations and should therefore be prevented at all times.

Other important aspects of the homopolymerisations are the molecular weights and the molecular-weight distributions. For the homopolymerisations of S and BA the evolution of  $M_n$  as a function of conversion is displayed in Figures 4.10.

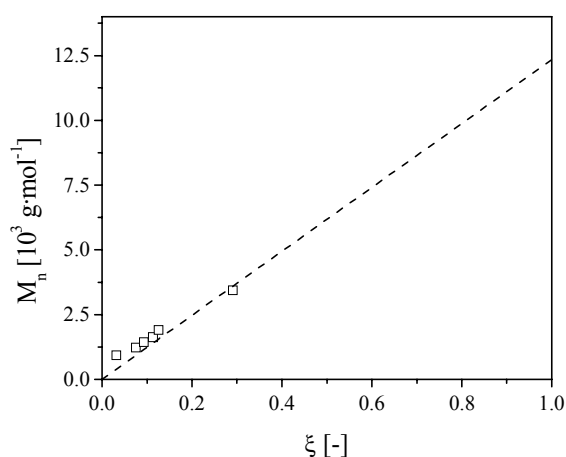


**Figure 4.10a** Evolution of  $M_n$  as a function of conversion for a homopolymerisation of S in p-xylene at 110°C; experimental data ( $\square$ ), expected from theory (---).

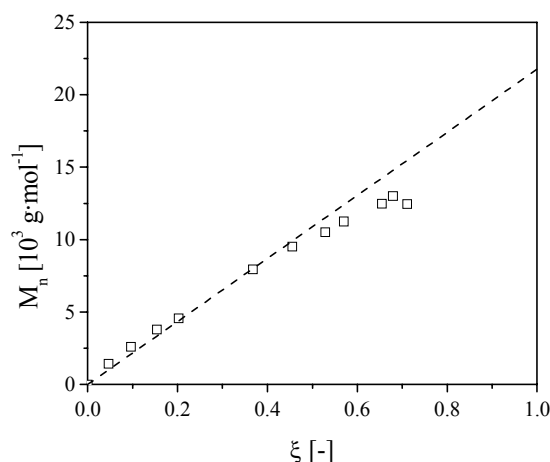


**Figure 4.10b** Evolution of  $M_n$  as a function of conversion for a homopolymerisation of BA in p-xylene at 110°C; experimental data ( $\square$ ), expected from theory (---).

These plots show that control of molecular weight is well possible for homopolymerisations of S and BA. Molecular weights increase linearly with conversion, which is the proof for the living character of the ATRP system. Furthermore, polydispersities are low and always stay below 1.3.

Knowing that the ATRP system with  $\text{Cu}/(\text{dHbpy})_2$  as catalyst is suitable for the polymerisation S and BA and having optimised the experimental conditions, we are now ready to investigate the homopolymerisation kinetics in order to quantify the deactivation rate coefficients.

#### 4.4.3.2 Kinetic experiments

It has to be stressed that these experiments were carried out in the presence of deactivating species, *i.e.*  $\text{Cu}^{2+}$  in the form of  $\text{CuBr}_2$ , at the beginning of the reaction. The evolution of  $-\ln(1-\xi)$  in time for duplo homopolymerisations of S and BA are displayed in Figures 4.11a and b, respectively. Note that the differences between the

evolutions of  $-\ln(1-\xi)$  for the duplo reactions are caused by differences in  $[I-Br]_0$ ,  $[Cu^+]_0$  and  $[Cu^{2+}]_0$ .

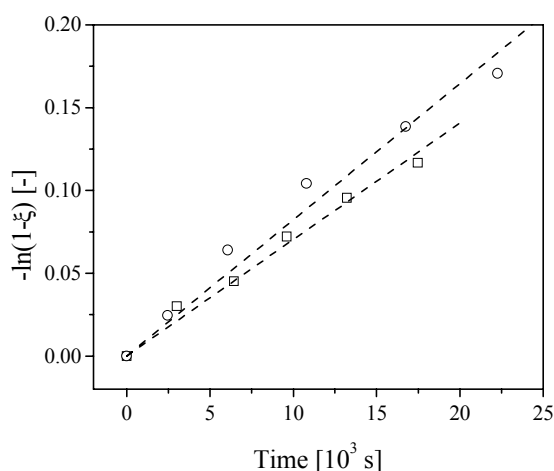


**Figure 4.11a** Evolution of  $-\ln(1-\xi)$  in time for a homopolymerisation of S in p-xylene at 110°C in the presence of 5% of  $Cu^{2+}$ ; reaction 1 (○) and 2 (□).

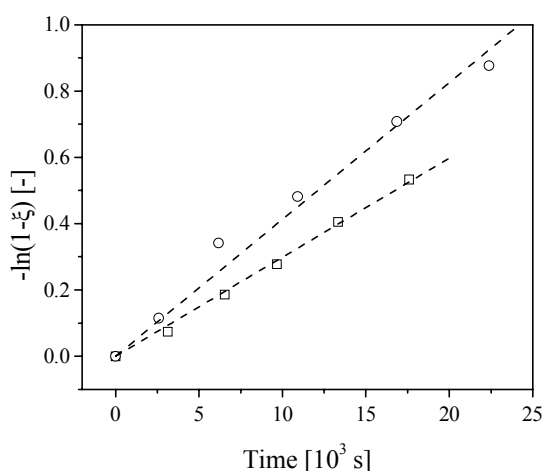


**Figure 4.11b** Evolution of  $-\ln(1-\xi)$  in time for a homopolymerisation of BA in p-xylene at 110°C in the presence of 5% of  $Cu^{2+}$ ; reaction 1 (○) and 2 (□).

The data in Figures 4.11 show that Eq. (3.15) is obeyed, although it should be noted that BA homopolymerisations give less scatter. There is no explanation for this at this moment. According to Eq. (3.15), in order to calculate the deactivation rate coefficients for PS and PBA dormant species, the initial concentrations of alkyl halide initiator,  $[I-Br]_0$ , catalyst,  $[Cu^+]$ , and deactivator,  $[Cu^{2+}]$ , need to be known. For both the S homopolymerisations and the BA homopolymerisations, the initial concentrations are collected in Table 4.4, together with the slopes ( $\alpha$ ) of the linear fits from Figures 4.11 and the calculated deactivation rate coefficients,  $k_{deact}^S$  and  $k_{deact}^{BA}$ .

**Table 4.4** Calculated deactivation rate coefficients for S and BA homopolymerisations in p-xylene at 110°C in the presence of 5%  $Cu^{2+}$ .

Reaction	$[I-Br]_0$ $mol \cdot L^{-1}$	$[Cu^+]_0$ $mol \cdot L^{-1}$	$[Cu^{2+}]_0$ $mol \cdot L^{-1}$	$\alpha$ -	$k_{act}$ $L \cdot mol^{-1} \cdot s^{-1}$	$k_p$ $L \cdot mol^{-1} \cdot s^{-1}$	$k_{deact}$ $L \cdot mol^{-1} \cdot s^{-1}$
S 1	$4.10 \cdot 10^{-2}$	$3.89 \cdot 10^{-2}$	$2.14 \cdot 10^{-3}$	$7.03 \cdot 10^{-6}$	0.43	$1.58 \cdot 10^3$	$7.2 \cdot 10^7$
S 2	$4.19 \cdot 10^{-2}$	$3.95 \cdot 10^{-2}$	$2.18 \cdot 10^{-3}$	$8.22 \cdot 10^{-6}$	0.43	$1.58 \cdot 10^3$	$6.3 \cdot 10^7$
BA 1	$3.71 \cdot 10^{-2}$	$3.43 \cdot 10^{-2}$	$2.02 \cdot 10^{-3}$	$3.18 \cdot 10^{-5}$	0.075	$7.84 \cdot 10^4$	$1.2 \cdot 10^8$
BA 2	$3.91 \cdot 10^{-2}$	$3.47 \cdot 10^{-2}$	$2.21 \cdot 10^{-3}$	$4.13 \cdot 10^{-5}$	0.075	$7.84 \cdot 10^4$	$8.7 \cdot 10^7$

From Table 4.4, it can be concluded that the deactivation rate coefficients for PS and PBA dormant species in *p*-xylene can be derived with a reasonable error interval of 10-15%. In order to investigate the effect of solvent on the deactivation rate coefficients, the kinetic experiments have also been carried out in butyl acetate. This is particularly important in view of the copolymerisations of S and BA, where composition drift occurs during polymerisation. The results for the kinetic experiments in butyl acetate are summarised in Table 4.5.

**Table 4.5** Calculated deactivation rate coefficients for S and BA homopolymerisations in butyl acetate at 110°C in the presence of 5% Cu<sup>2+</sup>.

Reaction	$[I-Br]_0$ <i>mol·L<sup>-1</sup></i>	$[Cu^+]_0$ <i>mol·L<sup>-1</sup></i>	$[Cu^{2+}]_0$ <i>mol·L<sup>-1</sup></i>	$\alpha$ -	$k_{act}$ <i>L·mol<sup>-1</sup>·s<sup>-1</sup></i>	$k_p$ <i>L·mol<sup>-1</sup>·s<sup>-1</sup></i>	$k_{deact}$ <i>L·mol<sup>-1</sup>·s<sup>-1</sup></i>
S	$4.35 \cdot 10^{-2}$	$3.96 \cdot 10^{-2}$	$2.09 \cdot 10^{-3}$	$6.37 \cdot 10^{-6}$	0.27	$1.58 \cdot 10^3$	$5.5 \cdot 10^7$
BA	$3.82 \cdot 10^{-2}$	$3.61 \cdot 10^{-2}$	$1.76 \cdot 10^{-3}$	$5.50 \cdot 10^{-5}$	0.086	$7.84 \cdot 10^4$	$1.1 \cdot 10^8$

We assume that the propagation rate coefficient,  $k_p$ , is not dependent on solvent. It is striking to see that the calculated deactivation rate coefficients from Table 4.5 do not show a significant solvent dependence. The deactivation rate coefficient for PBA dormant species does not even show the slightest decrease upon employing a more polar solvent, whereas the activation rate coefficient did. The equivalent coefficient for PS dormant species seems to be somewhat lower than in *p*-xylene, but is still very close. It should therefore be concluded that the deactivation process is less solvent dependent than the activation process.

## 4.5 CONCLUSIONS

In order to describe the copolymerisation of S and BA in ATRP, and ultimately control the chemical composition distribution, detailed knowledge on the homopolymerisations is indispensable.

By feasibility studies, it was shown that the ATRP homopolymerisations of S and BA can be conducted fairly easily. Molecular weights show a linear dependence on conversion and the polydispersities stay below 1.3, even at higher conversions.

Activation and deactivation rate coefficients have been determined using nitroxide exchange experiments and subsequent analysis by HPLC. The activation of PS dormant species in *p*-xylene at 110°C is much faster than the activation of PBA

dormant species:  $k_{act}^S = 0.43 \text{ L}\cdot\text{mol}^{-1}\cdot\text{s}^{-1}$  and  $k_{act}^B = 0.075 \text{ L}\cdot\text{mol}^{-1}\cdot\text{s}^{-1}$ . Solvent seems to have a significant influence on the activation process.

The deactivation rate coefficients have been determined by performing ATRP homopolymerisations in the presence of an initial amount of  $\text{CuBr}_2$ . By doing this, the impact of inaccuracies in termination rate coefficients as well as activation and deactivation rate coefficients of the alkyl halide initiator is minimised. The deactivation rate coefficients are similar for  $\text{PS}\cdot$  and  $\text{PBA}\cdot$  radicals and seem to be less dependent on solvent than the activation rate coefficient.

The activation and deactivation rate coefficients have been determined with reasonable accuracy in this chapter, but they still contain a considerable error of roughly 10-20%. When describing the homopolymerisation of S or BA, therefore, one should always bear in mind these inaccuracies. This is especially important when it is attempted to describe the ATRP copolymerisation of S and BA.

## REFERENCES

- <sup>1</sup> Olaj, O.F.; Bitai, I.; Hinkelmann, F. *Makromol. Chem.* **1987**, *188*, 1689
- <sup>2</sup> Buback, M.; Gilbert, R.G.; Hutchinson, R.A.; Klumperman, B.; Kuchta, R.-D.; Manders, B.G.; O'Driscoll, K.F.; Russell, G.T.; Schweer, J. *Macromol. Chem. Phys.* **1995**, *196*, 3267
- <sup>3</sup> Manders, B.G. *Ph.D. thesis*; Technische Universiteit Eindhoven: Eindhoven, 1999; Chapter 5
- <sup>4</sup> Von Smoluchowski, M. *Z. Phys. Chem., Stoichiom. Verwandtschaftsl.* **1917**, *92*, 129
- <sup>5</sup> Fischer, H.; Paul, H. *Acc. Chem. Res.* **1987**, *20*, 200
- <sup>6</sup> Griffiths, M.C.; Strauch, J.; Monteiro, M.J.; Gilbert, R.G. *Macromolecules* **1998**, *31*, 7835
- <sup>7</sup> Piton, M.C.; Gilbert, R.G.; Chapman, B.E.; Kuchel, P.W. *Macromolecules* **1993**, *26*, 4472
- <sup>8</sup> Ohno, K.; Goto, A.; Fukuda, T.; Xia, J.; Matyjaszewski, K. *Macromolecules* **1998**, *31*, 2699
- <sup>9</sup> Goto, A.; Fukuda, T. *Macromol. Rapid Commun.* **1999**, *20*, 633
- <sup>10</sup> Bon, S.A.F.; Chambard, G.; German, A.L. *Macromolecules* **1999**, *32*, 8269
- <sup>11</sup> Bowry, V.W.; Ingold, K.U. *J. Am. Chem. Soc.* **1992**, *114*, 4992
- <sup>12</sup> De Kock, J.B.L., *Ph.D. thesis*; Technische Universiteit Eindhoven: Eindhoven, 1999
- <sup>13</sup> Matyjaszewski, K.; Patten, T.E.; Xia, J. *J. Am. Chem. Soc.* **1997**, *119*, 674
- <sup>14</sup> Hutchinson, R.A.; Paquet, D.A.; McMinn, J.H.; Beuermann, S.; Fuller, R.E.; Jackson, C. *DEHEMA Monogr.* **1995**, *131*, 467
- <sup>15</sup> Trathnigg, B.; Kollroser, M.; Berek, D.; Nguyen, S.H.; Hunkeler, D. *ACS Symp. Ser.* **1999**, *731*, 95
- <sup>16</sup> Lide, D.R., Frederikse, H.P.R. *CRC Handbook of Chemistry and Physics*, 78<sup>th</sup> ed.; CRC Press: New York, 1997
- <sup>17</sup> Arehart, S.V.; Matyjaszewski, K. *Macromolecules* **1999**, *32*, 2221

- <sup>18</sup> Haddleton, D.M.; Shooter, A.J.; Heming, A.M.; Crossman, M.C.; Duncalf, D.J.; Morsley, S.R. In *Controlled Radical Polymerization*; Matyjaszewski, K., Ed.; ACS Symposium Series No. 685; American Chemical Society: Washington DC, 1997; p 284
- <sup>19</sup> Chambard, G.; de Man, P.A.P.; Klumperman, B. *Macromol. Symp.* **2000**, *150*, 45
- <sup>20</sup> Moad, G.; Rizzardo, E.; Solomon, D.H.; Beckwith, A.L.J. *Polym. Bull. (Berlin)* **1992**, *29*, 647
- <sup>21</sup> Fukuda, T.; Goto, A.; Ohno, K. *Macromol. Rapid Commun.* **2000**, *21*, 151



# 5

## *ATRP Copolymerisation of Styrene and Butyl Acrylate*

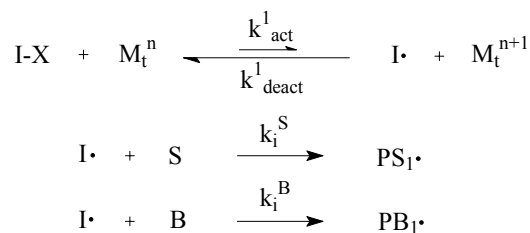
**Synopsis:** In this chapter, the reactivity ratios as well as the activation and deactivation rate coefficients,  $k_{act}$  and  $k_{deact}$ , respectively, for polystyrene and poly(butyl acrylate) dormant species are transposed to the ATRP copolymerisation of styrene and butyl acrylate. The temperature dependence of the reactivity ratios in the free-radical copolymerisation of styrene and butyl acrylate is investigated. Furthermore, the impact of the ATRP equilibria on the observed reactivity ratios is assessed. Kinetic experiments are performed and the living character of the copolymerisation is verified. It is endeavoured to link the conversion to the reaction time by comparing experimental data with model predictions. By using the basic kinetic parameters from chapter 4, the copolymerisation of styrene and butyl acrylate in ATRP can be described and control of chemical composition distribution is accomplished.



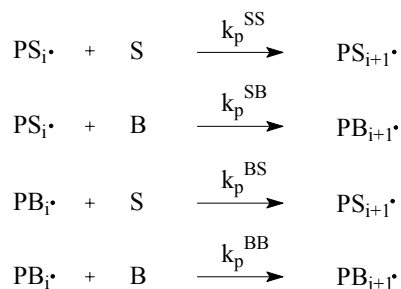
## 5.1 COPOLYMERISATION MODELS

Just as was done in chapter 4 for the homopolymerisation of styrene (S) and butyl acrylate (BA), it is useful to consider the reaction scheme of their copolymerisation. As already mentioned in chapter 2, several models to describe free-radical copolymerisation exist<sup>1,2,3,4,5</sup>. For reasons of simplicity, only the terminal unit model<sup>1,2</sup> and the penultimate unit model<sup>3,4</sup> will be considered in this chapter.

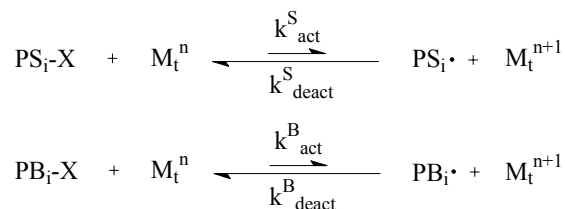
*Initiation:*



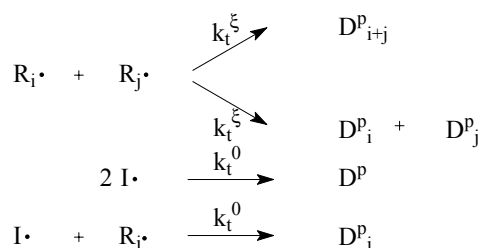
*Propagation:*



*ATRP equilibria:*



*Bimolecular termination:*



**Scheme 5.1 Terminal model reaction scheme for the copolymerisation of S and BA in ATRP.**

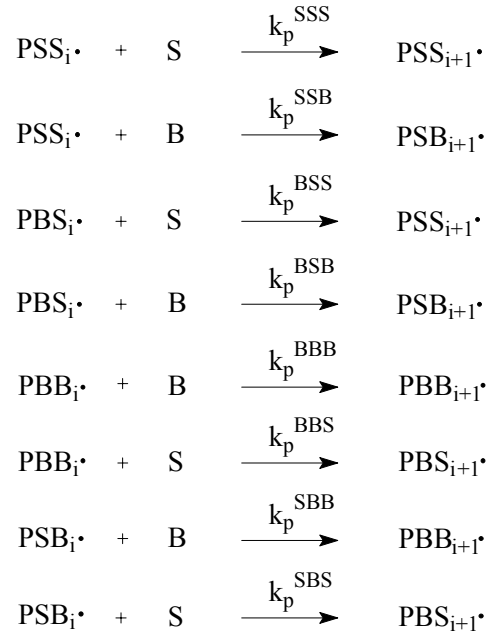
For the terminal unit model (TUM), the reaction scheme for the copolymerisation of S and BA is given in Scheme 5.1. Note that butyl acrylate is abbreviated with B, and dead material with D. As can be seen in Scheme 5.1, the initiation step now involves two reactions, *i.e.* the reaction of the alkyl halide derived radical with S and with BA. The initiation rate coefficients are, as in chapter 4, assumed to be not significantly different from the respective homopropagation rate coefficients. Therefore,  $k_i^S = k_p^{SS}$  and  $k_i^B = k_p^{BB}$ . The propagation steps are now given by four reactions, each governed by the corresponding propagation rate coefficient. For the copolymerisation of S and BA, the reactivity ratios are defined as the ratios of homopropagation rate coefficients and crosspropagation rate coefficients, see chapter 2.

$$r_S = \frac{k_p^{SS}}{k_p^{SB}} \quad \text{and} \quad r_B = \frac{k_p^{BB}}{k_p^{BS}}$$

Dubé *et al.*<sup>6</sup> evaluated  $r_S$  and  $r_B$  in bulk free-radical copolymerisation thoroughly and estimated them to be 0.95 for S and 0.18 for BA at 50°C.

Since two different dormant species and radicals exist, two ATRP equilibria are taken into account: one between the styrene-ended radical and its corresponding dormant species, and the other between the butyl acrylate-ended radical and its corresponding dormant species. Finally, the bimolecular termination reactions are assumed to be governed by the same chain-length-dependent termination rate coefficient,  $k_t$ .

The TUM generally describes the instantaneous chemical composition of the copolymer as a function of monomer composition at the locus of polymerisation reasonably well, which is also the case for the system S/BA. However, the copolymerisation of S and BA, as most copolymerisation systems, is not well characterised by the TUM in terms of the average propagation rate coefficient as a function of monomer composition<sup>7,8</sup> and for this reason it is necessary to consider the penultimate unit model (PUM)<sup>9</sup>. For the PUM we also have to take into account the effect of the penultimate unit on the propagation reaction. The following eight propagation steps are then obtained:



**Scheme 5.2 Penultimate unit model propagation reactions for the copolymerisation of S and BA.**

In addition to these propagation steps, it is assumed that after formation of the alkyl halide derived radical the initiation reactions of this species with S and BA immediately yield  $\text{PSS}_1\cdot$  and  $\text{PBB}_1\cdot$ , respectively. Furthermore, since the PUM is meant to describe the average propagation rate coefficient, the penultimate unit effect is only accounted for in the propagation reactions. It is assumed that the penultimate unit does not affect the rate coefficients in other reactions. For instance, a penultimate unit effect in the activation and deactivation processes are extremely difficult to determine experimentally and, as a consequence, only two ATRP equilibria between dormant species and growing radicals will be taken into account, namely the ones depicted in Scheme 5.1. Like in the TUM, reactivity ratios have been defined in the PUM as well.

$$\begin{array}{l}
r_{SS} = \frac{k_p^{\text{SSS}}}{k_p^{\text{SSB}}} \\
r_{BB} = \frac{k_p^{\text{BBB}}}{k_p^{\text{BBS}}} \\
r_{BS} = \frac{k_p^{\text{BSS}}}{k_p^{\text{BSB}}} \\
r_{SB} = \frac{k_p^{\text{SBB}}}{k_p^{\text{SBS}}}
\end{array}
\qquad
\begin{array}{l}
S_S = \frac{k_p^{\text{BSS}}}{k_p^{\text{SSS}}} \\
S_B = \frac{k_p^{\text{SBB}}}{k_p^{\text{BBB}}}
\end{array}$$

In the explicit penultimate unit model  $r_{SS} \neq r_{BS}$  and  $r_{BB} \neq r_{SB}$ <sup>10</sup>. In this chapter we will only deal with the implicit penultimate unit model, *i.e.*  $r_{SS} = r_{BS}$  and  $r_{BB} = r_{SB}$ .

For  $r_{SS}$  and  $r_{BB}$  the values of the TUM are used, *i.e.* 0.95 and 0.18 respectively. The  $s$ -values are not accurately known and may be amenable to a significant error. Davis *et al.*<sup>7</sup> evaluated the copolymerisation of S and BA at 50°C and estimated  $s_S = 0.90$  and  $s_B = 0.11$ . Unfortunately, Davis *et al.* used an inaccurate homopropagation rate coefficient of BA in their analysis, which causes the  $s$ -values to be incorrect. Using their data together with the correct homopropagation rate coefficient of BA<sup>11</sup> and recalculating the  $s$ -values yields  $r_S = 0.48$  and  $r_B = 0.06$ <sup>12</sup>.

## 5.2 REACTIVITY RATIOS IN THE S/BA COPOLYMERISATION

### 5.2.1 General

The copolymerisation reactivity ratios of S and BA have been a matter of discussion for decades. Probably the first thorough investigation was done by Bradbury and co-workers<sup>13</sup>, who reported reactivity ratios of the copolymerisation in bulk and in benzene. High-conversion bulk copolymerisations were reported by Gruber and Knell<sup>14</sup>. More recently, Kaszás *et al.*<sup>15</sup> investigated the reactivity ratios and the rate of initiation in bulk polymerisation and as solution polymerisation in benzene. As already mentioned, Dubé *et al.*<sup>6</sup> extensively studied the S/BA system as well and reported reactivity ratios  $r_S$  and  $r_B$  of 0.95 and 0.18, respectively. An extension to this work was performed by Davis and co-workers<sup>7</sup>, who reported  $s$ -values at 50°C. All these investigations focus on the copolymerisation at low or moderate temperatures, *i.e.* 20°C to 50°C.

Although reactivity ratios are believed to be approximately temperature-independent, O'Driscoll theoretically evaluated the temperature dependence of reactivity ratios<sup>16</sup>. According to O'Driscoll, the reactivity ratios should go towards unity upon increasing temperature. Therefore, when copolymerisations of S and BA are performed at higher temperatures, for instance 110°C, different reactivity ratios might be expected.

### 5.2.2 Determination of reactivity ratios in ATRP

In free-radical copolymerisation, reactivity ratios are generally determined by performing low-conversion experiments with various initial monomer compositions. The average chemical compositions of the resulting copolymers are analysed, *e.g.* by <sup>1</sup>H NMR. It is known that copolymer composition is generally well-described by the TUM and the copolymer composition vs. monomer composition is therefore fitted

with the differential copolymer composition equation<sup>1</sup>, as was also stated in chapter 2. In order to obtain statistically correct estimates of the reactivity ratios, non-linear least squares methods should be applied<sup>17,18</sup>.

For the copolymerisation of S and BA, the differential copolymer composition equation<sup>1</sup> is given in Eq. (5.1).

$$F_S = \frac{r_S f_S^2 + f_S(1-f_S)}{r_S f_S^2 + 2f_S(1-f_S) + r_B(1-f_S)^2} \quad (5.1)$$

The differential copolymer composition equation only holds when chains are very long to exclude the influence of possible preferential addition of one of the monomers onto the initiator-derived radical. Additionally, this equation is derived under the assumption that the relative radical concentrations,  $[PS_i^\cdot]$  and  $[PB_i^\cdot]$ , are constant during the growth of a polymeric chain. As a consequence, the crosspropagation rates are equal during the growth of a polymeric chain. It very important to realise that the radical concentrations are in a pseudo-steady state, *i.e.* the concentration ratio of both radicals may change during the course of the polymerisation due to the occurrence of composition drift of the residual monomer.

In ATRP, however, the situation is completely different. After all, it is not useful to determine copolymer composition at low conversion, since all polymeric chains are growing throughout the complete reaction time. At low conversion, therefore, the chains are too short to allow accurate determination of reactivity ratios. Hence, one has to seek resort to the application of the integrated form of the copolymerisation equation, see Eq. (5.2)<sup>19,20</sup>.

$$\xi = 1 - \left( \frac{f_S}{f_S^0} \right)^{\frac{r_B}{1-r_B}} \left( \frac{1-f_S}{1-f_S^0} \right)^{\frac{r_S}{1-r_S}} \left( \frac{f_S^0 - \delta}{f_S - \delta} \right)^{\frac{1-r_B}{2-r_S-r_B}} \quad (5.2)$$

In Eq. (5.2),  $\xi$  is the fractional total conversion on a molar basis,  $f_S^0$  the initial mole fraction of S based on the total amount of monomer and  $\delta$  a function of the reactivity ratios according to:

$$\delta = \frac{1 - r_S r_B}{(1 - r_S)(1 - r_B)}$$

Eq. (5.2), although being much more complicated, can also be used to estimate reactivity ratios<sup>21,22</sup>. Moreover, it meets the requirement that it should be applicable up to high conversion. With gas chromatography<sup>23</sup> or on-line techniques such as Raman spectroscopy<sup>24,25</sup> the total conversion and comonomer ratio of the residual monomer can be monitored. Since both monomer composition and total conversion are calculated from the monomer concentration data, one has to take into account the experimental error in both variables. Fitting the data to Eq. (5.2) should therefore be perpetrated with two-dimensional non-linear least squares parameter estimation, eventually leading to estimates for the reactivity ratios,  $r_S$  and  $r_B$ .

In literature, several research groups attempted to investigate the reactivity ratios in ATRP copolymerisations. Haddleton and coworkers<sup>26</sup> investigated the copolymerisation of methyl methacrylate (MMA) and *n*-butyl methacrylate (BMA) using various polymerisation techniques, among which ATRP. For the ATRP reactions, however, Haddleton *et al.* performed low-conversion copolymerisations and used copolymer composition data in conjunction with Eq. (5.1). Despite this incorrect approach, they came to the conclusion that the reactivity ratios are very similar to those known for conventional free-radical copolymerisations<sup>27</sup>. Sawamoto *et al.*<sup>28</sup> reported the ATRP copolymerisation of S and MMA and also applied Eq. (5.1) to obtain the reactivity ratios. Although these authors used the Fineman-Ross method<sup>29</sup> to evaluate their data, they obtained reactivity ratios that are similar to those for conventional free-radical copolymerisation. Moineau *et al.*<sup>30</sup> investigated the ATRP copolymerisation of MMA and BA. Unfortunately, these authors assessed copolymer composition vs. monomer composition data for low-conversion copolymerisations (<5%). Moineau *et al.* observed a small difference in reactivity ratios when compared to the ones they obtained for conventional free-radical copolymerisation. These authors imputed this discrepancy to interactions of the metal centre with the growing radical. They ignored the fact that at low conversions, the copolymer composition is influenced to a large extent by possible preferential addition of one of the monomers to the alkyl halide derived radical. The reactivity ratios, as a consequence, may differ significantly when copolymers having low molecular weights are analysed. Roos and Müller<sup>31</sup> determined reactivity ratios for the ATRP system MMA/BA using the Kelen-Tüdös<sup>32</sup> method and the Jaacks<sup>33</sup> methods. Although the approach of Roos and Müller in principle is not correct either, they obtained reactivity ratios that were comparable with the free-radical reactivity ratios. Arehart and Matyjaszewski<sup>34</sup> thoroughly investigated the ATRP copolymerisation of S and BA and used high-conversion data together with Eq. (5.2) to evaluate reactivity ratios. Although they used the correct copolymer composition equation, they considered only a one-dimensional error structure. However, their results agree well

with literature values on the reactivity ratios for conventional free-radical S/BA copolymerisations<sup>6</sup>.

### 5.2.3 Effect of the ATRP equilibria on the observed reactivity ratios

Eq. (5.2) has been derived under the same assumption as Eq. (5.1), *i.e.* the concentrations of both  $PS_i\cdot$  and  $PB_i\cdot$  are constant during the growth of a polymeric chain and, as a consequence, the crosspropagation rates are equal:

$$k_p^{SB}[PS_i\cdot][BA] = k_p^{BS}[PB_i\cdot][S] \quad (5.3)$$

Using this steady-state assumption the radical ratio,  $[PS_i\cdot]/[PB_i\cdot]$ , can be eliminated in the derivation of Eqs. (5.1) and (5.2). So, it is clear that when the pseudo-steady-state situation is attained, the crosspropagation rate coefficients,  $k_p^{SB}$  and  $k_p^{BS}$ , and therefore the reactivity ratios, govern the radical ratio in conventional free-radical copolymerisation. In this case, the reactivity ratios that are calculated with Eqs. (5.1) and (5.2) will be a true representation of the intrinsic reactivity ratios as defined above.

In conventional free-radical copolymerisation, the steady-state assumption is indeed valid, but not necessarily in ATRP. All things considered, two ATRP equilibria involving PS and PBA dormant species and PS and PBA radicals play a role as well and Eq. (5.3) must be written accordingly:

$$k_p^{BS} \cdot [PB_i\cdot][S] - k_p^{SB} \cdot [PS_i\cdot][BA] + k_{act}^S \cdot [PS - X][M_t^n] - k_{deact}^S \cdot [PS\cdot][M_t^{n+1}] = 0$$

$$k_p^{BS} \cdot [PB_i\cdot][S] - k_p^{SB} \cdot [PS_i\cdot][BA] + k_{act}^B \cdot [PB - X][M_t^n] - k_{deact}^B \cdot [PB\cdot][M_t^{n+1}] = 0$$

These relations reduce to Eq. (5.3) when the system has reached both equilibria between dormant species and growing radicals. The radical ratio, from which the reactivity ratios are determined, could well be altered in the beginning of the polymerisation, when the system is not yet in the steady state with respect to the equilibria between dormant species and growing radicals. Since this radical ratio is responsible for the observed reactivity ratios, the values of the latter may well differ from the intrinsic reactivity ratios. This has consequences when drawing conclusions from the evaluation of the ATRP reactivity ratios, since a difference in observed reactivity ratios does not necessarily imply that ATRP does not obey free-radical copolymerisation kinetics. Furthermore, when the ATRP equilibria strongly influence

the kinetics of the system, free-radical reactivity ratios may not be used to predict the copolymer composition as a function of conversion. It is therefore crucial to evaluate the reactivity ratios in order to estimate to what extent the ATRP equilibria influence the radical ratio during polymerisation.

To test the possible effect of the ATRP equilibria on the radical ratio during polymerisation, simulations can be of great help. Let us consider an ATRP copolymerisation of S and BA in *p*-xylene at 110°C, using the kinetic knowledge on the activation, deactivation and propagation rate coefficients and applying the TUM as depicted in Scheme 5.1. A possible influence of the ATRP equilibria on the observed reactivity ratios is suspected when the radical ratio,  $[PS_i\cdot]/[PB_i\cdot]$ , during the polymerisation reaction is different from the ratio observed in conventional free-radical copolymerisation using identical kinetic parameters. Two sets of simulations with  $f_S^0=0.75$  and 0.25 have therefore been performed with Mathematica 4.0 software, see the appendix, in order to compare the results for the conventional free-radical copolymerisation with the ATRP copolymerisation of S and BA. In the simulation for the free-radical system, a conventional initiator has been used with an arbitrary dissociation rate coefficient of  $2.0\cdot 10^{-6} \text{ s}^{-1}$ . All input values used in the simulations are summarised in Table 5.1. Reactivity ratios of 0.95 for S and 0.18 for BA have been used.

**Table 5.1 Initial concentrations and parameters used in the simulations of the ATRP system as depicted in Scheme 5.1 and free-radical copolymerisation.**

<i>Parameter / Concentration</i>	<i>ATRP system</i>	<i>Free-radical system</i>
$f_S^0$	0.75 and 0.25	0.75 and 0.25
$[M_t^n]_0$	$5\cdot 10^{-2} \text{ mol}\cdot\text{L}^{-1}$	-
$[I-X]_0$	$5\cdot 10^{-2} \text{ mol}\cdot\text{L}^{-1}$	$5\cdot 10^{-2} \text{ mol}\cdot\text{L}^{-1}$
$k_p^{SS}$	$1.58\cdot 10^3 \text{ L}\cdot\text{mol}^{-1}\cdot\text{s}^{-1}$	$1.58\cdot 10^3 \text{ L}\cdot\text{mol}^{-1}\cdot\text{s}^{-1}$
$k_p^{BB}$	$7.84\cdot 10^4 \text{ L}\cdot\text{mol}^{-1}\cdot\text{s}^{-1}$	$7.84\cdot 10^4 \text{ L}\cdot\text{mol}^{-1}\cdot\text{s}^{-1}$
$k_{act}^1$	$0.43 \text{ L}\cdot\text{mol}^{-1}\cdot\text{s}^{-1}$	-
$k_{deact}^1$	$6.8\cdot 10^7 \text{ L}\cdot\text{mol}^{-1}\cdot\text{s}^{-1}$	-
$r_S$	0.95	0.95
$r_B$	0.18	0.18
$k_{act}^S$	$0.43 \text{ L}\cdot\text{mol}^{-1}\cdot\text{s}^{-1}$	-
$k_{act}^B$	$7.5\cdot 10^{-2} \text{ L}\cdot\text{mol}^{-1}\cdot\text{s}^{-1}$	-
$k_{deact}^S$	$6.8\cdot 10^7 \text{ L}\cdot\text{mol}^{-1}\cdot\text{s}^{-1}$	-
$k_{deact}^B$	$1.0\cdot 10^8 \text{ L}\cdot\text{mol}^{-1}\cdot\text{s}^{-1}$	-
$k_{dis}$	-	$2.0\cdot 10^{-6} \text{ s}^{-1}$
$k_t^0$	$1.0\cdot 10^8 \text{ L}\cdot\text{mol}^{-1}\cdot\text{s}^{-1}$	$1.0\cdot 10^8 \text{ L}\cdot\text{mol}^{-1}\cdot\text{s}^{-1}$



The results for the simulations with  $f_S^0=0.75$  are displayed in Figure 5.1, where the radical ratio is plotted against the overall monomer conversion.

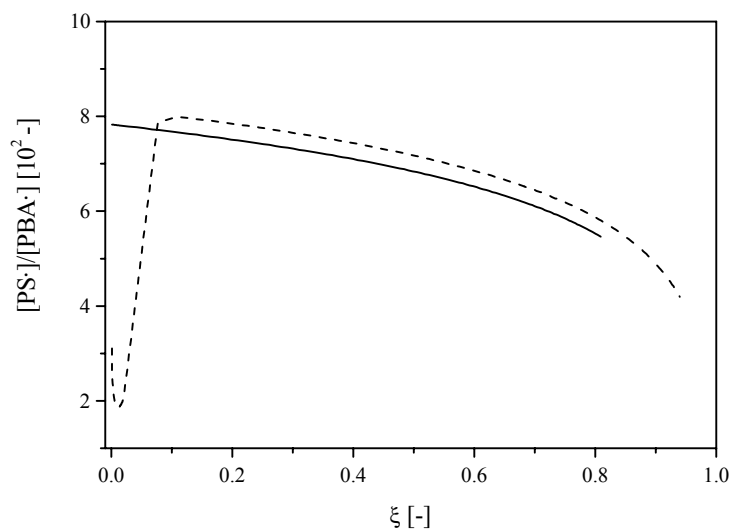


**Figure 5.1** Radical ratios vs. fractional conversion for simulations of a conventional free-radical copolymerisation (—) and an ATRP copolymerisation (---) of S and BA with the parameters listed in Table 5.1

As can be seen in Figure 5.1, the radical ratios, which govern the observed reactivity ratios, are not the same for free-radical and ATRP copolymerisation. In the beginning of the polymerisation, up to about 10% conversion, the radical ratio in the ATRP system shows a dramatic dip before it stabilises. This is due to the fact that the system has not yet reached a steady state in the equilibria between dormant species and growing radical chain. This period of non-equilibrium conditions also has a marked effect on the remaining part of the copolymerisation, which is reflected in the small shift in radical ratio compared to the ratio obtained in free-radical copolymerisation. This small offset in ATRP copolymerisation is probably caused by the change in monomer composition during the first part of the reaction when  $\xi < 0.10$ .

The monomer composition as a function of conversion is therefore an interesting issue to discuss. For the conventional free-radical and ATRP copolymerisation simulations with  $f_S^0=0.75$ , the fraction of S in the residual monomer vs. total conversion is plotted in Figure 5.2.

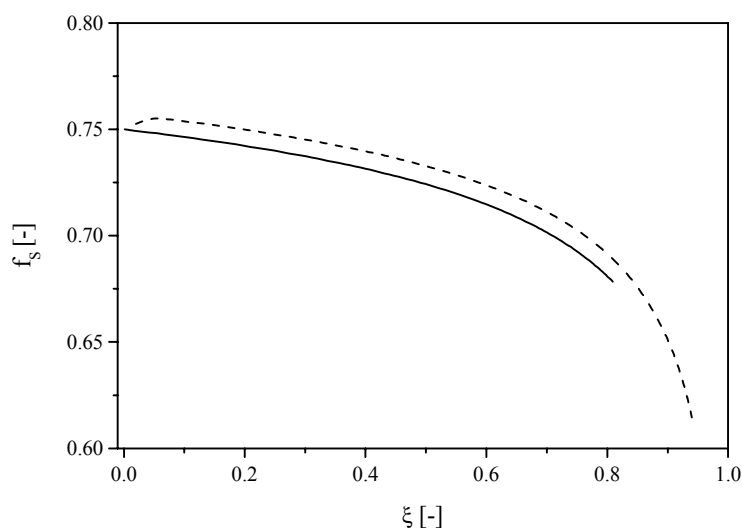


**Figure 5.2** Fraction of *S* in residual monomer vs. total conversion for simulations of a conventional free-radical copolymerisation (—) and an ATRP copolymerisation (---) of *S* and BA with the parameters listed in Table 5.1

From Figure 5.2 it is clear that the evolution of the monomer composition as a function of conversion is slightly different between both cases. In the beginning of the polymerisation, a small difference in monomer composition as a function of conversion is established, but after that both simulated lines stay parallel throughout the whole polymerisation.

Since the evolution of monomer composition as a function of conversion is proven to be slightly different from that in free-radical polymerisation, it is to be expected that when fitting Eq. (5.2) to these data, different reactivity ratios from those listed in Table 5.1 will be obtained. Indeed, when this exercise is performed, the reactivity ratios differ slightly from the input values. This is depicted in Figure 5.3, where the point estimate together with the 95% joint-confidence interval is shown. Note that the 95% joint-confidence interval does not even embrace the original input reactivity ratios.

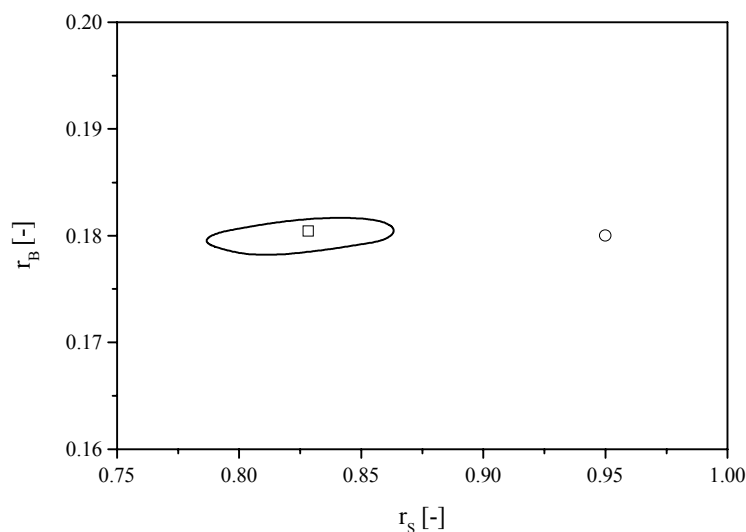


**Figure 5.3** 95% joint-confidence interval for the copolymerisation of S and BA with the parameters listed in Table 5.1. The ATRP point estimates (□) yields the following reactivity ratios:  $r_S=0.83$  and  $r_B=0.18$ ; input values (○).

For the free-radical copolymerisation point estimates, no 95% joint-confidence interval is plotted, since the error in the fit is very small. Figure 5.3 demonstrates that using Eq. (5.2), which holds for conventional free-radical polymerisation kinetics, in ATRP copolymerisations is in principle incorrect. Considering the effect that the ATRP equilibria can have on the kinetics of copolymerisation, care should be taken when abstracting reactivity ratios from high-conversion ATRP copolymerisation. As already stated, a difference in reactivity ratios as compared to free-radical copolymerisation reactivity ratios does not conclusively signify that the system does not follow classical free-radical kinetics. Moreover, the results of these simulations demonstrate that in principle free-radical reactivity ratios cannot be used as such to predict the development of monomer composition as a function of conversion in ATRP reactions. This certainly is the case when the system very slowly approaches the ATRP equilibria. To circumvent this problem, it is absolutely necessary to take into account the ATRP equilibria and to use a complete model (e.g. Scheme 5.1) in the kinetic evaluation.

#### 5.2.4 Summary

Since reactivity ratios are possibly dependent on temperature and, in addition, the impact of the ATRP equilibria on the kinetics is not known beforehand, it is necessary to cast a closer look on the reactivity ratios in free-radical copolymerisation and ATRP first. The temperature dependence of the reactivity ratios in conventional free-radical copolymerisation will therefore be evaluated. Similarly, although simulations

indicate that the ATRP equilibria do not significantly affect the kinetics, the actual system will be subjected to thorough investigation. The outcome might give an indication on the correctness of the proposed model.

### 5.2.5 Experimental

#### *Materials:*

The copper ligand, 4,4'-di-*n*-heptyl-2,2'-bipyridine (dHbpy), was synthesised according to a literature procedure<sup>35</sup>. Styrene (S, Aldrich, 99%) and butyl acrylate (BA, Aldrich, 99+%) were distilled and stored over molecular sieves. *p*-Xylene (Aldrich, 99+% HPLC grade) was stored over molecular sieves and used without further purification. CuBr (98%, Aldrich) and tosylchloride (TsCl, 99%, Aldrich) were used as received.

#### *Procedure for the low-conversion copolymerisations:*

S/BA copolymers were prepared at 50°C, 90°C, 100°C, 110°C and 120°C in bulk. Optimal monomer compositions were calculated applying the Tidwell-Mortimer criterion<sup>36</sup> and using literature values of the reactivity ratios<sup>6</sup>. At both optimal values of  $f_S^0$ , five copolymerisations were carried out. Conversion was determined gravimetrically and was kept below 1% in most cases. Hereafter, the reaction mixtures were freeze-dried and subsequently dried in a vacuum oven at room temperature for 1 day.

Copolymer composition was determined by <sup>1</sup>H NMR on a 400 MHz Bruker at 50°C in CDCl<sub>3</sub>. Peak areas of the proton resonances at  $\delta=7$  ppm (phenyl) and  $\delta=3.8$  ppm (methoxyl) were taken to calculate the copolymer composition. Monomer composition versus copolymer composition data was evaluated using non-linear least squares fitting which yields the most accurate values of both reactivity ratios<sup>17,18</sup>.

#### *Procedure for the ATRP copolymerisations:*

A typical copolymerisation of S and BA with  $f_S^0=0.827$  was performed using the following procedure. In a 100 mL three-necked round-bottom flask equipped with a magnetic stirrer *p*-xylene (12.00 g) was mixed with S (8.095 g, 0.0777 mol), BA (2.082 g, 0.0162 mol) and dHbpy (0.580 g,  $1.65 \cdot 10^{-3}$  mol). Hereafter, the reaction mixture was degassed by purging with dry argon for at least 45 minutes. After this, CuBr (0.100 g,  $6.97 \cdot 10^{-4}$  mol) was added and the reaction mixture was homogenised and purged with dry argon for another 15 minutes. The reaction mixture was then placed in a thermostatically controlled oil bath at 110°C. The reaction was started by addition of previously degassed solution of TsCl (0.182 g,  $9.55 \cdot 10^{-4}$  mol) in *p*-xylene. Samples from the reaction mixture were withdrawn through a septum with a syringe

and cooled down immediately. Partial monomer conversions were determined by gas chromatography using a HP 5890 gas chromatograph equipped with an AT Wax column (Alltech, length 30 m, film thickness 1.0  $\mu\text{m}$ ) and an auto sampler. The remainders of the samples were first passed through a column with aluminumoxide (activated, neutral, Brockman I, STD grade approx. 150 mesh, 58 $\text{\AA}$ , Aldrich) to remove the copper catalyst using stabilized tetrahydrofuran (AR, Biosolve) as eluent. After subsequent drying, the polymers were dissolved in stabilised tetrahydrofuran at 1  $\text{mg}\cdot\text{mL}^{-1}$  and filtrated using 0.2  $\mu\text{m}$  filters. The molecular weights were determined by size exclusion chromatography (SEC) with a Waters Model 510 pump and Waters 712 WISP using 4 PL-gel mix C columns (300 $\text{mm}\times 7.5\text{mm}$ , Polymer Laboratories) at 40 $^{\circ}\text{C}$  and tetrahydrofuran as eluent. The eluent flow rate was 1.0  $\text{mL}\cdot\text{min}^{-1}$ . Calibration was performed with polystyrene standards with narrow molecular-weight distributions (Polymer Laboratories). All molecular weights were calculated relative to polystyrene. A Waters 410 differential refractometer and a Waters 440 UV detector operating at 254 nm were used for detection. Data acquisition was done with Millennium-32 3.05 software.

## 5.2.6 Results and discussion

### 5.2.6.1 Low-conversion free-radical copolymerisations

Low-conversion copolymerisations of S and BA have been carried out at 50 $^{\circ}\text{C}$ , 90 $^{\circ}\text{C}$ , 100 $^{\circ}\text{C}$ , 110 $^{\circ}\text{C}$  and 120 $^{\circ}\text{C}$  and the reactivity ratios have been calculated by fitting the data with Eq. (5.1). The 95% joint-confidence intervals are plotted in Figure 5.4.

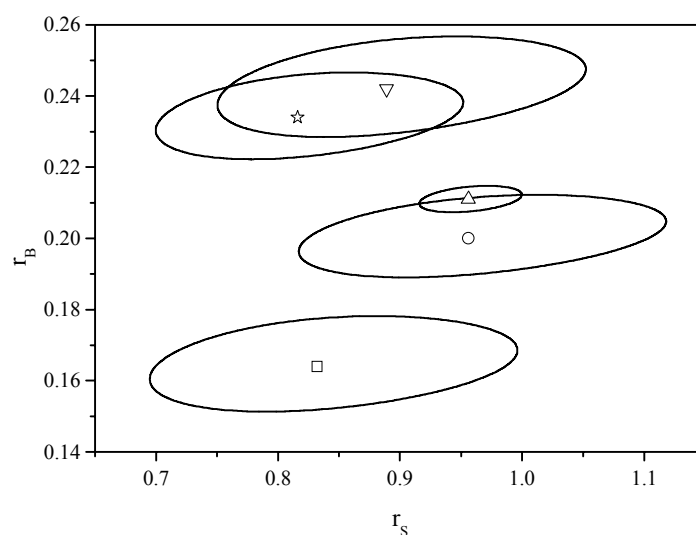


*Figure 5.4 95% joint-confidence intervals of free-radical copolymerisations of S and BA at 50 $^{\circ}\text{C}$  (□), 90 $^{\circ}\text{C}$  (○), 100 $^{\circ}\text{C}$  (△), 110 $^{\circ}\text{C}$  (▽) and 120 $^{\circ}\text{C}$  (☆).*

What immediately catches the eye when looking at Figure 5.4 is that the reactivity ratios are temperature dependent. However, it seems that only  $r_B$  is temperature dependent, since the 95% joint-confidence intervals do not overlap for  $r_B$ . The reactivity ratio for S, on the contrary, does not seem to exhibit a significant temperature dependence. The value of  $r_B$  seems to increase with increasing temperature, although this trend is violated when looking at the data at 110°C.

The temperature dependence of  $r_B$  can be quantified when plotting  $\ln(r_B)$  against  $T^{-1}$ , see Figure 5.5. The point estimate at 110°C has not been taken into account in the fitting procedure.

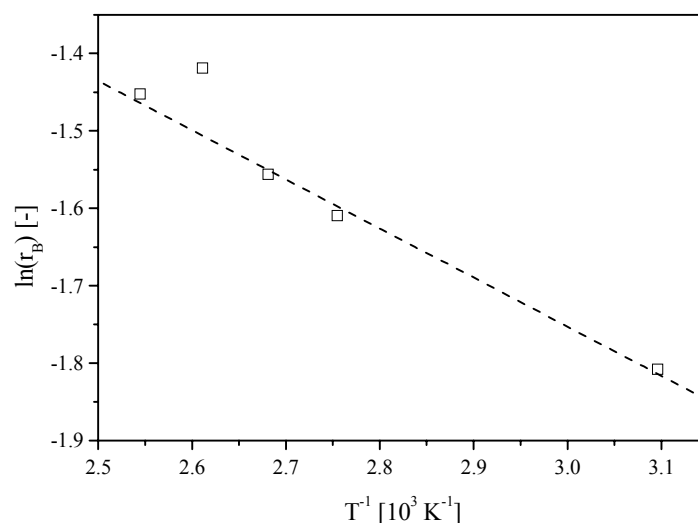


**Figure 5.5**  $r_B$  as a function of temperature; experimental data ( $\square$ ) and calculated fit (---) with  $\ln(r_B) = a + b/T$ , with  $a = 0.15$  and  $b = -634 \text{ K}^{-1}$ .

The fit through the data yields a slope of  $-634 \text{ K}^{-1}$  and an intercept of 0.15. From the slope, one can calculate that the difference in activation energy between homopropagation and crosspropagation, *i.e.*  $E_a^{BB} - E_a^{BS}$ , equals  $5.3 \cdot 10^3 \text{ J} \cdot \text{mol}^{-1}$ . This difference is relatively small and demonstrates that the temperature dependence of  $r_B$  is not very strong. Using the data from Figure 5.5,  $r_B$  can be calculated at any desired temperature. At 110°C, the reactivity ratio of BA equals 0.22. The literature values for the reactivity ratios at 50°C,  $r_S = 0.95$  and  $r_B = 0.18$ <sup>6</sup>, compare very well with the values presented in Figure 5.4. In the description of the ATRP copolymerisations  $r_B = 0.22$  will be used together with  $r_S = 0.95$  in first approximation.

These reactivity ratios have been determined in bulk, while the ATRP copolymerisations will be conducted in *p*-xylene solution. In principle it is possible that the reactivities of the radicals in *p*-xylene differ from those in bulk. Fernández-García and co-workers<sup>37</sup> investigated this possibility for S/BA copolymerisations in

benzene and benzonitrile at 50°C. They found that the reactivity ratios were different for solution copolymerisations in benzonitrile, but that they were similar to bulk values when benzene was used as a solvent. Fernández-García *et al.* concluded that in non-polar solvents preferential solvation of one of the monomers does not occur. It is therefore reasonable to assume that the reactivity ratios in *p*-xylene will be comparable to those calculated with our data for bulk polymerisations.

### 5.2.6.2 Reactivity ratios in ATRP

To investigate the reactivity ratios in ATRP, four copolymerisations have been carried out at different  $f_S^0$ . Values for  $f_S^0$  were chosen where a large composition drift was expected, *i.e.* at  $f_S^0=0.251$ , 0.271, 0.694 and 0.827. The monomer composition and overall conversion data was fitted to Eq. (5.2) using non-linear least squares parameter estimation. The 95% joint-confidence intervals for these copolymerisations are collected in Figure 5.6.

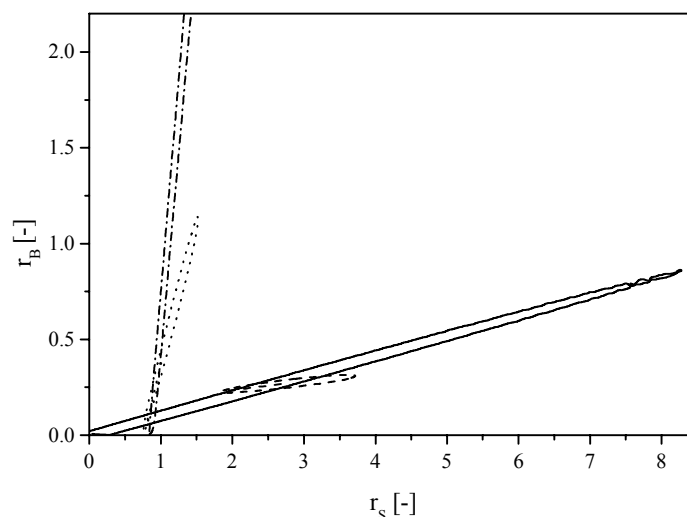


**Figure 5.6** 95% joint-confidence intervals for the ATRP copolymerisation of S and BA at four different initial monomer compositions;  $f_S^0=0.251$  (—),  $f_S^0=0.271$  (---),  $f_S^0=0.694$  (-·-·-),  $f_S^0=0.827$  (- - -)

The 95% joint-confidence intervals in Figure 5.7 are a two-dimensional representation of the three-dimensional error space. It has been assured that in all copolymerisations the same number of samples has been taken. Therefore, in the analysis of the monomer composition vs. overall conversion data, the same statistical treatment could be performed for all samples.

As can be seen from Figure 5.6, the shape of the joint confidence intervals is strongly dependent on  $f_S^0$ . For high  $f_S^0$ , the  $r_S$  is well-determined, but the error in  $r_B$  is large. When applying a low fraction of styrene in the monomer mixture, the situation is

exactly opposite. To obtain a reliable joint-confidence interval for both reactivity ratios, the sum of the squared residuals spaces of experiments at different initial monomer composition must be combined. The combined sum of squared residuals space can be visualized, leading to an estimation of reactivity ratios, see Figure 5.7. The point estimates are  $r_S=0.89$  and  $r_B=0.17$ .

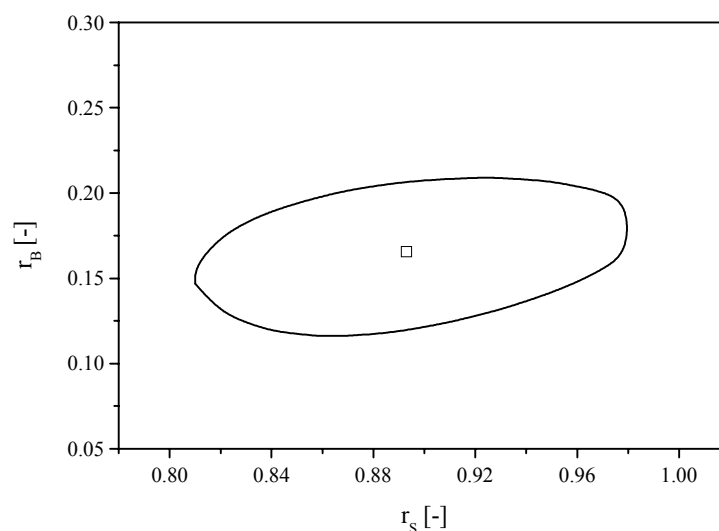


**Figure 5.7** 95% Joint confidence interval resulting from the four joint confidence intervals presented in Figure 5.6.  $r_S=0.89$  and  $r_B=0.17$ .

The reactivity ratios that are obtained via combination of the sum of squared residuals spaces of the high-conversion copolymerisations are in very good agreement with free-radical literature values<sup>6</sup>, as well as with the results obtained by Arehart *et al.*<sup>34</sup>. Furthermore, the reactivity ratios depicted in Figure 5.7 are also very similar to those obtained from the bulk copolymerisations.

As expected from simulations, the experimentally obtained reactivity ratios point to an insignificant interference of the ATRP equilibria in the instantaneous copolymer composition. This suggests a fast approach of the equilibria between dormant and radical species. The reactivity ratios from conventional free-radical polymerisation will therefore be used in an attempt to describe the ATRP copolymerisation reaction in order to ultimately control the copolymer composition distribution.



## 5.3 MODELLING OF THE ATRP COPOLYMERISATIONS OF S AND BA

### 5.3.1 Evolution of $-\ln(1-\xi)$

Having the knowledge that the observed reactivity ratios for the ATRP copolymerisation of S and BA do not deviate significantly from those in conventional free-radical copolymerisation, it is now possible to try to develop a mathematical description for the actual copolymerisation reaction. In order to be able to control the incorporation of monomers into the polymeric chain and to produce polymers with a pre-defined intramolecular composition distribution, the strategy is to link the rate of polymerisation with reaction time. In this way, the reaction time and monomer conversion (and therefore copolymer composition) are interchangeable. In this section, therefore, special attention is paid to the evolution of  $-\ln(1-\xi)$  with time.

As in ATRP homopolymerisation, a closer look has to be cast on the chain-length-dependent termination coefficient in copolymerisations. It is known that this coefficient not only depends on chain length, but also on the chemical composition of the polymeric radical. A model proposed by Fukuda *et al.*<sup>38</sup> seems to describe bimolecular termination in copolymerisation reasonably well:

$$\left(k_{t,copo}^{\xi}\right)^{-1} = \left(k_{t,11}^{\xi}\right)^{-1} \cdot F_1 + \left(k_{t,22}^{\xi}\right)^{-1} \cdot F_2 \quad (5.4)$$

This equation relates the bimolecular termination rate coefficient in copolymerisation ( $k_{t,copo}^{\xi}$ ) to the termination rate coefficients for homopolymerisation ( $k_{t,11}^{\xi}$  and  $k_{t,22}^{\xi}$ ) as well as to the overall chemical composition of the polymeric radicals involved ( $F_1$  and  $F_2$ ). It is based on the assumption that bimolecular termination is a diffusion-controlled process and seems to describe the copolymerisation termination kinetics of acrylate/methacrylate systems fairly well<sup>39</sup>. The termination rate coefficients for homopolymeric radicals can be calculated with Eq. (4.9), see chapter 4:

$$k_{t,ii}^{\xi} = k_t^0 \left( 1 + \frac{[M]_0}{[I-X]_0} \xi \right)^{-(0.664+2.02 \cdot w_{M,0} \cdot \xi)} \quad (4.9)$$

Consequently, in all ATRP copolymerisations, chain length, conversion as well as chemical composition of the radicals is important and should be taken into account to calculate  $k_{t,copo}^{\xi}$ .

However, an important aspect to look at before performing the copolymerisations, is whether a small initial amount of deactivator, *i.e.*  $\text{CuBr}_2$ , in the polymerisation will have the same beneficial consequences as in the homopolymerisations. As in chapter 4, simulations can be performed to trace whether the effect of the initiation process or the chain-length-dependent termination rate coefficient can be ruled out by the addition of a small amount of  $\text{Cu}^{2+}$  (in the form of  $\text{CuBr}_2$ ) in the recipe.

Simulations have been carried out varying the activation rate coefficient for the alkyl halide,  $k_{act}^I$ , and  $k_t^0$ . The influence of  $k_{deact}^I$  on the kinetics has not been assessed, since it has been shown in chapter 4 to be analogous to the influence of  $k_{act}^I$ . The TUM in Scheme 5.1 is used as the copolymerisation model and the initial concentrations and parameters are summarised in Table 5.1. In the simulation with  $\text{CuBr}_2$  present at the beginning of the reaction  $[\text{CuBr}_2]_0$  is set to  $2.5 \cdot 10^{-3} \text{ mol} \cdot \text{L}^{-1}$ . The results for the simulations are depicted in Figures 5.8a (effect of  $k_{act}^I$ ) and b (effect of  $k_t^0$ ).

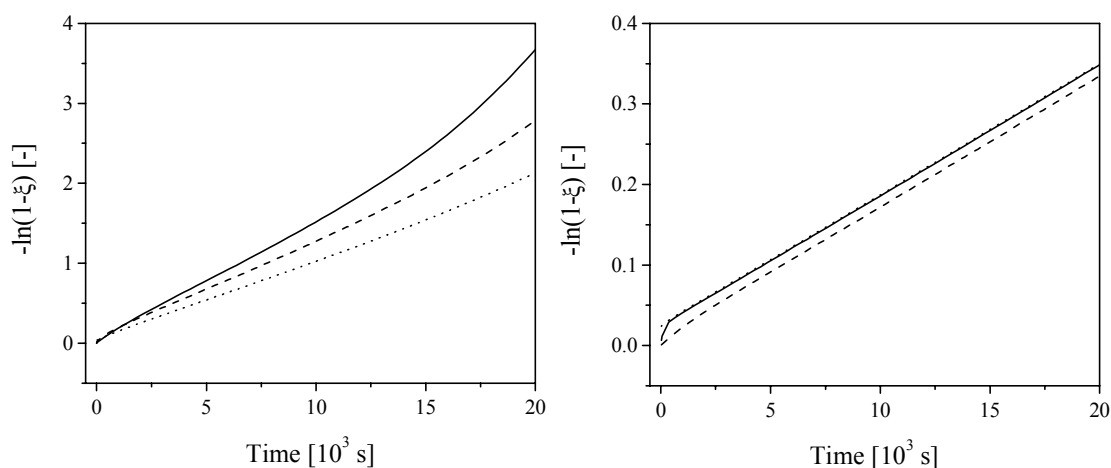


**Figure 5.8a** Influence of  $k_{act}^I$  on the evolution of  $-\ln(1-\xi)$  with time for simulations of ATRP copolymerisations of S and BA using the model in Scheme 5.1 and the parameters in Table 5.1. Left: without initial  $\text{CuBr}_2$ ; Right:  $[\text{CuBr}_2]_0 = 0.0025 \text{ mol} \cdot \text{L}^{-1}$ ;  $k_{act}^I = 0.43 \text{ L} \cdot \text{mol}^{-1} \cdot \text{s}^{-1}$  (—),  $k_{act}^I = 0.043 \text{ L} \cdot \text{mol}^{-1} \cdot \text{s}^{-1}$  (---) and  $k_{act}^I = 4.3 \text{ L} \cdot \text{mol}^{-1} \cdot \text{s}^{-1}$  (···).

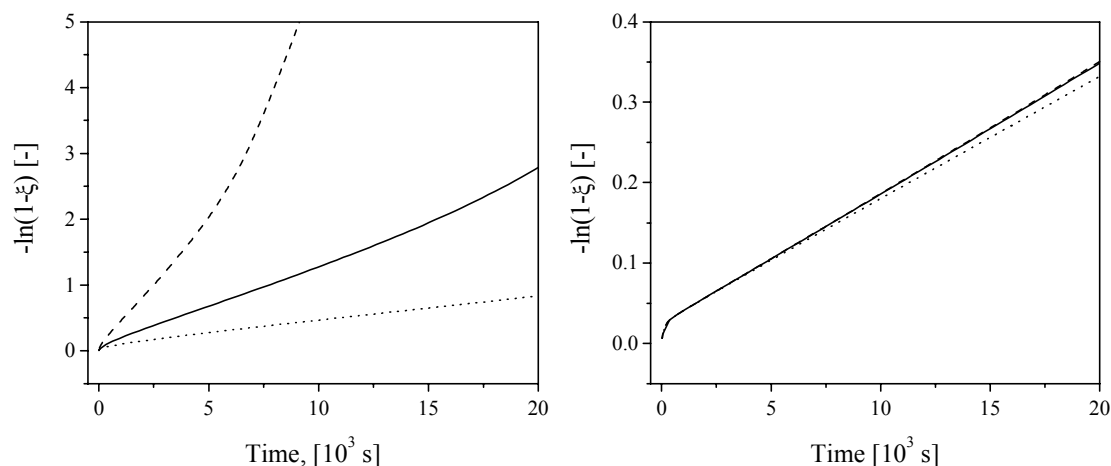


**Figure 5.8b** Influence of  $k_t^0$  on the evolution of  $-\ln(1-\xi)$  with time for simulations of ATRP copolymerisations of S and BA using the model in Scheme 5.1 and the parameters in Table 5.1. Left: without initial  $\text{CuBr}_2$ ; Right:  $[\text{CuBr}_2]_0 = 0.0025 \text{ mol}\cdot\text{L}^{-1}$ ;  $k_t^0 = 1 \cdot 10^8 \text{ L}\cdot\text{mol}^{-1}\cdot\text{s}^{-1}$  (—),  $k_t^0 = 1 \cdot 10^7 \text{ L}\cdot\text{mol}^{-1}\cdot\text{s}^{-1}$  (---) and  $k_t^0 = 1 \cdot 10^9 \text{ L}\cdot\text{mol}^{-1}\cdot\text{s}^{-1}$  (⋯).

Figures 5.8 clearly show that in the copolymerisation of S and BA the addition of  $\text{CuBr}_2$  at the start of the reaction is beneficial as well. According to Figure 5.8a, the initiation process does not seem to have a significant impact on the course of the polymerisation reaction when  $\text{CuBr}_2$  is added. Additionally, errors in the description of  $-\ln(1-\xi)$  in time that might be introduced through inaccuracies in the bimolecular termination rate coefficient are greatly reduced when 5%  $\text{CuBr}_2$  is added, see Figure 5.8b. The addition of deactivator at the beginning of the reaction, therefore, will be standard for all following copolymerisations of S and BA.

### 5.3.2 Experimental

#### Materials:

The copper ligand, 4,4'-di-*n*-heptyl-2,2'-bipyridine (dHbpy), was synthesised according to a literature procedure<sup>35</sup>. Styrene (S, Aldrich, 99%) and butyl acrylate (BA, Aldrich, 99+%) were distilled and stored over molecular sieves. *p*-Xylene (Aldrich, 99+% HPLC grade) was stored over molecular sieves and used without further purification.  $\text{CuBr}$  (99,999%, Aldrich) was stored in a glove box, while  $\text{CuBr}_2$  (99%, Aldrich) and ethyl 2-bromoisobutyrate (98%, Aldrich) were used as received.

#### Procedure for the copolymerisations:

A typical copolymerisation of S and BA with  $f_S^0 = 0.5$  is as follows. In a 100 mL three-necked round-bottom equipped with a magnetic stirrer, *p*-xylene (5.00 g) was mixed with S (2.50 g, 0.0240 mol), BA (3.08 g, 0.0240 mol), dHbpy (0.338 g,

$9.60 \cdot 10^{-4}$  mol),  $\text{CuBr}_2$  (0.0055 g,  $2.46 \cdot 10^{-5}$  mol) and ethyl 2-bromoisobutyrate (0.0940 g,  $4.82 \cdot 10^{-4}$  mol). While stirring, the reaction mixture was degassed by purging with dry argon for at least 45 minutes. Hereafter,  $\text{CuBr}$  (0.0670 g,  $4.67 \cdot 10^{-4}$  mol) was added and the reaction mixture was homogenised and purged with dry argon for another 15 minutes. After this, the reaction mixture was placed in a thermostatically controlled oil bath at  $110^\circ\text{C}$ . Samples from the reaction mixture were withdrawn through a septum with a syringe and cooled down immediately. Monomer conversion was determined by gas chromatography using a HP 5890 gas chromatograph equipped with an AT Wax column (Alltech, length 30 m, film thickness  $1.0 \mu\text{m}$ ) and an auto sampler. The remainder of the samples was used for molecular weight and copolymer composition analysis. For these purposes, the samples were first passed through a column with aluminumoxide (activated, neutral, Brockman I, STD grade approx. 150 mesh,  $58\text{\AA}$ , Aldrich) to remove the copper catalyst using stabilized tetrahydrofuran (AR, Biosolve) as eluent. After subsequent drying, the polymers were dissolved in stabilised tetrahydrofuran at  $1 \text{ mg}\cdot\text{mL}^{-1}$  and filtrated using  $0.2 \mu\text{m}$  filters. The molecular weights were determined by size exclusion chromatography (SEC) with a Waters Model 510 pump and Waters 712 WISP using 4 PL-gel mix C columns ( $300\text{mm} \times 7.5\text{mm}$ , Polymer Laboratories) at  $40^\circ\text{C}$  and tetrahydrofuran as eluent. The eluent flow rate was  $1.0 \text{ mL}\cdot\text{min}^{-1}$ . Calibration was performed with polystyrene standards with narrow molecular-weight distributions (Polymer Laboratories). All molecular weights were calculated relative to polystyrene. A Waters 410 differential refractometer was used for detection. Data acquisition was done with Millennium-32 3.05 software.

For the copolymer composition analysis, 10 wt% solutions of the copolymers in  $\text{CDCl}_3$  were subjected to  $^1\text{H}$  NMR using a 400 MHz Bruker operating at  $20^\circ\text{C}$ . Peak areas of the proton resonances at  $\delta=7$  ppm (phenyl) and  $\delta=3.8$  ppm (methoxyl) were taken to calculate copolymer composition.

### 5.3.3 Results and discussion

#### 5.3.3.1 Assessment of living character

In order to assess the living character of the ATRP copolymerisations of S and BA, the evolution of  $M_n$  vs. conversion should be investigated. A linear increase of  $M_n$  as a function of conversion is one of the indications for proper control of the polymerisation reaction. The molecular weights for two typical copolymerisations of S and BA ( $f_S^0=0.3$  and  $0.5$ ) in *p*-xylene at  $110^\circ\text{C}$  are plotted in Figure 5.9. The results clearly demonstrate the living character of the polymerisation.

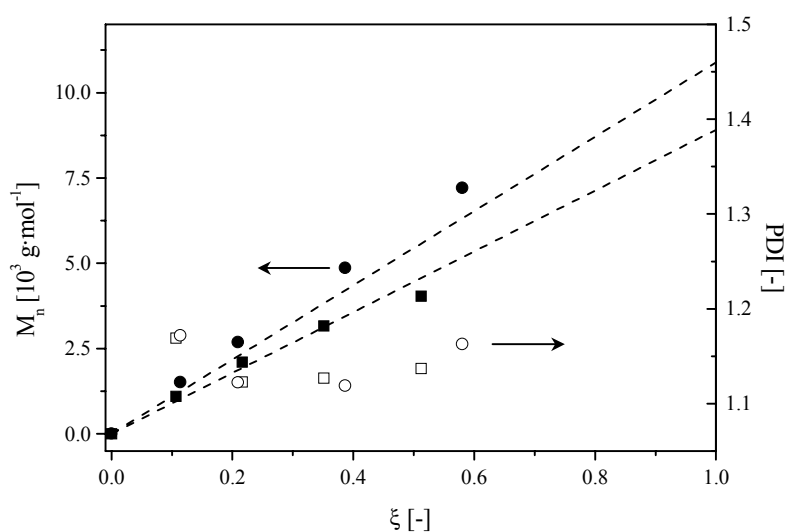


**Figure 5.9** Evolution of molecular weight and polydispersity index (PDI) as a function of total conversion in two ATRP copolymerisations of S and BA;  $f_S^0=0.3$  ( $M_n$ : ● and PDI: ○) and  $f_S^0=0.5$  ( $M_n$ : ■ and PDI: □). Theoretical predictions for  $M_n$  (---).

Although the linear increase in  $M_n$  with conversion suggests good control of the reaction, it does not necessarily point to a minimisation of bimolecular termination in the system. It does, however, indicate that chain-transfer processes play a minor role. Since we are dealing here with the *number-average* molecular weight, the effect of chain transfer occurring during polymerisation would be much more pronounced than that of bimolecular termination. However, the molecular-weight distributions evidently show that the functionality of the dormant species is retained throughout the reaction and that termination only plays a marginal role. Polydispersities do not seem to increase during the reaction and stay well below 1.2.

It is also interesting to look at the chemical composition of the copolymers as a function of total conversion and compare the results with theory. When determining the chemical composition by, for instance,  $^1\text{H}$  NMR one should bear in mind that the cumulative chemical composition is obtained. Since the TUM generally describes the copolymer composition well, we compare the experimental data with a theoretical prediction of the cumulative fraction of S in the copolymer using the TUM with  $r_S=0.95$  and  $r_B=0.22$ , see Figure 5.10.

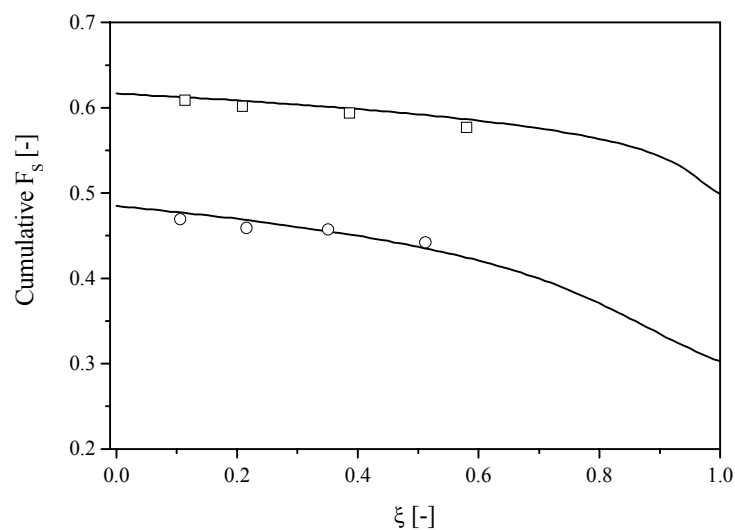


**Figure 5.10** Cumulative fraction of styrene in the copolymer as a function of total conversion for two ATRP copolymerisations of S and BA;  $f_S^0=0.3$  ( $\circ$ ),  $f_S^0=0.5$  ( $\square$ ) and their respective theoretical predictions.

The results in Figure 5.10 demonstrate that the model predictions of the cumulative fraction of S in the copolymer using the reactivity ratios  $r_S=0.95$  and  $r_B=0.22$  agree well with the experimental data. Nevertheless, the cumulative copolymer composition is a relatively poor instrument to distinguish between different models or parameters and the significance of Figure 5.10 therefore has to be considered in that perspective.

### 5.3.3.2 Evolution of $-\ln(1-\xi)$ as a function of $f_S^0$

Three copolymerisations have been carried out at three different initial monomer compositions:  $f_S^0=0.3$ , 0.5 and 0.7. The evolution of  $-\ln(1-\xi)$  in time for these copolymerisations is plotted in Figure 5.11.

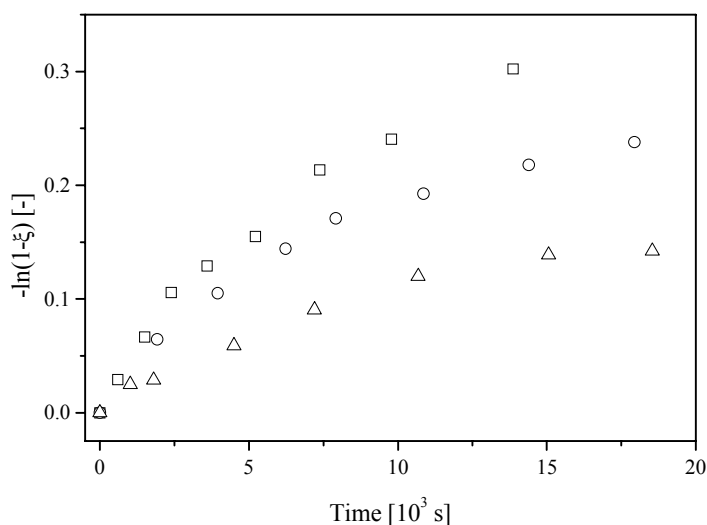


**Figure 5.11**  $-\ln(1-\xi)$  vs. time for ATRP copolymerisations of S and BA in *p*-xylene at 110°C at three different initial monomer compositions;  $f_S^0 = 0.7$  ( $\Delta$ ),  $f_S^0 = 0.5$  ( $\circ$ ) and  $f_S^0 = 0.3$  ( $\square$ ).

The evolution of  $-\ln(1-\xi)$  with time shows a marked dependence on the initial monomer composition, as can be seen in Figure 5.11. Apparently, the polymerisation reaction proceeds at a higher rate when the fraction of butyl acrylate in the monomer mixture is higher. Bearing in mind the homopropagation rate coefficients of S and BA at 110°C,  $1.58 \cdot 10^3 \text{ L} \cdot \text{mol}^{-1} \cdot \text{s}^{-1}$  and  $7.84 \cdot 10^4 \text{ L} \cdot \text{mol}^{-1} \cdot \text{s}^{-1}$ , respectively, one would indeed expect an increased rate of polymerisation. After all, the average propagation rate coefficient will gradually increase when more BA is present in the monomer mixture. The way in which it is exactly dependent on the monomer composition is of course governed by the detailed kinetics of the copolymerisation system.

There is, however, an opposing effect. It concerns the activation and deactivation rate coefficients for PS and PBA dormant species. As was demonstrated in chapter 4, the deactivation rate coefficients for both dormant species are quite similar, while the activation rate coefficient of PBA in *p*-xylene is almost 6 times lower than that of PS dormant species. Upon increasing BA content in the monomer composition, the relative amount of PBA dormant species will also increase. As a result, the ‘average activation rate coefficient’ will decrease and, consequently, the rate of polymerisation will drop.

As stated before, these opposing effects cannot be described in an analytical way and are therefore very difficult to predict. The results depicted in Figure 5.11 will therefore be compared with simulations using the TUM, see Scheme 5.1, or the PUM, see Scheme 5.2. All simulations are carried out with Mathematica 4.0 software using the algorithms listed in the appendix.

### 5.3.3.3 Modelling of the ATRP copolymerisations of S and BA

In this section, the results of the copolymerisations will be compared with three different models, namely the TUM with  $r_S=0.95$  and  $r_B=0.22$ , the PUM with  $r_{SS}=0.95$ ,  $r_{BB}=0.22$ ,  $s_S=0.90$  and  $s_B=0.11$ <sup>7</sup> and the PUM with  $r_{SS}=0.95$ ,  $r_{BB}=0.22$ ,  $s_S=0.48$  and  $s_B=0.06$ <sup>12</sup>. The concentrations of all species were used as input values in the simulations.

For the copolymerisations with  $f_S^0=0.3$ , 0.5 and 0.7 the evolution of  $-\ln(1-\xi)$  with time of both experimental data and simulations are depicted in Figure 5.12a, b and c, respectively.

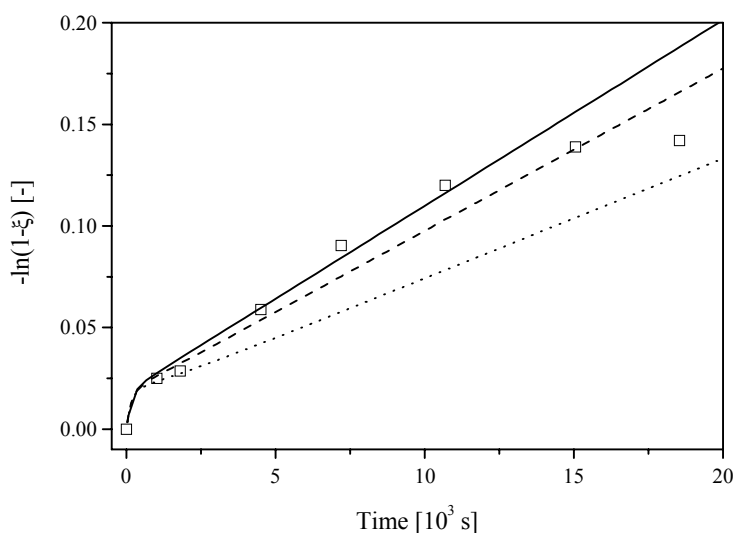


**Figure 5.12a** Evolution of  $-\ln(1-\xi)$  with time for the ATRP copolymerisation of S and BA with  $f_S^0=0.7$ ; experimental data ( $\square$ ), TUM simulation with  $r_S=0.95$  and  $r_B=0.22$  (—) and PUM simulation with  $r_{SS}=0.95$ ,  $r_{BB}=0.22$ ,  $s_S=0.90$  and  $s_B=0.11$  (---)  $r_{SS}=0.95$ ,  $r_{BB}=0.22$ ,  $s_S=0.48$  and  $s_B=0.06$  (···).



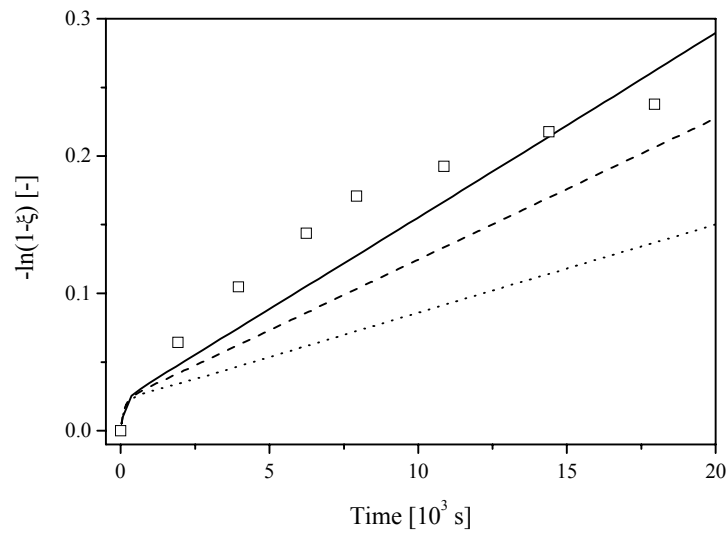


**Figure 5.12b** Evolution of  $-\ln(1-\xi)$  with time for the ATRP copolymerisation of *S* and *BA* with  $f_S=0.5$ ; experimental data ( $\square$ ), TUM simulation with  $r_S=0.95$  and  $r_B=0.22$  (—) and PUM simulation with  $r_{SS}=0.95$ ,  $r_{BB}=0.22$ ,  $s_S=0.90$  and  $s_B=0.11$  (---)  $r_{SS}=0.95$ ,  $r_{BB}=0.22$ ,  $s_S=0.48$  and  $s_B=0.06$  (···).

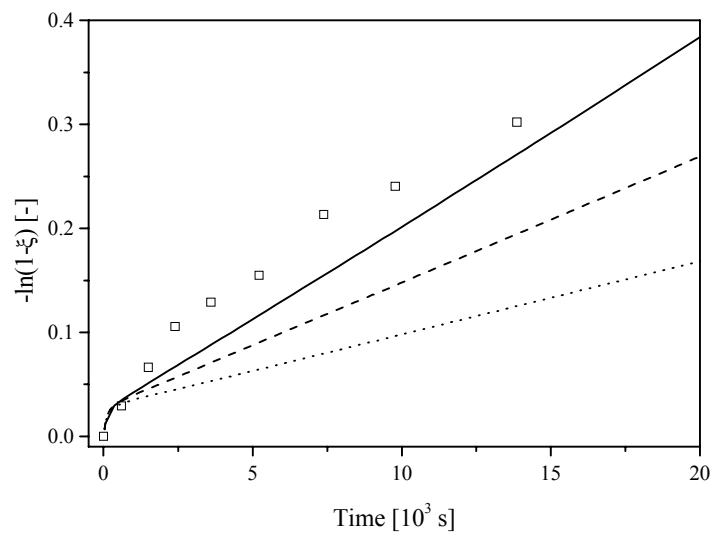


**Figure 5.12c** Evolution of  $-\ln(1-\xi)$  with time for the ATRP copolymerisation of *S* and *BA* with  $f_S=0.3$ ; experimental data ( $\square$ ), TUM simulation with  $r_S=0.95$  and  $r_B=0.22$  (—) and PUM simulations with  $r_{SS}=0.95$ ,  $r_{BB}=0.22$ ,  $s_S=0.90$  and  $s_B=0.11$  (---) and with  $r_{SS}=0.95$ ,  $r_{BB}=0.22$ ,  $s_S=0.48$  and  $s_B=0.06$  (···).

It is very interesting to see how the simulations compare with the experimental data. Two aspects immediately catch the eye. First, it seems that the penultimate unit model

fails to describe the kinetics of ATRP copolymerisation, whereas the terminal unit model closer approaches the experimental data. Second, the ATRP copolymerisation can be well described for a high  $f_S^0$ . At  $f_S^0=0.7$ , the model prediction fits the experimental data very well, while at higher BA contents the model predictions deviate systematically from the experimental data.

The first observation is totally unexpected, since the conventional free-radical copolymerisation kinetics of S and BA at 50°C is well-described by the PUM<sup>7</sup>. The answer might lie in the fact that we conducted our copolymerisations at a higher temperature, *viz.* 110°C, whereas copolymerisations of S and BA in literature are mostly performed at temperatures of 20°C or 50°C. At these moderate temperatures, possible effects of the penultimate unit on the reactivity of the radical-chain end are still noticeable. At 110°C, however, the influence of this penultimate unit may be negligible and there is no difference between  $k_p^{iii}$  and  $k_p^{jii}$ , *i.e.*  $s_S$  and  $s_B$  are likely to become equal to unity. In this case, the PUM would simply reduce to the TUM. In order to verify this bold hypothesis, one should conduct pulsed-laser polymerisations at various initial monomer compositions at 110°C, to fit average  $k_p$  vs.  $f_S$  data. This, however, is impeded by the high homopropagation rate coefficient of BA and the dominant contribution of chain-transfer processes.

The observation that the TUM describes the experimental data better for higher  $f_S^0$  might indicate that the reactivity ratio of S is somewhat overestimated in the simulations or that the reactivity ratio of BA is slightly underestimated. The effects of these errors are much less pronounced at high styrene fractions than when the BA content in the monomer mixture is high. This is rather evident: at a high S content, the homopropagation of S dominates, while the crosspropagation rate coefficient, which is related to the reactivity ratio of S, does not really influence the reaction rate due to the low concentration of BA. On the other hand, crosspropagation of S radicals will be much more marked when the concentration of BA in the monomer mixture is high. Similarly, a higher  $r_B$  would predict less crosspropagation and more homopropagation. Since the reactivity of a BA-ended radical is much higher than that of a S-ended radical, the net effect is an enhanced reaction rate.

When comparing the simulations with the experimental data, it should be noted that the attention is focused on the initial stages of the copolymerisation reaction. As already mentioned earlier, withdrawal of samples in order to determine monomer conversion and monomer composition may lead to the introduction of oxygen in the system. This leads to a decreased reaction rate and the data may not be compared with the simulations, where absolute exclusion of oxygen is assumed.

### 5.3.3.4 Influence of reactivity ratios, $k_{act}$ and $k_{deact}$

So far, the kinetics of ATRP copolymerisation are not optimally described, especially at low styrene contents in the monomer mixture. Bearing in mind that  $r_S$  and  $r_B$  might have a great influence on the description of the ATRP copolymerisation kinetics it seems to be a good idea to adjust  $r_S$  or  $r_B$  in the simulations. Looking at Figure 5.4, the reactivity ratio for S can vary from 0.7 to 1.1, and therefore  $r_S=0.95$  seemed to be a reasonable estimate. However, in literature one often finds lower values for  $r_S$ <sup>15,40</sup> and it is therefore realistic to assume that in our copolymerisations we should apply a lower value for this parameter. The reactivity ratio of BA in Figure 5.4 does not seem to be very much higher than 0.22 and any inaccuracy in this parameter will therefore not be taken into consideration.

The simulations to predict the ATRP copolymerisations of S and BA have therefore been performed again, but now with  $r_S=0.80$  using only the TUM. The results are displayed in Figure 5.13.

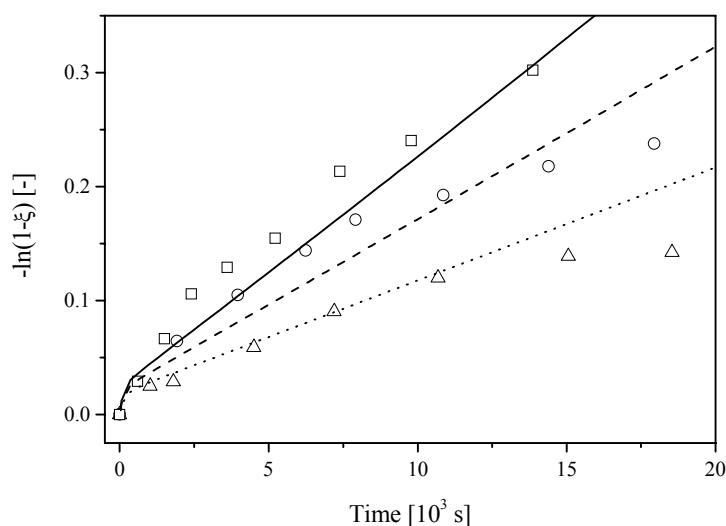


**Figure 5.13** Evolution of  $-\ln(1-\xi)$  in time for the ATRP copolymerisation of S and BA compared with simulations using TUM with  $r_S=0.80$  and  $r_B=0.22$ ;  $f_S^0=0.7$  ( $\Delta$ : experimental data,  $\cdots$ : simulation),  $f_S^0=0.5$  ( $\circ$ : experimental data,  $---$ : simulation) and  $f_S^0=0.3$  ( $\square$ : experimental data,  $—$ : simulation).

By changing the reactivity ratio for S from 0.95 to 0.80, it is clear that the ATRP copolymerisations of S and BA, as depicted in Figure 5.13, are better described. Nevertheless, it should be noticed that especially at higher BA content, the predictions do not exactly match the experimental data. The deviations, therefore, cannot only be fully explained by inaccuracies in the reactivity ratio of S.

Two other parameters that influence the evolution of  $-\ln(1-\xi)$  in time significantly are the activation and deactivation rate coefficients for PS and PBA dormant species. From chapter 4, the activation and deactivation rate coefficients have been determined with reasonable accuracy, but still with a relative error of about 10%. Since the predictions of the simulations are consistently too low in comparison with the experimental data, it seems that either the activation rate coefficients have been underestimated or the deactivation rate coefficients have been overestimated. Furthermore, since the predictions are more accurate when the fraction of S in the monomer mixture is higher, we might expect that the activation or deactivation rate coefficients of BA in the simulations are inaccurate.

Simulations have therefore been carried out with different values for  $k_{act}^B$  and  $k_{deact}^B$ . The former is now taken  $0.15 \text{ L}\cdot\text{mol}^{-1}\cdot\text{s}^{-1}$  (100% error) and the latter is set to  $6.8\cdot 10^7 \text{ L}\cdot\text{mol}^{-1}\cdot\text{s}^{-1}$  (equal to  $k_{deact}^S$ ). The reactivity ratio of S is still assumed to be equal to 0.80 in these simulations. The resulting predictions, together with the experimental data are depicted in Figures 5.14a and b.

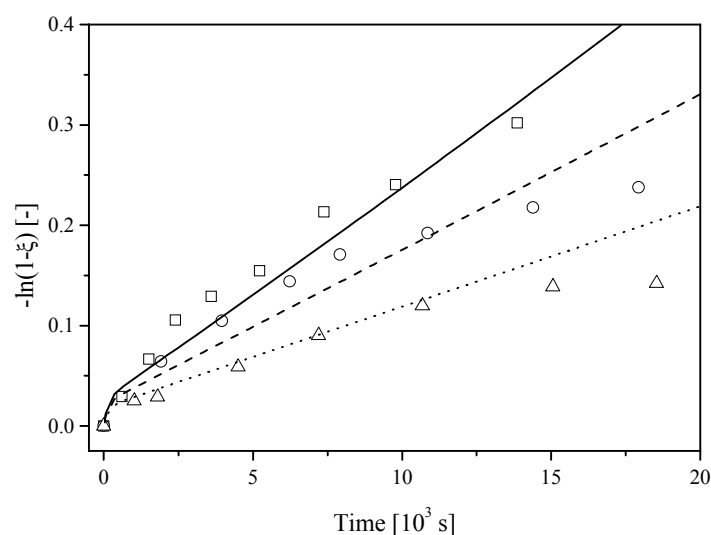


**Figure 5.14a** Evolution of  $-\ln(1-\xi)$  in time for the ATRP copolymerisation of S and BA compared with simulations using TUM with  $r_S=0.80$  and  $r_B=0.22$  and  $k_{act}^B=0.15 \text{ L}\cdot\text{mol}^{-1}\cdot\text{s}^{-1}$ ;  $f_S^0=0.7$  ( $\Delta$ : experimental data,  $\cdots$ : simulation),  $f_S^0=0.5$  ( $\circ$ : experimental data,  $---$ : simulation) and  $f_S^0=0.3$  ( $\square$ : experimental data,  $—$ : simulation).

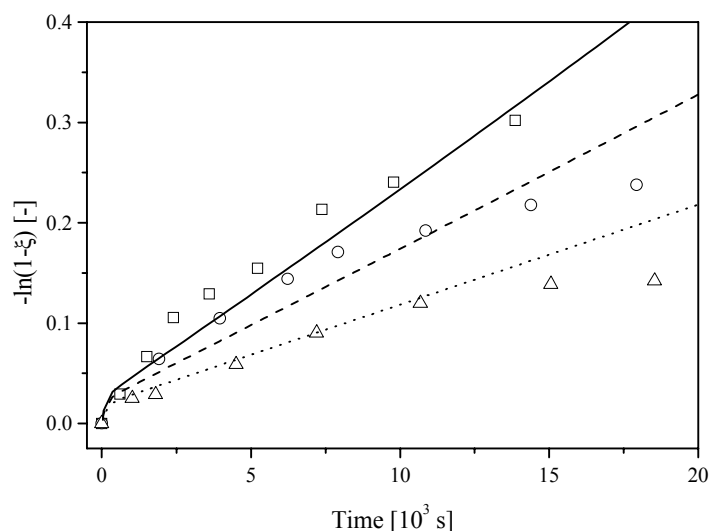


**Figure 5.14b** Evolution of  $-\ln(1-\xi)$  in time for the ATRP copolymerisation of S and BA compared with simulations using TUM with  $r_S=0.80$  and  $r_B=0.22$  and  $k_{deact}^B=6.8\cdot 10^7 \text{ L}\cdot\text{mol}^{-1}\cdot\text{s}^{-1}$ ;  $f_S^0=0.7$  ( $\Delta$ : experimental data,  $\cdots$ : simulation),  $f_S^0=0.5$  ( $\circ$ : experimental data,  $---$ : simulation) and  $f_S^0=0.3$  ( $\square$ : experimental data,  $—$ : simulation).

From Figures 5.14 one sees that the variations of activation and deactivation rate coefficients do not lead to a significantly improved description of the ATRP copolymerisation of S and BA.

The reason for the small discrepancy between the experimental data and the predictions from simulations does not lie in possible inaccuracies in the model parameters. Reactivity ratios, activation and deactivation coefficients, as well as the homopropagation rate coefficients do not influence the reaction rate in the simulations to such an extent that they could account for the observed differences. The underlying reasons should either concern the assumed model or external factors. It is theoretically possible that ATRP does not obey conventional free-radical kinetics and in principle the TUM or PUM cannot be used to predict the ATRP copolymerisation. However, the reactivity ratios do not support this hypothesis, but strongly favour a free-radical mechanism. Since the rate of polymerisation is consistently higher than the model predictions, and in view of the fact that the discrepancy, although still small, increases with increasing BA content, it would suggest an enhanced reactivity of BA in ATRP copolymerisation.

The other possibility could be that external factors have played a role in the copolymerisations, although it should be stressed that this is not very plausible. This would mean that, for instance, temperature control in the ATRP copolymerisations is worse at higher BA fraction in the monomer mixture. It has nevertheless been assured that temperature was always within 1-2°C of the target temperature of 110°C.

Nonetheless, it has been shown that the ATRP copolymerisation of S and BA can be described by the TUM using quantitative information on the activation and deactivation rate coefficients obtained from the ATRP homopolymerisations. The reactivity ratios from conventional free-radical copolymerisation can be used in ATRP copolymerisation. The optimal description of the ATRP copolymerisation of S and BA is obtained when  $r_S=0.80$  and  $r_B=0.22$ .

## 5.4 CONCLUSIONS

The quantitative description of the ATRP copolymerisation is possible using the kinetic data from ATRP homopolymerisation and conventional free-radical copolymerisation parameters. It has been shown that the terminal model describes the rate of polymerisation better than more comprehensive models, such as the penultimate unit model. However, a minor discrepancy exists between experimental data and the model predictions, which is more pronounced at higher BA content in the initial monomer mixture. The origin of these discrepancies has been investigated by assessing possible inaccuracies in the model parameters. It seems that  $r_S=0.95$  is an overestimation and  $r_S=0.80$  yields a better fit at low S content in the initial monomer mixture. The description of the ATRP copolymerisations, however, is satisfactory to control the intramolecular chemical composition distribution in semi-batch copolymerisations.

## REFERENCES

- <sup>1</sup> Mayo, F.R.; Lewis, F.M., *J. Am. Chem. Soc.* **1944**, *66*, 1594
- <sup>2</sup> Alfrey Jr., T.; Goldfinger, G., *J. Chem. Phys.* **1944**, *12*, 205
- <sup>3</sup> Merz, E.; Alfrey Jr., T.; Goldfinger, G., *J. Polym. Sci.* **1946**, *1*, 75
- <sup>4</sup> Ham, G.E., *J. Polym. Sci.* **1954**, *14*, 87
- <sup>5</sup> Cais, R.E.; Farmer, R.G.; Hill, D.J.T.; O'Donnell, J.H., *Macromolecules* **1979**, *12*, 835
- <sup>6</sup> Dubé, M.A.; Penlidis, A.; O'Driscoll, K.F. *Can. J. Chem. Eng.* **1990**, *68*, 974
- <sup>7</sup> Davis, T.P.; O'Driscoll, K.F.; Piton, M.C.; Winnik, M.A. *Polymer Int.* **1991**, *24*, 65

- 8 Fernández-García, M.; Fernández-Sanz, M.; López Madruga, E.; Fernández-Monreal, C. *Macromol. Chem. Phys.* **1999**, *200*, 199
- 9 Fukuda, T.; Ma, Y.-D.; Inagaki, H. *Makromol. Chem. Rapid Commun.* **1987**, *8*, 495
- 10 Fukuda, T.; Ma, Y.-D.; Kubo, K.; Inagaki, H. *Macromolecules* **1991**, *24*, 370
- 11 Manders, B.G. *Ph.D. thesis*; Technische Universiteit Eindhoven: Eindhoven, 1999; Chapter 5
- 12 Van Herk, A.M., *private communications*
- 13 Bradbury, J.H.; Melville, H.W. *Proc. R. Soc., London* **1954**, *A 222*, 456
- 14 Gruber, E.; Knell, W.L. *Makromol. Chem.* **1978**, *179*, 733
- 15 Kaszás, G.; Földes-Bereznich, T.; Tüdös, F. **1984**, *20 (4)*, 395
- 16 O'Driscoll, K.F. *J. Macromol., Sci.-Chem.* **1969**, *A3 (2)*, 307
- 17 Van Herk, A.M. *J. Chem. Ed.* **1995**, *72*, 138
- 18 Van Herk, A.M.; Dröge, T. *Macromol. Theory Simul.* **1997**, *6*, 1263
- 19 Skeist, I. *J. Am. Soc.* **1946**, *68*, 1781
- 20 Meyer, V.E.; Lowry, G.G. *J. Polym. Sci., Part A* **1965**, *3*, 2843
- 21 Meyer, V.E. *J. Polym. Sci., Part A-1* **1966**, *4*, 2819
- 22 Plaumann, H.P.; Branston, R.E. *J. Polym. Sci., Part A: Polym. Chem.* **1989**, *27*, 2819
- 23 German, A.L.; Heikens, D. *Anal. Chem.* **1971**, *43*, 1940
- 24 Haigh, J.; Brookes, A.; Hendra, P.J.; Strawn, A.; Nickolas, C.; Purbrick, M. *Spectrochim. Acta, Part A* **1997**, *53*, 9
- 25 Van den Brink, M., *Ph.D. thesis*; Technische Universiteit Eindhoven: Eindhoven, 1999
- 26 Haddleton, D.M.; Crossman, M.C.; Hunt, K.H.; Topping, C.; Waterson, C.; Suddaby, K.G. *Macromolecules* **1997**, *30*, 3992
- 27 Manders, B.G.; Smulders, W.; Aerts, A.M.; Van Herk, A.M. *Macromolecules* **1997**, *30*, 322
- 28 Kotani, Y.; Kamigaito, M.; Sawamoto, M. *Macromolecules* **1998**, *31*, 5582
- 29 Fineman, M.; Ross, S.D. *J. Polym. Sci.* **1950**, *5*, 259
- 30 Moineau, G.; Minet, M.; Dubois, Ph.; Teyssié, Ph.; Senninger, T.; Jérôme, R. *Macromolecules* **1999**, *32*, 27
- 31 Roos, S.G.; Müller, A.H.E.; Matyjaszewski, K. *Macromolecules* **1999**, *32*, 8331
- 32 Kelen, T.; Tüdös, F. *J. Macromol. Sci. Chem.* **1975**, *A9*, 1
- 33 Jaacks, N. *Makromol. Chem.* **1972**, *161*, 161
- 34 Arehart, S.V.; Matyjaszewski, K. *Macromolecules* **1999**, *32*, 2221
- 35 Matyjaszewski, K.; Patten, T.E.; Xia, J. *J. Am. Chem. Soc.* **1997**, *119*, 674
- 36 Tidwell, P.W.; Mortimer, G.A. *J. Polym. Sci.* **1965**, *A3*, 369
- 37 Fernández-García, M.; Fernández-Sanz, M.; López Madruga, E.; Cuervo-Rodríguez, R.; Hernández-Gordo, V.; Fernández-Monreal, M. C. *J. Pol. Sci.: Part A: Pol. Chem.* **2000**, *38*, 60
- 38 Fukuda, T.; Ide, N.; Ma, Y.-D. *Macromol. Symp.* **1996**, *111*, 305
- 39 Kowollik, C., *Ph.D. thesis*; Göttingen University: Göttingen, 1999
- 40 Guillaume, J.L.; Pichot, C.; Revillon, A. *Makromol. Chem. Suppl.* **1985**, *10/11*, 69

# 6

## *Synthesis and Characterisation of Intramolecularly Heterogeneous Copolymers*

**Synopsis:** The experience with atom transfer radical polymerisation and the kinetic insights acquired in chapter 5 are used to control the synthesis of copolymers of styrene and butyl acrylate with intramolecularly heterogeneous composition distributions. Two classes of copolymers are assessed. First, the synthesis of block copolymers is highlighted, as well as the complications arising during the process. Second, a strategic approach to produce gradient copolymers is developed on the basis of the kinetic knowledge on conventional free-radical copolymerisation together with activation and deactivation rate parameters. The occurrence of micro-phase separation in the block and gradient copolymers is investigated with differential scanning calorimetry. The block length of the block copolymers has a significant influence on their phase separation behaviour. Gradient copolymers do not seem to exhibit phase separation, indicating good intramolecular compatibility.



## 6.1 INTRODUCTION

In chapter 5, the activation and deactivation rate coefficients together with the monomer reactivity ratios have been used in a model for the ATRP copolymerisation of styrene (S) and butyl acrylate (BA). It has been shown that a reasonable prediction of the rate of reaction is possible.

In this chapter, the experience and knowledge gained on the ATRP system will be employed for the controlled synthesis of intramolecularly compositionally heterogeneous copolymers of S and BA as an alternative for conventional living polymerisation techniques. The attention will be focused on the synthesis of block and gradient copolymers. Furthermore, the phase separation behaviour of these block and gradient copolymers will be investigated. It is suspected that block copolymers of S and BA will show phase separation, due to the incompatibility of the corresponding homopolymers<sup>1,2</sup>. The dependence of this behaviour on block length will be investigated. The phase separation behaviour of gradient copolymers is currently not known. From this point of view, it is interesting to find out whether or not their behaviour is similar to that of the block copolymers.

Bearing in mind the main objective of the thesis, it is stressed that this chapter is meant to have a qualitative character. The focus of this chapter, therefore, is the synthesis and characterisation of intramolecularly heterogeneous copolymers by atom transfer radical polymerisation. It is beyond the scope of this thesis to deal with the phase separation process quantitatively.

## 6.2 BLOCK COPOLYMERISATION

### 6.2.1 Definition and application

According to the IUPAC definition<sup>3</sup>, block copolymers consist of linear arrangements of blocks of varying monomer composition. A diblock copolymer, for instance, is composed of two monomer species that are completely segregated and thus form two different blocks linked together by a covalent bond. These blocks generally exhibit the macroscopic properties, *e.g.* glass transition temperature ( $T_g$ ), of the corresponding homopolymers.

Block copolymers are becoming more and more important in today's life<sup>4,5</sup>. In many cases, incompatibility between two different phases needs to be prevented. The amphiphilic properties of block copolymers are often exploited to create thermodynamic stability between these phases. For example, Gaillard *et al.*<sup>6</sup>

developed block copolymers of styrene and butadiene used as compatibilising agent between polystyrene and polybutadiene. Duivenvoorde *et al.*<sup>7</sup> used block copolymers of  $\epsilon$ -caprolactone and 2-vinyl pyridine as dispersants in powder coatings, where sufficient stabilisation of the pigment particles in the polyester matrix material is thus created. In other areas block copolymers are used to favour adhesion between two materials differing in polarity, such as poly(ethylene-*co*-butylene)-*b*-poly(styrene-*co*-maleic anhydride) copolymers that enable adhesion of polyolefins onto a metal substrate<sup>8</sup>. Another important application can be found in emulsion polymerisation, where block copolymers of styrene sulfonate and styrene proved to be efficient stabilisers for the emulsion polymerisation of styrene<sup>9</sup>.

### 6.2.2 Phase separation

The compatibility of two homopolymers determines whether phase separation will occur. The occurrence of phase separation in a system comprising two homopolymers is thermodynamically governed by the change in Gibbs free energy,  $\Delta G$ . When upon mixing two homopolymers  $\Delta G > 0$ , the homopolymers are not miscible and phase separation will occur. In the case of a block copolymer, the two homopolymers are linked together with a covalent bond. When the two blocks are incompatible, *i.e.*  $\Delta G > 0$ , phase separation in principle can also take place, albeit on a microphase scale. Generally, however, the extent of segregation of a system is expressed with the reduced parameter  $\chi N$ , where  $\chi$  is the Flory-Huggins interaction parameter<sup>10</sup> and  $N$  the chain length. Above a critical value,  $(\chi N)_{cr}$ , a system of two homopolymers or a block copolymer will show micro-phase separation. This critical value of  $\chi N$  is lower in the case of a system consisting of two homopolymers than for a system consisting of a block copolymer, *i.e.*  $(\chi N)_{cr} = 2.0$  and  $(\chi N)_{cr} = 10.5$ , respectively. Evidently, a higher molecular weight is needed to obtain phase separation in block copolymers compared to a mixture of homopolymers.

Phase separation in block copolymers consisting of two non-crystallising blocks can take place in different ways. Lamellar structures, cylindrical and even spherical morphologies are generally observed. Alternating layers of the first and second block have been observed<sup>11</sup>, while spherical morphologies, in which the first block is embedded in the second block, have also been reported<sup>12</sup>. A cylindrical morphology has been found for block copolymers of styrene and butadiene<sup>13</sup>.

The occurrence of phase separation in block copolymers depends on various parameters, in particular temperature, the molecular weights of both blocks and the chemical composition of the block copolymer, see Figure 6.1.

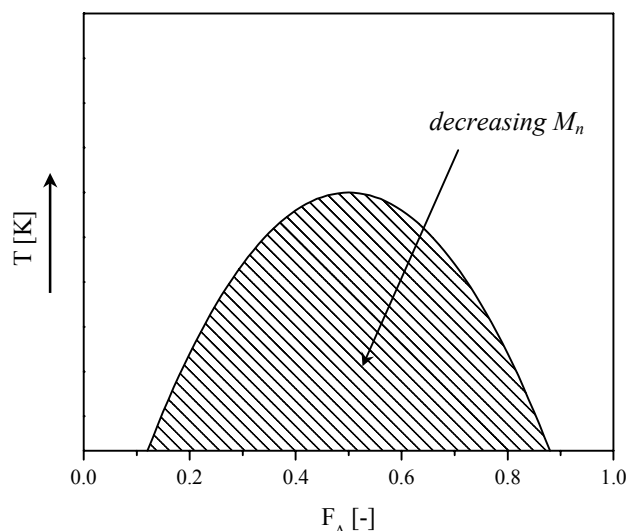


**Figure 6.1** Schematic phase diagram of a poly(A-b-B) block copolymer; the phase separation behaviour depends on the temperature ( $T$ ), the copolymer composition ( $F_A$ ) and molecular weight ( $M_n$ ).

In Figure 6.1, the curved line represents the transition from a completely homogeneous block copolymer poly(A-b-B), where no phase separation takes place, to a heterogeneous system. The shaded area under this curve reflects the conditions where phase separation takes place. Upon decreasing molecular weight, this area becomes smaller and the block copolymer will show less tendency to phase separate. Similarly, upon increasing temperature, the system generally exhibits less phase separation.

Phase separation in block copolymer systems can be investigated with a number of techniques. Differential scanning calorimetry (DSC) is a powerful tool to study the thermal properties of the block copolymer. When two glass transition temperatures are observed, the block copolymer shows micro-phase separation and the two blocks essentially form two different domains as if they were consisted of homopolymers. On the other hand, when the block copolymer is completely homogeneous, only one value for  $T_g$  will be observed. In general, this  $T_g$  value lies in between the  $T_g$  values of the corresponding homopolymers. DSC is a useful tool to obtain information on the micro-phase separation of block copolymers.

Other important methods to investigate the occurrence of microdomain formation in block copolymers are transmission electron microscopy (TEM) and small angle X-ray scattering (SAXS). With these techniques the morphology of the block copolymer can be elucidated. For TEM it should be noted that enough contrast has to be obtained to differentiate between the two domains. An additional problem arises when copolymers with soft blocks are involved. In these cases a thin film must be sliced

cryogenically to avoid destruction of the existing morphology, an often meticulous and impracticable task.

### 6.2.3 Synthesis

The simultaneous conventional free-radical polymerisation of two monomer species in general does not lead to the formation of block copolymers. The synthesis of block copolymers is therefore most often performed using so-called living polymerisation techniques, such as anionic polymerisation<sup>14</sup>. Generally, a multi-step synthesis is applied, where the different blocks are sequentially polymerised. To this end, it is of utmost importance that the precursor from the previous stage bears sufficient functionality to allow the growth of the consecutive block. Although anionic polymerisation is the most widely applied technique to synthesise block copolymers, it is susceptible to impurities and can only be used with a limited number of monomers.

In this chapter, ATRP will be applied as a useful and versatile tool to synthesise block copolymers. Many groups reported on the block copolymer synthesis by means of ATRP. Early papers demonstrated the application of ATRP only to polymerise a second block onto a macroinitiator that was previously prepared via living techniques. Chen and co-workers<sup>15</sup> used a polyisobutene macroinitiator capped on each side by several S monomer units and a chloride atom to polymerise S onto both ends via ATRP. Similarly, Coca *et al.*<sup>16</sup> synthesised PS macroinitiators with chlorine chain ends via cationic polymerisation. Subsequently, S, methyl acrylate (MA) or methyl methacrylate (MMA) was polymerised via ATRP in the second step. Gaynor *et al.*<sup>17</sup> combined step-growth polymerisation techniques to prepare the functional macroinitiator, after which the second monomer was polymerised with ATRP.

Many groups reported the successful synthesis of block copolymers using exclusively ATRP<sup>18</sup>. Particularly interesting are the block copolymers comprising a high and a low  $T_g$  block. Uegaki *et al.*<sup>19</sup> prepared block copolymers of MMA with BA and MA, which was reported by Shipp and co-workers<sup>20</sup> not long after that. In the same category, Cassebras *et al.*<sup>21</sup> synthesised block copolymers of S and BA at 130°C, starting from both PS and PBA chloride-functional macroinitiators. In this study, 10 vol% of *N,N*-dimethylformamide was added to the reaction mixture to dissolve the Cu/(bpy)<sub>2</sub> catalyst. Cassebras and co-workers<sup>21</sup> observed a higher rate of reaction for the S polymerisation compared to that for the BA polymerisation. Cassebras *et al.* concluded that the equilibrium between dormant species and active species is shifted further towards the dormant species in the case of BA. This conclusion is in agreement with our own observations, see chapter 4, where the equilibrium constant of the equilibrium between dormant species and growing radicals is about eight times

higher for S than for BA. However, in our case, the ATRP polymerisation of BA still proceeds faster than a corresponding S polymerisation due to the difference in propagation rate constant. In the case of Cassebras and co-workers, thermal initiation probably played a significant role in the polymerisations, which led to the formation of additional radicals. As a result, the reaction rate increased and simultaneously the molecular-weight distribution broadened. The latter was also observed by Cassebras and co-workers, who reported rather elevated polydispersities of 1.31. In this respect, the addition of 10% dimethylformamide is suspicious. As reported in chapter 4, the activation rate coefficient of S dormant species in polar media is significantly increased, while that of BA dormant species does not seem to be affected to the same extent. Cassebras *et al.* argued that in view of the low equilibrium constant in the case of BA, the best strategy for block copolymer synthesis is to start from a PS precursor and polymerising BA in a following step. These authors stated, rather arbitrary, that the low equilibrium constant would not lead to quantitative reactivation of the chlorine-functional PBA macroinitiator. When a PS macroinitiator was used to polymerise BA in the second step, polydispersities initially increase from 1.31 up to 1.93, indicating that there was no control of the molecular-weight distribution. Nevertheless, because they were polymerising a very long block of BA onto a relatively short PS block, the molecular-weight distribution narrowed after about 15% conversion. When the block copolymer was synthesised starting from a PBA macroinitiator and successive polymerisation of S, Cassebras *et al.*<sup>21</sup> obtained block copolymers with much more narrow molecular-weight distributions. Considering these experimental results, it is rather surprising that Cassebras *et al.*<sup>21</sup> in their paper concluded that chain extension of a PS macroinitiator with BA is the preferred strategy to produce well-defined block copolymers of S and BA.

#### 6.2.4 Experimental

##### *Materials:*

The copper ligand, 4,4'-di-*n*-heptyl-2,2'-bipyridine (dHbpy), was synthesised according to a literature procedure<sup>22</sup>. Styrene (S, Aldrich, 99%) and butyl acrylate (BA, Aldrich, 99+%) were distilled and stored over molecular sieves. *p*-Xylene (Aldrich, 99+% HPLC grade) was stored over molecular sieves and used without further purification. CuBr (Aldrich, 98%) and ethyl 2-bromoisobutyrate (Aldrich, 98%) were used as received.

#### *Macroinitiator synthesis:*

PS and PBA macroinitiators with different molecular weights were synthesised with ATRP. A typical procedure to prepare a PS macroinitiator is the following. *p*-Xylene (5.04 g), S (5.02 g, 0.0481 mol), ethyl 2-bromoisobutyrate (0.122 g,  $6.15 \cdot 10^{-4}$  mol) and dHbpy (0.490 g,  $1.39 \cdot 10^{-3}$  mol) were mixed in a 100 mL round-bottom flask. The mixture was purged with argon for 30 min, after which CuBr (0.0960 g,  $6.69 \cdot 10^{-4}$  mol) was added. No extra CuBr<sub>2</sub> was added. The reaction mixture was then homogenized and purged with argon for another 30 min, after which the reaction mixture was placed in a thermostatically controlled oil bath at 110 °C. After a certain time, depending on the desired molecular weight, the reaction mixture was quenched by rapid cooling to room temperature. The samples were passed through a column with aluminumoxide (activated, neutral, Brockman I, STD grade approx. 150 mesh, 58Å, Aldrich) to remove the copper catalyst using stabilized tetrahydrofuran (AR, Biosolve) as eluent. Hereafter, the samples were subjected to drying and subsequently analysed.

The procedure for the synthesis of PBA macroinitiators is analogous to the procedure described above.

#### *Block formation; chain extensions of the macroinitiators:*

A chain extension of a PBA macroinitiator with  $M_n = 2300 \text{ g} \cdot \text{mol}^{-1}$  and a polydispersity of 1.16 to a total target molecular weight of  $1 \cdot 10^4 \text{ g} \cdot \text{mol}^{-1}$  was performed using the following procedure. *p*-Xylene (5.00 g), S (5.00 g, 0.0480 mol), PBA macroinitiator (1.32 g,  $4.80 \cdot 10^{-3}$  mol) and dHbpy (0.200 g,  $5.68 \cdot 10^{-4}$  mol) were mixed in a 100 mL round-bottom flask. The mixture was purged with argon for 30 min, after which CuBr (0.0344 g,  $2.40 \cdot 10^{-4}$  mol) was added. No extra CuBr<sub>2</sub> was added. The reaction mixture was then homogenized and purged with argon for another 30 min, after which the reaction mixture was emerged in a thermostatically controlled oil bath at 110 °C.

Samples were withdrawn from the reaction mixture through a septum with a syringe at timed intervals. The samples were cooled down immediately after withdrawal. Monomer conversions were determined either gravimetrically, or by residual monomer analysis with gas chromatography. Thereto, a HP 5890 gas chromatograph equipped with an AT Wax column (Alltech, length 30 m, film thickness 1.0 µm) and an auto sampler was used. The remainder of the samples was first passed through a column with aluminumoxide (activated, neutral, Brockman I, STD grade approx. 150 mesh, 58Å, Aldrich) to remove the copper catalyst using stabilized tetrahydrofuran (AR, Biosolve) as eluent. Hereafter, the samples were subjected to drying and subsequently analysed.

### *Analysis:*

To determine the molecular weight and the molecular-weight distributions, the dry polymers were dissolved in stabilised tetrahydrofuran at  $1 \text{ mg}\cdot\text{mL}^{-1}$  and filtrated using  $0.2 \mu\text{m}$  filters. The molecular weights were determined by size exclusion chromatography (SEC) with a Waters Model 510 pump and Waters 712 WISP using 4 PL-gel mix C columns ( $300\text{mm}\times 7.5\text{mm}$ , Polymer Laboratories) at  $40^\circ\text{C}$  and tetrahydrofuran as eluent. The eluent flow rate was  $1.0 \text{ mL}\cdot\text{min}^{-1}$ . Calibration was performed with polystyrene standards with narrow molecular-weight distributions (Polymer Laboratories). All molecular weights were calculated relative to polystyrene. A Waters 410 differential refractometer and a Waters 440 UV detector operating at  $254 \text{ nm}$  were used for detection. Data acquisition was done with Millennium-32 3.05 software.

Some block copolymer samples have been fractionated with SEC and the fractions were subsequently analysed by infrared spectroscopy (IR). A Waters 717 Plus Autosampler was used together with 2 PL-gel mix B columns ( $300\text{mm}\times 7.5\text{mm}$ , Polymer Laboratories) at  $35^\circ\text{C}$  and tetrahydrofuran as eluent. The eluent flow rate was  $0.5 \text{ mL}\cdot\text{min}^{-1}$ . A Spectra Physics UV 150 operating at  $260 \text{ nm}$  and an Erma differential refractometer were used for detection. Data acquisition was done with Millennium-32 3.05 software. An LC-Transform Model 500 (Lab Connections) was used to evaporate the eluent and collect the fractionated sample onto a  $60 \text{ mm}$  germanium disc. The nozzle temperature was set at  $125^\circ\text{C}$ , sheath gas pressure was set at  $25 \text{ psi}$  and the nozzle height was adjusted to  $7 \text{ mm}$ . Nitrogen was used as nebuliser gas. The disc rotation speed was  $7.2 \text{ mm}\cdot\text{min}^{-1}$ . IR spectra were recorded on a Perkin Elmer Spectrum GX equipped with a liquid nitrogen cooled MCT detector. The sample and detector compartment were continuously purged with nitrogen gas dried by a Zander Adsorbtion Dryer Type KM5 TE. The spectra consisted of 32 scans. Gram-Schmidt chromatograms and chemigrams of carbonyl and aromatic C-H were constructed using Perkin Elmer Timebase. For the chemigram construction, the maximum peak height within a small wavenumber range was used. Band position were as follows: C=O at  $1733 \text{ cm}^{-1}$  and aromatic C-H at  $3027 \text{ cm}^{-1}$ .

For the copolymer composition analysis,  $10 \text{ wt}\%$  solutions of the copolymers in  $\text{CDCl}_3$  were subjected to  $^1\text{H}$  NMR using a  $400 \text{ MHz}$  Bruker operating at  $20^\circ\text{C}$ . Peak areas of the proton resonances at  $\delta=7 \text{ ppm}$  (phenyl) and  $\delta=3.8 \text{ ppm}$  (methoxyl) were taken to calculate copolymer composition.

Glass transition temperatures were measured with differential scanning calorimetry (DSC) using a Perkin-Elmer Pyris 1 equipment at a scan speed of  $10^{\circ}\text{C}\cdot\text{min}^{-1}$ .

High performance liquid chromatography (HPLC) measurements were conducted using an Alliance Waters 2690 Separation Module and a Jordi Gel DVB polyamine column ( $250\text{mm}\times 4.6\text{mm}$ , Alltech) at  $40^{\circ}\text{C}$ . The gradient program changed from 100% heptane to 100% dichloromethane in 15 min, then to 80/20 dichloromethane/THF in 25 min. Detection was carried out using a multi-wavelength and multi-angle PL-EMD 960 evaporative light scattering detector (ELSD) (Polymer Laboratories). Data acquisition was done using Millennium-32 3.05 software.

## 6.2.5 Results and discussion

Block copolymers of S and BA have been synthesised covering a range of S and BA block lengths. The proof of block existence will be discussed first. Hereafter, the attention will be focused on complications that were encountered during the synthesis of the block copolymers. Finally, the phase separation behaviour of the block copolymers will be dealt with.

### 6.2.5.1 Indications of block existence

It is of paramount importance to ascertain the formation of the block copolymers during the chain extension with the second monomer. After all, it might be that the second monomer is simply homopolymerised instead of being incorporated into the macroinitiator chains. Several methods to prove the existence of block copolymers can be used. The first indication that block copolymerisation takes place can be seen when the molecular weights of the polymeric material is plotted vs. monomer conversion ( $\xi$ ). As discussed in chapter 3, a linear increase in the number-average molecular weight,  $M_n$ , is expected in living polymerisation systems.

For a chain extension of a PBA macroinitiator ( $M_n=2300\text{ g}\cdot\text{mol}^{-1}$ ) with styrene, the molecular-weight evolution is plotted in Figure 6.2a and the corresponding SEC chromatograms are shown in Figure 6.2b.



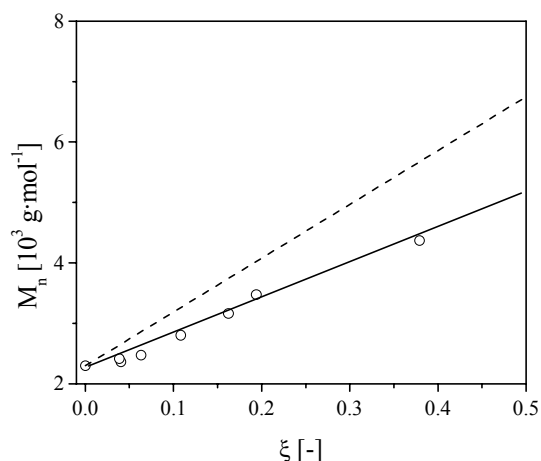


**Figure 6.2a** Chain extension PBA with S. Evolution of  $M_n$  as a function of fractional conversion; experimental data ( $\circ$ ), fit through data (—) and theoretically expected (---).

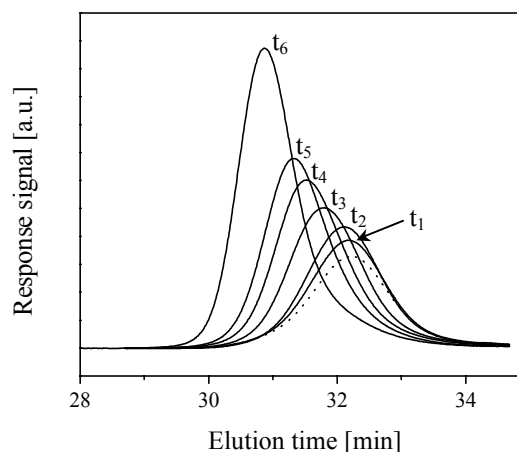


**Figure 6.2b** Chain extension of PBA with S. Evolution of the SEC chromatograms (DRI detector); The original macroinitiator ( $\cdots$ ). Note that the chromatograms have been scaled with conversion.

The linear increase in the number-average molecular weight,  $M_n$ , as a function of conversion is a fair indication that S is polymerised onto the PBA macroinitiator. All the more so when a look is cast on the molecular-weight distributions. They clearly show that the macroinitiator is consumed during the polymerisation reaction. Furthermore, the molecular-weight distributions remain very narrow, typically  $<1.2$ , which also is a clear indication that the S monomer is incorporated into the PBA macroinitiator chains.

When we use the response signal from the UV detector, it is possible to illustrate the contribution of the S block to the DRI signal. It can thus be verified whether the S units are homogeneously distributed in the block copolymer. In Figure 6.3, this has been done for the sample with the highest molecular weight depicted in Figures 6.2.

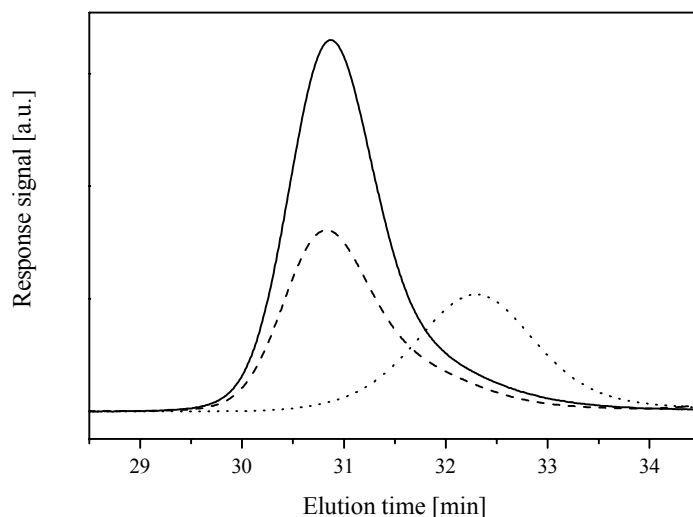


**Figure 6.3** SEC chromatograms of a PBA macroinitiator (···) extended with S visualised with different detectors; The DRI signal (—) and the UV response signal (---) are shown.

In the ideal case, the contribution of the PS in the copolymer should be evenly distributed over the whole molecular-weight distribution. From Figure 6.3, one can see that this is indeed the case: the dashed line representing the contribution of S units present in the polymeric chains is of the same form as the response signal from the differential refractometer representing the contribution of PS as well as PBA in the polymeric chains. The results displayed in Figure 6.3 therefore suggest a homogeneous block copolymer of S and BA, *i.e.* the PBA macroinitiator has been completely reinitiated and S has been incorporated into all macroinitiator chains.

The linear increase in molecular weight, as well as the analysis of the molecular-weight distributions are strong indications that block copolymers are produced in the chain extension experiments.

A proof of block existence can be obtained when investigating the presence of the PBA macroinitiator in the whole molecular-weight distribution. This can be done by subjecting the polymer sample to SEC analysis and subsequent investigation by infrared spectroscopy (IR). The polymer sample was studied in the IR spectrometer for the presence of S and BA by focusing on the absorption bands of  $3027\text{ cm}^{-1}$  and  $1733\text{ cm}^{-1}$ , respectively. The integral values of the specific bands are monitored as a function of the angle of the germanium disk. Since this angle is related to the elution time in the SEC, the distribution of S and BA over the molecular-weight distribution can be obtained. The results for the polymer sample depicted in Figure 6.3 is plotted in Figure 6.4.

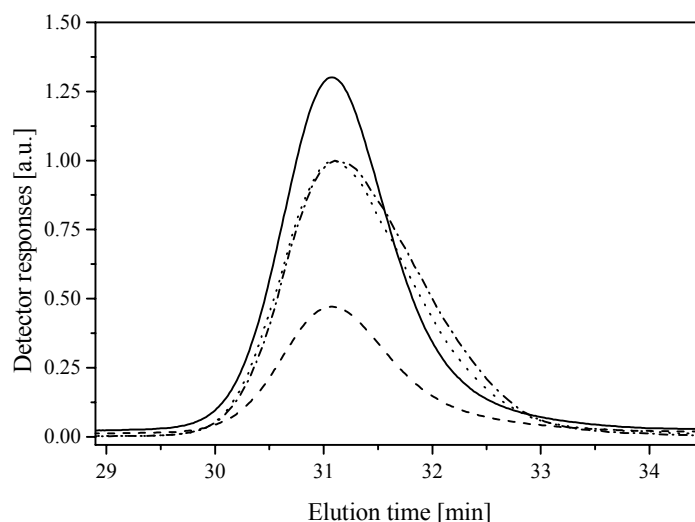


**Figure 6.4** Distribution of the phenyl (— · —) and carbonyl (···) over the complete molecular-weight distribution determined with IR spectroscopy for a chain extension of PBA with S in *p*-xylene at 110°C; the DRI (—) and the UV (---) response signals from the SEC run are also depicted.

Note that the curves in Figure 6.4 have not been normalised and that attention should be focused on their shapes. As can be seen from Figure 6.4, the S and BA units are homogeneously distributed over the whole molecular-weight distribution. This means that the PBA macroinitiator has added S monomer, *i.e.* the proof that we have a block copolymer.

### 6.2.5.2 Problems

The results shown so far all concerned chain extensions of PBA macroinitiators with S. Molecular weights increase linearly with conversion, polydispersities remain low, and HPLC analyses show that only small amounts of PBA macroinitiator are not reactivated in the chain extension step. However, when a block copolymer of S and BA is prepared starting from a PS macroinitiator and subsequent chain extension with BA, control of the polymerisation is less. Although molecular weights increase linearly with conversion, the molecular-weight distributions reveal loss of functionality during the polymerisation, see Figures 6.5a and b.

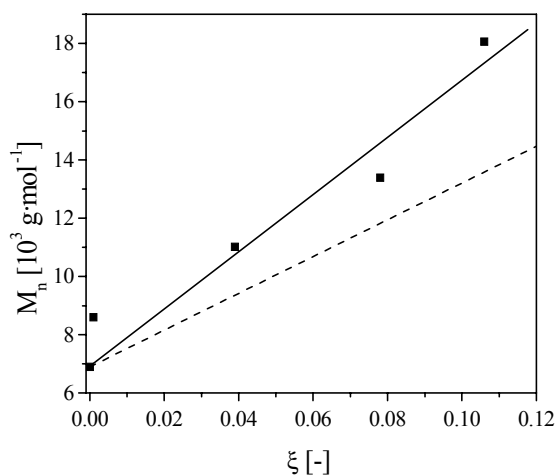


**Figure 6.5a** Chain extension of PS with BA. Evolution of  $M_n$  as a function of fractional conversion; experimental data (■), fit through data (—) and theoretically expected (---).

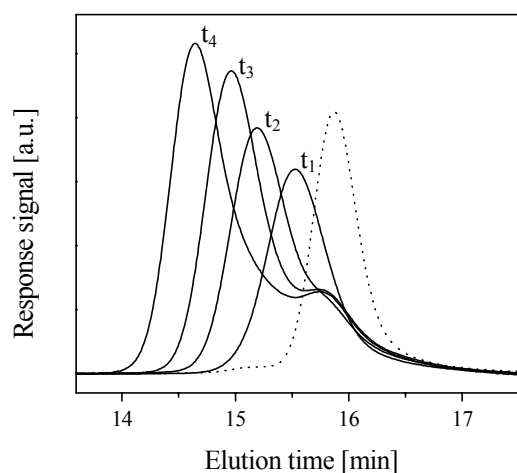


**Figure 6.5b** Chain extension of PS with BA. Evolution of the SEC chromatograms (DRI detector); The original macroinitiator (···).

In Figure 6.5b, one can very clearly observe that the molecular-weight distributions, which have been scaled with conversion, become bimodal as the polymerisation reaction proceeds. The peak at approximately 15.7 min does not seem to disappear but remains at a constant level, indicating that this fraction of the polymeric material with this molecular weight does not add monomer anymore. Our experiments consistently show bimodal distributions in SEC when block copolymers are prepared via chain extension of PS macroinitiators with BA. The total amount of polymeric material that does not polymerise anymore can be roughly estimated from the SEC chromatograms and in some cases represents 50% of the total amount of initial macroinitiator. Our experimental observations are in conflict with the statement made by Cassebras *et al.*<sup>21</sup>, who claimed that the preparation of S/BA block copolymers should be conducted via chain extension of a PS macroinitiator with BA. According to these authors, the activation of PBA dormant species is significantly more difficult.

What kind of polymeric material is responsible for the unchanging peak in SEC? According to the interpretation of Cassebras *et al.*<sup>21</sup>, it is likely that it consists of functional PS with a few BA monomer units attached to it. These BA units should then not be able to reactivate and restart polymerisation. However, this does not explain why a part of the dormant species is still polymerising and certainly does not support the excellent control in our chain extensions of PBA macroinitiators with S.

Another possibility is that the material eluting at 15.7 min in the SEC consists of non-functional polymeric material produced via bimolecular termination reactions. If this were the case, it is important and interesting to know when this so-called ‘dead’

material is formed. Two hypotheses can be raised as to where the dead polymeric material is coming from. First, the PS macroinitiator is not completely functionalised with a bromide at the chain end due to bimolecular termination reactions during the synthesis, resulting in incomplete re-initiation of the PS block. Second, during the first stages of the chain extension with BA, the amount of bimolecular termination is relatively high. This leads to the addition of a few BA monomer units to the PS block, after which bimolecular termination takes place. After the persistent radical concentration has been built up at the expense of a loss of dormant species, polymerisation proceeds normally.

In order to verify whether the synthesis of the PS macroinitiators is well controlled, the functionality of the PS macroinitiators was assessed using two different experimental techniques. First, as was done in chapter 4 to investigate the activation rate parameter, exchange experiments have been conducted to quantitatively transform all bromide-functional PS into trapped species. Exchange reactions using hydroxy-TEMPO have thereto been conducted at 110°C. It was assured that all bromide-functional chains were transformed into hydroxy-functional species by applying a reaction time of one hour. It should be noted that calibration for the different components has not been performed and the HPLC analyses therefore yield only rough estimates of the relative amount of functional PS. The results in all cases show that the PS macroinitiator was highly functionalised. An example is shown in Figure 6.6, where the estimated functionality is >83%. This macroinitiator has actually been applied in the chain extension experiment of which the molecular-weight distributions are displayed in Figure 6.5b.

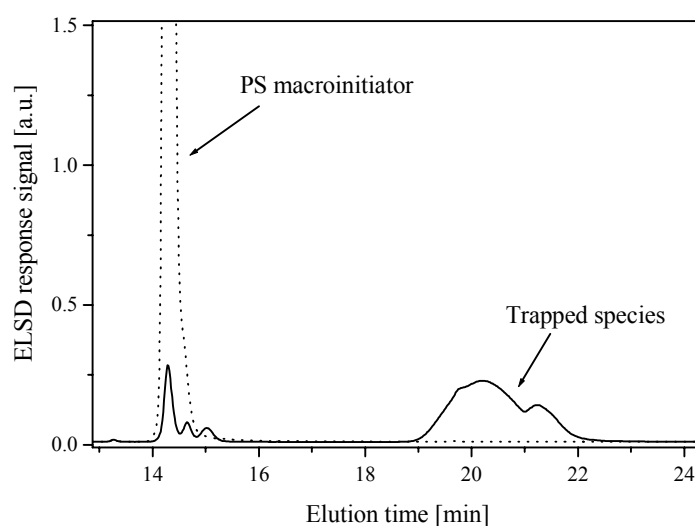


**Figure 6.6** Example of a PS macroinitiator with  $M_n = 6900 \text{ g}\cdot\text{mol}^{-1}$  before the exchange reaction ( $\cdots$ ) and after trapping with hydroxy-TEMPO. The exchange experiment was performed in *p*-xylene at 110°C for 1 hour.

Figure 6.6 clearly demonstrates that the macroinitiator at elution time 14.5 min has decreased after 1 hour of reaction and that the hydroxy-functional species has been formed. It proves that the PS macroinitiator is highly functional.

The second way to estimate the functionality of the PS macroinitiators has been conducted via  $^1\text{H}$  NMR. The attention is focused on the signals of the protons residing in the initiator fragment and the proton at the end of the dormant species chain, see Figure 6.7. The peak position of the two protons in the initiator fragment is found at  $\delta=3.6$ , while the one for the proton at the functional polymer chain end is about  $\delta=4.5$ . The ratio of the initiator and the end-group peaks in the  $^1\text{H}$  NMR spectrum is a measure of the fraction of chains that can still be activated. Ideally, the ratio should be 2.

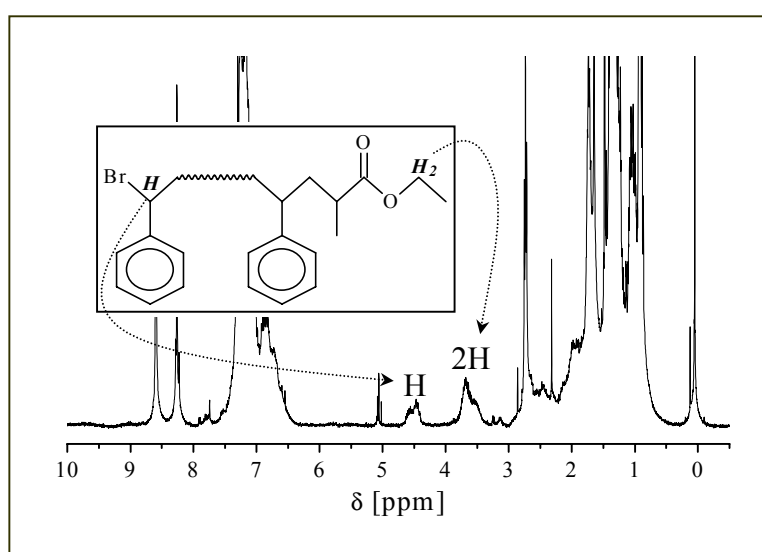


**Figure 6.7.**  $^1\text{H}$  NMR spectrum of a PS dormant species. The peak at  $\delta=4.5$  ppm originates from proton at the end of the polymer chain, while the peak at  $\delta=3.6$  ppm comes from the two protons in the initiator fragment.

It has been found that the functionality of all PS macroinitiators investigated was at least 80%, and in many cases even higher. It should be stressed, however, that the accuracy of the  $^1\text{H}$  NMR method is somewhat less at high chain lengths and reliable data can therefore only be obtained for PS macroinitiators with molecular weights up to about  $1 \cdot 10^4$   $\text{g} \cdot \text{mol}^{-1}$ .

Both the results of the exchange reactions with hydroxy-TEMPO and the  $^1\text{H}$  NMR spectra of PS macroinitiators demonstrate that the functionality of the PS macroinitiators is acceptable. The bimodal distributions, therefore, cannot be the result of insufficient re-initiation of the macroinitiator due to a lack of functionality.

They can only be explained by imperfections during the chain extension with BA in the second step. In order to determine whether the static peak in SEC is due to inadequate reactivation or to a loss of functionality during the early stages in the chain extension, it is necessary to identify the polymeric material that is responsible for the bimodality in the molecular-weight distributions. The polymer samples with bimodal distributions have thereto also been subjected to SEC analysis and subsequent investigation by infrared spectroscopy, but now in order to focus on the C-Br band at  $642\text{ cm}^{-1}$ . It proved to be impossible, however, to detect the C-Br absorption band in the copolymer samples, since a strong band coming from S at  $697\text{ cm}^{-1}$  completely overshadowed the C-Br band. It is possible to investigate the presence of S and BA over the complete molecular-weight distribution, see Figure 6.8.

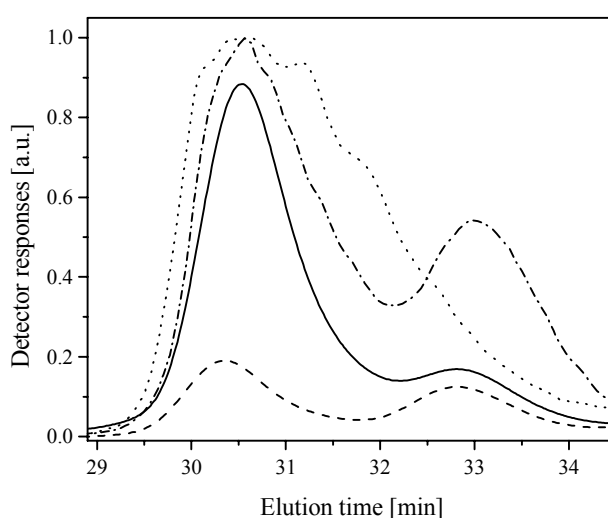


**Figure 6.8** Distribution of the phenyl (— · —) and carbonyl (···) over the complete molecular-weight distribution determined with IR spectroscopy for a chain extension of PS with BA in *p*-xylene at  $110^{\circ}\text{C}$ ; the DRI (—) and the UV (---) response signals from the SEC run are also depicted.

Figure 6.8 clearly demonstrates that the static peak at elution time 32.7 min is mostly consisting of S. Furthermore, a BA contribution can also be seen in this part of the molecular-weight distribution, so the polymeric material consists of PS with some BA monomer units attached to it. Unfortunately, however, whether or not the polymeric material at elution time 32.7 min is bromide-functional remains unclear. The fact that the static peak, *i.e.* at elution time 15.7 min in Figure 6.5b and 32.7 min in Figure 6.8, remains constant indicates that we are dealing with non-functional polymeric material.

The fact that we obtain improved control of the polymerisation when starting from a PBA macroinitiator and subsequent chain extension with S than in the reverse case,

can easily be explained by looking at the ratio of initiation and propagation in both synthesis routes. The initiation process is governed by the activation ( $k_{act}$ ) of a dormant species followed by the crosspropagation step ( $k_p^{ij}$ ). The propagation process is governed by the activation and subsequent homopropagation ( $k_p$ ) step. Note that the deactivation step has not been taken into account, since it is independent of the nature of the radical. When starting from a PBA macroinitiator and subsequent chain extension with S, the initiation process is governed by  $k_{act}^B \cdot k_p^{BS}$  and the propagation process by  $k_{act}^S \cdot k_p^{SS}$ . Taking into account the activation rate coefficients from chapter 4, *i.e.*  $k_{act}^S = 0.43 \text{ L}\cdot\text{mol}^{-1}\cdot\text{s}^{-1}$  and  $k_{act}^B = 0.075 \text{ L}\cdot\text{mol}^{-1}\cdot\text{s}^{-1}$  and the reactivity ratios from chapter 5, *i.e.*  $r_S = 0.80$  and  $r_B = 0.22$ , initiation is almost 40 times faster than propagation. When starting from a PS macroinitiator and subsequent chain extension with BA, initiation is about 7 times slower than propagation. These calculations show the importance of thorough knowledge about the kinetics of the ATRP system. The calculations also demonstrate that in the case of S/BA, the best way to form block copolymers is by starting from a PBA macroinitiator and chain extension with S.

### 6.2.5.3 Phase separation

In order to obtain information on the influence of the block lengths of S and BA as well as the overall composition on the phase separation behaviour, differential scanning calorimetry (DSC) has been used. To this end, the  $T_g$  values of the homopolymers were investigated first. The results are collected in Table 6.1.

**Table 6.1 Glass transition temperatures of PS and PBA homopolymers of various molecular weights.**

Polymer	$M_n \text{ g}\cdot\text{mol}^{-1}$	$T_g \text{ }^\circ\text{C}$
PS	3000	72.4
PS	6900	78.1
PS	10800	78.2
PBA	2500	-62.0
PBA	4900	-57.5
PBA	11700	-52.9

As expected<sup>23</sup>, the  $T_g$  values in Table 6.1 are increasing with increasing molecular weights. The data for the PS homopolymers agree reasonably well with the dependence of the  $T_g$  on the molecular weight found by Inoue and co-workers<sup>24</sup>. An important aspect in the interpretation of the  $T_g$  data is the presence of low-molecular-weight material in the polymer. This may significantly influence the  $T_g$  observed. For example, for a PS sample with  $M_n = 8200 \text{ g}\cdot\text{mol}^{-1}$  and a tailing on the low-molecular-



weight side in the molecular-weight distribution a  $T_g$  of 56.5°C was measured. In this light, the relatively low  $T_g$  value of the PS sample with  $M_n=10800 \text{ g}\cdot\text{mol}^{-1}$  in Table 6.1 can also be explained by the presence of low-molecular-weight material. The PBA homopolymers show the same trend: upon increasing chain length, the  $T_g$  values increases as well. For the PBA with  $M_n=11700 \text{ g}\cdot\text{mol}^{-1}$  one would also expect a somewhat higher  $T_g$  than the -52.9°C that is observed experimentally. However, as well as with the PS homopolymer with  $M_n=10800 \text{ g}\cdot\text{mol}^{-1}$ , this polymer also shows a low-molecular-weight tailing in the molecular-weight distribution and a resulting polydispersity of 1.28.

The block copolymers are also measured with DSC. The glass transition temperatures for these copolymers are listed in Table 6.2.

**Table 6.2 Glass transition temperatures for block copolymers of S and BA with various block lengths and compositions.**

Polymer	$M_n^{PS}, \text{g}\cdot\text{mol}^{-1}$	$M_n^{PBA}, \text{g}\cdot\text{mol}^{-1}$	$F_S$ -	$T_g^1, ^\circ\text{C}$	$T_g^2, ^\circ\text{C}$
S8 t <sub>end</sub>	1900	1600	0.59	-3.23	
S25 t <sub>2</sub>	3000	4600	0.45	-37.3	26.2
S18 t <sub>4</sub>	3200	4600	0.46	-30.8	
S13 t <sub>3</sub>	4400	4900	0.52	-34.3	75.2
S13 t <sub>end</sub>	8200	4900	0.67		31.0
S14 t <sub>4</sub>	6900	11100	0.43	-40.3	
S17 t <sub>end</sub>	9100	11700	0.49	-43.5	
S26 t <sub>end</sub>	10800	10400	0.56	-26.3	49.8
S16 t <sub>end</sub>	6900	30500	0.22	-44.2	

The data in Table 6.2 are quite inconsistent and therefore difficult to interpret. In general, one can state that block copolymers with one large block compared to the second one only show a single  $T_g$ . When taking a look at Table 6.2, samples S13 t<sub>end</sub>, S14 t<sub>4</sub> and S16 t<sub>end</sub> confirm this hypothesis. The explanation for these observations is probably the compatibilising behaviour of the large block. It forms the matrix material to, so to speak, solubilise the small block, hereby preventing phase separation to take place. Additionally, the  $T_g$  observed only seems to be dependent on the overall chemical composition of the block copolymer. Only a small molecular-weight dependence is observed.

When both blocks in the copolymer are of comparable size, phase separation occurs. Examples of these block copolymers are S13 t<sub>3</sub>, S25 t<sub>2</sub> and S26 t<sub>end</sub>. Both  $T_g$  values observed, e.g. -37.3°C and 26.2°C in the case of S25 t<sub>2</sub>, do not agree with the  $T_g$  values of the corresponding homopolymers. It is clear that in this case these  $T_g$  values

are influenced by the presence of the other phase. One should expect that these effects become less pronounced at higher molecular weights. Both blocks in sample S26  $t_{\text{end}}$  are larger and, as a result, the corresponding  $T_g$  value of the S phase is higher as compared to S25  $t_2$ . The  $T_g$  for the BA phase is also higher due to the higher  $F_S$ .

Note that although sample S8  $t_{\text{end}}$  has two comparable blocks, they are too small to enable phase separation. Furthermore, when low-molecular-weight material is present in the block copolymer, this will act like a compatibiliser and prevent phase separation. This is probably the case in sample S18  $t_4$  and S17  $t_{\text{end}}$ , which have broad molecular-weight distributions.

Another important note is that no clear trend seems to be present as far as phase separation for block copolymers with a bimodal molecular-weight distribution are concerned. Samples S14  $t_4$ , S16  $t_{\text{end}}$ , S18  $t_4$ , S25  $t_2$  and S26  $t_{\text{end}}$  all have bimodal molecular-weight distributions, but only S26  $t_{\text{end}}$  and S25  $t_2$  show two  $T_g$  values.

### 6.2.6 Concluding remarks

The synthesis of block copolymers using ATRP has proven to be possible. However, the success of the block formation greatly depends on the synthesis route that is chosen. When starting from a PBA macroinitiator and subsequent chain extension with S, good control is obtained over the polymerisation process. Molecular weight increases linearly with conversion and polydispersities remain low. In contrast to this route is the one where a PS macroinitiator is extended with BA. In this case, although molecular weights increase with conversion, bimodal distributions are obtained. Beside a part of the polymeric chains that is able to propagate, a considerable fraction of the chains does no longer seem to participate in the polymerisation process. It remains unclear whether this material is still bromide-functional.

Phase separation in the block copolymers occurs when both blocks are of approximately the same length. In these cases, two glass transition temperatures are observed in DSC. Nonetheless, when a significant amount of low-molecular-weight polymeric material is present, which is reflected in the polydispersity of the polymer, this will act as compatibiliser and no phase separation can be detected with DSC. If one of the two blocks is significantly larger than the other, the block copolymer only shows a single glass transition temperature, indicating that phase separation does not occur.

## 6.3 GRADIENT COPOLYMERISATION

Gradient, or tapered, copolymers consist of two monomer species that are distributed in such a way that the composition changes gradually along the polymer chain<sup>25</sup>. At one end, the polymer chain primarily consists of the first monomer, whereas the other end mostly contains the second monomer. As far as the composition distribution is concerned, gradient copolymers are situated between block and random copolymers. Although their properties are not well known, they are also expected to lie between those of block and random copolymers.

### 6.3.1 Synthesis

Little is known in literature on the synthesis of gradient copolymers. Although the synthesis of gradient copolymers via free-radical polymerisation techniques has been reported<sup>26</sup>, gradient copolymers, like block copolymers, were until recently only synthesised by means of anionic polymerisation<sup>13,27</sup>. However, living radical polymerisation techniques have proven to be an excellent alternative in recent years. Zaremskii and co-workers<sup>28</sup> produced gradient copolymers of S and methyl acrylate (MA) using *O,O'*-diisopropylxantogen iniferters. Although broad molecular-weight distributions were obtained, the authors synthesised “compositionally homogeneous gradient copolymers”. Arehart *et al.*<sup>29</sup> used S and BA to produce tapered copolymers via ATRP, while Greszta and co-workers<sup>30</sup> polymerised S and acrylonitrile (AN). All these groups, however, used the same strategy for the synthesis of their gradient copolymers. In all cases, the copolymerisation kinetics, *i.e.* reactivity ratios, is used to change the residual monomer composition. This composition drift of the monomer mixture is then imposed onto the growing polymeric chains, hereby creating a compositional gradient along the chain. This is a very convenient way to produce gradient copolymers, since it concerns a one-step synthesis. However, in many cases the reactivity ratios do not allow the gradients to be very ‘steep’, *i.e.* the copolymer still bears the character of a random copolymer. For example, the fraction of S in the gradient copolymers of S and MA reported by Zaremskii *et al.*<sup>28</sup> gradually decreases from 0.366 to 0.221, a very subtle change in composition.

For an ATRP copolymerisation of S/BA with an initial monomer composition,  $f_S^0$ , of 0.5, the instantaneous copolymer composition as a function of conversion as calculated from Eq. (5.1) is plotted in Figure 6.9. For the reactivity ratios, the optimised values from chapter 5 are used, *viz.*  $r_S=0.80$  and  $r_B=0.22$ .

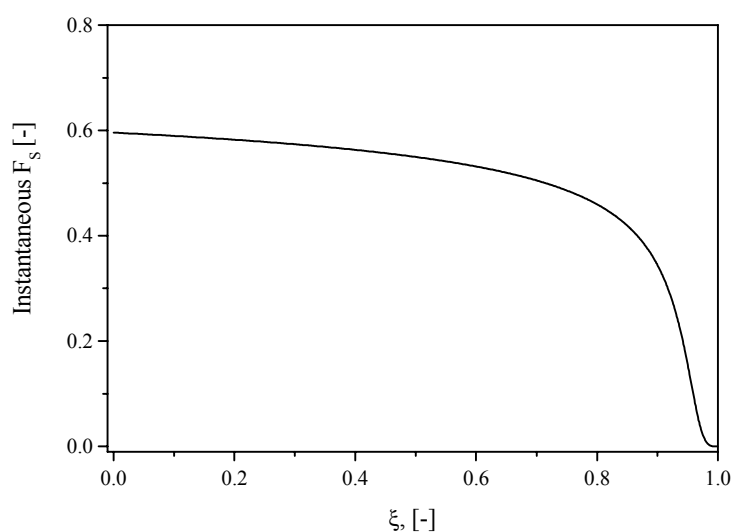


**Figure 6.9** Instantaneous copolymer composition ( $F_s$ ) as a function of total conversion for an ATRP copolymerisation of S/BA with initial monomer composition,  $f_s^0$ , of 0.5.

The instantaneous copolymer composition as a function of conversion as depicted in Figure 6.9 in fact reflects the copolymer composition at a certain position in the chain. It is evident from Figure 6.9 that the composition of the S/BA copolymer does not change significantly even up to a total conversion of 80%. For many copolymerisation systems, therefore, this strategy is not optimal for the production of gradient copolymers.

Two other strategies can yield much more pronounced gradients. The first one is the semi-batch copolymerisation, where the least reactive monomer is added to the reaction mixture during polymerisation. To this end, an optimal addition profile can be calculated when the kinetics of the copolymerisation system is exactly known. The advantage of this approach is that any gradient can be obtained by changing the addition profile. However, a major disadvantage is that even the slightest uncertainty in the kinetics will cause an inaccuracy in the addition profile. As a consequence, the rate of polymerisation will no longer correspond to the expected kinetics. This snowball effect will eventually lead to different gradient copolymers than originally targeted for.

A safer strategy is to start a copolymerisation with an initial monomer composition, which is very rich in the more reactive monomer 1. After a certain conversion a pulse of the second monomer is added to the system, hereby altering the monomer composition. It should be assured that the monomer composition after addition of the second monomer leads to preferential incorporation of the first monomer. As a result, the composition of the residual monomer mixture will change and becomes abundant

in monomer 2. When the conditions are optimised, this approach may lead to the production of tapered copolymers. The great advantage of this method is that only limited knowledge of the kinetics is required. Inaccuracies do not lead to a loss of control of the chemical composition distribution. This technique is schematically depicted for the copolymerisation of S and BA in Figure 6.10, where the composition of the instantaneously formed copolymer is plotted as a function of monomer composition. Eq. (5.1) from chapter 5 has been used together with  $r_S=0.80$  and  $r_B=0.22$ .

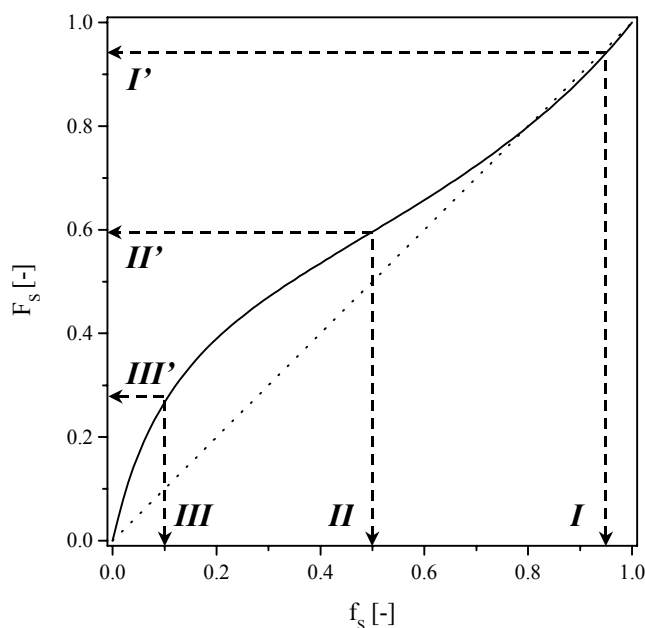


**Figure 6.10** Momentary copolymer composition ( $F_S$ ) as a function of monomer composition ( $f_S$ ) for the copolymerisation of S and BA (—); diagonal (···); for the explanations of the arrows, see text.

A useful strategy in the copolymerisation would be to start at an initial monomer composition **I**,  $f_S^0=0.95$ . At this monomer composition, a copolymer with approximately 95% S (**I'**) would be formed. With the monomer composition, the free-radical copolymerisation kinetics and the activation and deactivation parameters, one can calculate at what time the desired block length has been attained. Furthermore, the concentrations of all reacting species can be calculated as well. At this stage, a certain amount of BA is added to the reaction mixture to reach  $f_S^0=0.50$ , e.g. **II**. The block that is added onto the first S-rich block will still be relatively rich in S (composition **II'**). As a consequence, composition drift of the monomer composition occurs and the monomer mixture will become richer in BA. This composition drift is imposed on the polymer chains and, consequently, the composition of the second block gradually changes from S-rich towards more BA-rich. After a certain time period, another

quantity of BA is added to the reaction mixture, resulting in the monomer composition *III*. The instantaneous copolymer composition is now very low, which implies that the third block abounding in BA is formed. It is clear that in this strategy, knowledge on the kinetics is only required to calculate when the first pulse of BA should be added and what the amount should be. Since the copolymerisation system then spontaneously shows composition drift, one should only assure that the second pulse of BA is enough to ensure the formation of a block with an excess of BA. Note that Fukuda *et al.*<sup>31</sup> reported a similar strategy for the synthesis of block copolymers of S and AN comprising random sequences with narrow polydispersities.

As was shown in chapter 5, the copolymerisation kinetics of the system S/BA are well-described by the terminal unit model (TUM) in combination with the kinetic parameters obtained in chapter 4. This description is more accurate at high S fractions in the monomer mixture. For the three-step-synthesis approach, it is necessary to be able to predict the total conversion and the concentrations of the various species reasonably accurately. This is especially important for the determination when the first pulse of BA should be added. Fortunately, the three-step strategy starts with a high fraction of S in the monomer mixture, and so one can precisely predict when and how much BA should be added at the end of the first step.

In the next sections, a gradient copolymer of S and BA will be synthesised according to the three-step strategy. The aim is to produce a gradient copolymer with a steep intramolecular compositional gradient. A block abounding in S will thereto be formed, onto which a second transition block is polymerised, after which the third BA rich block should be attached.

### 6.3.2 Experimental

#### *Materials:*

The copper ligand, 4,4'-di-*n*-heptyl-2,2'-bipyridine (dHbpy), was synthesised according to a literature procedure<sup>13</sup>. Styrene (S, Aldrich, 99%) and butyl acrylate (BA, Aldrich, 99+%) were distilled and stored over molecular sieves. *p*-Xylene (Aldrich, 99+% HPLC grade) were stored over molecular sieves and used without further purification. CuBr (Aldrich, 98%) and ethyl 2-bromoisobutyrate (Aldrich, 98%) were used as received.

#### *Gradient copolymerisation; the three-step synthesis:*

*p*-Xylene (3.97 g), S (3.08 g, 0.0296 mol), BA (0.203 g,  $1.58 \cdot 10^{-3}$  mol) ethyl 2-bromoisobutyrate (0.140 g,  $7.18 \cdot 10^{-4}$  mol), CuBr<sub>2</sub> ( $8.38 \cdot 10^{-3}$  g,  $3.75 \cdot 10^{-5}$  mol) and dHbpy (0.593 g,  $1.68 \cdot 10^{-3}$  mol) were mixed in a 100 mL round-bottom flask. The mixture was purged with argon for 30 min, after which CuBr (0.108 g,  $7.53 \cdot 10^{-4}$  mol)

was added. The reaction mixture was then homogenized and purged with argon for another 30 min, after which the reaction mixture was placed in a thermostatically controlled oil bath at 110 °C. With these concentrations, simulations of this system were conducted with Mathematica 4.0 using the TUM, see the appendix. To obtain a first block of about  $1 \cdot 10^3 \text{ g} \cdot \text{mol}^{-1}$ , it was calculated that the first pulse of BA (4.22 g, 0.0329 mol) should be added approximately 260 min after the start of the reaction. This amount of BA was degassed in a dropping funnel and added to the reaction mixture, after which it was allowed to react for 19 hours.

To assure a reasonable rate of polymerisation, the second pulse of BA (8.18 g, 0.0638 mol) was mixed with dHbpy (0.455 g,  $1.29 \cdot 10^{-3}$  mol) and subsequently degassed for about 15 min. Hereafter, CuBr (0.0725 g,  $5.05 \cdot 10^{-4}$  mol) was added. This mixture was added to the polymerisation system approximately 23 hours after the start of the reaction.

Reaction samples were withdrawn from the reaction mixture at timed intervals. The samples were quenched immediately. Partial monomer conversions were determined by gas chromatography using a HP 5890 gas chromatograph equipped with an AT Wax column (Alltech, length 30 m, film thickness 1.0  $\mu\text{m}$ ) and an auto sampler. The remainder of the samples was passed through a column with activated alumina to remove the copper catalyst. After subsequent drying, the polymers were dissolved in stabilised tetrahydrofuran at  $1 \text{ mg} \cdot \text{mL}^{-1}$  and filtrated using 0.2  $\mu\text{m}$  filters. The molecular weights were determined by size exclusion chromatography (SEC) with a Waters Model 510 pump and Waters 712 WISP using 4 PL-gel mix C columns (300mm $\times$ 7.5mm, Polymer Laboratories) at 40°C and tetrahydrofuran as the eluent. The eluent flow rate was  $1.0 \text{ mL} \cdot \text{min}^{-1}$ . Calibration was performed with polystyrene standards with narrow molecular-weight distributions (Polymer Laboratories). The molecular weights of the gradient copolymers are all relative to polystyrene.

### 6.3.3 Results and discussion

The gradient copolymerisation was conducted using the strategy outlined in section 6.3.1. The molecular-weight evolution, as well as the molecular-weight-distributions are depicted in Figure 6.11a and b, respectively.

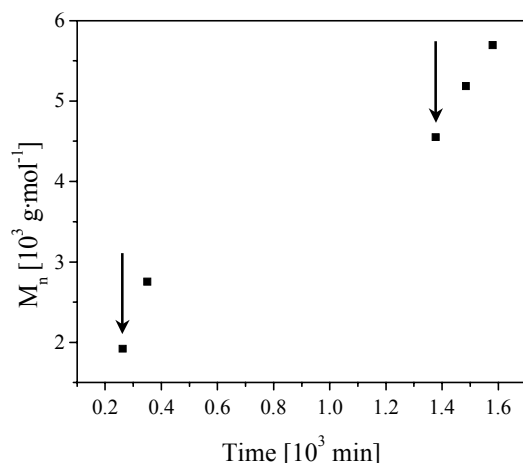


**Figure 6.11a** Three-step synthesis of a gradient copolymer of *S* and BA. Evolution of  $M_n$  with time. The arrows indicate addition of BA.

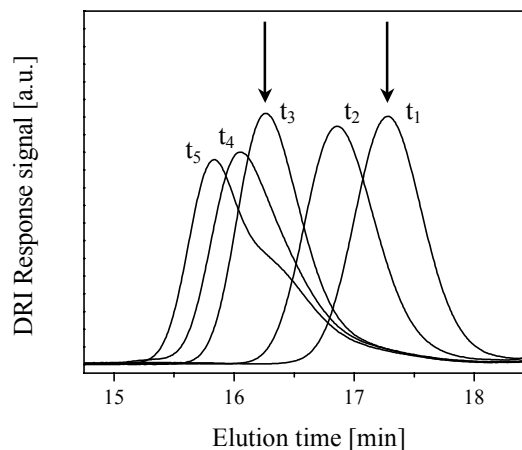


**Figure 6.11b** Three-step synthesis of a gradient copolymer. Evolution of the SEC chromatograms (DRI detector). The arrows indicate the addition of BA.

The molecular weights in Figure 6.11a have been plotted against time, since the total conversion in the three-step synthesis is difficult to calculate. As can be seen, molecular weights increase with time, indicating that the system bears living character. The molecular-weight distributions in Figure 6.11b confirm this, although it should be noted that they have not been corrected for conversion. After the addition of the second pulse of BA, *viz.* after the 4<sup>th</sup> sample in Figure 6.11b, we see that a low-molecular-weight shoulder appears in the molecular-weight distributions. We suspect that this shoulder arises from bimolecular termination products that are no longer able to propagate. This might be related to the problems discussed earlier concerning the chain extension of PS macroinitiators with BA.

Beside molecular-weight analysis, the samples were also subjected to gas chromatography to determine the composition of the residual monomer and to <sup>1</sup>H NMR to investigate the cumulative copolymer composition ( $F_S^{tot}$ ). The results are collected in Table 6.3.

**Table 6.3** Molecular weights, chemical composition and monomer composition during various stages of the gradient copolymerisation of *S* and BA at 110°C.

Time / event	$M_n$ , g.mol <sup>-1</sup>	$F_S^{tot}$ , [-]	$f_S$ , [-]
initially	0	-	0.95
after first BA addition	1921	0.91	0.38
before second BA addition	4531	0.70	0.34
after second BA addition	4531	0.70	0.092
end of reaction	5695	0.59	0.082



The monomer composition at the start of the reaction, just after the first BA addition and just after the second BA addition correspond to the compositions **I**, **II** and **III** in Figure 6.10, respectively. The monomer composition data listed in Table 6.3 can be depicted together with the curve that relates the instantaneous monomer composition to the composition of the instantaneously formed copolymer for a S/BA copolymerisation. As in Figure 6.10, Eq. (5.1) has been used with  $r_S=0.80$  and  $r_B=0.22$ .

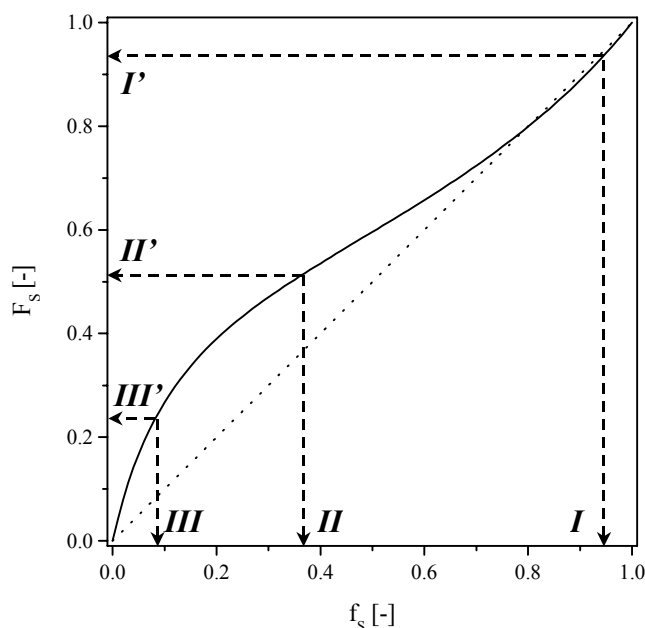


**Figure 6.12** Momentary copolymer composition ( $F_S$ ) as a function of monomer composition ( $f_S$ ) for the copolymerisation of S and BA (—); diagonal (···). The monomer compositions at  $t=0$  (**I**), just after the first BA addition (**II**) and second BA addition (**III**) are given by the arrows.

According to theory, *i.e.* using Eq (5.1), the eventual gradient copolymer should consist of a first block containing approximately 94% S, a second part with about 51% S and 49% BA, and finally a third block of about 76% BA. For our experiment, it is possible to determine the average chemical composition of each block with the molecular weight and the composition data of the whole copolymer. The chemical composition of the first block,  $F_S^I$ , equals 0.91, see Table 6.3. This is in fair agreement with the calculated copolymer composition using Eq. (5.1) and the reactivity ratios. According to theory, the first block should contain 94% S.

The composition of the second block,  $F_S^{II}$ , can easily be calculated with Eq. (6.1), using the molecular weights and the overall chemical composition:

$$F_S^{tot} = F_S^I \cdot x^I + F_S^{II} \cdot x^{II} \quad (6.1)$$

In Eq. (6.1),  $x^I$  and  $x^{II}$  are the mole fractions of the first and the second block in the copolymer of  $M_n=4531 \text{ g}\cdot\text{mol}^{-1}$ , respectively. Using the data from Table 6.3, it follows that the second block contains 53% S. According to the calculations, the instantaneously formed copolymer should contain 51% S, which is again in good accordance with the experimentally obtained composition.

The composition of the third block, can be calculated with the following relation:

$$F_S^{tot} = F_S^I \cdot x^I + F_S^{II} \cdot x^{II} + F_S^{III} \cdot x^{III} \quad (6.2)$$

Using this equation, together with the data in Table 6.3, one can calculate that the composition of the third block,  $F_S^{III}$ , equals 0.21. Calculations would predict a composition of the instantaneously formed copolymer of 24% S.

These results show that a copolymer with a ‘steep’ compositional gradient can be synthesised relatively easy using this strategy. The composition of the copolymer gradually changes from  $F_S=0.90$  at one end of the polymeric chain to  $F_S=0.21$ , *i.e.* approximately 80% BA, at the other end. The gradient copolymer is schematically depicted in Scheme 6.1.



**Scheme 6.1** Gradient copolymer of S and BA obtained in the three-step synthesis, schematically shown. The first block of  $M_n=1921 \text{ g}\cdot\text{mol}^{-1}$  contains 94% S, the second block of  $M_n=2610 \text{ g}\cdot\text{mol}^{-1}$  contains 53% S and the third block of  $M_n=1164 \text{ g}\cdot\text{mol}^{-1}$  contains 21% S.

### Phase separation:

The samples taken from the gradient polymerisation were also subjected to analysis by DSC. The results are listed in Table 6.4.

**Table 6.4** Glass transition temperatures ( $T_g$ ) of samples taken from the gradient copolymerisation of S and BA at 110°C.

Sample	$M_n$ , g·mol <sup>-1</sup>	$F_S^{tot}$ , [-]	$T_g$ , °C
t1	1921	0.91	2.51
t3	4457	0.70	-1.21
t7	5187	0.63	-12.3
t <sub>end</sub>	5695	0.59	-21.5

As can be seen from Table 6.4, only one glass transition temperature is observed. This indicates that phase separation does not occur. Although block copolymers with the same molecular weight and overall composition are not directly available, it is expected that they might show phase separation from molecular weights of  $5 \cdot 10^3$  g·mol<sup>-1</sup> on. In the gradient copolymers, even at relatively high molecular weights and almost equal amounts of S and BA present, *e.g.* sample t<sub>end</sub>, only one  $T_g$  value is observed. Another interesting point is the decreasing  $T_g$  with increasing fraction of BA in the copolymer despite the increase in molecular weight. Apparently, the chemical composition of the copolymer influences the  $T_g$  value much more than the molecular weight does. If the glass transition temperature of sample t<sub>end</sub> is compared with a block copolymer of similar overall composition, *e.g.* sample S8 t<sub>end</sub> in Table 6.3, it is remarkable that for the gradient copolymer it is much lower. This is related to the chemical composition distribution of the gradient copolymer, where the presence of BA in the S-rich first block is enough to ensure a low value for  $T_g$ .

### 6.3.4 Concluding remarks

The three-step-synthesis approach proved to be an excellent method to produce gradient copolymers with a steep compositional gradient along the polymeric chain. The kinetic model from chapter 5 can easily be used in this strategy. Despite the fact that they partly resemble the block copolymers in terms of segregation of both monomers in the polymeric chain, one can conclude that the gradient copolymers behave as random copolymers, since only one value for  $T_g$  is observed, which increases with increasing fraction of S in the copolymer. The fact that complete segregation between the two monomer species is absent in the gradient copolymer indicates sufficient compatibility within the polymeric chain.

## 6.4 CONCLUSIONS

It has been shown that ATRP can be used to produce intramolecularly heterogeneous copolymers of S and BA. Block copolymers with varying S and BA blocks have been synthesised. When these block copolymers were synthesised starting from a PBA macroinitiator and subsequent chain extension with S, excellent control of the polymerisation was obtained. However, applying the opposite pathway, *i.e.* starting from a PS macroinitiator followed by chain extension with BA, resulted in bimodal molecular-weight distributions. Further analysis of this system led us to conclude that during the second step a part of the macroinitiator does not propagate anymore. The best way to synthesise block copolymers of S and BA is to start from a PBA macroinitiator followed by chain extension with S.

The kinetic insights in the ATRP copolymerisation of S and BA can successfully be implemented to produce gradient copolymers of S and BA. A three-step-synthesis strategy proved to be an excellent way to produce tapered copolymers. It has been shown that a fairly steep gradient can be accomplished in this way.

DSC results indicate that the phase separation behaviour in block copolymers is dependent on the length of both S and BA blocks. The presence of low-molecular-weight material prevents phase separation to take place. The gradient copolymers did not show any phase separation. It is therefore plausible to assume that the smooth transition of composition along the polymeric chain ensures enough compatibility.

## REFERENCES

- <sup>1</sup> Hughes, L.J.; Britt, G.E. *J. Appl. Pol. Sci.* **1961**, *V (15)*, 337
- <sup>2</sup> Krause, S. *J. Macromol. Sci. – Revs. Macromol. Chem.* **1972**, *C7 (2)*, 251
- <sup>3</sup> IUPAC Commission on Macromolecular Nomenclature, *Pure Appl. Chem.* **1974**, *40*, 479
- <sup>4</sup> Goodman, I., *Developments in Block Copolymers – 2*; Elsevier Applied Science Publishers Ltd.: London, 1985
- <sup>5</sup> Riess, G.; Hurtrez, G. Bahadur, P. *Encyclopedia of Polymer Science and Engineering – 2*; Mark, H.F., Kroschwitz, J.I., Eds.; Wiley; New York, 1985
- <sup>6</sup> Gaillard, P.; Ossenbach-Sauter, M.; Riess, G. In *Polymer Compatibility and Incompatibility, Vol 2*; Solc, K., Ed.; Harwood Academic Publishers: New York, 1982; p 289
- <sup>7</sup> Duivenvoorde, F.L.; van Es, J.J.G.S.; van Nostrum, C.F.; Van der Linde, R. *Macromol. Chem. Phys.* **2000**, *201*, 656
- <sup>8</sup> De Brouwer, H.; Schellekens, M.A.J.; Klumperman, B.; Monteiro, M.J.; German, A.L. *J. Pol. Sci., Part A: Pol. Chem.* **2000**, *38 (19)*, 3596

- <sup>9</sup> Bouix, M.; Gouzi, J.; Charleux, B.; Vairon, J.-P.; Guinot, P. *Macromol. Rapid Commun.* **1998**, *19*, 209
- <sup>10</sup> Flory, P.J. , *Principles of Polymer Chemistry*; Cornell University Press: Ithaca, 1953
- <sup>11</sup> Hashimoto, T.; Shibayama, M.; Kawai, H. *Macromolecules* **1980**, *13*, 1237
- <sup>12</sup> Hashimoto, H.; Fujimura, M.; Hashimoto, T.; Kawai, H. *Macromolecules* **1981**, *14*, 844
- <sup>13</sup> Hashimoto, T.; Tsukahara, Y.; Tachi, K.; Kawai, H. *Macromolecules* **1983**, *16*, 648
- <sup>14</sup> Iván, B.; Kennedy, J.P. *Macromolecules* **1990**, *23*, 2880
- <sup>15</sup> Chen, X.; Iván, B.; Kops, J.; Batsberg, W. *Polym. Prepr.* **1997**, *38* (1), 715
- <sup>16</sup> Coca, S.; Matyjaszewski, K. *Polym. Prepr.* **1997**, *38* (1), 693
- <sup>17</sup> Gaynor, S.G.; Edelman, S.Z.; Matyjaszewski, K. *Polym. Prepr.* **1997**, *38* (1), 703
- <sup>18</sup> Matyjaszewski, K., *Controlled Radical Polymerization*; ACS Symposium Series No. 685; American Chemical Society: Washington DC, 1997
- <sup>19</sup> Uegaki, H.; Kotani, Y.; Kamigaito, M.; Sawamoto, M. *Macromolecules* **1998**, *31*, 6756
- <sup>20</sup> Shipp, D. A.; Wang, J.-L.; Matyjaszewski, K. *Macromolecules* **1998**, *31*, 8005
- <sup>21</sup> Cassebras, M.; Pascual, S.; Polton, A.; Tardi, M.; Vairon, J.-P. *Macromol. Rapid Commun.* **1999**, *20*, 261
- <sup>22</sup> Matyjaszewski, K.; Patten, T.E.; Xia, J. *J. Am. Chem. Soc.* **1997**, *119*, 674
- <sup>23</sup> Fischer, H.; Poser, S. *Acta Polymer.* **1996**, *47*, 413
- <sup>24</sup> Inoue, T.; Onogi, T.; Yao, M.-L.; Osaki, K. *J. Polym. Sci.: Part B: Polym. Phys.* **1999**, *37*, 389
- <sup>25</sup> Zelinski, R.P.; Childers, C.W. *Rubber Chem. Technol.* **1968**, *41*, 161
- <sup>26</sup> Semchikov, Yu.D.; Smirnova, L.A.; Knyazeva, T.Ye.; Bulgakova, S.A.; Sherstyanykh, V.I. *Eur. Polym. J.* **1990**, *26* (8), 883
- <sup>27</sup> Szwarc, M.; Levy, M.; Milkovich, R. *J. Am. Chem. Soc.* **1956**, *78*, 2656
- <sup>28</sup> Zaremskii, M.Yu.; Luzin, A.A.; Garina, E.S.; Golubev, V.B.; Lachinov, M.B. *Pol. Sci.* **1997**, *39* (8), 858
- <sup>29</sup> Arehart, S.V.; Greszta, D.; Matyjaszewski, K. *Polym. Prepr.* **1997**, *38* (1), 705
- <sup>30</sup> Greszta, D.; Matyjaszewski, K.; Pakula, T. *Polym. Prepr.* **1997**, *38* (1), 709
- <sup>31</sup> Fukuda, T.; Terauchi, T.; Goto, A.; Tsujii, Y.; Miyamoto, T.; Shimizu, Y. *Macromolecules* **1996**, *29*, 3050

# Epilogue

In society nowadays, a strong trend can be observed towards the application of specialty polymeric materials. Block copolymers constitute a large part of these top-end polymers, which are produced through living polymerisation techniques such as anionic polymerisation. The choice of monomers, however, is limited and the process demands stringent reaction conditions.

A challenge in this respect lies in the development of straightforward polymerisation techniques to open the door to the facile and controlled synthesis of a wider range of copolymers with well-defined intramolecular chemical composition distributions. In this thesis, therefore, the attention has been focused on advanced radical polymerisation techniques.

The results of the investigations on the conventional free-radical copolymerisation of styrene and butyl acrylate demonstrated that this approach could, to the best of our knowledge, never lead to control of monomer sequence distributions. It should be further investigated whether this could be achieved in other copolymerisations involving a more polar monomer, such as methacrylic acid with styrene. Thorough knowledge may lead to control of the incorporation process by manipulation of the preferential absorption coefficient or the bootstrap distribution coefficient by choosing the right reaction conditions.

This thesis has given a fundamental and profound investigation on the ATRP homo- and copolymerisation of styrene and butyl acrylate. *System knowledge* has been provided and should be considered as the major fundamental contribution of this thesis. Strategic parameters have been pinpointed in chapter 4 and convenient approaches to determine them have been suggested. These methods can easily be transposed to other ATRP copolymerisation systems involving other catalysts, comonomer pairs or reaction conditions. Considering the results of the investigations in chapter 5, one can suppose that the ATRP equilibria can be regarded as features additional to the conventional free-radical polymerisation kinetics.

Beside system knowledge, the investigations in this thesis have provided *product synthesis knowledge*. Unlike many statements reported in literature, the success of the synthesis of block copolymers depends in a great deal on the strategy followed. Depending on the properties of the eventual block copolymer, approaches for the synthesis of well-defined block copolymers of styrene and butyl acrylate have been

suggested in chapter 6. An underexposed class of intramolecularly heterogeneous copolymers are gradient copolymers. When amphiphilic properties are desired, but phase separation needs to be prevented, a three-step-synthesis approach is provided to produce copolymers bearing a steep compositional gradient along the chain. It has been shown throughout the thesis that ATRP is a promising tool in the controlled synthesis of well-defined polymeric materials, provided that thorough knowledge on the system is available.

Future studies should primarily be focused on two areas. First, more detailed fundamental knowledge on the mechanism of ATRP is of utmost importance. A still better understanding of the ATRP system will allow one to manipulate and control important reaction parameters. In this respect, the adequate characterisation of polymerisation products is a crucial point. Size exclusion chromatography combined with infrared spectroscopy has proven to be a valuable tool in the determination of chemical composition distributions of copolymers of styrene and butyl acrylate as a function of their molecular-weight distribution. However, other characterisation techniques are potentially very interesting. Matrix-assisted laser desorption ionisation (MALDI) can be of great importance, although the lack of understanding of the underlying mechanism has certainly limited its applicability so far.

A second area relates to the scaling-up of ATRP to produce high-performance materials in large quantities. In view of the robustness of the ATRP system as compared with conventional living polymerisation techniques, this is only a matter of time. As in conventional free-radical polymerisation processes, one should exclude oxygen from the reaction mixture to prevent the catalyst from oxidising. The main challenge in the scaling-up of ATRP lies in obtaining higher turnover ratios. The application of ATRP in emulsion systems has already proven to be possible, although latex stability and copper removal still hamper its use on a large scale. In this field, therefore, a significant effort has to be put into development of methods to remove the copper catalyst. In this light, heterogeneous ATRP systems are a competitive option, since the catalyst removal can be done in a single separation step. An additional advantage is that the catalyst can easily be recycled and used in a second polymerisation reaction.

In conclusion, the future prospects for Atom Transfer Radical Polymerisation seem very promising. Further research is of utmost importance to fully exploit its possibilities. The work presented in this thesis should be considered as a contribution to solve the complicated jigsaw that will eventually lead to complete understanding of the ATRP system.

# Appendix: Simulation Programs

## ATRP Homopolymerisations:

```
SetDirectory["E:\\gregs data\\mathematica\\ATRP homopolymerisation"]

Off[General::spell1];

ks = 1580; kini = 0.45; ktr = 1.1 107;
kas = 0.45; kas = 1.1 107; k0 = 1 108;
S00 = 4.2; EiB00 = 0.05;

EiB0 = 0.05;
EiBr0 = 0;
S0 = 4.2;
Sr0 = 0;
PSBr0 = 0;
CuI0 = 0.05;
CuII0 = 0;

k[t]= k0(1+(S00-S[t])/EiB00)^(-1.674)+ 1.01 (S[t]/S00);

solut[interval_, EiB0_, EiBr0_, S0_, Sr0_, PSBr0_, CuI0_, CuII0_]:=
#[interval]&/@({EiB, EiBr, S, Sr, PSBr, CuI, CuII}/.First[
NDSolve[{EiB'[t] == -kini EiB[t]CuI[t] + ktr EiBr[t]CuII[t],
EiBr'[t] == kini EiB[t]CuI[t] - ktr EiBr[t]CuII[t] - ks EiBr[t]S[t] -
2k[t](EiBr[t])2 - 2k[t] EiBr[t]Sr[t],
S'[t] == -ks Sr[t]S[t] - ks EiBr[t]S[t],
Sr'[t] == kas PSBr[t]CuI[t] - kas Sr[t]CuII[t] - 2k[t](Sr[t])2 + ks EiBr[t]S[t] -
2k[t] EiBr[t]Sr[t],
PSBr'[t] == -kas PSBr[t]CuI[t] + kas Sr[t]CuII[t],
CuI'[t] == -kas PSBr[t]CuI[t] + kas Sr[t]CuII[t] - kini EiB[t]CuI[t] +
ktr EiBr[t]CuII[t],
CuII'[t] == kas PSBr[t]CuI[t] - kas Sr[t]CuII[t] + kini EiB[t]CuI[t] -
ktr EiBr[t] CuII[t],
EiB[0] == EiB0,
EiBr[0] == EiBr0,
S[0] == S0,
Sr[0] == Sr0,
PSBr[0] == PSBr0,
CuI[0] == CuI0,
CuII[0] == CuII0}], {EiB, EiBr, S, Sr, PSBr, CuI, CuII},
{t, 0, interval}]]

Clear[x]; x=0; ttijd=0; sol[0]={ttijd, EiB0, EiBr0, S0, Sr0, PSBr0, CuI0, CuII0};
While[ttijd < 10*3600,
interval=If[ttijd ≤ 3000, 30, 150];
{dummy, EiB0, EiBr0, S0, Sr0, PSBr0, CuI0, CuII0}=
sol[+x]= Prepend[solut[interval, EiB0, EiBr0, S0, Sr0, PSBr0, CuI0, CuII0],
ttijd += interval]//Timing

oplossing = Array[sol, x-1, 1];
{ttijd, EiBt, EiBrt, St, Srt, PSBrt, CuIt, CuIIIt}=Transpose[oplossing];
Conv = (S00 - St)/S00;
lnConv = -Log[1 - Conv];
Export["Raw data S ATRP.txt",
Transpose[{ttijd, EiBt, EiBrt, St, Srt, PSBrt, CuIt, CuIIIt, Conv, lnConv}], "Table"];
```



## ATRP Copolymerisations; TUM:

```

SetDirectory["E:/Gregs Data/Mathematica/ATRP copolymerisation/TUM"]
Off[General::spell1];

kSS = 1580; kBS = 435000; kBB = 78400; kSB = 1663; kini = 0.43;
kaS = 0.43; kdS = 6.8 107; k0 = 108; kaB = 0.075; kdB = 1 108;
S00 = 3; B00 = 1; EiB00 = 0.05;
EiB0 = 0.05;
EiBr0 = 0;
S0 = 3;
B0 = 1;
Sr0 = 0;
Br0 = 0;
PSBr0 = 0;
PBBr0 = 0;
CuI0 = 0.05;
CuII0 = 0;

k[t] = k0(1 + (S00+B00-S[t]-B[t])/EiB00)^(-1.674+(S[t]+B[t])/(S00+B00));

solut[interval_, EiB0_, EiBr0_, S0_, B0_, Sr0_, Br0_, PSBr0_, PBBr0_, CuI0_,
CuII0_] := # [interval] & / @ ( {EiB, EiBr, S, B, Sr, Br, PSBr, PBBr, CuI, CuII} /. First[
NDSolve[ {EiB'[t] == -kini EiB[t] CuI[t] + kaS EiBr[t] CuII[t],
EiBr'[t] == kini EiB[t] CuI[t] - kdS EiBr[t] CuII[t] - kSS EiBr[t] S[t] - kBS EiBr[t] B[t],
S'[t] == -kSS Sr[t] S[t] - kBS Br[t] S[t] - kSS EiBr[t] S[t],
B'[t] == -kBS Br[t] B[t] - kSB Sr[t] B[t] - kBB EiBr[t] B[t],
Sr'[t] == kSS EiBr[t] S[t] + kaS PSBr[t] CuI[t] - kdS Sr[t] CuII[t] + kBS Br[t] S[t] -
kSB Sr[t] B[t] - 2k[t](Sr[t])2 - 2k[t]Sr[t]Br[t],
Br'[t] == kBS EiBr[t] B[t] + kaB PBBr[t] CuI[t] - kdB Br[t] CuII[t] + kSB Sr[t] B[t] -
kBS Br[t] S[t] - 2k[t](Br[t])2 - 2k[t]Sr[t]Br[t],
PSBr'[t] == -kaS PSBr[t] CuI[t] + kdS Sr[t] CuII[t],
PBBr'[t] == -kaB PBBr[t] CuI[t] + kdB Br[t] CuII[t],
CuI'[t] == -kaS PSBr[t] CuI[t] - kaB PBBr[t] CuI[t] + kdS Sr[t] CuII[t] +
kdB Br[t] CuII[t] - kini EiB[t] CuI[t] + kaS EiBr[t] CuII[t],
CuII'[t] == kaS PSBr[t] CuI[t] + kaB PBBr[t] CuI[t] - kdS Sr[t] CuII[t] -
kdB Br[t] CuII[t] + kini EiB[t] CuI[t] - kdS EiBr[t] CuII[t],
EiB[0] == EiB0,
EiBr[0] == EiBr0,
S[0] == S0,
B[0] == B0,
Sr[0] == Sr0,
Br[0] == Br0,
PSBr[0] == PSBr0,
PBBr[0] == PBBr0,
CuI[0] == CuI0,
CuII[0] == CuII0,
{EiB, EiBr, S, B, Sr, Br, PSBr, PBBr, CuI, CuII},
{t, 0, interval}]]

Clear[x]; x=0; ttijd=0;
sol[0]={ttijd, EiB0, EiBr0, S0, B0, Sr0, Br0, PSBr0, PBBr0, CuI0, CuII0};
While[ttijd < 10*3600, interval = If[ttijd ≤ 30, 1, 30];
{dummy, EiB0, EiBr0, S0, B0, Sr0, Br0, PSBr0, PBBr0, CuI0, CuII0}=
sol[+x]= Prepend[solut[interval, EiB0, EiBr0, S0, B0, Sr0, Br0, PSBr0, PBBr0, CuI0,
CuII0], ttijd += interval]//Timing

```

```

oplossing = Array[sol, x-1, 1];
{ttijd, EiBt, EiBrt, St, Bt, Srt, Brt, PSBrt, PBBrt, CuIt, CuIIIt}=
Transpose[oplossing];
p1 = Srt/(Srt + Brt);
f1 = St/(St + Bt);
p2 = Brt/(Srt + Brt);
f2 = Bt/(St + Bt);
RadTot = Srt + Brt;
radratio = p1/p2;
Conv = ((S00 + B00) - (St + Bt))/(S00 + B00);
lnConv = -Log[1 - Conv];
kp = kSS p1 f1 + kBS p2 f1 + kBB p2 f2 + kSB p1 f2;
Export["Raw Data TUM.txt", Transpose[{ttijd, Srt, Brt, RadTot, St, Bt}], "Table"];
Export["Data TUM.txt", Transpose[{ttijd, Conv, lnConv, radratio, f1, kp}], "Table"];

```

## ATRP Copolymerisations; PUM:

```

SetDirectory["E:\\gregs data\\mathematica\\ATRP\\copolymerisation\\PUM"]
Off[General::spell1];

kSSS = 1580; kBBB = 78400; kBBS = 435000; kSBB = 1663;
kBSS = 759; kSBB = 4704; kBBS = 798; kSBS = 26133;
kini = 0.43; S0 = 2; B0 = 2; EiB0 = 0.05;
kaS = 0.43; kdS = 6.8 107; k0 = 108; kaB = 0.075;
kdB = 1 108;

EiB0 = 0.05;
EiBr0 = 0;
S0 = 2;
B0 = 2;
SSr0 = 0;
BSr0 = 0;
BBr0 = 0;
SBr0 = 0;
PSSBr0 = 0;
PBSBr0 = 0;
PBBBr0 = 0;
PSBBr0 = 0;
CuI0 = 0.05;
CuII0 = 0.0025;

k[t] = k0(1 + (S0+B0-S[t]-B[t])/EiB00)(-1.674+(S[t]+B[t])/(S0+B0));

solout[interval_, EiB0_, EiBr0_, S0_, B0_, SSr0_, BSr0_, BBr0_, SBr0_,
PSSBr0_, PBSBr0_, PBBBr0_, PSBBr0_, CuI0_, CuII0_] :=
#[interval]&@({EiB, EiBr, S, B, SSr, BSr, BBr, SBr, PSSBr, PBSBr, PBBBr,
PSBBr, CuI, CuII}/.First[NDSolve[
({EiB'[t] == -kini EiB[t]CuI[t] + kdS EiBr[t]CuII[t],
EiBr'[t] == kini EiB[t]CuI[t] - kdS EiBr[t]CuII[t] - kSSS EiBr[t]S[t] - kBBB EiBr[t]B[t],
S'[t] == -kSSS SSr[t]S[t] - kBSS BSr[t]S[t] - kBBS BBr[t]S[t] - kSBS SBr[t]S[t] -
kSSS EiBr[t]S[t],
B'[t] == -kBBB BBr[t]B[t] - kSBB SBr[t]B[t] - kSBB SSr[t]B[t] - kSBB BSr[t]B[t] -
kBBB EiBr[t]B[t],
SSr'[t] == kSSS EiBr[t]S[t] + kaS PSSBr[t]CuI[t] - kdS SSr[t]CuII[t] + kBSS BSr[t]S[t] -
kSBB SSr[t]B[t] - 2k[t](SSr[t])2 - 2k[t]SSr[t]BSr[t] - 2k[t]SSr[t]BBr[t] -
2k[t]SSr[t]SBr[t],
BSr'[t] == kaS PBSBr[t]CuI[t] - kdS BSr[t]CuII[t] - kBSS BSr[t]S[t] - kSBB BSr[t]B[t] +
kBBS BBr[t]S[t] + kSBS SBr[t]S[t] - 2k[t](BSr[t])2 - 2k[t]BSr[t]BBr[t] -
2k[t]BSr[t]SBr[t] - 2k[t]BSr[t]SSr[t],
BBr'[t] == kBBB EiBr[t]B[t] + kaB PBBBr[t]CuI[t] - kdB BBr[t]CuII[t] + kSBB SBr[t]B[t] -
kBBS BBr[t]S[t] - 2k[t](BBr[t])2 - 2k[t]BBr[t]SBr[t] - 2k[t]BBr[t]BSr[t] -
2k[t]BBr[t]SSr[t],
SBr'[t] == kaB PSBBr[t]CuI[t] - kdB SBr[t]CuII[t] - kSBB SBr[t]B[t] - kSBS SBr[t]S[t] +
kSBB SSr[t]B[t] + kSBB BSr[t]B[t] - 2k[t](SBr[t])2 - 2k[t]SBr[t]BBr[t] -
2k[t]SBr[t]BSr[t] - 2k[t]SBr[t]SSr[t],
PSSBr'[t] == -kaS PSSBr[t]CuI[t] + kdS SSr[t]CuII[t],
PBSBr'[t] == -kaS PBSBr[t]CuI[t] + kdS BSr[t]CuII[t],
PBBBr'[t] == -kaB PBBBr[t]CuI[t] + kdB BBr[t]CuII[t],
PSBBr'[t] == -kaB PSBBr[t]CuI[t] + kdB SBr[t]CuII[t],
CuI'[t] == -kaS PSSBr[t]CuI[t] - kaS PBSBr[t]CuI[t] - kaB PBBBr[t]CuI[t] -
kaB PSBBr[t]CuI[t] + kdS SSr[t]CuII[t] + kdS BSr[t]CuII[t] + kdB BBr[t]CuII[t] +
kdB SBr[t]CuII[t] - kini EiB[t]CuI[t] + kdS EiBr[t]CuII[t],
CuII'[t] == kaS PSSBr[t]CuI[t] + kaS PBSBr[t]CuI[t] + kaB PBBBr[t]CuI[t] +
kaB PSBBr[t]CuI[t] - kdS SSr[t]CuII[t] - kdS BSr[t]CuII[t] - kdB BBr[t]CuII[t] -
kdB SBr[t]CuII[t] + kini EiB[t]CuI[t] - kdS EiBr[t]CuII[t],

```

```

EiB[0] == EiB0,
EiBr[0] == EiBr0,
S[0] == S0,
B[0] == B0,
SSr[0] == SSr0,
BSr[0] == BSr0,
BBr[0] == BBr0,
SBr[0] == SBr0,
PSSBr[0] == PSSBr0,
PBSBr[0] == PBSBr0,
PBBBr[0] == PBBBr0,
PSBBr[0] == PSBBr0,
CuI[0] == CuI0,
CuII[0] == CuII0},
{EiB, EiBr, S, B, SSr, BSr, BBr, SBr, PSSBr, PBSBr, PBBBr, PSBBr, CuI, CuII},
{t, 0, interval}]]))

Clear[x]; x=0; ttijd=0;
sol[0] = {ttijd, EiB0, EiBr0, S0, B0, SSr0, BSr0, BBr0, SBr0, PSSBr0, PBSBr0, PBBBr0,
PSBBr0, CuI0, CuII0};
While[ttijd < 10*3600, interval = If[ttijd ≤ 300, 30, 300];
{dummy, EiB0, EiBr0, S0, B0, SSr0, BSr0, BBr0, SBr0, PSSBr0, PBSBr0, PBBBr0, PSBBr0,
CuI0, CuII0}=
sol[+x]= Prepend[solut[interval, EiB0, EiBr0, S0, B0, SSr0, BSr0, BBr0, SBr0, PSSBr0,
PBSBr0, PBBBr0, PSBBr0, CuI0, CuII0], ttijd += interval]]//Timing

oplossing = Array[sol, x-1, 1];
{ttijd, EiBt, EiBrt, St, Bt, SSrt, BSrt, BBrt, SBr, PSSBrt,
PBSBrt, PBBBrt, PSBBrt, CuIt, CuIIt} = Transpose[oplossing];
p11 = SSrt/(SSrt + BSrt + BBrt + SBr);
p12 = SBr/(SSrt + BSrt + BBrt + SBr);
p22 = BBrt/(SSrt + BSrt + BBrt + SBr);
p21 = BSrt/(SSrt + BSrt + BBrt + SBr);
RadTot = SSrt + BSrt + BBrt + SBr;
f1 = St/(St + Bt);
f2 = Bt/(St + Bt);
radratio = (p11 + p21)/(p22 + p12);
Conv = ((S00 + B00) - (St + Bt))/(S00 + B00);
kp = kSSS p11 f1 + kBSS p21 f1 + kBBS p22 f1 + kSBS p12 f1 + kBBB p22 f2 + kSBB p12 f2 +
kSSB p11 f2 + kBSS p21 f2;
Export["Raw Data PUM.txt", Transpose[{ttijd, SSrt, BSrt, BBrt, SBr, RadTot, St,
Bt}], "Table"];
Export["Data PUM.txt", Transpose[{ttijd, Conv, radratio, f1, kp}], "Table"];

```

## Conventional free-radical copolymerisations; TUM:

```

SetDirectory["E:/Gregs Data/Mathematica/Free-radical Polymerisation"]
Off[General::spell1];

kSS = 1580; kBS = 435000; kBB = 78400; kSB = 1663; kini = 2 10(-6);
k0 = 108;
S00 = 3; B00 = 1; AIBN00 = 0.05;
AIBN0 = 0.05;
AIBNr0 = 0;
S0 = 3;
B0 = 1;
Sr0 = 0;
Br0 = 0;

k[t] = k0;

solut[interval_, AIBN0_, AIBNr0_, S0_, B0_, Sr0_, Br0_] :=
#[interval]&@({AIBN, AIBNr, S, B, Sr, Br}/.First[
NDSolve[{AIBN'[t] == -kini AIBN[t],
AIBNr'[t] == kini AIBN[t] - kSS AIBNr[t]S[t] - kBB AIBNr[t]B[t],
S'[t] == -kSS Sr[t]S[t] - kBS Br[t]S[t] - kSS AIBNr[t]S[t],
B'[t] == -kBB Br[t]B[t] - kSB Sr[t]B[t] - kBB AIBNr[t]B[t],
Sr'[t] == kSS AIBNr[t]S[t] + kBS Br[t]S[t] - kSB Sr[t]B[t] - 2k[t](Sr[t])2 -
2k[t]Sr[t]Br[t],
Br'[t] == kBB AIBNr[t]B[t] + kSB Sr[t]B[t] - kBS Br[t]S[t] - 2k[t](Br[t])2 -
2k[t]Sr[t]Br[t],
AIBN[0] == AIBN0,
AIBNr[0] == AIBNr0,
S[0] == S0,
B[0] == B0,
Sr[0] == Sr0,
Br[0] == Br0},
{AIBN, AIBNr, S, B, Sr, Br}, {t, 0, interval}]]

Clear[x]; x = 0; ttijd = 0;
sol[0] = {ttijd, AIBN0, AIBNr0, S0, B0, Sr0, Br0};
While[ttijd < 10*3600, interval = If[ttijd ≤ 300, 30, 100];
{dummy, AIBN0, AIBNr0, S0, B0, Sr0, Br0} =
sol[++x] = Prepend[solut[interval, AIBN0, AIBNr0, S0, B0, Sr0, Br0],
ttijd += interval]]//Timing

oplossing = Array[sol, x-1, 1];
{ttijd, AIBNt, AIBNrt, St, Bt, Srt, Brt} = Transpose[oplossing];
p1 = Srt/(Srt + Brt);
f1 = St/(St + Bt);
p2 = Brt/(Srt + Brt);
f2 = Bt/(St + Bt);
RadTot = Srt + Brt;
radratio = p1/p2;
Conv = ((S00 + B00) - (St + Bt))/(S00 + B00);
kp = kSS p1 f1 + kBS p2 f1 + kBB p2 f2 + kSB p1 f2;
Export["Raw Data TUM.txt", Transpose[{ttijd, AIBNt, Srt, Brt, RadTot, St, Bt}],
"Table"];
Export["Data TUM.txt", Transpose[{ttijd, Conv, radratio, f1, kp}], "Table"];

```

# Glossary

## Parameters:

$c^*$	concentration at which polymeric coils start overlapping ( $\text{mol}\cdot\text{L}^{-1}$ )
$D_0$	diffusion coefficient of a monomer species ( $\text{m}^2\cdot\text{s}^{-1}$ )
$D_i$	diffusion coefficient of a polymeric radical with chain length $i$ ( $\text{m}^2\cdot\text{s}^{-1}$ )
$E_a$	activation energy ( $\text{J}\cdot\text{mol}^{-1}$ )
$f_i$	molar fraction of monomer $i$ in monomer mixture (-)
$f_i^0$	initial molar fraction of monomer $i$ in monomer mixture (-)
$F_i$	molar fraction of monomer $i$ in copolymer (-)
$k_{\text{act}}$	activation rate coefficient ( $\text{L}\cdot\text{mol}^{-1}\cdot\text{s}^{-1}$ )
$k_{\text{act}}^1$	activation rate coefficient of alkyl halide ( $\text{L}\cdot\text{mol}^{-1}\cdot\text{s}^{-1}$ )
$k_{\text{deact}}$	deactivation rate coefficient ( $\text{L}\cdot\text{mol}^{-1}\cdot\text{s}^{-1}$ )
$k_{\text{deact}}^1$	deactivation rate coefficient of alkyl halide derived radical ( $\text{L}\cdot\text{mol}^{-1}\cdot\text{s}^{-1}$ )
$k_{\text{act}}^i$	activation rate coefficient of species $i$ ( $\text{L}\cdot\text{mol}^{-1}\cdot\text{s}^{-1}$ )
$k_{\text{deact}}^i$	deactivation rate coefficient of species $i$ ( $\text{L}\cdot\text{mol}^{-1}\cdot\text{s}^{-1}$ )
$k_d$	dissociation rate coefficient of an alkoxyamine ( $\text{s}^{-1}$ )
$k_{\text{dis}}$	dissociation rate coefficient ( $\text{s}^{-1}$ )
$k_i$	initiation rate coefficient ( $\text{L}\cdot\text{mol}^{-1}\cdot\text{s}^{-1}$ )
$k_i^j$	initiation rate coefficient of primary radical with monomer $j$ ( $\text{L}\cdot\text{mol}^{-1}\cdot\text{s}^{-1}$ )
$k_p$	propagation rate coefficient ( $\text{L}\cdot\text{mol}^{-1}\cdot\text{s}^{-1}$ )
$k_p^i$	homopropagation rate coefficient of species $i$ ( $\text{L}\cdot\text{mol}^{-1}\cdot\text{s}^{-1}$ )
$k_p^{ii}$	homopropagation rate coefficient ( $\text{L}\cdot\text{mol}^{-1}\cdot\text{s}^{-1}$ )
$k_p^{ij}$	crosspropagation rate coefficient ( $\text{L}\cdot\text{mol}^{-1}\cdot\text{s}^{-1}$ )
$k_t$	termination rate coefficient ( $\text{L}\cdot\text{mol}^{-1}\cdot\text{s}^{-1}$ )
$\bar{k}_t$	average termination rate coefficient ( $\text{L}\cdot\text{mol}^{-1}\cdot\text{s}^{-1}$ )
$k_t^c$	termination rate coefficient for combination ( $\text{L}\cdot\text{mol}^{-1}\cdot\text{s}^{-1}$ )
$k_t^d$	termination rate coefficient for disproportionation ( $\text{L}\cdot\text{mol}^{-1}\cdot\text{s}^{-1}$ )
$k_{\text{tr}}$	transfer rate coefficient ( $\text{L}\cdot\text{mol}^{-1}\cdot\text{s}^{-1}$ )
$k_{\text{tr}}$	trapping rate coefficient ( $\text{L}\cdot\text{mol}^{-1}\cdot\text{s}^{-1}$ )
$k_t^{i,j}$	chain-length-dependent termination rate coefficient ( $\text{L}\cdot\text{mol}^{-1}\cdot\text{s}^{-1}$ )

$k_t^0$	termination rate coefficient for a polymer with chain length 1 ( $L \cdot mol^{-1} \cdot s^{-1}$ )
$k_t^\xi$	conversion-dependent termination rate coefficient ( $L \cdot mol^{-1} \cdot s^{-1}$ )
$k_{t,ii}^\xi$	conversion-dependent termination rate coefficient for homopolymer i ( $L \cdot mol^{-1} \cdot s^{-1}$ )
K	equilibrium constant (a.u.)
$K^A$	distribution coefficient in solvent A (-)
$M_n$	number-average molecular weight ( $g \cdot mol^{-1}$ )
$M_w$	weight-average molecular weight ( $g \cdot mol^{-1}$ )
$\sim M_i \cdot$	polymeric radical with monomer i as the radical bearing chain end
$N_A$	Avogadro's number ( $mol^{-1}$ )
p	probability (-)
p	spin multiplicity factor (-)
R	gas constant ( $J \cdot mol^{-1} \cdot K^{-1}$ )
$R_p$	rate of propagation ( $mol \cdot L^{-1} \cdot s^{-1}$ )
$R_t$	rate of termination ( $mol \cdot L^{-1} \cdot s^{-1}$ )
$R_{deact}$	rate of deactivation ( $mol \cdot L^{-1} \cdot s^{-1}$ )
$R_{ELSD}$	evaporative light scattering detector signal (mV)
$r_i$	terminal unit model monomer reactivity ratio (-)
$r_{ij}$	penultimate unit model monomer reactivity ratio (-)
$s_i$	radical reactivity ratio (-)
$S_t$	normalised area under the SEC chromatograms at time t (-)
$S_0$	initial normalised area under the SEC chromatograms (-)
$[S_i]$	concentration of species S with chain length i ( $mol \cdot L^{-1}$ )
$[S]$	concentration of species S ( $mol \cdot L^{-1}$ )
$[S]_0$	initial concentration of species S ( $mol \cdot L^{-1}$ )
t	time (s)
T	temperature (K)
$T_g$	glass transition temperature ( $^{\circ}C$ )
$w_p$	weight fraction of polymer (-)
$w_{M,0}$	initial weight fraction of monomer (-)
x	mole fraction (-)

*Greek symbols:*

$\alpha$	slope of linear fit (-)
$\delta$	chemical shift (ppm)
$\Delta$	tetrahedral field splitting (a.u.)
$\Delta G$	change in Gibbs free energy ( $\text{J}\cdot\text{mol}^{-1}$ )
$\epsilon$	dielectric constant (-)
$\lambda$	preferential absorption coefficient ( $\text{mL}\cdot\text{g}^{-1}$ )
$\xi$	fractional conversion (-)
$\sigma$	capture radius (m)
$\chi$	Flory-Huggins interaction parameter (-)
$\chi N$	reduced parameter (-)
$(\chi N)_{\text{cr}}$	critical reduced parameter (-)

*Acronyms and Symbols:*

AAM	acryl amide
AIBN	2,2'-azobis(isobutyronitrile)
AN	acrylonitrile
ATRA	atom transfer radical addition
ATRP	atom transfer radical polymerisation
BA	butyl acrylate
BMA	butyl methacrylate
BP	benzoyl peroxide
BuAc	butyl acetate
CTA	chain-transfer agent
dHbpy	4,4'-di- <i>n</i> -heptyl-2,2'-bipyridine
D <sup>p</sup>	dead polymeric material with chain length 1
D <sup>p</sup> <sub>i</sub>	dead polymeric material with chain length i
DMF	<i>N,N</i> -dimethylformamide
DRI	differential refractive index
DSC	differential scanning calorimetry
ELSD	evaporative light scattering detector
hydroxy-TEMPO	4-hydroxy-2,2,6,6-tetramethylpiperidine- <i>N</i> -oxyl
HPLC	high performance liquid chromatography
I <sub>2</sub>	initiator



I·	primary radical
I-X	alkyl halide initiator
IR	infrared spectroscopy
LRP	living radical polymerisation
LUMO	lowest unoccupied molecular orbital
MA	methyl acrylate
MAA	methacrylic acid
Me	methyl
$M_i$	monomer i
$M_t^{n+1}$	metal complex in its oxidised state
$M_t^{n+1}X$	metal complex in its oxidised state
$M_t^n$	metal complex in its reduced state
MLCT	metal to ligand charge transfer
MMA	methyl methacrylate
NMR	nuclear magnetic resonance
$PB_i\cdot$	butyl acrylate-ended polymer radical with chain length i
PBA	poly(butyl acrylate)
PBA-Br	poly(butyl acrylate) dormant species
$PBB_i\cdot$	butyl acrylate-ended polymer radical with a butyl acrylate penultimate unit and chain length i
$PBS_i\cdot$	styrene-ended polymer radical with a butyl acrylate penultimate unit and chain length i
$PS_i\cdot$	styrene-ended polymer radical with chain length i
$PSB_i\cdot$	butyl acrylate-ended polymer radical with a styrene penultimate unit and chain length i
$PSS_i\cdot$	styrene-ended polymer radical with a styrene penultimate unit and chain length i
PDI	polydispersity index
PS	polystyrene
PS-Br	polystyrene dormant species
PUM	penultimate unit model
R·	carbon-centred radical
$R_i\cdot$	carbon-centred radical with chain length i
RAFT	reversible addition-fragmentation transfer
R-OH	hydroxy-functional species

R-X	dormant species
S	styrene
SAXS	small angle X-ray scattering
SEC	size exclusion chromatography
T	species involved in transfer reactions
T	hydroxy-TEMPO
TEM	transition electron microscopy
TEMPO	2,2,6,6-tetramethylpiperidine- <i>N</i> -oxyl
TsCl	tosylchloride
TUM	terminal unit model



# Summary

Today's world demands polymeric materials with very specific properties. Copolymers with well-defined intramolecular chemical composition distributions, for instance, have found applications in many different areas. The production of these specialty copolymers, however, calls for outstanding control of the incorporation of the monomer units into the polymeric chain. In general, living polymerisation techniques are applied for the synthesis of well-defined copolymers; an often complicated and meticulous matter, which hampers a wider use of these copolymers.

This thesis attempts to provide a facile approach to synthesise copolymers having pre-defined and well-defined intramolecular composition distributions using straightforward free-radical polymerisation techniques. The comonomer pair styrene/butyl acrylate has been chosen as a model system.

The first line of research consisted of a feasibility study for the application of conventional free-radical copolymerisation to obtain compositionally heterogeneous polymeric chains. It was suspected that intramolecular composition drift might occur in the free-radical copolymerisation of styrene and butyl acrylate. The molecular-weight dependence of copolymer composition was thereto investigated by assessing the monomer reactivity ratios for polymerisations in the presence and absence of chain-transfer agent. Copolymerisations were performed at 50°C and 90°C. At both temperatures, no significant difference in reactivity ratios was observed. This approach, therefore, was considered not viable to control intramolecular composition distributions.

As a result, the application of living radical polymerisation techniques seemed to be inevitable. Atom Transfer Radical Polymerisation (ATRP) was chosen, since it appears to be the most versatile living radical polymerisation technique. Given that ATRP still is underexposed from a detailed kinetic point of view, the strategy of the second line of research was aimed at investigating and understanding the ATRP homopolymerisations. The leitmotif was to transpose the important kinetic parameters from the ATRP homopolymerisations of styrene and butyl acrylate to their ATRP copolymerisation.

In a first stage, the important kinetic parameters of the ATRP homopolymerisations of styrene and butyl acrylate were investigated. Attention was focused on the determination of activation and deactivation rate coefficients. It was shown that the activation rate coefficients could be obtained experimentally by performing so-called nitroxide exchange experiments. In these experiments, the bromide atom at the

dormant species chain end was replaced with a hydroxy-functional stable nitroxide. Subsequent analysis was by high performance liquid chromatography, where the non-functional and hydroxy-functional species were separated. In *p*-xylene, the activation rate coefficient of polystyrene dormant species proved to be almost a factor of 6 higher than the one for poly(butyl acrylate) dormant species. The activation rate coefficients are strongly dependent on solvent. The deactivation rate coefficients were obtained by performing ATRP homopolymerisations with an initial amount of deactivating species present. Unlike the activation rate coefficients, the deactivation rate coefficients do not seem to depend significantly on solvent.

In a second step, it was tried to transpose the activation and deactivation rate coefficients, as well as the monomer reactivity ratios from conventional free-radical copolymerisation, to the ATRP copolymerisation of styrene and butyl acrylate. Thereto, the influence of the ATRP equilibria on the reactivity ratios was investigated by performing high-conversion ATRP copolymerisations. It was found that the observed reactivity ratios did not change significantly. Model predictions confirmed these findings.

In a next step, it was endeavoured to link the total monomer conversion to the reaction time. ATRP copolymerisations were performed at different initial monomer compositions and were compared with *ab initio* simulations. In these simulations, the terminal unit model and the penultimate unit model were assessed. The former was proven to describe the ATRP copolymerisation of styrene and butyl acrylate most accurately. A peculiar fact in this case was that model predictions described the ATRP copolymerisation more accurately at high fractions of styrene in the initial monomer composition. Nevertheless, the results enabled us to predict the evolution of monomer conversion in time reasonably accurately.

The application of the kinetic insights in ATRP to produce copolymers with pre-defined intramolecular chemical composition distributions formed the last step. Block copolymers of styrene and butyl acrylate were synthesised and it was shown that the most efficient way to do so is by polymerising styrene in a second stage onto a poly(butyl acrylate) macroinitiator prepared in the first stage. Proof of block existence was provided by size exclusion chromatography, nuclear magnetic resonance and infrared spectroscopy.

A three-step-synthesis strategy proved to be an excellent way to produce gradient copolymers. In the first step, the first block rich in styrene was produced. The kinetic knowledge on the ATRP copolymerisation was used to predict when the first pulse of butyl acrylate should be added. The second block consisted of both styrene and butyl acrylate. In the third step, another pulse of butyl acrylate was added to obtain a third block rich in butyl acrylate.

The phase separation behaviour of the block and gradient copolymers was studied by means of differential scanning calorimetry. This technique revealed that the phase separation behaviour of the block copolymers is dependent on the length of both styrene and butyl acrylate blocks. The gradient copolymers did not show any phase separation, indicating good compatibility.



# Résumé

L'époque actuelle réclame des matériaux polymères aux propriétés très spécifiques. Par exemple, certains copolymères à la composition chimique intramoléculaire bien définie trouvent des applications dans des domaines divers. Cependant, la production de ces polymères de spécialité requiert un excellent contrôle de l'incorporation des unités monomères dans les chaînes polymères. En général, des techniques de polymérisation vivante sont utilisées pour synthétiser ces copolymères à la composition bien définie. Ces techniques sont hélas souvent compliquées et demandent une très grande rigueur ce qui empêche leur utilisation étendue.

Dans cette thèse, de simples techniques de polymérisation radicalaire sont utilisées pour tenter de faciliter la synthèse de copolymères ayant des distributions de composition intramoléculaire à la fois pre-définies et bien-définies. La paire de monomères styrène/acrylate de butyle a été choisie comme modèle.

Une étude de faisabilité a été menée en premier lieu afin d'évaluer la possibilité de produire des polymères ayant une composition hétérogène par des méthodes traditionnelles de copolymérisation radicalaire. Pour le système styrène/acrylate de butyle, une variation dans la composition intramoléculaire était supposée se produire lors d'une réaction de copolymérisation radicalaire. Les rapports de réactivité en présence ou non d'agent de transfert ont donc été calculés afin d'établir l'influence de la masse moléculaire sur la composition des copolymères. Les réactions de copolymérisation ont été conduites à 50°C et à 90°C. Dans aucun cas une différence significative dans les rapports de réactivité n'a pu être observée. Cette approche a donc été jugée non adaptée pour le contrôle de la distribution intramoléculaire de composition chimique.

En conséquence, l'utilisation des techniques de polymérisation radicalaire vivante a paru indispensable. La technique dite *Atom Transfer Radical Polymerisation* (ATRP) a été choisie car elle semble être la plus prometteuse des techniques de polymérisation radicalaire vivante. Ce type de polymérisation n'est cependant toujours pas complètement élucidé d'un point de vue cinétique et c'est pourquoi une seconde ligne de recherche a été consacrée à l'étude et la compréhension de l'homopolymérisation par ATRP. La démarche a consisté à transposer les paramètres cinétiques importants de l'homopolymérisation à la copolymérisation des monomères styrène et acrylate de butyle par ATRP.

Dans un premier temps les paramètres cinétiques importants de l'homopolymérisation par ATRP du styrène et de l'acrylate de butyle ont été étudiés et une attention toute



particulière a été portée aux coefficients d'activation et de désactivation. Il a été démontré que des expériences dites d'échange de nitroxyde pouvaient conduire à la détermination des coefficients d'activation. Ces expériences consistent à remplacer l'atome de brome situé au bout des chaînes dormantes par un groupe nitroxyde stable possédant une fonction hydroxyde. Les espèces avec et sans groupe fonctionnel ont ensuite été séparées et quantifiées par chromatographie en phase liquide (HPLC). Les résultats ont montré que dans le *p*-xylène le coefficient d'activation des espèces dormantes est six fois plus grand pour le polystyrène comparé au poly-acrylate de butyle. Il a pu être montré que les coefficients d'activation dépendent fortement du solvant utilisé. Des expériences d'homopolymérisation par ATRP en présence d'une quantité initiale d'espèces désactivantes ont permis de déterminer les coefficients de désactivation. Contrairement aux coefficients d'activation, ceux-ci ne sont pas significativement dépendant du solvant utilisé.

Le but fixé dans un second temps a été de tenter de transposer les coefficients d'activation et de désactivation ainsi que les rapports de réactivité de la copolymérisation radicalaire conventionnelle à la copolymérisation par ATRP pour les deux monomères styrène et acrylate de butyle. Ainsi, des copolymérisations par ATRP ont été menées jusqu'à hautes conversions afin d'étudier l'influence de l'équilibre caractérisant le mécanisme ATRP sur les rapports de réactivité. Les résultats ont montré que les rapports de réactivité ainsi observés ne changent pas de façon significative. Les prédictions obtenues par modélisation ont confirmé cette observation.

Par la suite, la conversion des monomères a été reliée au temps de réaction. Des copolymérisations par ATRP ont été menées en faisant varier la composition initiale en monomères. Les résultats ont été comparés à ceux obtenus par simulation de la totalité du système. Les modèles dits *terminal* et *penultimate* ont été utilisés en parallèle dans les simulations. C'est le modèle terminal qui est apparu le plus adapté pour décrire la copolymérisation du styrène et de l'acrylate de butyle par ATRP. Il est à noter que dans ce cas les prédictions du modèle décrivent la copolymérisation par ATRP de façon plus exacte lorsque la fraction initiale en monomère styrène est élevée. Quoiqu'il en soit, ces résultats nous ont permis de prédire la conversion des monomères dans le temps avec une bonne précision.

Enfin, les informations obtenues sur la cinétique de la polymérisation par ATRP ont été utilisées pour produire des copolymères possédant une distribution de composition chimique pré-établie. Des copolymères blocs de styrène et d'acrylate de butyle ont été synthétisés. Il a pu être montré que la manière la plus adaptée pour atteindre ce but est de former dans un premier temps un macro-amorceur de poly-acrylate de butyle et de l'utiliser ensuite pour polymériser le styrène. Des analyses par chromatographie

d'exclusion stérique, résonance magnétique nucléaire et spectroscopie infra-rouge ont prouvé l'existence de blocs dans ces polymères.

Une synthèse en trois étapes s'est révélée être une méthode tout à fait adaptée pour produire des copolymères à gradient de composition. Dans la première étape, un bloc riche en styrène a été formé. Pour la seconde étape, les données cinétiques de la copolymérisation par ATRP déjà accumulées ont été utilisées pour prédire l'instant auquel l'acrylate de butyle a dû être ajouté. Ainsi le second bloc contenait à la fois du styrène et de l'acrylate de butyle. Un autre apport en acrylate de butyle a marqué le début de la troisième étape et l'obtention d'un dernier bloc enrichi en ce monomère.

Le comportement des polymères blocs et gradients en ce qui concerne les phénomènes de séparation de phase a été étudié par calorimétrie différentielle. Cette technique a montré que la séparation de phase dépend de la longueur des blocs styrène et acrylate de butyle. Les copolymères à gradient de composition n'ont pas induit de phénomènes de séparation de phase démontrant ainsi une grande compatibilité.



# Samenvatting

Vandaag de dag stelt men aan polymere materialen zeer hoge eisen en dienen deze vaak zeer specifieke eigenschappen te bezitten. Zo worden copolymeren met een goed gedefinieerde intramoleculaire sequentieverdeling tegenwoordig in tal van toepassingen gebruikt. De bereiding van deze speciale copolymeren vergt echter een nauwgezette beheersing van de inbouw van de beide monomeren in de keten. In het algemeen worden copolymeren met een goed gedefinieerde intramoleculaire chemische samenstellingsverdeling dan ook geproduceerd met behulp van zogenaamde levende-polymerisatietechnieken. Deze technieken zijn echter bijzonder gevoelig voor spootjes verontreinigingen in het reactiemengsel, zoals bijvoorbeeld water bij anionische polymerisatie, wat de verdere toepassing van de genoemde copolymeren in de weg staat.

Dit proefschrift poogt een eenvoudig alternatief te bieden voor de bereiding van copolymeren met een goed gedefinieerde, vooraf bepaalde intramoleculaire chemische samenstellingsverdeling, daarbij gebruik makende van vrije-radicaal-polymerisatietechnieken. Er is gekozen voor het modelsysteem styreen/butylacrylaat. Een eerste onderzoekslijn richtte zich op de haalbaarheid van conventionele vrije-radicaalpolymerisatietechnieken. De ketenlengteafhankelijkheid van de chemische samenstelling werd daartoe onderzocht door de monomere reactiviteitsverhoudingen in polymerisaties in aan- en afwezigheid van een chain-transfer agent te bepalen. Deze copolymerisaties werden uitgevoerd bij 50°C en 90°C. Een significant verschil in reactiviteitsverhoudingen werd bij beide temperaturen niet waargenomen. De conclusie luidt dan ook dat conventionele vrije-radicaalpolymerisatie van styreen en butylacrylaat niet kan worden toegepast om de intramoleculaire chemische samenstellingsverdeling te beheersen.

Deze slotsom noopte tot het toepassen van levende-radicaalpolymerisatietechnieken. Atom Transfer Radical Polymerisation (ATRP) werd hiervoor gekozen, vanwege zijn reeds bewezen veelzijdigheid. De strategie van de tweede onderzoekslijn was bewust gericht op het vergroten van inzicht in fundamentele aspecten van ATRP. Met name kinetische aspecten van ATRP zijn in de literatuur onderbelicht. De kerngedachte hierbij is dat de fundamentele reactiestappen, die bij homopolymerisaties optreden, ook terugkomen bij de copolymerisaties.

In eerste instantie werd de kinetiek van de ATRP homopolymerisaties van zowel styreen als butylacrylaat grondig onderzocht. Daarbij werd voornamelijk de aandacht gevestigd op de bepaling van activerings- en deactiveringsnelheidscoëfficiënten.

Gebleken is dat de activeringssnelheidscoëfficiënten konden worden bepaald door middel van zogenaamde nitroxide-uitwisselingsexperimenten. In deze experimenten werd het broomatoom aan het ketenuiteinde van de slapende ketens vervangen door een hydroxy-functioneel stabiel nitroxide. De niet-functionele en monofunctionele polymeren konden vervolgens met *high performance liquid chromatography* worden gescheiden. De activeringssnelheidscoëfficiënt van niet-reagerende ketens met een styreen als ketenuiteinde bleek in *p*-xyleen ongeveer 6 maal hoger te zijn dan de corresponderende waarde voor de niet-reagerende ketens met een butylacrylaat als ketenuiteinde. De activeringssnelheidscoëfficiënten bleken erg sterk afhankelijk te zijn van oplosmiddel. De deactiveringssnelheidscoëfficiënten werden bepaald met behulp van ATRP homopolymerisaties waarbij een kleine hoeveelheid deactivator was toegevoegd aan het reactiemengsel. In tegenstelling tot de activeringssnelheidscoëfficiënten waren de waarden voor de deactiveringssnelheidscoëfficiënten praktisch niet afhankelijk van oplosmiddel.

In de tweede stap werd geprobeerd de activerings- en deactiveringssnelheidscoëfficiënten, tezamen met de monomere reactiviteitsverhoudingen van de conventionele vrije-radicaalpolymerisaties te vertalen naar de ATRP copolymerisatie van styreen en butylacrylaat. Het effect van de ATRP evenwichten op de reactiviteitsverhoudingen werd onderzocht door middel van hoge-conversie-ATRP copolymerisaties. De reactiviteitsverhoudingen bleken slechts in geringe mate te worden beïnvloed door de ATRP evenwichten, hetgeen ook door modelberekeningen werd ondersteund.

In de daarop volgende stap werd getracht de totale monomeerconversie mathematisch te verbinden aan de reactietijd. ATRP copolymerisaties werden uitgevoerd met verschillende initiële monomeersamenstellingen en werden vergeleken met *ab initio* modelberekeningen. Het *terminal unit* en het *penultimate unit* model werden geëvalueerd, waarbij werd vastgesteld dat de eerstgenoemde de beste benadering opleverde voor de experimentele resultaten van de ATRP copolymerisatie van styreen en butylacrylaat. Een eigenaardige bijkomstigheid in dezen was de betere beschrijving van het systeem bij hoge fracties styreen in het monomeermengsel. Over het algemeen genomen was de beschrijving echter bevredigend te noemen.

De toepassing van de opgedane kinetische kennis van ATRP voor de synthese van copolymeren met een vooraf gedefinieerde intramoleculaire samenstellingsverdeling vormt de laatste stap van dit proefschrift. Blokcopolymeren van styreen en butylacrylaat werden gemaakt en het bleek dat dit doel het meest efficiënt werd bereikt door styreen te polymeriseren op een polybutylacrylaat macroinitiator. Het bewijs voor de aanwezigheid van de blokken werd geleverd door *size exclusion chromatography*, *nuclear magnetic resonance spectroscopy* en *infrared spectroscopy*.

Een synthese strategie om gradiëntcopolymeren te produceren in drie stappen bleek een doeltreffende concept te zijn voor het verkrijgen van zogenaamde steile gradiënten. In de eerste stap, waarin de kinetische kennis van het ATRP systeem werd toepast, werd een styreenrijk blok gesynthetiseerd. Er werd berekend wanneer en hoeveel butylacrylaat moest worden toegevoegd. Het tweede blok bestond uit een mengsel van styreen en butylacrylaat. In de derde en laatste stap werd een tweede hoeveelheid butylacrylaat toegevoegd om ervoor te zorgen dat het derde blok voornamelijk uit butylacrylaat bestond.

Het fasenscheidingsgedrag van de blok- en gradiëntcopolymeren werd bestudeerd met *differential scanning calorimetry*. Het fasenscheidingsgedrag van de blokcopolymeren bleek afhankelijk te zijn van de beide bloklengten. De gradiëntcopolymeren vertoonden geen fasenscheiding, wat duidt op voldoende mengbaarheid en compatibiliteit.



# Dankwoord

Aan het einde van vier jaren van noeste arbeid, wil ik graag een paar woorden van dank uiten aan diegenen die mij in die periode hebben gesteund.

Ik dank Ton German voor zijn niet-aflatende interesse en voor de bijna spreekwoordelijk geworden geboden vrijheid. I would like to thank professor Fukuda for taking part in my promotion committee as second promotor. Professor Haddleton is also acknowledged for taking part in my examination committee. Mijn begeleider en copromotor Bert Klumperman wil ik graag bedanken voor de vele discussies die we de afgelopen jaren gevoerd hebben. Jan Meuldijk bedank ik voor zijn motiverend enthousiasme en voor het zorgvuldig doorlezen en corrigeren van het manuscript.

Mijn huisgenoten Frank en Bastiaan, waarmee ik, vaak onder het genot van vele aangename alcoholische versnaperingen, menig discussie heb gevoerd en die bij tijd en wijle mijn wetenschappelijke zorgen telkenmale deden verdwijnen. Ik wil ook zeker niet voorbij gaan aan de steun die ik van mijn vrienden heb gekregen in de afgelopen vier jaren. Roel, Karin en Wouter, zonder vooral jullie vriendschap en hulp was dit boek zeker niet tot stand gekomen. Karin, bedankt voor de ontzettend stijlvolle omslag!

Voorts wil ik iedereen in de vakgroep polymeerchemie bedanken voor de prettige werksfeer, die mij altijd weer met plezier aan het werk deed gaan. Een aantal mensen wil ik met name bedanken. Hans de Brouwer en Bas Pierik ben ik erg veel dank verschuldigd voor het lezen en corrigeren van het manuscript. Ook Mike Schellekens verdient hiervoor lof. Mijn ex-kamergenoten Stefan, Dominique, Eelco, Camiel, Michel en Bas ben ik zeer erkentelijk voor hun luisterend oor en voor de broodnodige afleiding tussen de werkzaamheden door. Mijn studenten Mayk Senden, Mark Wubbels, Jarl Ivar van der Vlugt, Patrick de Man en Frank de Wit wil ik noemen voor al hun inspanningen die ze in het kader van mijn onderzoek hebben verricht. Helly en Caroline, bedankt voor de geboden hulp wanneer het weer eens 'stressen' was.

Erik Vonk ben ik erkentelijk voor de vele metingen die hij aan mijn polymeren heeft verricht. Hetzelfde kan ik zeggen van Sander Kok van TNO, die in het laatste stadium van het onderzoek de SEC-IR metingen aan de blokcopolymeren heeft uitgevoerd. Hartmut Fischer wil ik bedanken voor de interessante en leerzame discussies op het gebied van polymere eigenschappen.



Ik heb bijna twee jaar moeten wachten om Paul Cools op mijn beurt te kunnen bedanken voor de vele bakjes koffie en de sportieve afleiding. Paul, bij dezen! Martin de Jong wil ik graag bedanken voor zijn positieve bijdrage op zowel wetenschappelijk als persoonlijk vlak (jawohl Herr Kapellmeister!). Uiteraard wil ik niet de mensen vergeten, met wie ik regelmatig –zo niet overmatig– verlichtende gesprekken en discussies heb gevoerd bij de geliefde koffieautomaat. Ik noem mijn trouwe Riskbondgenoot Hans, Robert, voor het introduceren van Bohnanza en uiteraard voor het wekelijks etaleren van zijn talenten bij de zaalvoetbalcompetitie, Frank, Dominique, Mike, Amaia (¡por cierto, hasta luego!), Bas en Francis als voornaamste bondgenoten in dit dagelijks meermaals terugkerende ritueel. Je voudrais aussi remercier Thibault, pour son enthousiasme assidu pendant les matchs de squash. On fera un autre bientôt!

Natuurlijk kan en wil ik niet voorbij gaan aan mijn familie, die in feite weinig direct met mijn onderzoek te maken heeft gehad, maar die altijd haar interesse en vertrouwen in mijn kunnen heeft getoond. Papa, mama, Sylvain en Tessa, ontzettend bedankt voor die nimmer wijkende positieve instelling die mij meer dan eens de motivatie heeft gegeven in mindere tijden!

Finalement, un très grand merci pour Martine, tout d’abord pour son amour et aussi pour m’avoir aidé et ‘supporté’ tout le long du trajet. J’espère ne pas avoir été trop perfectionniste... Martine, merci!

# *Curriculum Vitae*

Grégory Chambard was born on the 25<sup>th</sup> of November 1972 in Prinsenbeek, The Netherlands. In 1991, he completed his secondary education at the Onze-Lieve-Vrouwe Lyceum in Breda. In the same year, he started his studies at the Faculty of Chemical Engineering and Chemistry at the Eindhoven University of Technology. In 1996 he graduated with distinction, after which he started a Ph.D. project in the Polymer Chemistry Department of prof. dr. ir. A.L. German. Since November 2000, he has been working for the Dow Chemical Company at the Engineering Plastics R&D department in Terneuzen, The Netherlands.